

Mitochondria, Inflammation and Stem Cells in Gastrointestinal and Hepatic Disease

Meng Li 栗梦

Cover layout: Ridderprint BV, the Netherlands

Source of image: <https://www.shutterstock.com/image-illustration/winter-landscape-oil-paintings-village-digital-743093230>

Printed by: Ridderprint BV, the Netherlands

Financial support for printing this thesis was kindly provided by

Erasmus MC – University Medical Center Rotterdam

© Meng Li, 2020

For all articles published, the copyright has been transferred to the respective publisher. No part of this thesis may be reproduced, stored in a retrieval system, or transmitted in any form or any means without written permission of the author or when appropriate from the publisher

ISBN: 978-94-6375-952-6

Mitochondria, Inflammation and Stem Cells in Gastrointestinal and Hepatic Disease

Mitochondria, ontsteking en stamcellen in ziekte van darmen en lever

Thesis

**To obtain the degree of Doctor from the
Erasmus University Rotterdam
by command of the
rector magnificus**

Prof. dr. R.C.M.E. Engels

and in accordance with the decision of the Doctorate Board

The public defense shall be held on

Wednesday 8th July 2020 at 11:30

by

Meng Li

Born in Harbin, Heilongjiang Province, China

Erasmus University Rotterdam



DOCTORAL COMMITTEE

Promotor

Prof. dr. M.P. Peppelenbosch

Inner Committee

Prof. dr. C.J. van der Woude

Prof. dr. L.J.W. van der Laan

Dr. C.A. Spek

Co-promotor

Dr. Q. Pan

Contents

CHAPTER 1	1
General introduction and aim of the thesis	
CHAPTER 2	15
Mitochondrial Fusion Via OPA1 and MFN1 Supports Liver Tumor Cell Metabolism and Growth....	
<i>Cells, 2020, 9(1), 121; https://doi.org/10.3390/cells9010121.</i>	
CHAPTER 3	41
The complex I and III of mitochondrial electron transport chain are therapeutically targetable in liver cancer	
<i>In preparation.</i>	
CHAPTER 4	63
Cancer-associated fibroblasts provide a stromal niche for liver cancer organoids that confers trophic effects and therapy resistance	
<i>In preparation.</i>	
CHAPTER 5	105
Modeling liver cancer and therapy responsiveness using organoids derived from primary mouse liver tumors	
<i>Carcinogenesis. 2019 Mar 12;40(1):145-154.</i>	
CHAPTER 6	139
LGR5 marks targetable tumor-initiating cells in liver cancer	
<i>Nat Commun. 2020 Apr 23;11(1):1961.</i>	
CHAPTER 7	221
Pregnane X Receptor Activation Constrains Mucosal NF- κ B Activity in Active Inflammatory Bowel Disease	
<i>PLoS One. 2019 Oct 3;14(10):e0221924</i>	
CHAPTER 8	249
Risk for complications in cancer patients treated with checkpoint inhibitors.....	
<i>Clin Res Hepatol Gastroenterol. 2018 Dec 26. pii: S2210-7401(18)30278-X.</i>	
CHAPTER 9	259
General discussion and summary.....	

CHAPTER 10	273
-------------------------	-----

Nederlandse samenvatting	
--------------------------------	--

Dutch summary.....	
--------------------	--

Appendix	277
-----------------------	-----

Acknowledgements	
------------------------	--

Publications.....	
-------------------	--

PhD portfolio	
---------------------	--

Curriculum Vitae.....	
-----------------------	--

CHAPTER 1

General introduction and aim of the thesis

1. Liver cancer

Liver cancer has a relatively high prevalence and in combination with a paucity of curative and therapeutic options, it remains a leading cause of mortality worldwide [1]. With increasing age incidence of liver cancer increases and thus the globally increasing life expectancy will further provoke more cases of this deadly disease [2,3]. According to the report provided by GLOBOCAN 2018, an estimated 18,1 million new cases of this cancer cases occurred in that year, while 9,6 million cancer deaths were a consequence of this disease [4]. It is thus evident that liver cancer is a major health problem warranting further research.

Liver cancer is a term that groups various subtypes of disease, including hepatocellular carcinoma (HCC; the most prevalent form), cholangiocarcinoma (CCA) and various other rare types of disease. In conjunction they constitute the fourth leading cause of cancer-related death [4]. HCC accounts for 75% - 85% of liver cancer and is often the consequence of other aetiologies that provoke chronic inflammatory liver diseases culminating in oncogenic transformation [5]. In the principle this would provide a window for prevention and early diagnosis of disease at a potentially curative stage, but unfortunately effective prevention, timely diagnosis and treatment remain challenging. Main issues in this respect are the absence of symptoms and liver cancer progresses silently without specific manifestations, whereas once disease has been established it is highly resistant to therapy [6]. Insights into the characteristics of the cells that initiate the disease, how the cells involved acquire their resistance towards therapeutic intervention, and how physiology of these cells is different from non-transformed cells may all prove necessary to devise novel avenues for the rational treatment of disease. These are all aspects of liver cancer I have aimed to explore in thesis.

2. Mitochondria and cancer metabolism

The liver is metabolically the most important organ in the body [7]. In metabolism, the mitochondria play a usually prominent role. It thus stands to reason that understanding liver pathology would require investigation of this class of organelles. Mitochondria play central roles in cell functionality, as the main source of ATP but for instance also being an important intermediate in the cellular stress response [8,9]. Being the powerhouse of the cell, mitochondria show highly dynamic adaptation in response to alterations of the

metabolic environment, as also evident by morphologic changes in mitochondria ultrastructure driven by constantly fission (division of mitochondria) and fusion (elongation of mitochondria) of these organelles [10,11]. Mitochondria are comprised of an outer membrane and an inner membrane. Mitochondrial fusion mixes not only the mitochondrial membranes but also the contents of the mitochondrial matrix [12]. The controlling step in regulation of mitochondrial fusion is the coordinated joining of both the outer and inner mitochondrial membranes of two adjacent mitochondria. Principal mediators of this process are the Mfn1 and Mfn2 mitofusins, which are GTPases localized to the outer mitochondrial membrane [13]. In addition, the inner membrane protein OPA1 is essential for mitochondrial fusion [14]. Mitochondrial fusion is critical for control of mitochondrial shape and also for maintenance of mitochondrial function [15]. Mitochondrial dysfunction with respect to fusion and fission has pleiotropic effects affecting multiple cell functions [16].

In the context of cancer, the Warburg effect describes the metabolic reprogramming in cancer cells, maybe related to altered energy demand during oncogenesis [17]. Mitochondria play a central role in the bioenergetic reprogramming of cancer cells [18]. Mitochondrial dynamics with respect to mitochondrial number and their degree of biogenesis, are often observed to be imbalanced in many cancer cells [19]. Both expression of key regulators of mitochondrial fission as well as their functionality was reported to be influenced in different cancer types including liver cancer [20,21]. Cancer cells alter mitochondrial fission to adapt to metabolic transformation to support tumor proliferation, metastasis, and drug resistance. The molecular mechanisms driving these changes remain largely obscure, although a study in triple-negative breast cancer cells indicated that mitochondrial fusion was induced by MYC signalling [22].

However, in liver cancer, the basic biology of mitochondrial fusion remains much to be explored, and the liver being the metabolic nexus of the body, these dynamics are likely to be highly relevant. In this thesis I shall thus aim to explore biology of changes in mitochondrial ultrastructure in the context of liver pathology.

The focus on mitochondrial dynamics is supported by the observation that metabolic reprogramming universally occurs in cancer. Besides mitochondrial dynamics, also the

mitochondrial electron transport chain (ETC) is involved in cancer cell bioenergetic functionality [23]. The mitochondrial electron transport chain (ETC), a group of molecules that includes complexes I-IV and the electron transporters ubiquinone and cytochrome c, is present in mitochondrial inner membrane. There are two electron flows in mitochondrial ETC to produce ATP: Complex I/III/IV, using NADH as a substrate and complex II/III/IV, with succinic acid as a substrate [24]. Due to the large electron flow, ETC is the major source of mitochondrial and also cellular reactive oxygen species (ROS). ROS perform functions in cell proliferation, hypoxia adaptation and cell fate determination, but excessive ROS can cause irreversible cell damage and even cell death [25]. The occurrence and development of cancer are closely related to imbalance in ROS production, scavenging and subcellular localization [26]. Besides, ETC itself impacts apoptosis. Therefore, the mitochondria ETC represents an intriguing therapeutic target in cancer in general and targeting the ETC may provide a valuable therapeutic option for the future treatment of liver cancer specifically [27].

A large number of agents like metformin, have been classified as mitochondria ETC-targeting agents and the clinical effects of such agent are increasingly being linked to mitochondrial dysfunctions [28]. Metformin, used for treating diabetes for decades, is currently under investigation for its potential in cancer treatment [29]. In addition to these relatively new agents, it has become clear that old pharmaceutical agents target the ETC and can be used for cancer treatment. In this thesis I therefore included investigations as to which of such agents, inhibiting the mitochondrial ETC, may be useful as novel anti-cancer drugs in liver cancer.

3. Cancer associated fibroblasts

Mitochondria involve the interior of the cell, but the exterior, interaction between the cells, in the cancer process may also yield important novel targets for therapy. In this context cancer-associated fibroblasts (CAFs) attract attention, as they are a major component of the tumor microenvironment. It is thought that they play an important role in cancer progression and drug resistance [30]. Investigation of the interaction between CAFs and the cancer cells remained challenging. Potentially, *in vitro* models that involve co-cultures of CAFs and cancer cells may be used to establish a 'more clinically relevant' tumor model and better mimic the real situation *in vivo*. Various types of co-culture systems

implementing mutual interaction between CAFs and cancer cells have been explored in previous studies and have attracted attention in the cancer research field, encouraging me to further explore possibilities here [31,32]. Among the relevant cellular interactions within the tumor microenvironment, especially the interaction between (presumptive) cancer cells and fibroblasts is known to contribute to tumor initiation, progression and metastasis in many cancer types [33-35]. These models have also been used to test anticancer agents, but progress is hampered by the reliance of cancer cell lines and/or fibroblast cell lines which has not allowed to fully capture the mechanistic details of the interactions involved. Thus, in this thesis I aimed to explore how isolated cancer-associated fibroblasts (CAFs) promote the proliferation and angiogenesis of liver tumor cells in an organoid system, that resembles tumors much better as compared to previous approaches.

4. LGR5 and Organoids

As also evident from the above, tissue and organ biology studies are very challenging in animal models and particularly in humans, and especially the abundant use of immortal transformed cell lines has proven inadequate with respect to capturing the clinical situation as encountered by oncologists and other physicians. However, progress in stem cell culture achieved in the last decade has made it possible to derive in vitro 3D tissue cultures called organoids [36]. Organoids are stem cell derived, but organ-like in many respects. Organoids system not only offer a promising platform for stem cell study but could also be used for modeling a wide range of diseases [37].

Stem cells in cancer are considered to be responsible for tumor initiation and growth, therapy resistance and tumor recurrence due to their unique feature of self-renew to give birth to offspring which remain the stemness [38]. Their physiology remains partly understood and also markers identifying these cells have not yet been conclusively defined. As in other systems, also LGR5 may provide such a marker. LGR5 is the leucine-rich-repeat-containing G-protein-coupled receptor 5 and marks group of stem cells proliferating after liver injury induced by carbon tetrachloride (CCL4) [39]. LGR5 in cancer cells marks a cancer stem cell population with high tumorigenesis, evident by their remarkable capacity to form tumors when transplanted into immunodeficient mice [40]. Cancer stem cells have been reported to be able to fuel the tumor initiation and tumor growth, which make them attractive cancer targets [38]. However, many cancer stem cell markers also present on

adult stem cells, making it difficult to target cancer cells without killing important healthy cells. Encouraging results, however, have been obtained with antibody-drug conjugates. The anti-LGR5-antibody-drug conjugates selectively target and deplete LGR5 stem cells in colon cancer and impede the growth of the primary tumor without a major effect on normal stem cell pool [41]. These observations make LGR5-targeting an attractive novel strategy for combating cancer stem cells.

Therefore, organoid system might be useful for modeling liver cancer in long-term cultures aimed at expanding cancer cells. In turn these be used to extract personalized information regarding response to therapy and to further explore cancer cell properties in general and stem cell population composed of LGR5 positive cells in particular. In the present thesis I set out to test this notion directly and addressed the idea that targeting cancer stem cells may yield improved therapy directly.

5. Inflammatory bowel disease

As mentioned earlier, liver cancer often originates in a liver that is subject to chronic inflammation [42]. Chronic inflammation is a relevant clinical problem even without the link to oncological transformation [43]. Better understanding pathogenesis and treatment of chronic inflammation is thus highly relevant. In this thesis I chose to study chronic inflammation in the context of Inflammatory bowel disease (IBD). For IBD many clinical strategies with respect to its management have already been developed and is also better accessible to experimental sampling as compared to liver inflammation which would otherwise have been more logical to study in the context of this thesis [44,45]. There are two major distinct phenotypes of IBD: Crohn's disease (CD) and ulcerative colitis (UC). CD is characterized by trans-mural and patchy inflammation that can occur in the entire GI tract but mostly involves the terminal ileum and colon, while UC is characterized by superficial inflammation involving the large bowel only. IBD is a multifactorial disease in which the onset of disease and also the progression to IBD related colorectal cancer (CRC) [46]. The Pregnane X Receptor (PXR) is a principal signal transducer in mucosal responses to xenobiotic stress, and is expressed in the intestine but also in the liver [47]. Investigations into PXR in the context of IBD may thus have value for understanding hepatic inflammation as well. In the intestine, to facilitate regenerative responses PXR impedes activity of Nuclear Factor- κ B (NF- κ B), the main transcription factor controlling

inflammatory responses [48]. Although it is well-recognized that IBD is accompanied by xenobiotic stress (an important factor in liver disease as well), the importance of PXR in limiting inflammatory responses in IBD had not been investigated and I pursued this in the present thesis. Conversely, I also investigated iatrogenic inflammation in the intestine as provoked by immunostimulation for treating cancer. This form of IBD (which may represent a manifestation of IBD separate from CD or UC) often occurs following immunostimulation to combat oncological disease and understanding the processes involved may thus also help devising better immunotherapy for liver cancer as well.

With respect to the above, checkpoint inhibition provokes an IBD-like colitis. Check point inhibition is an immunomodulatory strategy used to boost immune responses against the cancer [49]. When the immune system fails to response to disease like cancer, introduction of check point inhibitors restores T cell activation, proliferation and cytokine production. These inhibitors target various immunological pathways including cytotoxic T lymphocyte associated antigen 4 (CTLA-4) and programmed death-1 (PD-1), which in turn are linked to cell cycle arrest and apoptosis [50]. The monoclonal antibodies that constitute check point inhibitors are widely used and have become standard of care in many cancers [51-53]. Their significant clinical impact has highlighted their immune-related side effects including IBD-like colitis which in turn influences pharmacokinetics proprieties through loss of antibody in the intestine. I shall evaluate theoretically how the mitigate the effects involved in this thesis.

Aim of the thesis

In [chapter 2](#) of this thesis, I aim to provide a current view of how mitochondrial dynamics involve in liver cancer development. Mitochondria act as the hubs of bioenergetics and metabolism. The morphodynamics of mitochondria, as a consequence of mitochondrial fusion and fission processes, are closely associated with alternative mitochondrial function and are often dysregulated in cancer. It is thus interesting to investigate the mitochondrial morphodynamics and its functional consequences in human liver cancer and in this chapter I pursue this line of investigation. Exploiting the insights gained for improved clinical care is, however, still far away and thus I decided to investigate alternative approaches.

Apart from controlling mitochondrial morphology, also mitochondrial biochemistry is essential for the liver cancer process and thus may represent a *bona fide* target for the treatment of disease. In [chapter 3](#), I explore this notion and try to provide more insights into the potential use of ETC inhibitors in HCC. Metabolism of cancer cells is different from the normal hepatocyte which may allow strategies exploiting these differences in this respect. I shall conclude, however, that a large body of preclinical and clinical work is still required for this ambitious objective to become a clinical reality, prompting exploration of alternative avenues.

In [chapter 4](#), I decided to explore the interaction of the stroma with the cancer and this end I present an organoid-based co-culture model that integrates tumor organoids with CAFs. Cancer associated fibroblasts that were activated by tumor cells in co-culture conditions, demonstrated increases in α -SMA expression and migratory activity. Proliferation of tumor cells was significantly promoted in co-culture group compared to the control group. I also showed the existence of a reciprocal interaction between tumor organoids and fibroblasts, components of the surrounding microenvironment. I feel that this co-culture system could be further used to study the tumor microenvironment and for evaluation of drug screening and especially in combination with other strategies open the way for improved treatment.

A potential target for such combined strategies may be the cancer stem cell compartment. Thus prompted, in [chapter 5](#) and [chapter 6](#), I aim to investigate the interrelationship of the

proliferative LGR5 stem cells in liver cancer. In [chapter 5](#), we aim to establish malignant organoids models from mouse injury primary liver tumors and demonstrate their applications in liver cancer research in [chapter 6](#). The studies involved do not yet fully capture the influence of immune component in the liver cancer process and thus I decided to explore these aspects better in the last two chapters of this thesis.

For reasons explained above, in [chapter 7](#) I aim to investigate correlation of PXR levels with NF- κ B target gene expression in IBD. PXR is also relevant in the liver but the intestine is more easy to study and apart from that IBD is related to cholangiocarcinoma and constitutes an important subject for research *per se*. Treatment with rifampicin reduces NF- κ B activity showing that PXR activity is a rate-limiting step with respect to CD-associated NF- κ B activity. These effects were also verified in vitro. Our data suggest that the presence of PXR is the main mechanism counteracting and limiting the epithelial NF- κ B activity in patients with active IBD. Modulation of PXR activity thus holds therapeutic promise in the clinical management of CD and further studies should highlight the importance of PXR for liver inflammation as well.

In [chapter 8](#) I explore the side effects of check point inhibition. Check point inhibition is an immunomodulatory strategy used to boost immune responses against the cancer but is hampered by side effects, including IBD-like colitis. I provide a theoretical evaluation how to mitigate the effects involved in this chapter.

In conjunction, in this thesis I explore the ultrastructure of liver cancer (mitochondria biochemistry and organelle biology), the stem cell compartment leading to liver cancer development and the interactions of liver cancer cells with environment (fibroblasts and immune system). I hope to with this multifaceted approach to have contributed to better understanding and care of this deadly disease.

References

1. Gravitz, L. Liver cancer. *Nature* **2014**, *516*, S1, doi:10.1038/516S1a.
2. Petrick, J.L.; Braunlin, M.; Laversanne, M.; Valery, P.C.; Bray, F.; McGlynn, K.A. International trends in liver cancer incidence, overall and by histologic subtype, 1978-2007. *Int J Cancer* **2016**, *139*, 1534-1545, doi:10.1002/ijc.30211.
3. Wang, F.; Mubarik, S.; Zhang, Y.; Wang, L.; Wang, Y.; Yu, C.; Li, H. Long-Term Trends of Liver Cancer Incidence and Mortality in China 1990-2017: A Joinpoint and Age-Period-Cohort Analysis. *Int J Environ Res Public Health* **2019**, *16*, doi:10.3390/ijerph16162878.
4. Bray, F.; Ferlay, J.; Soerjomataram, I.; Siegel, R.L.; Torre, L.A.; Jemal, A. Global cancer statistics 2018: GLOBOCAN estimates of incidence and mortality worldwide for 36 cancers in 185 countries. *CA Cancer J Clin* **2018**, *68*, 394-424, doi:10.3322/caac.21492.
5. Gores, G.J. Decade in review-hepatocellular carcinoma: HCC-subtypes, stratification and sorafenib. *Nat Rev Gastroenterol Hepatol* **2014**, *11*, 645-647, doi:10.1038/nrgastro.2014.157.
6. Llovet, J.M.; Montal, R.; Sia, D.; Finn, R.S. Molecular therapies and precision medicine for hepatocellular carcinoma. *Nat Rev Clin Oncol* **2018**, *15*, 599-616, doi:10.1038/s41571-018-0073-4.
7. Knell, A.J. Liver function and failure: the evolution of liver physiology. *J R Coll Physicians Lond* **1980**, *14*, 205-208.
8. Nunnari, J.; Suomalainen, A. Mitochondria: in sickness and in health. *Cell* **2012**, *148*, 1145-1159, doi:10.1016/j.cell.2012.02.035.
9. Hatefi, Y. ATP synthesis in mitochondria. *Eur J Biochem* **1993**, *218*, 759-767, doi:10.1111/j.1432-1033.1993.tb18431.x.
10. Tronstad, K.J.; Nooteboom, M.; Nilsson, L.I.; Nikolaisen, J.; Sokolewicz, M.; Grefte, S.; Pettersen, I.K.; Dyrstad, S.; Hoel, F.; Willems, P.H., et al. Regulation and quantification of cellular mitochondrial morphology and content. *Curr Pharm Des* **2014**, *20*, 5634-5652, doi:10.2174/1381612820666140305230546.
11. Chan, D.C. Mitochondria: dynamic organelles in disease, aging, and development. *Cell* **2006**, *125*, 1241-1252, doi:10.1016/j.cell.2006.06.010.
12. van der Bliek, A.M.; Shen, Q.; Kawajiri, S. Mechanisms of mitochondrial fission and fusion. *Cold Spring Harb Perspect Biol* **2013**, *5*, doi:10.1101/cshperspect.a011072.
13. Chen, H.; Detmer, S.A.; Ewald, A.J.; Griffin, E.E.; Fraser, S.E.; Chan, D.C. Mitofusins Mfn1 and Mfn2 coordinately regulate mitochondrial fusion and are essential for embryonic development. *J Cell Biol* **2003**, *160*, 189-200, doi:10.1083/jcb.200211046.
14. Del Dotto, V.; Fogazza, M.; Carelli, V.; Rugolo, M.; Zanna, C. Eight human OPA1 isoforms, long and short: What are they for? *Biochim Biophys Acta Bioenerg* **2018**, *1859*, 263-269, doi:10.1016/j.bbabi.2018.01.005.
15. Chen, H.; Chomyn, A.; Chan, D.C. Disruption of fusion results in mitochondrial heterogeneity and dysfunction. *J Biol Chem* **2005**, *280*, 26185-26192, doi:10.1074/jbc.M503062200.
16. Mishra, P.; Chan, D.C. Metabolic regulation of mitochondrial dynamics. *J Cell Biol* **2016**, *212*, 379-387, doi:10.1083/jcb.201511036.
17. Schwartz, L.; Supuran, C.T.; Alfaro, K.O. The Warburg Effect and the Hallmarks of Cancer. *Anticancer Agents Med Chem* **2017**, *17*, 164-170, doi:10.2174/1871520616666161031143301.
18. Wallace, D.C. Mitochondria and cancer. *Nat Rev Cancer* **2012**, *12*, 685-698, doi:10.1038/nrc3365.
19. Senft, D.; Ronai, Z.A. Regulators of mitochondrial dynamics in cancer. *Curr Opin Cell Biol* **2016**, *39*, 43-52, doi:10.1016/j.ceb.2016.02.001.
20. Serasinghe, M.N.; Chipuk, J.E. Mitochondrial Fission in Human Diseases. *Handb Exp Pharmacol* **2017**, *240*, 159-188, doi:10.1007/164_2016_38.
21. Huang, Q.; Zhan, L.; Cao, H.; Li, J.; Lyu, Y.; Guo, X.; Zhang, J.; Ji, L.; Ren, T.; An, J., et al. Increased mitochondrial fission promotes autophagy and hepatocellular carcinoma cell survival through

- the ROS-modulated coordinated regulation of the NFKB and TP53 pathways. *Autophagy* **2016**, *12*, 999-1014, doi:10.1080/15548627.2016.1166318.
22. von Eyss, B.; Jaenicke, L.A.; Kortlever, R.M.; Royla, N.; Wiese, K.E.; Letschert, S.; McDuffus, L.A.; Sauer, M.; Rosenwald, A.; Evan, G.I., et al. A MYC-Driven Change in Mitochondrial Dynamics Limits YAP/TAZ Function in Mammary Epithelial Cells and Breast Cancer. *Cancer Cell* **2015**, *28*, 743-757, doi:10.1016/j.ccell.2015.10.013.
 23. Rich, P.R.; Marechal, A. The mitochondrial respiratory chain. *Essays Biochem* **2010**, *47*, 1-23, doi:10.1042/bse0470001.
 24. Mitchell, P. Coupling of phosphorylation to electron and hydrogen transfer by a chemi-osmotic type of mechanism. *Nature* **1961**, *191*, 144-148, doi:10.1038/191144a0.
 25. Zhao, R.Z.; Jiang, S.; Zhang, L.; Yu, Z.B. Mitochondrial electron transport chain, ROS generation and uncoupling (Review). *Int J Mol Med* **2019**, *44*, 3-15, doi:10.3892/ijmm.2019.4188.
 26. Sabharwal, S.S.; Schumacker, P.T. Mitochondrial ROS in cancer: initiators, amplifiers or an Achilles' heel? *Nat Rev Cancer* **2014**, *14*, 709-721, doi:10.1038/nrc3803.
 27. Rohlena, J.; Dong, L.F.; Ralph, S.J.; Neuzil, J. Anticancer drugs targeting the mitochondrial electron transport chain. *Antioxid Redox Signal* **2011**, *15*, 2951-2974, doi:10.1089/ars.2011.3990.
 28. Neuzil, J.; Dong, L.F.; Rohlena, J.; Truksa, J.; Ralph, S.J. Classification of mitocans, anti-cancer drugs acting on mitochondria. *Mitochondrion* **2013**, *13*, 199-208, doi:10.1016/j.mito.2012.07.112.
 29. Mallik, R.; Chowdhury, T.A. Metformin in cancer. *Diabetes Res Clin Pract* **2018**, *143*, 409-419, doi:10.1016/j.diabres.2018.05.023.
 30. Kalluri, R. The biology and function of fibroblasts in cancer. *Nat Rev Cancer* **2016**, *16*, 582-598, doi:10.1038/nrc.2016.73.
 31. Cadamuro, M.; Nardo, G.; Indraccolo, S.; Dall'olmo, L.; Sambado, L.; Moserle, L.; Franceschet, I.; Colledan, M.; Massani, M.; Stecca, T., et al. Platelet-derived growth factor-D and Rho GTPases regulate recruitment of cancer-associated fibroblasts in cholangiocarcinoma. *Hepatology* **2013**, *58*, 1042-1053, doi:10.1002/hep.26384.
 32. Koliarakis, V.; Pallangyo, C.K.; Greten, F.R.; Kollias, G. Mesenchymal Cells in Colon Cancer. *Gastroenterology* **2017**, *152*, 964-979, doi:10.1053/j.gastro.2016.11.049.
 33. Friedrich, J.; Seidel, C.; Ebner, R.; Kunz-Schughart, L.A. Spheroid-based drug screen: considerations and practical approach. *Nat Protoc* **2009**, *4*, 309-324, doi:10.1038/nprot.2008.226.
 34. Kalluri, R.; Zeisberg, M. Fibroblasts in cancer. *Nat Rev Cancer* **2006**, *6*, 392-401, doi:10.1038/nrc1877.
 35. Aref, A.R.; Huang, R.Y.; Yu, W.; Chua, K.N.; Sun, W.; Tu, T.Y.; Bai, J.; Sim, W.J.; Zervantonakis, I.K.; Thiery, J.P., et al. Screening therapeutic EMT blocking agents in a three-dimensional microenvironment. *Integr Biol (Camb)* **2013**, *5*, 381-389, doi:10.1039/c2ib20209c.
 36. Clevers, H. Modeling Development and Disease with Organoids. *Cell* **2016**, *165*, 1586-1597, doi:10.1016/j.cell.2016.05.082.
 37. Dutta, D.; Heo, I.; Clevers, H. Disease Modeling in Stem Cell-Derived 3D Organoid Systems. *Trends Mol Med* **2017**, *23*, 393-410, doi:10.1016/j.molmed.2017.02.007.
 38. Greten, F.R. Cancer: Tumour stem-cell surprises. *Nature* **2017**, *543*, 626-627, doi:10.1038/543626a.
 39. Cao, W.; Chen, K.; Bolkestein, M.; Yin, Y.; Versteegen, M.M.A.; Bijvelds, M.J.C.; Wang, W.; Tuysuz, N.; Ten Berge, D.; Sprengers, D., et al. Dynamics of Proliferative and Quiescent Stem Cells in Liver Homeostasis and Injury. *Gastroenterology* **2017**, *153*, 1133-1147, doi:10.1053/j.gastro.2017.07.006.
 40. de Sousa e Melo, F.; Kurtova, A.V.; Harnoss, J.M.; Kljavin, N.; Hoeck, J.D.; Hung, J.; Anderson, J.E.; Storm, E.E.; Modrusan, Z.; Koepfen, H., et al. A distinct role for Lgr5(+) stem cells in primary and metastatic colon cancer. *Nature* **2017**, *543*, 676-680, doi:10.1038/nature21713.

41. Junttila, M.R.; Mao, W.; Wang, X.; Wang, B.E.; Pham, T.; Flygare, J.; Yu, S.F.; Yee, S.; Goldenberg, D.; Fields, C., et al. Targeting LGR5+ cells with an antibody-drug conjugate for the treatment of colon cancer. *Sci Transl Med* **2015**, *7*, 314ra186, doi:10.1126/scitranslmed.aac7433.
42. Ray, K. Liver cancer: A complex interplay between inflammation and immunity in liver cancer. *Nat Rev Gastroenterol Hepatol* **2018**, *15*, 3, doi:10.1038/nrgastro.2017.165.
43. Medzhitov, R. Inflammation 2010: new adventures of an old flame. *Cell* **2010**, *140*, 771-776, doi:10.1016/j.cell.2010.03.006.
44. Kelly, P.N. A way to switch off IBD. *Science* **2017**, *356*, 497, doi:10.1126/science.356.6337.497-d.
45. Ray, K. IBD: The changing epidemiology of IBD. *Nat Rev Gastroenterol Hepatol* **2017**, *14*, 690, doi:10.1038/nrgastro.2017.159.
46. Choi, C.R.; Bakir, I.A.; Hart, A.L.; Graham, T.A. Clonal evolution of colorectal cancer in IBD. *Nat Rev Gastroenterol Hepatol* **2017**, *14*, 218-229, doi:10.1038/nrgastro.2017.1.
47. Azuma, K.; Casey, S.C.; Urano, T.; Horie-Inoue, K.; Ouchi, Y.; Blumberg, B.; Inoue, S. Pregnane X receptor knockout mice display aging-dependent wearing of articular cartilage. *PLoS One* **2015**, *10*, e0119177, doi:10.1371/journal.pone.0119177.
48. Zhou, C.; Tabb, M.M.; Nelson, E.L.; Grun, F.; Verma, S.; Sadatrafiei, A.; Lin, M.; Mallick, S.; Forman, B.M.; Thummel, K.E., et al. Mutual repression between steroid and xenobiotic receptor and NF-kappaB signaling pathways links xenobiotic metabolism and inflammation. *J Clin Invest* **2006**, *116*, 2280-2289, doi:10.1172/JCI26283.
49. Wolchok, J.D. PD-1 Blockers. *Cell* **2015**, *162*, 937, doi:10.1016/j.cell.2015.07.045.
50. Farkona, S.; Diamandis, E.P.; Blasutig, I.M. Cancer immunotherapy: the beginning of the end of cancer? *BMC Med* **2016**, *14*, 73, doi:10.1186/s12916-016-0623-5.
51. De Felice, F.; Marchetti, C.; Palaia, I.; Ostuni, R.; Muzii, L.; Tombolini, V.; Benedetti Panici, P. Immune check-point in cervical cancer. *Crit Rev Oncol Hematol* **2018**, *129*, 40-43, doi:10.1016/j.critrevonc.2018.06.006.
52. Hodi, F.S.; Chiarion-Sileni, V.; Gonzalez, R.; Grob, J.J.; Rutkowski, P.; Cowey, C.L.; Lao, C.D.; Schadendorf, D.; Wagstaff, J.; Dummer, R., et al. Nivolumab plus ipilimumab or nivolumab alone versus ipilimumab alone in advanced melanoma (CheckMate 067): 4-year outcomes of a multicentre, randomised, phase 3 trial. *Lancet Oncol* **2018**, *19*, 1480-1492, doi:10.1016/S1470-2045(18)30700-9.
53. Ferris, R.L.; Blumenschein, G., Jr.; Fayette, J.; Guigay, J.; Colevas, A.D.; Licitra, L.; Harrington, K.; Kasper, S.; Vokes, E.E.; Even, C., et al. Nivolumab for Recurrent Squamous-Cell Carcinoma of the Head and Neck. *N Engl J Med* **2016**, *375*, 1856-1867, doi:10.1056/NEJMoa1602252.

CHAPTER 2

Mitochondrial Fusion Via OPA1 and MFN1 Supports Liver Tumor Cell Metabolism and Growth

Meng Li¹, Ling Wang¹, Yijin Wang², Shaoshi Zhang¹, Guoying Zhou¹, Ruby Lieshout³, Buyun Ma¹, Jiaye Liu¹, Changbo Qu¹, Monique M. A. Verstegen³, Dave Sprengers¹, Jaap Kwekkeboom¹, Luc J. W. van der Laan³, Wanlu Cao¹, Maikel P. Peppelenbosch¹ and Qiuwei Pan^{1*}

¹ Department of Gastroenterology and Hepatology, Erasmus MC-University Medical Center, Rotterdam, The Netherlands.

² Department of Pathology and Hepatology, Beijing 302 Hospital, Beijing, China.

³ Department of Surgery, Erasmus MC-University Medical Center, Rotterdam, The Netherlands.

Cells. 2020 Jan 4;9(1).

Abstract

Metabolic reprogramming universally occurs in cancer. Mitochondria act as the hubs of bioenergetics and metabolism. The morphodynamics of mitochondria, comprised of fusion and fission processes, are closely associated with mitochondrial functions and are often dysregulated in cancer. In this study, we aim to investigate the mitochondrial morphodynamics and its functional consequences in human liver cancer. We observed excessive activation of mitochondrial fusion in tumor tissues from hepatocellular carcinoma (HCC) patients and in vitro cultured tumor organoids from cholangiocarcinoma (CCA). The knockdown of the fusion regulator genes, OPA1 (Optic atrophy 1) or MFN1 (Mitofusin 1), inhibited the fusion process in HCC cell lines and CCA tumor organoids. This resulted in inhibition of cell growth in vitro and tumor formation in vivo, after tumor cell engraftment in mice. This inhibitory effect is associated with the induction of cell apoptosis, but not related to cell cycle arrest. Genome-wide transcriptomic profiling revealed that the inhibition of fusion predominately affected cellular metabolic pathways. This was further confirmed by the blocking of mitochondrial fusion which attenuated oxygen consumption and cellular ATP production of tumor cells. In conclusion, increased mitochondrial fusion in liver cancer alters metabolism and fuels tumor cell growth.

Keywords: mitochondrial dynamics; liver cancer; OPA1; MFN1

Introduction

Primary liver cancer, including hepatocellular carcinoma (HCC) and intrahepatic cholangiocarcinoma (CCA), is one of the leading causes of cancer related death. This is mainly attributed to the global prevalence of hepatitis virus infections and the rising prevalence of non-alcoholic fatty liver disease [1]. Liver cancer is well-known for its resistance to classical chemotherapy, and therefore very limited therapeutic options are available [2]. Over the past decade, the research of cancer metabolism has largely extended our understanding of cancer biology and provided opportunities for therapeutic development [3].

Mitochondria, as double-membrane-bound organelles, are the cellular powerhouses in almost all eukaryotic organisms [4]. Metabolic reprogramming, a hallmark of cancer, is critical for the tumor initiation and development [5]. The Warburg hypothesis proposed that metabolism was altered due to mitochondrial defects, leading to an increase in glycolysis [3]. In addition to mitochondrial energetic metabolism transitions, the morphology of mitochondria is also dynamic in cancer [6,7]. Mitochondrial morphology is under control of the mitochondrial dynamics network, which continuously exists in cells and is comprised of fusion and fission processes [8]. Mitochondrial fusion, facilitated by Optic atrophy 1 (OPA1) and Mitofusin 1/2 (MFN1/2), is reported to be able to attenuate damage to mitochondrial DNA (mtDNA), proteins and lipids by mixing and dilution of mitochondrial matrix and membranes [9]. Therefore, larger and more efficient mitochondria may prevent excessive damage accumulation and better serve the metabolic needs of proliferating cells [10].

As the heart of the mitochondrial fusion process, OPA1 and MFN1/2 are respectively responsible for inner membrane and outer membrane fusion [11]. OPA1 plays a key role in mitochondrial cristae structure maintenance while cristae, invaginated by the inner membrane, are required for cellular adaptation to metabolic demand [12]. OPA1 deficiency in mice is lethal [13] and tissue specific depletions of OPA1 have demonstrated that mitochondrial fusion is vital for cellular metabolism [14]. OPA1 downregulation has also been reported to sensitize HCC cells to sorafenib treatment [15]. However, the detailed role of mitochondrial fusion in liver cancer remains largely elusive. In this study, we have investigated mitochondrial morphodynamics and its functional relevance in liver cancer.

Materials and Methods

1. Cells and Organoids Culture

Human HCC cell lines, Huh7 and SNU449, and human embryonic kidney epithelial cell line HEK 293T cells were maintained in Dulbecco's modified Eagle's medium (Lonza, Basel, Basel-Stadt, Switzerland) supplemented with 10% fetal bovine serum (Sigma-Aldrich, St. Louis, Missouri, USA) and 1% streptomycin/penicillin (Gibco, Thermo Fisher Scientific, Waltham, Massachusetts, USA). The obtained mycoplasma-free human cell lines were commercially checked monthly by GATC Biotech (GATC Biotech, Konstanz, Baden-Württemberg, Germany) and their identity verified by the molecular pathology department of the Erasmus MC as described previously [16]. Healthy liver, adjacent liver, and CCA organoids were cultured as previously described [17-19]. Informed consent was obtained from all patients and the use of patient materials was approved by the medical ethical committee of Erasmus Medical Center, Rotterdam (MEC-2014-060 and MEC-2013-143).

2. Gene Knockdown by Lentiviral Vectors

For gene knockdown, pLKO.1-based vectors targeting OPA1 and MFN1 and scramble were kindly provided by the Biomix Center in Erasmus Medical Center. Lentiviral-shRNA vectors packaging and infection were performed as described before [20]. Subsequently, Huh7 and SNU449 cells were selected by 3 µg/mL puromycin (Sigma-Aldrich, St. Louis, Missouri, USA) to generate stable knockdown cells. After selection, knockdown cells were cultured without puromycin for at least one month before use in further experiments. The generation of knockdown organoids was performed as described before [21].

3. Immunofluorescence of Live Cells and Frozen Tissues

We used tetramethylrhodamine (TMRM) to quantify the mitochondrial morphology of live cells, in a manner that is dependent on the maintenance of the mitochondrial membrane potential [22]. TMRM and Hoechst 33342 were purchased from Thermo Fisher.

Frozen tissues were sectioned at 8 µm and fixed in 4% paraformaldehyde. The stainings of the Voltage-dependent anion-selective channel 1 (VDAC1) and DAPI were performed as previously described [23]. Nonspecific staining was blocked by phosphate-buffered saline (PBS) supplemented with 5% serum, 1% bovine serum albumin and 0.2% Triton X-100 for 1 h. Samples were incubated with primary antibody VDAC1 (ab15895, Abcam, Cambridge, United Kingdom) diluted at 1: 200 at 4 °C overnight and subsequently with goat anti-rabbit secondary antibody conjugated with Alexa Fluor 488 (BD biosciences, Franklin Lakes, New Jersey, USA) diluted at 1:1000 for 2 h at room temperature.

All images were acquired with a Zeiss LSM510META confocal microscope and quantified with ImageJ software (version 1.51, National Institute of Mental Health, Bethesda, Maryland, USA).

4. Colony Formation Assay and Alamar Blue Assay

Cells were seeded in 6-well plates (400 cells/well for Huh7 and 800 cells/well for SNU449), and cultured for 10 days. Formed colonies were washed with PBS and fixed by 3.7% formaldehyde for 10 min. Colonies were counterstained with Giemsa and their numbers were counted.

Organoid proliferation was evaluated for 3 days with an Alamar Blue assay according to the manufacturer's manual (Life Technologies, Thermo Fisher Scientific, Waltham, Massachusetts, USA).

5. Analysis of Cell Cycle and Cell Apoptosis

Cells were trypsinized and washed with PBS. After being fixed in cold 70% ethanol overnight at 4 °C, the cells were washed with PBS and incubated with 20 µg/mL RNase at 37 °C for 30 min. Subsequently, the samples with 50 µg/mL propidium iodide (PI) at 4 °C for 30 min, were analyzed by FACS for cell cycle.

Cell apoptosis analysis was performed by staining cells with Annexin V-FITC and PI as described before [24].

6. Xenograft Mouse Model in Nude Mice

The xenograft tumor model was established in 4–6 weeks female nude mice breeding in SPF environment. Mice were injected subcutaneously with knockdown cells and corresponding control cells into the lower left or right flank of the same mice ($5 \times 10^6/200 \mu\text{L}$ cells per mouse; $n = 6$ mice per group), 1: 1 mixed with matrigel. After the cell engrafting, tumor formation was monitored and measured on the first, seventeenth, nineteenth, twenty fourth and twenty seventh day. Then mice were sacrificed, and tumors were harvested and weighted. All animal experiments were approved by the Committee on the Ethics of Animal Experiments of the Erasmus Medical Center.

7. RNA Isolation and Sequencing

Cell lines and organoids were isolated according to manufacturer's guidelines with total RNA isolation protocol (Invitrogen, Carlsbad, California, USA). The quantity of total RNA was measured by a NanoDrop 2000 and the quality of total RNA was measured by Bioanalyzer RNA 6000 Picochip as a quality-control step. RNA sequencing was performed by Novogene with paired-end 150 bp (PE 150) sequencing strategy.

8. Real-Time PCR

Expression of mRNA in different samples were measured according to the manufacturer's instructions [25]. GAPDH was considered as reference gene for normalization. The forward and reverse primers for OPA1 were as follows: TCAAGAAAACTTGATGCTTTCA and GCAGAGCTGATTATGAGTACGATT. The forward and reverse primers for MFN1 were as follows: TGTTTTGGTCGCAAACTCTG and CTGTCTGCGTACGTCTTCCA.

9. Oxygen Consumption and ATP Production Measurement

The oxygraph-2k (O2k, OROBOROS instruments) was used for respiration measurements. Hepes/Tris buffer (adjusted to pH 7.4 with Tris) containing 4.2 mM KCl, 132 mM NaCl, 10 mM Hepes, 1.2 mM MgCl₂ and 1 mM CaCl₂, was used to incubate intact cells. The experiments were performed at 37 °C.

An ATP determination kit (Invitrogen, Carlsbad, California, USA) was used for ATP measurement of cells. The final results were normalized by cell numbers or total protein concentration.

10. Measurement of Reactive Oxygen Species (ROS) Production

Cellular ROS Assay Kit (ab186027, Abcam) was used for ROS production measurements. The measurements were performed according to the manufacturer's instructions. Cells were plated overnight in growth medium and harvested at 10^4 – 4×10^4 cells/100 µL per well. Further, 100 µL/well of ROS Red Working Solution was added into the cell plate and incubated at room temperature or in a 37 °C/5% CO₂ incubator for one hour. Fluorescence activity was measured at Ex/Em = 520/605 nm (cut off 590 nm) with bottom read mode. The final results were normalized by cell numbers or total protein concentration.

11. Glucose Consumption Measurement

Glucose Assay Kit (ab65333, Abcam) was used for glucose level measurements. The measurements were performed according to the manufacturer's instructions. Cells were plated overnight in growth medium and were harvested at 2×10^6 cells/100 µL per well. Further, 100 µL/well of assay buffer was added into the cell plate. Cells were homogenized quickly by pipetting up and down a few times before being centrifuged for 2 min at 4 °C at top speed in a cold microcentrifuge to remove any insoluble material. Supernatant was collected and transferred to a clean tube. These enzymes were removed from sample by using Deproteinizing Sample Preparation Kit - TCA (ab204708, Abcam). Subsequently, 50 µL of reaction mix was prepared for each reaction. Cell plate was incubated at 37 °C/5% CO₂ incubator for half an hour. The value was measured on a microplate reader at OD 570 nm. The final results were normalized by cell numbers or total protein concentration.

12. Lactate Measurement

A Lactate Assay Kit (ab65331, Abcam) was used for lactate level measurements. The measurements were performed according to the manufacturer's instructions. The final results were normalized by cell numbers or total protein concentration.

13. Statistical Analysis

All data are presented as mean ± SEM. Statistical comparisons were performed with paired t test for paired samples or Mann-Whitney test for non-paired independent samples. For all experiments, a p-value less than 0.05 was considered as significant.

Results

1. Activation of Mitochondrial Fusion in Liver Cancer

Initially, we employed paired frozen tissues from thirteen HCC patients and one CCA patient by staining mitochondria with VDAC1, one of the most abundant proteins in the outer mitochondrial membrane. Details of the patient information were shown in Table 1. Of each patient, we included tumor tissue and adjacent tissue (Figure 1A). Immunofluorescence analysis showed that cells in tumor tissue and cells in adjacent tissue contained different mitochondrial morphology. In 10 out of 14 paired tissues mitochondrial volume per cell was larger in tumor tissue compared to adjacent tissue (Figure 1B). Interestingly, in all paired tissues tumor cells possessed stronger VDAC1 fluorescence intensity and integrated density (Figure 1C and 1D, respectively). We further examined mitochondrial morphology in paired HCC and adjacent tissue derived from an HBV positive patient by electron microscopy. Consistently, mitochondria size is larger in tumor tissue (Supplementary Figure S1).

To investigate the clinical and functional relevance of mitochondrial morphodynamics in liver cancer, we examined key fusion proteins involved in mitochondrial dynamics. A previous study revealed that MFN1 mRNA levels are slightly elevated in liver while MFN2 is expressed at low levels in liver in contrast with heart and muscle [26]. Thus, our study mainly focused on OPA1 and MFN1. Analysis of the Oncomine online database, containing five cohorts of HCC patients, revealed that both OPA1 and MFN1 are more highly expressed in HCC tumor tissue compared to liver tissue in the majority of cohorts (Figure 1E and 1F).

We concluded that mitochondria in tumor and tumor surrounding tissues possessed different morphology and structural integrity.

2. Mitochondrial Fusion Sustains CCA Organoid Growth

We also observed a similar phenomenon in patient-derived CCA organoids (Figure 2A). One pair (up row) included normal organoids derived from the adjacent tissue and tumor organoids derived from the tumor tissue of the same patient. Another pair (lower row) included normal organoids derived from the donor liver and tumor organoids derived from another patient. Mitochondria in normal organoids are more sphere- or ovoid- like compared with the long filaments of mitochondria in tumor organoids. Further, 83.5% of organoids in tumor cells possessed elongated mitochondria, which is more than that in normal organoids (Figure 2B).

We consequently performed gene knockdown of OPA1 and MFN1 respectively in human CCA organoids and confirmed at both mRNA (Figure 2C) and protein levels (Supplementary Figure S2A). Consistently, this resulted in mitochondrial morphology transition (Figure 2D) and reduced mitochondrial length (Figure 2E). This functionally inhibited CCA organoid growth (Figure 2F).

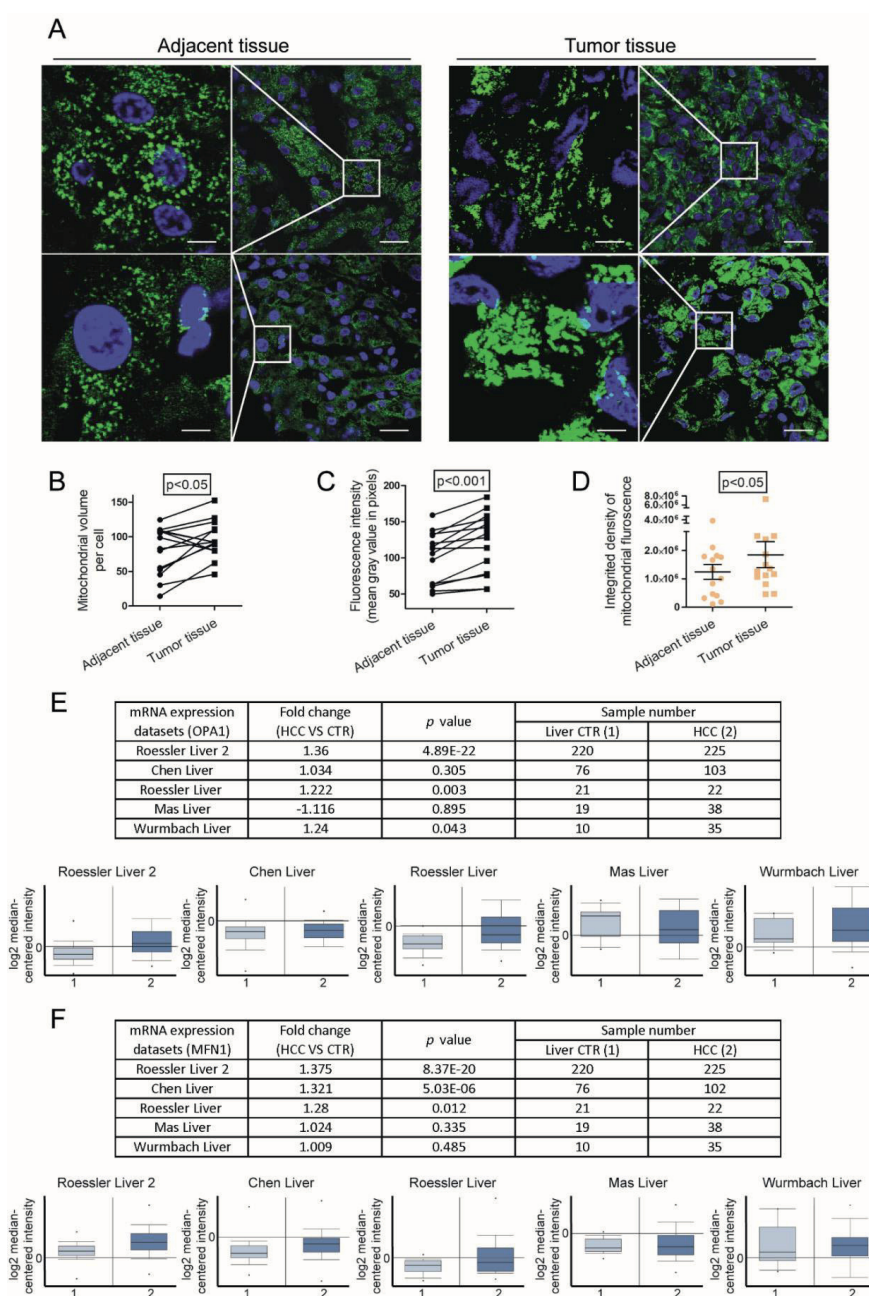


Figure 1. Activation of mitochondrial fusion in liver cancer. **(A)** Representative confocal images of mitochondria with VDAC1 staining in cryosection from paired tumor or adjacent liver tissues of two HCC patients. The white boxed regions were further magnified in the expanded images (left row). Scale bar = 5 μ m (left row). Scale bar = 20 μ m (right row). **(B)** Images of paired tissue were analyzed by ImageJ software. Mitochondrial volume per cell was determined by fluorescence area in pixels (Adjacent vs. Tumor: 80.29 ± 9.285 vs. 96.29 ± 7.24 ; $n = 14$ patients). **(C)** Fluorescent intensity represented the mean gray value of different images (Adjacent vs. Tumor: 100.3 ± 9.555 vs. 120.9 ± 11.18 ; $n = 14$ patients). **(D)** Integrated density was calculated by the product of area and mean gray value (Adjacent vs. Tumor: $1.245e+006 \pm 260.203$ vs. $1.848e+006 \pm 459.958$;

n = 14 patients). Histograms show means \pm SEM with p value derived by two tailed paired Student's *t* test. (E) The Oncomine microarray database (<https://www.oncomine.org>) was searched to analyze mRNA expression of OPA1 in HCC patients. In total, five cohorts of 423 HCC tumor tissues compared with 346 paired tumor-free tissues were identified. The expression level of OPA1 mRNA was demonstrated in five cohorts. (F) The Oncomine microarray database (<https://www.oncomine.org>) was searched to analyse mRNA expression of MFN1 in HCC patients. In total, five cohorts of 422 HCC tumor tissues compared with 346 paired tumor-free tissues were identified. The expression level of MFN1 mRNA was demonstrated in five cohorts. Histograms are mean \pm SEM, with p values by Student's *t* test.

Table 1. Patient Characteristics.

Characteristics	HCC Patient (n = 13)	CCA Patient (n = 1)
Age at surgery (years)		
Mean \pm SD	64.9 \pm 13.4	60
Median (range)	70 (37–79)	-
sex (%)		
Male	8 (62)	1 (100)
Female	5 (38)	-
Etiology (%)		
Unknown liver disease	6 (46)	-
Alcohol abuse	1 (8)	1 (100)
Chronic HBV	3 (23)	-
Hemochromatosis	1 (8)	-
Hemochromatosis and alcohol abuse	2 (15)	-
Cirrhosis (%)		
Yes	2 (15)	-
No	11 (85)	1 (100)
Tumor differentiation (%)		
Well	1 (8)	-
Moderate	9 (69)	-
Poor	2 (15)	-
Unknown	1 (8)	1 (100)
Vascular invasion (%)		
Micro-invasion	6 (46)	-
Vaso-invasion	2 (15)	-
Severe vaso-invasion	2 (15)	1 (100)
No	3 (23)	-
AFP (pre-operative) (μg/L)		
Mean \pm SD	4076.2 \pm 12607.2	3.8
Median (range)	16 (3-45803)	-

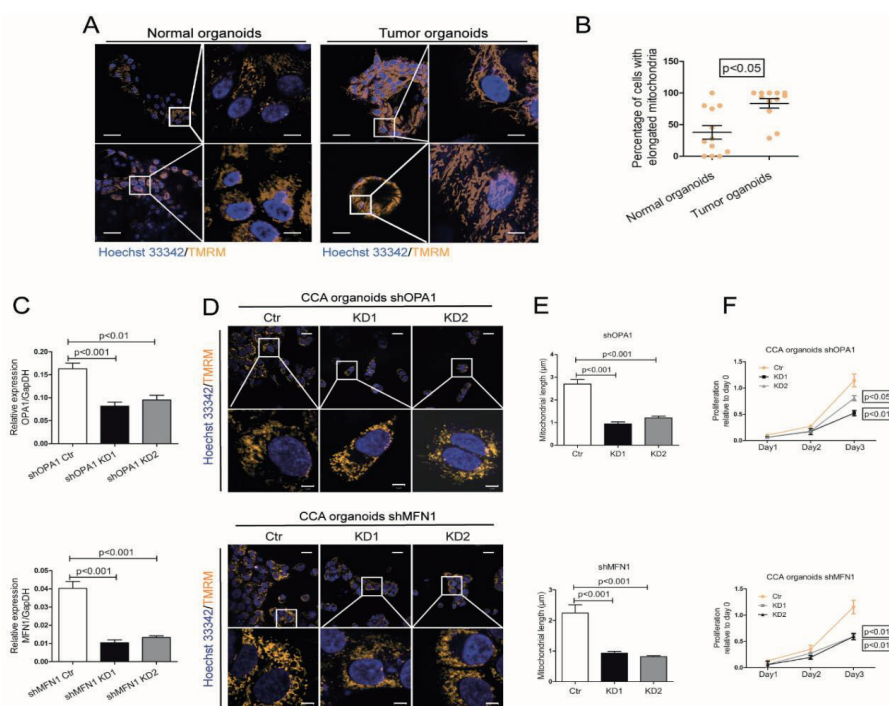


Figure 2. Silencing of OPA1 or MFN1 inhibits mitochondrial fusion and the growth of CCA organoids. **(A)** Representative confocal images of mitochondria with TMRM staining in in vitro cultured organoids from two tumor tissue, one matched adjacent liver tissue and one donor liver tissue. The white boxed regions were further magnified in the expanded images (right row). Scale bar = 50 μ m (left row). Scale bar = 10 μ m (right row). **(B)** Images of tumor and non-tumor “normal” liver organoids were quantified (Normal vs. Tumor: 37.93 ± 10.62 vs. 83.5 ± 7.34 ; $n = 6$ images/sample). **(C)** CCA organoids were transduced with mock lentivirus (Ctr) or shOPA1/shMFN1 lentivirus (KD1 and KD2) respectively. Gene knockdown efficiency of OPA1 was quantified by Real-time PCR ($n = 6$). **(D)** Representative live cell confocal images of mitochondria with TMRM staining in CCA organoids with OPA1/MFN1 knockdown. The white boxed regions were further magnified in the expanded images (lower row). Scale bar = 20 μ m (upper row). Scale bar = 5 μ m (lower row). **(E)** Quantified measurements of mitochondrial length in control and KD cells of CCA organoids ($n = 3$ images/sample). **(F)** The Alamar Blue fluorescence level of CCA organoids was measured at Day 0/1/2/3 for cell viability and data at day 0 was set as control of each group ($n = 3$). Histograms show means \pm SEM with p value derived by the Mann Whitney test.

3. Dysfunction of Mitochondrial Fusion Inhibits Liver Cancer Cell Growth in Vitro and in Vivo

To further investigate the underlying mechanism, we stably knocked down gene OPA1 or MFN1 by lentiviral transfection in two HCC cell lines Huh7 and SNU449. The successful knockdown was confirmed at mRNA (Figure 3A) and protein levels (Figure S2B). The down-regulation of OPA1 or MFN1 induced mitochondrial fragmentation and a decrease of mitochondrial length, indicating the inhibition of mitochondrial fusion (Figure 3B and Figure 3C). This functionally resulted in dramatic inhibition of ability of single cell colony formation (Figure 3D). The colony units of Huh7 shMFN1 dropped from average 71 per well to 20 and 9, and of Huh7 shOPA1 dropped from 31 to none. Similar results were observed in SNU449 cells.

Upon subcutaneous engraftment in immunodeficient nude mice, we demonstrated that knockdown of OPA1 or MFN1 dramatically inhibited tumor formation and growth of HCC cells in vivo (Figure 4A and 4B).

We found that knockdown of mitochondrial fusion regulators has no effect on cell cycle (Supplementary Figure S3) but triggered the induction of cell apoptosis. This effect was much stronger in Huh7 shOPA1 cells compared to Huh7 shMFN1 cells. The percentage of apoptotic cells increased from 4.44% to 24.45% or 13.84% with the decrease of OPA1 gene expression, while the percentages of apoptotic cells increased from 3.17% to 4.79% or 4.64% with the decrease of MFN1 gene expression (Figure 5A and Figure 5B). The apoptotic cells in SNU449 also showed the same trend with mitochondrial fusion dysfunction (Figure 5C and 5D). Interestingly, OPA1/MFN1 knockdown increased the ratio of Bax/Bcl-2 expression at mRNA levels in SNU449 and CCA organoids. This appears consistent with the observed increase of apoptosis in OPA1/MFN1 knockdown cells (Supplementary Figure S4). Taken together, these data suggest that dysfunction of mitochondrial fusion induces tumor cell apoptosis.

4. Mitochondrial Fusion Fuels Cellular Metabolism of Liver Cancer Cells

To obtain insight in the potential mechanisms that mediate acceleration of tumor cell growth by mitochondrial fusion in liver cancer, we performed genome-wide transcriptomic analysis by RNA sequencing in OPA1 knockdown Huh7. We identified 552 differentially expressed genes between the control cells and the shOPA1 cells ($p < 0.05$, $\log_2\text{Fc} > 1$), consisting of 332 genes downregulated and 220 genes upregulated (Figure 6A). KEGG pathway enrichment analysis revealed the alteration of several pathways, but most prominently of the metabolism pathway (Figure 6B), involving 33 differentially expressed genes (Figure 6C).

The dysfunction of mitochondrial fusion by OPA1/MFN1 knockdown was also found to be correlated to increased ROS levels in SNU449 and CCA organoids (Figure 6D and Figure 6E). Furthermore, we performed the glucose consumption and lactate secretion measurement in SNU449 and CCA organoids (Figure S5 and Figure S6). Glucose consumption was down-regulated when mitochondrial fusion was inhibited. The lactate level was also reduced when knocking down OPA1/MFN1, which indicated that glycolysis was not stimulated upon mitochondrial inhibition.

To provide further evidence for dysregulation of mitochondrial metabolism in cell lines, the mitochondrial metabolism of oxygen consumption and ATP production were measured in Huh7 (Figure 7A and Figure 7B). The oxygen consumption rate (OCR) dropped from 37.68 pmol/s/ 10^6 cells to 26.78 pmol/s/ 10^6 cells and 21.63 pmol/s/ 10^6 cells in Huh7 shOPA1 cells, while ATP content dropped to 79.27% and 76.22% compared with control group. Similar results were observed in Huh7 shMFN1 cells. Alterations of mitochondrial metabolism were also observed in CCA organoids, including a decrease in oxygen consumption (Figure 7C) and a reduction in ATP production reduction (Figure 7D). Therefore, enhanced mitochondrial fusion fuels cellular metabolism to functionally support liver cancer.

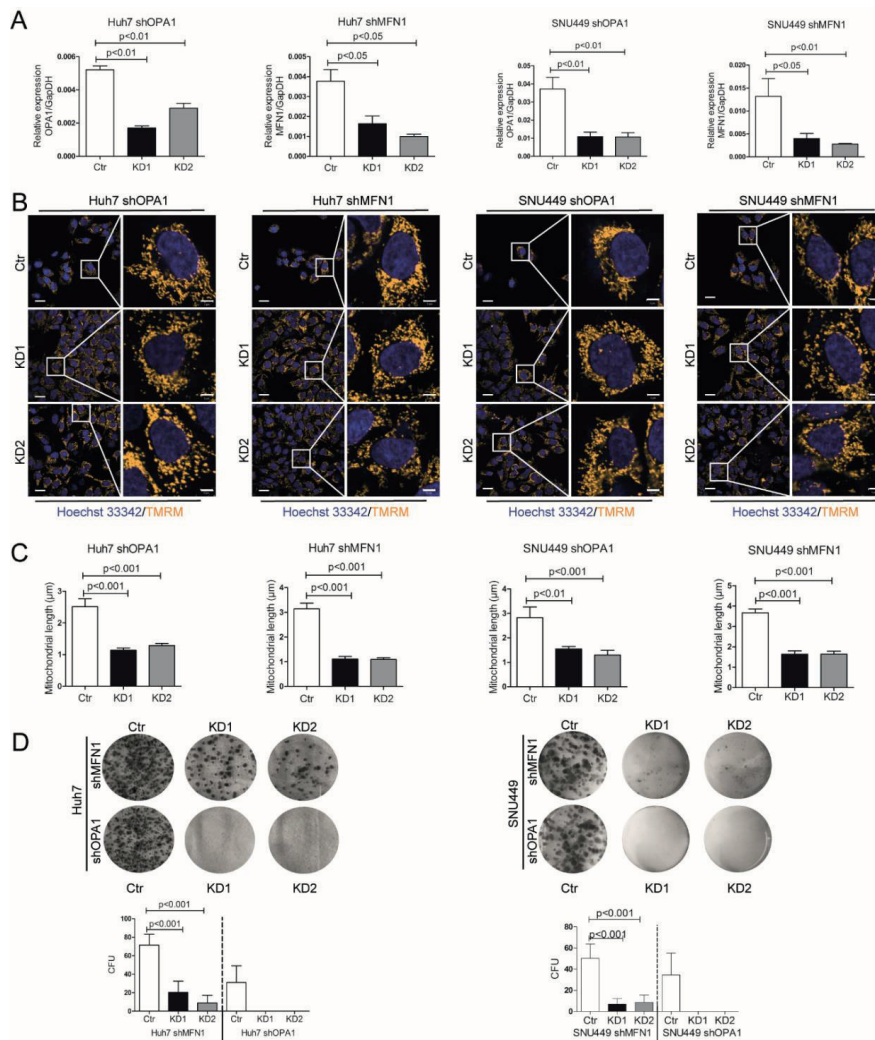


Figure 3. Knockdown of OPA1 or MFN1 inhibits mitochondrial fusion. Inhibition of mitochondrial fusion attenuates cancer cell growth in vitro. **(A)** Real-time PCR analysis of OPA1 expression in Huh7/SNU449 shOPA1 cells and MFN1 expression in Huh7/SNU449 shMFN1 cells. Huh7/SNU449 shOPA1 cells were transfected with mock lentivirus (Ctr) and shOPA1 lentivirus (KD1 and KD2) respectively. Huh7/SNU449 shMFN1 cells were transfected with mock lentivirus (Ctr) and shMFN1 lentivirus (KD1 and KD2) respectively. Gene knockdown efficiency was quantified (n = 6). **(B)** Representative confocal images of mitochondria with TMRM staining in live cells with OPA1 and MFN1 knockdown respectively. The white boxed regions were further magnified in the expanded images (right row). Scale bar = 20 μm (left row). Scale bar = 5 μm (right row). **(C)** Quantified measurements of mitochondrial length in control and KD cells (n = 3 images/sample). **(D)** Representative images of colony formation assay of Huh7/SNU449 shOPA1 cells and shMFN1 cells. Cells were fixed and stained by Giemsa (n = 9). The number of colony forming units (CFU) was quantified by ImageJ software. Histograms show means ± SEM with p value by Mann Whitney test.

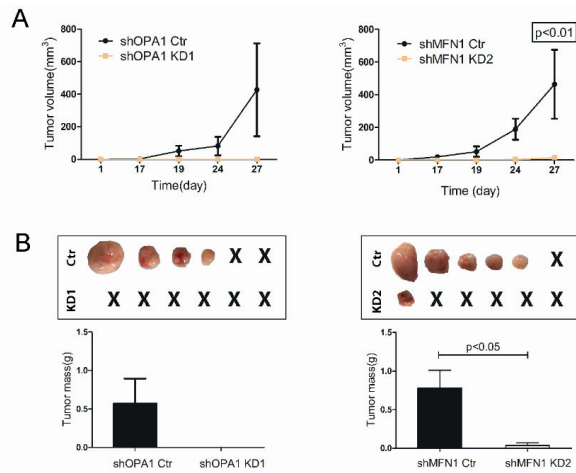


Figure 4. Mitochondrial fusion dysfunction inhibited tumor formation and growth in vivo. **(A)** Huh7 shOPA1 and control cells were injected subcutaneously into nude mice. Tumor size was measured at post-injection days 1/17/19/24/27 ($n = 4$ pairs). Huh7 shMFN1 and control cells were injected and tumor size was measured in the same way ($n = 5$ pairs). **(B)** Tumors were harvested from nude mice at day 27 and weighed. Histograms show means \pm SEM with p value derived by the Mann Whitney test.

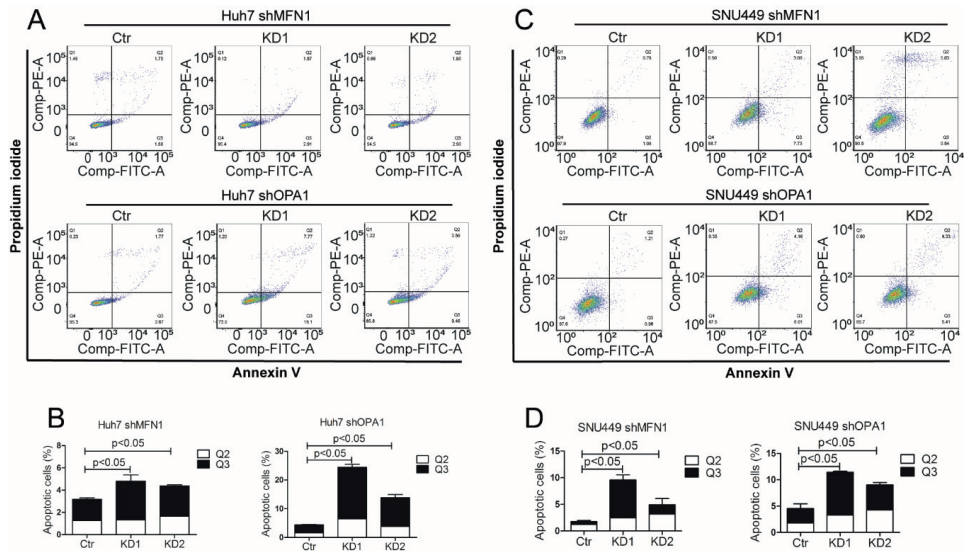


Figure 5. Mitochondrial fusion dysfunction inhibited tumor growth through cell apoptosis induction **(A–B)** Apoptotic cells were quantified by flow cytometry using Annexin V and propidium iodide co-staining in Huh7 shOPA1 and Huh7 shMFN1 cells ($n = 3$). **(C–D)** Apoptotic cells were quantified by flow cytometry using Annexin V and propidium iodide co-staining in SNU449 shOPA1 and SNU449 shMFN1 cells ($n = 3$). Histograms show means \pm SEM with p value derived by the Mann Whitney test.

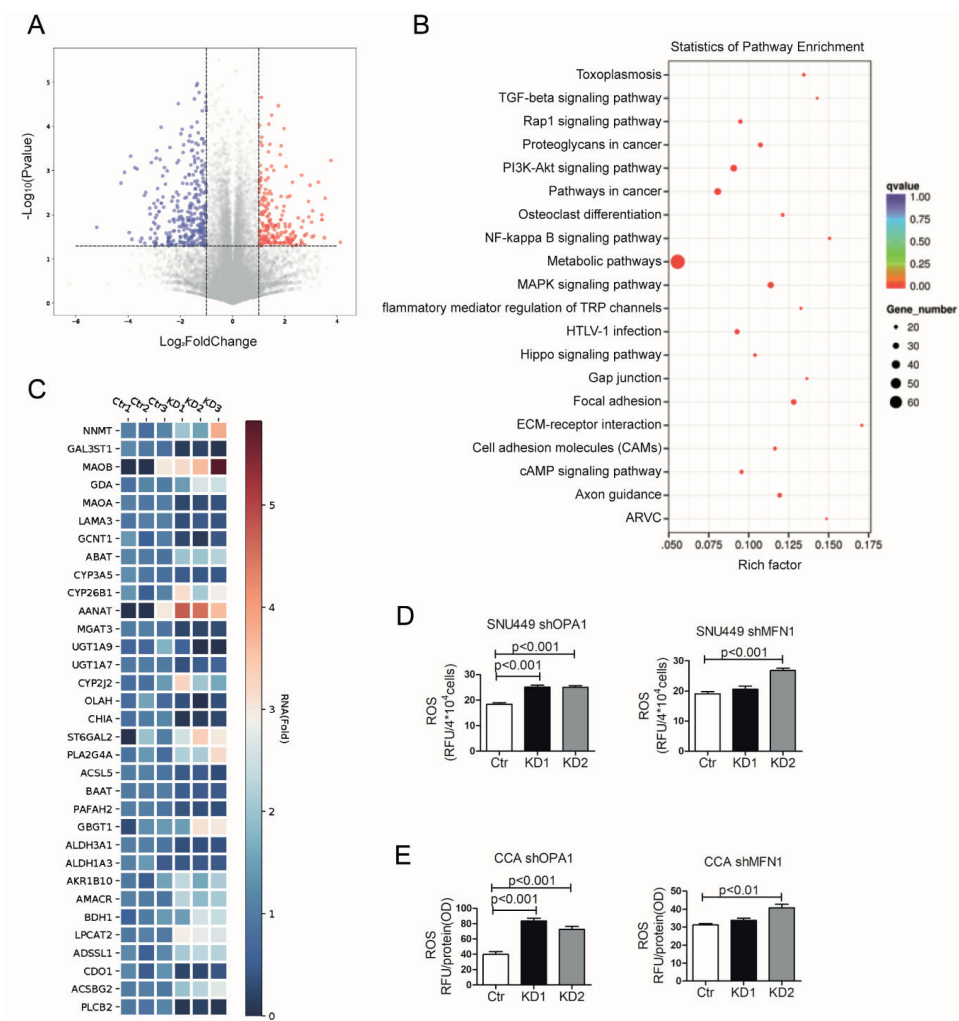


Figure 6. Inhibition of mitochondrial fusion affects cellular metabolism. **(A)** Volcano plot of statistical significance ($p < 0.05$) against fold change (ratio of KD/Ctr group), demonstrating the most significantly differentially expressed genes by genome-wide transcriptomic analysis between Ctr and shOPA1 Huh7 cells ($n = 3$). **(B)** KEGG pathway enrichment analysis within the complete set of differentially expressed genes ($n = 3$). **(C)** Heat map of color-coded expression levels of differentially expressed genes from metabolism pathway (two way ANOVA) ($n = 3$). **(D)** The ROS product level of SNU449 cells with OPA1/MFN1 downregulation showed increased ROS level compared with control group ($n = 6$). **(E)** The ROS product level of CCA organoids with OPA1/MFN1 downregulation showed increased ROS level compared with control group ($n = 6$). Histograms are mean \pm SEM, with p values by Mann Whitney test.

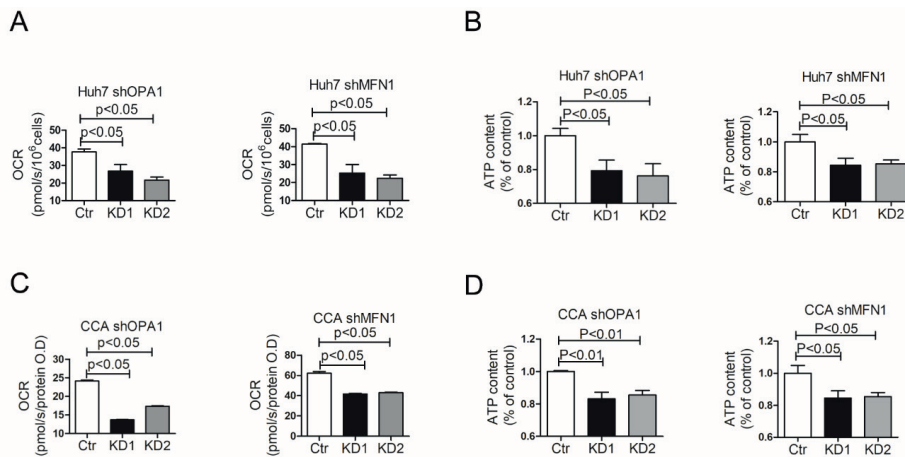


Figure 7. Inhibition of mitochondrial fusion affects Oxygen Consumption Rate and ATP production. **(A)** Real-time analysis of basal Oxygen Consumption Rate (OCR) in Huh7 shOPA1 and shMFN1 cells ($n = 3$). **(B)** ATP production of Huh7 cells with OPA1/MFN1 downregulation was reduced compared with control group ($n = 6$). **(C)** Real-time analysis of basal OCR in CCA organoids with shOPA1 and shMFN1 ($n = 3$). **(D)** ATP production of CCA tumor organoids with OPA1/MFN1 downregulation was reduced compared with control group ($n = 6$). Histograms show means \pm SEM with p value derived by the Mann Whitney test.

Discussion

Although the early Warburg hypothesis proposed glycolysis as the major metabolic process for energy production and anabolic growth in cancer cells due to mitochondrial defects, it recently became more clear that mitochondria also play key roles in oncogenesis [27]. In addition to the bioenergetic functions, mitochondria represent a cell signaling hub regulating cancer cell growth and fate [28]. The function of mitochondria is closely associated with their morphodynamics comprising of the fusion and fission processes. In this study, we found excessive activation of mitochondrial fusion in liver cancer, which provides a metabolic advantage to sustain tumor growth.

Hepatitis virus infections, namely HBV and HCV, are one of the leading causes of HCC. Mitochondrial fission has been frequently observed in HBV and HCV infections [29,30], which has been implicated in the attenuation of cell apoptosis. Whether this has an effect on malignant transformation towards the development of HCC remains unclear. In our HCC patients, we observed a clear enhancement of mitochondrial fusion in the tumor tissues compared to the adjacent liver tissues. Among all the tissues, only two pairs were HBV positive. Whether this discrepancy is attributed to the distinct etiologies of HCC remains to be further investigated.

In general, mitochondrial fission and its key regulator Drp1 has been widely studied in various types of cancers. Drp1 has been reported to be overexpressed in oncocytic thyroid tumors [31]

but decreased in malignant colon and lung cancer tissues, whereas no change was observed in breast and prostate cancer [32]. Overall, fission is thought to be pro-tumorigenic, although it remains a matter of debate whether it has pro- or anti-apoptotic function [33]. Since, in our study, we found a clear elevation of mitochondrial fusion in HCC patient tissues and in vitro cultured tumor organoids from CCA patients, we thus focused on the functional relevance of this process. By genetic knockdown of the key fusion regulators OPA1 or MFN1, we inhibited mitochondrial fusion in HCC cell lines and CCA tumor organoids. This functionally inhibited cell growth in vitro and in vivo tumor formation in mice. This is in line with a previous study showing that the oncogene MYC increases membrane polarization and mitochondrial fusion in mammary epithelial cells to enhance cell proliferation [34].

We found that the inhibition of fusion did not affect cell cycling, but triggered apoptosis, pointing to an anti-apoptotic role of mitochondrial fusion in HCC. In this setting, it is likely the activation of the intrinsic apoptotic pathway, because no specific ligand was added. This intrinsic pathway is mainly triggered by non-receptor stimuli and characterized by the permeabilization of the outer mitochondrial membrane. This leads to the release of pro-apoptotic factors from the mitochondrial inter-membrane space into the cytosol [35]. Our results appear to be in line with the previous findings that mitochondrial fusion protein is responsible for maintenance of mitochondrial membrane structure, matrix homogeneity and mitochondrial genome integrity, which are vital for cell survival [36,37]. However, the exact mechanisms by which mitochondrial fusion modulates this apoptotic process remain to be investigated.

In MYC transformed cells, it has been demonstrated that fusion promotes mitochondrial metabolism to enhance cell proliferation [38,39]. Thus, we have performed genome-wide transcriptomic analysis and, consistently, the inhibition of fusion affected the metabolic pathway most predominantly. Functionally, we have demonstrated that the knockdown of fusion genes inhibited oxygen consumption and ATP production, the hallmarks of mitochondrial metabolism, in HCC cell lines and CCA tumor organoids. We also found the reduced glucose consumption and lactate secretion in fusion gene knockdown cells. In mouse embryonic fibroblasts, mitochondrial fragmentation impairs cell growth, showing widespread heterogeneity in mitochondrial membrane potential and suffered reduced respiratory capacity [40]. Although fission has been widely recognized as pro-tumorigenic, it has also been reported to decrease mitochondrial oxygen consumption rate and ATP production in malignant cells [41]. Cancer cells without mtDNA remain viable, although they are unable to form tumors, whereas reconstitution of oxidative phosphorylation again endows the tumorigenic capability [42]. Growing evidence demonstrates cross-talk between metabolic intermediates and ROS in cancer [43]. Mitochondrial dynamics and ROS processes influence each other in various cancers [44,45]. Our studies found that the dysfunction of mitochondrial fusion could increase ROS level in liver cancer cells. The morphodynamics and functions of mitochondria are rather multifaceted, highly depending on the cancer types and specific

context. Thus, the distinct observations from different studies appear but may not be necessarily contradictory.

In summary, we found that the process of mitochondrial fusion is activated in liver cancer. This enhances mitochondrial metabolism to fuel tumor growth while resisting cell apoptosis. These findings bear important implications for understanding liver cancer biology and developing potential mitochondria-targeted therapy and more effective treatment modalities.

Supplementary Materials: The following are available online at www.mdpi.com/xxx/s1, Figure S1: Mitochondrial morphology in an HBV-related HCC patient. Figure S2: Western blot analysis of mitochondrial fusion genes in liver cancer cells SNU449 and CCA organoids. Figure S3: Dysfunction of mitochondrial fusion inhibited tumor cell growth independent of cell cycle arrest. Figure S4: Dysfunction of mitochondrial fusion is correlated with increased ratio of Bax/Bcl-2 gene expression in liver cancer cells. Figure S5: Dysfunction of mitochondrial fusion down-regulated glucose level in liver cancer cells. Figure S6: Dysfunction of mitochondrial fusion down-regulated lactate level in liver cancer cells.

Author Contributions: Conceptualization, M.L., W.C. and Y.W.; Methodology, M.L., W.C., B.M.; Software, M.L., W.C.; Validation, M.L., S.Z., L.W. and W.C.; Formal analysis, M.L., J.L.; Investigation, M.L., C.Q.; Resources, R.L., G.Z.; Data curation, M.L., W.C.; Writing—original draft preparation, M.L.; Writing—review and editing, M.L., L.V., J.K., D.S., M.V.; Supervision, Q.P.; Project administration, M.P.

Funding: This research is supported by a KWF Young Investigator Grant (No. 10140) from the Dutch Cancer Society and a VIDI grant (No. 91719300) from the Netherlands Organization for Scientific Research (NWO) to Q. Pan. This research is also financially supported by an InnoSysTox grant from ZonMW (No. 114027003 – LJW van der Laan), and a China Scholarship Council PhD fellowship (File No. 201506100033) to Meng Li.

Acknowledgments: We thank Dr. Werner Koopman for support and suggestions regarding optimization of images; Ehsan Shokrollahi and Dr. Nicolaas J. H. Raat from Laboratory of Experimental Anesthesiology of Erasmus MC for facilitating mitochondrial metabolism measurements.

Conflicts of Interest: The authors declare no conflict of interest.

References

1. Bray, F.; Ferlay, J.; Soerjomataram, I.; Siegel, R.L.; Torre, L.A.; Jemal, A. Global cancer statistics 2018: Globocan estimates of incidence and mortality worldwide for 36 cancers in 185 countries. *CA Cancer J. Clin.* **2018**, *68*, 394–424.
2. Sia, D.; Villanueva, A.; Friedman, S.L.; Llovet, J.M. Liver cancer cell of origin, molecular class, and effects on patient prognosis. *Gastroenterology* **2017**, *152*, 745–761.
3. Wallace, D.C. Mitochondria and cancer. *Nat. Rev. Cancer* **2012**, *12*, 685–698.
4. Chandel, N.S. Evolution of mitochondria as signaling organelles. *Cell Metab.* **2015**, *22*, 204–206.
5. Ward, P.S.; Thompson, C.B. Metabolic reprogramming: A cancer hallmark even warburg did not anticipate. *Cancer Cell* **2012**, *21*, 297–308.
6. Grandemange, S.; Herzig, S.; Martinou, J.C. Mitochondrial dynamics and cancer. *Semin. Cancer Biol.* **2009**, *19*, 50–56.
7. Srinivasan, S.; Guha, M.; Kashina, A.; Avadhani, N.G. Mitochondrial dysfunction and mitochondrial dynamics-the cancer connection. *Biochim. Biophys. Acta Bioenerg.* **2017**, *1858*, 602–614.
8. Alavi, M.V.; Fuhrmann, N. Dominant optic atrophy, opa1, and mitochondrial quality control: Understanding mitochondrial network dynamics. *Mol. Neurodegener.* **2013**, *8*, 32.
9. Zorzano, A.; Liesa, M.; Sebastian, D.; Segales, J.; Palacin, M. Mitochondrial fusion proteins: Dual regulators of morphology and metabolism. *Semin. Cell Dev. Biol.* **2010**, *21*, 566–574.
10. Youle, R.J.; van der Bliek, A.M. Mitochondrial fission, fusion, and stress. *Science* **2012**, *337*, 1062–1065.
11. Hoppins, S.; Lackner, L.; Nunnari, J. The machines that divide and fuse mitochondria. *Annu. Rev. Biochem.* **2007**, *76*, 751–780.
12. Patten, D.A.; Wong, J.; Khacho, M.; Soubannier, V.; Mailloux, R.J.; Pilon-Larose, K.; MacLaurin, J.G.; Park, D.S.; McBride, H.M.; Trinkle-Mulcahy, L.; et al. Opa1-dependent cristae modulation is essential for cellular adaptation to metabolic demand. *EMBO J.* **2014**, *33*, 2676–2691.
13. Wakabayashi, J.; Zhang, Z.; Wakabayashi, N.; Tamura, Y.; Fukaya, M.; Kensler, T.W.; Iijima, M.; Sesaki, H. The dynamin-related gtpase drp1 is required for embryonic and brain development in mice. *J. Cell Biol.* **2009**, *186*, 805–816.
14. Zhang, Z.; Wakabayashi, N.; Wakabayashi, J.; Tamura, Y.; Song, W.J.; Sereda, S.; Clerc, P.; Polster, B.M.; Aja, S.M.; Pletnikov, M.V.; et al. The dynamin-related gtpase opa1 is required for glucose-stimulated atp production in pancreatic beta cells. *Mol. Biol. Cell* **2011**, *22*, 2235–2245.
15. Zhao, X.; Tian, C.; Puszyk, W.M.; Ogunwobi, O.O.; Cao, M.; Wang, T.; Cabrera, R.; Nelson, D.R.; Liu, C. Opa1 downregulation is involved in sorafenib-induced apoptosis in hepatocellular carcinoma. *Lab. Investig.* **2013**, *93*, 8–19.
16. Liu, P.; Cao, W.; Ma, B.; Li, M.; Chen, K.; Sideras, K.; Duitman, J.W.; Sprengers, D.; Khe Tran, T.C.; Ijzermans, J.N.M.; et al. Action and clinical significance of ccaat/enhancer-binding protein delta in hepatocellular carcinoma. *Carcinogenesis* **2019**, *40*, 155–163.

17. Broutier, L.; Andersson-Rolf, A.; Hindley, C.J.; Boj, S.F.; Clevers, H.; Koo, B.K.; Huch, M. Culture and establishment of self-renewing human and mouse adult liver and pancreas 3d organoids and their genetic manipulation. *Nat. Protoc.* **2016**, *11*, 1724–1743.
18. Broutier, L.; Mastrogiovanni, G.; Verstegen, M.M.; Francies, H.E.; Gavarro, L.M.; Bradshaw, C.R.; Allen, G.E.; Arnes-Benito, R.; Sidorova, O.; Gaspersz, M.P.; et al. Human primary liver cancer-derived organoid cultures for disease modeling and drug screening. *Nat. Med.* **2017**, *23*, 1424–1435.
19. Vicent, S.; Lieshout, R.; Saborowski, A.; Verstegen, M.M.A.; Raggi, C.; Recalcati, S.; Invernizzi, P.; van der Laan, L.J.W.; Alvaro, D.; Calvisi, D.F.; et al. Experimental models to unravel the molecular pathogenesis, cell of origin and stem cell properties of cholangiocarcinoma. *Liver Int.* **2019**, *39*, 79–97.
20. Xu, L.; Zhou, X.; Wang, W.; Wang, Y.; Yin, Y.; Laan, L.J.; Sprengers, D.; Metselaar, H.J.; Peppelenbosch, M.P.; Pan, Q. Ifn regulatory factor 1 restricts hepatitis e virus replication by activating stat1 to induce antiviral ifn-stimulated genes. *FASEB J.* **2016**, *30*, 3352–3367.
21. Drost, J.; Artegiani, B.; Clevers, H. The generation of organoids for studying wnt signaling. *Methods Mol. Biol.* **2016**, *1481*, 141–159.
22. Petrat, F.; Pindiur, S.; Kirsch, M.; de Groot, H. “Mitochondrial” photochemical drugs do not release toxic amounts of 1o(2) within the mitochondrial matrix space. *Arch. Biochem. Biophys.* **2003**, *412*, 207–215.
23. Cao, W.; Chen, K.; Bolkestein, M.; Yin, Y.; Verstegen, M.M.A.; Bijvelds, M.J.C.; Wang, W.; Tuysuz, N.; Ten Berge, D.; Sprengers, D.; et al. Dynamics of proliferative and quiescent stem cells in liver homeostasis and injury. *Gastroenterology* **2017**, *153*, 1133–1147.
24. Chen, K.; Cao, W.; Li, J.; Sprengers, D.; Y Hernandez, P.; Kong, X.; Jw van der Laan, L.; Man, K.; Kwekkeboom, J.; J Metselaar, H.; et al. Differential sensitivities of fast- and slow-cycling cancer cells to inosine monophosphate dehydrogenase 2 inhibition by mycophenolic acid. *Mol. Med.* **2016**, *21*, 792–802.
25. Ma, B.; Chen, K.; Liu, P.; Li, M.; Liu, J.; Sideras, K.; Sprengers, D.; Biermann, K.; Wang, W.; Ijzermans, J.N.M.; et al. Dichotomous functions of phosphorylated and unphosphorylated stat1 in hepatocellular carcinoma. *J. Mol. Med. (Berl.)* **2019**, *97*, 77–88.
26. Santel, A.; Frank, S.; Gaume, B.; Herrler, M.; Youle, R.J.; Fuller, M.T. Mitofusin-1 protein is a generally expressed mediator of mitochondrial fusion in mammalian cells. *J. Cell Sci.* **2003**, *116*, 2763–2774.
27. Porporato, P.E.; Filigheddu, N.; Pedro, J.M.B.; Kroemer, G.; Galluzzi, L. Mitochondrial metabolism and cancer. *Cell Res.* **2018**, *28*, 265–280.
28. Ortmayr, K.; Dubuis, S.; Zampieri, M. Metabolic profiling of cancer cells reveals genome-wide crosstalk between transcriptional regulators and metabolism. *Nat. Commun.* **2019**, *10*, 1841.
29. Kim, S.J.; Khan, M.; Quan, J.; Till, A.; Subramani, S.; Siddiqui, A. Hepatitis b virus disrupts mitochondrial dynamics: Induces fission and mitophagy to attenuate apoptosis. *PLoS Pathog.* **2013**, *9*, e1003722.
30. Kim, S.J.; Syed, G.H.; Khan, M.; Chiu, W.W.; Sohail, M.A.; Gish, R.G.; Siddiqui, A. Hepatitis c virus triggers mitochondrial fission and attenuates apoptosis to promote viral persistence. *Proc. Natl. Acad. Sci. USA* **2014**, *111*, 6413–6418.

31. Ferreira-da-Silva, A.; Valacca, C.; Rios, E.; Populo, H.; Soares, P.; Sobrinho-Simoes, M.; Scorrano, L.; Maximo, V.; Campello, S. Mitochondrial dynamics protein drp1 is overexpressed in oncocyctic thyroid tumors and regulates cancer cell migration. *PLoS ONE* **2015**, *10*, e0122308.
32. Kim, Y.Y.; Yun, S.H.; Yun, J. Downregulation of drp1, a fission regulator, is associated with human lung and colon cancers. *Acta Biochim. Biophys. Sin. (Shanghai)* **2018**, *50*, 209–215.
33. Maycotte, P.; Marin-Hernandez, A.; Goyri-Aguirre, M.; Anaya-Ruiz, M.; Reyes-Leyva, J.; Cortes-Hernandez, P. Mitochondrial dynamics and cancer. *Tumour Biol.* **2017**, *39*, 1010428317698391.
34. von Eyss, B.; Jaenicke, L.A.; Kortlever, R.M.; Royla, N.; Wiese, K.E.; Letschert, S.; McDuffus, L.A.; Sauer, M.; Rosenwald, A.; Evan, G.I.; et al. A myc-driven change in mitochondrial dynamics limits yap/taz function in mammary epithelial cells and breast cancer. *Cancer Cell* **2015**, *28*, 743–757.
35. Brenner, D.; Mak, T.W. Mitochondrial cell death effectors. *Curr. Opin. Cell Biol.* **2009**, *21*, 871–877.
36. Cogliati, S.; Frezza, C.; Soriano, M.E.; Varanita, T.; Quintana-Cabrera, R.; Corrado, M.; Cipolat, S.; Costa, V.; Casarin, A.; Gomes, L.C.; et al. Mitochondrial cristae shape determines respiratory chain supercomplexes assembly and respiratory efficiency. *Cell* **2013**, *155*, 160–171.
37. Frezza, C.; Cipolat, S.; De Brito, O.M.; Micaroni, M.; Beznoussenko, G.V.; Rudka, T.; Bartoli, D.; Polishuck, R.S.; Danial, N.N.; De Strooper, B.; et al. Opa1 controls apoptotic cristae remodeling independently from mitochondrial fusion. *Cell* **2006**, *126*, 177–189.
38. Graves, J.A.; Wang, Y.; Sims-Lucas, S.; Cherok, E.; Rothermund, K.; Branca, M.F.; Elster, J.; Beer-Stolz, D.; Van Houten, B.; Vockley, J.; et al. Mitochondrial structure, function and dynamics are temporally controlled by c-myc. *PLoS ONE* **2012**, *7*, e37699.
39. Dang, C.V. Myc, metabolism, cell growth, and tumorigenesis. *Cold Spring Harb. Perspect. Med.* **2013**, *3*, a014217.
40. Chen, H.; Chomyn, A.; Chan, D.C. Disruption of fusion results in mitochondrial heterogeneity and dysfunction. *J. Biol. Chem.* **2005**, *280*, 26185–26192.
41. Serasinghe, M.N.; Wieder, S.Y.; Renault, T.T.; Elkholi, R.; Asciolla, J.J.; Yao, J.L.; Jabado, O.; Hoehn, K.; Kageyama, Y.; Sesaki, H.; et al. Mitochondrial division is requisite to ras-induced transformation and targeted by oncogenic mapk pathway inhibitors. *Mol. Cell* **2015**, *57*, 521–536.
42. Bajzikova, M.; Kovarova, J.; Coelho, A.R.; Boukalova, S.; Oh, S.; Rohlenova, K.; Svec, D.; Hubackova, S.; Endaya, B.; Judasova, K.; et al. Reactivation of dihydroorotate dehydrogenase-driven pyrimidine biosynthesis restores tumor growth of respiration-deficient cancer cells. *Cell Metab.* **2019**, *29*, 399–416.e10.
43. Panieri, E.; Santoro, M.M. ROS homeostasis and metabolism: a dangerous liason in cancer cells. *Cell Death Dis.* **2016**, *7*, e2253.
44. Huang, Q.; Zhan, L.; Cao, H.; Li, J.; Lyu, Y.; Guo, X.; Zhang, J.; Ji, L.; Ren, T.; An, J.; et al. Increased mitochondrial fission promotes autophagy and hepatocellular carcinoma cell survival through the ros-modulated coordinated regulation of the nfkb and tp53 pathways. *Autophagy* **2016**, *12*, 999–1014.

45. Hu, J.; Zhang, Y.; Jiang, X.; Zhang, H.; Gao, Z.; Li, Y.; Fu, R.; Li, L.; Li, J.; Cui, H.; et al. Ros-mediated activation and mitochondrial translocation of camkii contributes to drp1-dependent mitochondrial fission and apoptosis in triple-negative breast cancer cells by isorhamnetin and chloroquine. *J. Exp. Clin. Cancer Res.* **2019**, *38*, 225.

Supplementary data for

Mitochondrial fusion via OPA1 and MFN1 supports liver tumor cell metabolism and growth

Meng Li, Ling Wang, Yijin Wang, Shaoshi Zhang, Guoying Zhou, Ruby Lieshout, Buyun Ma, Jiaye Liu, Changbo Qu, Monique M. A. Verstegen, Dave Sprengers, Jaap Kwekkeboom, Luc J. W. van der Laan, Wanlu Cao, Maikel P. Peppelenbosch, Qiuwei Pan

Table of contents

Supplementary Figure 1

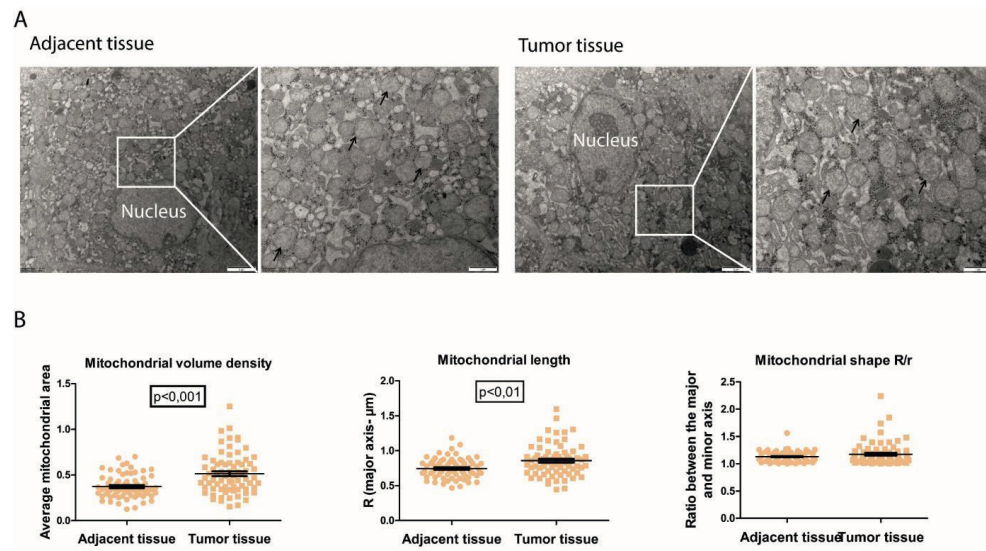
Supplementary Figure 2

Supplementary Figure 3

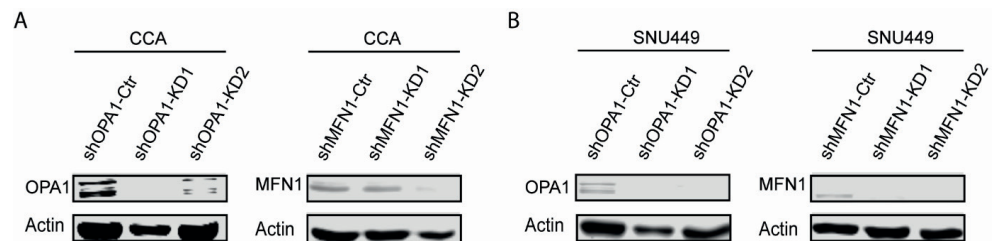
Supplementary Figure 4

Supplementary Figure 5

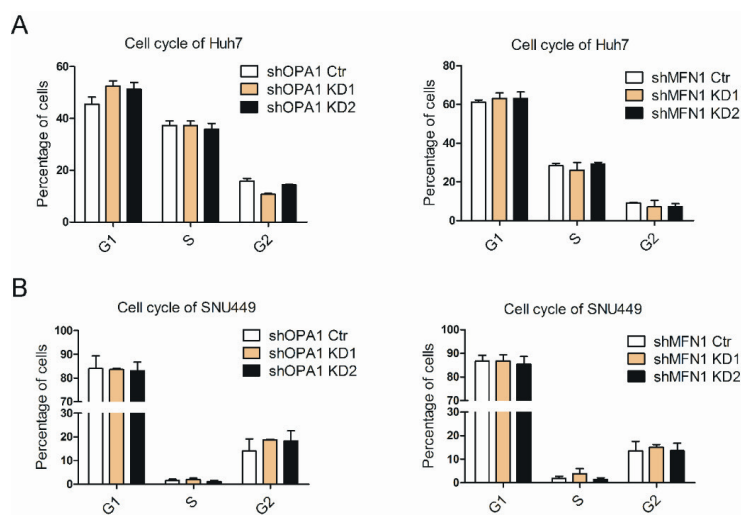
Supplementary Figure 6



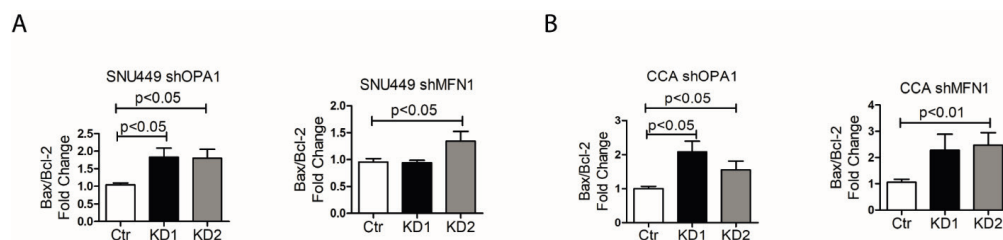
Supplementary Fig 1 Mitochondrial morphology in a HBV-related HCC patient. **A** Representative electron microscopy images of cells from adjacent tissue and tumor tissue of the HCC patient (scale bar = 2 µm). The white boxed regions were further magnified in the expanded images (right side) (scale bar = 1 µm). Mitochondria (arrows) were observed. **B** Images of paired tissue were analysed by ImageJ software (n = 5 images/sample). Mitochondrial volume (mitochondrial area) per cell and mitochondrial length (mitochondrial major axis) were valued. Mitochondrial shape was calculated by the ratio of major axis and minor axis. Histograms are mean ± SEM, with *p* values by Mann Whitney test.



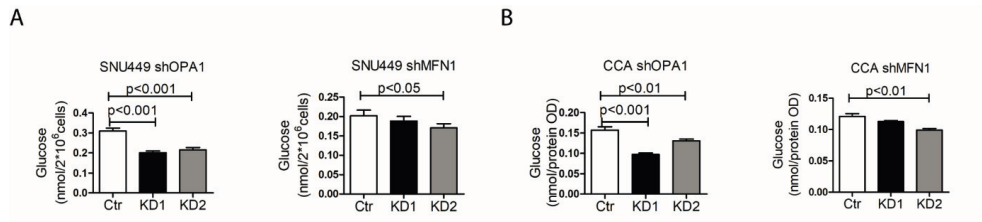
Supplementary Fig 2 Western blot analysis of mitochondrial fusion genes in liver cancer cells SNU449 and CCA organoids. **A** OPA1/MFN1 protein level of CCA organoids with OPA1/MFN1 downregulation. **B** OPA1/MFN1 protein level of SNU449 cells with OPA1/MFN1 downregulation.



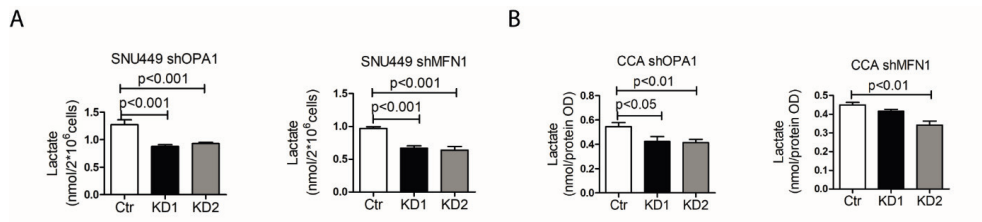
Supplementary Fig 3 Dysfunction of mitochondrial fusion inhibited tumor cell growth independent of cell cycle arrest. **A** The distribution of Huh7 cells with OPA1/MFN1 downregulation did not show significantly difference with control group ($n = 3$). **B** The distribution of SNU449 cells with OPA1/MFN1 downregulation did not show significantly difference with control group ($n = 3$). Histograms are mean \pm SEM.



Supplementary Fig 4 Dysfunction of mitochondrial fusion is correlated with increased ratio of Bax/Bcl-2 gene expression in liver cancer cells. **A** Bax/Bcl-2 fold change of SNU449 cells with OPA1/MFN1 downregulation increased compared with control group ($n = 6$). **B** Bax/Bcl-2 fold change of CCA organoids with OPA1/MFN1 downregulation increased compared with control group ($n = 6$). Histograms are mean \pm SEM, with p values by Mann Whitney test.



Supplementary Fig 5 Dysfunction of mitochondrial fusion down-regulated glucose level in liver cancer cells. **A** The glucose product level of SNU449 cells with OPA1/MFN1 downregulation showed decreased glucose level compared with control group (n = 6). **B** The glucose product level of CCA organoids with OPA1/MFN1 downregulation showed decreased glucose level compared with control group (n = 6). Histograms are mean \pm SEM, with *p* values by Mann Whitney test.



Supplementary Fig 6 Dysfunction of mitochondrial fusion down-regulated lactate level in liver cancer cells. **A** The lactate product level of SNU449 cells with OPA1/MFN1 downregulation showed decreased lactate level compared with control group (n = 6). **B** The lactate product level of CCA organoids with OPA1/MFN1 downregulation showed decreased lactate level compared with control group (n = 6). Histograms are mean \pm SEM, with *p* values by Mann Whitney test.

CHAPTER 3

The complex I and III of mitochondrial electron transport chain are therapeutically targetable in liver cancer

Meng Li ^{1*}, Qin Yang ^{1,2*}, Jiaye Liu ¹, Changbo Qu ¹, Yang Li ¹, Maikel P. Peppelenbosch ¹ and Qiuwei Pan ¹

¹ Department of Gastroenterology and Hepatology, Erasmus MC-University Medical Center Rotterdam, The Netherlands.

² Department of general surgery, The Third People's Hospital of Chengdu & the Affiliated Hospital of Southwest Jiaotong University & the second medical school of Chengdu affiliated to Chongqing medical university, Chengdu, Sichuan 610031, P.R. China.

In preparation

Abstract

Liver cancer is one of the most common and deadliest types of oncological diseases worldwide, with limited treatment options available. New treatment modalities are urgently called for and their development is hampered in a lack of insight into the molecular mechanisms underlying disease. It is clear, however, that metabolic reprogramming in general and alternative mitochondrial function in particular is intimately linked to the liver cancer process, prompting exploration of mitochondrial biochemistry as a potential therapeutic target. Here we report that in various preclinical models of liver cancer including cell lines, liver cancer organoids and murine xenografts, depletion of mitochondrial DNA, pharmacologic inhibition or genetic knockdown of mitochondrial electron transport chain (mETC) complex I or pharmacological inhibition of mETC complex III limits cancer cell growth and cancer cell clonogenic ability. The inhibition of liver cancer by targeting mETC complex I and III was associated with production of reactive oxygen species, apoptosis induction and reduced ATP generation. Thus, our results reveal the mETC compartment of mitochondria as a potential therapeutic target in liver cancer.

Introduction

Liver cancer, mainly consisting of hepatocellular carcinoma (HCC) and cholangiocarcinoma (CCA), is the sixth most common cancer and one of the leading causes of cancer related-death [1]. The risk factors for contracting HCC include Hepatitis B, Hepatitis C as well as metabolic syndrome and type II diabetes amongst others. How these risk factors translate in cancer development and the molecular details of further disease progression are less clear, which hampers rational efforts to develop new therapy. Apart from surgery no curative options exist while clinical management of HCC is further hampered by high recurrence rates and the resistance to systemic chemotherapy [2]. Hence, increased insight into the liver cancer progress is urgently needed.

Hepatocytes are in many aspects a unique cell type and of the defining characteristics is the high abundance of mitochondria in their cytoplasm, which appear involved in oncogenic transformation of this cell type [3]. Liver cancer progression is accompanied by a sequence of fairly defined genetic alterations while concomitantly cellular metabolism shows considerable reprogramming, in particular aerobic glycolysis becomes prominent [1,4]. The central role of the mitochondrion in hepatocyte metabolism has given rise to speculation that this organelle can provide for novel therapeutic targets, although fair to say that our knowledge on the functionality of these organelles in the HCC process is far from complete [5].

Mitochondria are complex multimembrane structures with their own DNA and own translational machinery, although mitochondrial function is also critically dependent on import of proteins from the cytosol [6,7]. The most central element in mitochondrial biochemistry is the mitochondrial electron transport chain (mETC) which is located in the inner mitochondrial membrane and consists of four complexes that in conjunction enable oxidative phosphorylation [8]. Encouragingly, chronic use of Metformin-like drugs that target mETC complex I reduces risk for HCC development, which may also relate to the role of mETC in energy production, membrane potential maintenance and redox balance control [9-12]. More direct studies on the importance of mitochondria in HCC are, however, required to better determine the promise of mETC-directed therapy in liver cancer.

Prompted by the above mentioned considerations we attempted to investigate the importance of mETC components in liver cancer. The results identify mitochondrial DNA in general and mETC complex I and III in particular as essential components in HCC physiology. Our results further demonstrated the possibility of therapeutically targeting the mETC in liver cancer cells and may guide the development of novel rational avenues for the treatment of HCC.

Materials and Methods

Reagents and antibodies

Rotenone (ROT), Metformin (Met), 2-Thenoyltrifluoroacetone (TTFA), Antimycin A (AMA), Myxothiazol (MYXO), puromycin, uridine, diphenyleneiodonium chloride, ethidium bromide (EtBr), and Potassium cyanide (KCN) were purchased from Sigma-Aldrich (St. Louis, MO). The rabbit polyclonal antibody against cytochrome b (CYTB) and mouse monoclonal antibody against NDUFS1 were purchased from Sigma-Aldrich (St. Louis, MO). The rabbit monoclonal antibody against cleaved caspase-3 was purchased from cell signalling technology.

Cell culture

Human cell lines HepG2, PLC/PRF/5, and Snu-449 were kindly provided from Department of Viroscience, Erasmus Medical Center and cultured in Dulbecco's modified Eagle medium (DMEM) (Lonza Biowhittaker, Verviers, Belgium) supplemented with 10% (v/v) heat-inactivated fetal bovine serum (FBS, Thermo Fisher Scientific), 100 IU/ml penicillin and 100 IU/ml streptomycin. A mitochondrial DNA (mtDNA)-depleted cell model was established by co-culturing with EtBr (50 ng/ml), pyruvate (100 µg/ml) and uridine (50 µg/ml) for 5 days as described early [13]. For knockdown of mETC complex I, cells were transduced with an appropriate short hairpin RNA (shRNA) and transduced cells were selected by culturing with 3 µg/ml puromycin in DMEM according to previously described procedures [14]. The Plko.1-based shRNA lentiviral vectors sequence was: NDUFS1, 5'-CCGGGCAAGCAGATAGAAGGCCATACTCGAGTATGGCCTTCTATCTGCTTGCTTTT-3'.

Organoids were derived and cultured as described early [15]. The study was approved by the medical ethical committee of Erasmus Medical Center. In addition, the study protocol conforms to the ethical guidelines of the 1975 Declaration of Helsinki.

Proliferation assay of cells and organoids

Cell proliferation was measured by reduction of 3-(4, 5-Dimethylthiazol-2-yl)-2, 5-diphenyltetrazolium bromide (MTT, MilliporeSigma) and Alamar Blue™ Cell Viability reagent (Thermo Fisher, CA), essentially as described earlier [16]. In short, for the MTT assay, cells were seeded into a 96-well plate with or without mETC complex inhibitors and cultured for 48 hours. Then, 15 µl of 10% MTT solution (5 mg/ml) per well was added to the wells followed by incubation at 37 °C in a 5% CO₂ for 4 hours. The medium was removed and 100 µl DMSO was added to each well and shaken for 30 min. The absorbance of each well was read on a microplate absorbance reader (Bio-Rad, Hercules, CA, USA) at a wavelength of 490nm.

For the Alamar Blue assay, after treating the cells or organoids with inhibitors as appropriate for 48 hours, the medium was removed and exchanged for fresh culture medium supplemented with 5% Alamar Blue and cultured at 37 °C with 5% CO₂ for 4 hours. Fluorescence (excitation 530 nm, emission 590 nm) of each well was measured on a FLUO STAR OPTIMA microplate reader (BMG Labtech, Durham, NC, USA).

Colony formation efficiency assay

After treatment of the cells with appropriate inhibitors, cells were cultured in drug-free medium for approximately 14 days. The cells were fixed with methanol and stained with crystal violet for one hour, and then washed with water and dried before counting of colonies. A total number of colonies that contained more than 50 cells were counted and the colony formation efficiency (CFE) was calculated. The results were normalized to the unexposed control (set to 100% plating efficiency).

$$\text{CFE\%} = \frac{\text{number of colonies in exposure cultures}}{\text{number of colonies in unexposed cultures}} \times 100\%$$

Analysis of cell apoptosis

Cell apoptosis was measured by quantitatively determining cell surface phosphatidylserine in apoptotic cells using Annexin V-FITC/PI apoptosis detection kit (Becton Dickinson). Experiments being performed according to the manufacturer's instruction. The treated cells were washed with cold PBS after co-culturing with the appropriate complex inhibitors for 48 hours and suspended by 1 X Binding Buffer. FITC Annexin V and PI (1:1) were added into 100 μL suspension (1×10^4 cells) and incubated for 15 min at room temperature (25 °C) in the dark. The samples were tested by FACS within 1 hour [17]. Cell apoptosis rate was analysed by FlowJo_V10 software. For each treatment, two independent wells were tested for PLC/PRF/5, C I-knockdown and mtDNA-depleting cell lines for three times. The mean and standard error were calculated for each condition.

Xenograft Mouse Model in Nude Mice

The xenograft tumour model was established in female nude mice injected subcutaneously with knockdown cells and corresponding control cells into the lower left or right flank of the same mice ($5 \times 10^6/200 \mu\text{L}$ cells per mouse; $n = 5$ mice per group), 1: 1 mixed with matrigel. Xenograft mouse model was performed as described before [18]. All animal experiments were approved by the Committee on the Ethics of Animal Experiments of the Erasmus Medical Center.

Reactive oxygen species measurements

Cellular reactive oxygen species (ROS) was measured using CM-H2DCFDA (General Oxidative Stress Indicator) kit (ThermoFisher). Cell lines were seeded into 6-well plates and pretreated with diphenylene iodonium (DPI, 10 μM) for 1 hour prior to appropriate complex inhibitor treatment for 3 hours. The positive control was induced by adding 100 μM H_2O_2 for 15 min. Cells were washed with PBS and incubated with non-serum medium containing 5 μM CM-H2DCFDA at 37 °C for 30 min. Then, the cells were washed with PBS for three times and suspended by 500 μL PBS. The samples were tested by a FACS and ROS production was analysed by FlowJo_V10 software.

Adenosine triphosphate (ATP) production measurement

An ATP Bioluminescence Assay Kit HS II was used to measure the ATP content of cells according to the manufacturer's instructions (Roche Life Science, Penzberg, Germany). Cells were seeded into a 96-well plate with or without mETC complex inhibitors and cultured for 48 hours. Then, cells were harvested and suspended in dilution buffer at a concentration of $1 \times 10^5 \text{ ml}^{-1}$. The same volume of cell lysis reagent was added into the above cell suspension and incubated at 15 °C for 5 min and for an extra 2 min at 100 °C. Subsequently, the cell suspension was centrifuged at $10,000 \times g$ for 60 s and the supernatant was transferred to a fresh tube. Samples were kept on ice until measurement. A mixture of 50 µl luciferase reagent was added to 50 µl supernatant or standards provided by ATP Assay kit. Luminescence was detected after 1 second delay using a microplate reader (LumiStar Optima Luminescence Counter, BMG Labtech, Offenburg, Germany) (excitation=535 nm; emission=587 nm).

Real-time quantitative Polymerase Chain Reaction (PCR)

RNA was isolated with a Machery-NucleoSpin RNA kit (Bioke, Leiden, the Netherlands) and quantified with a Nanodrop ND-1000 (Wilmington, DE). The iScript cDNA synthesis kit (Takara Bio INC.) was used to acquire cDNA from total RNA. Quantitative real-time PCR analyses were performed by the StepOne Real-Time PCR system and the Step-One v2.0 software (Applied Biosystem, Darmstadt, Germany). Primer sequences are provided in Supplementary Table 1. All the expression levels are depicted relative to the expression of GAPDH.

Western blot assay

Western blotting was performed according to routine procedure [19]. In short, total protein (100 µg) was loaded in each lane, subjected to sodium dodecyl sulfate-polyacrylamide (SDS-PAGE) gel (12%) electrophoresis and then transferred onto polyvinylidene difluoride (PVDF) membranes (Invitrogen). Subsequently, the membranes were blocked for 1 hour at room temperature followed by incubation with antibodies overnight at 4 °C. Membranes were washed 3 times before incubating with secondary antibodies for 2 hours. Protein bands were detected with Odyssey 3.0 Infrared Imaging System (LI-COR Biosciences) after washing 3 times.

Statistical Analysis

All data are presented as mean \pm SEM. Prism software (GraphPad Software) was used for all statistical analysis. N= repeated times of experiments. Statistical analysis was performed one-way ANOVA if multi-group of samples were analyzed otherwise Mann-Whitney test was performed. For all experiments, a *p*-value less than 0.05 was considered as significant.

Results

Growth of liver cancer cell lines requires functional mETC complex I and III.

To study the effects of targeting mETC complexes in liver cancer, SNU449, PLC/prf/5 and HepG2 liver cancer cell lines was challenged with six pharmacological inhibitors targeting the four mETC complexes (I, II, III, and IV) and effects on cell survival were assessed. Pharmacological of neither complex II (using TTFA) nor complex IV (using KCN) inhibitors showed obvious effects in this respect (supplementary Fig S1). However, inhibition of either mETC complex I (employing ROT or Metformin) or III (using AMA or MYXO) was not compatible with liver cancer cell line survival at concentrations. These results showed inhibitors targeting mETC can impact on liver cancer cell line survival (Figure 1A and 1B). In apparent agreement, pharmacological inhibition of either mETC complex I or mETC complex III reduced the colony formation efficiency of all three cell lines to less than 50 % as compared to untreated controls (Figure 1C and 1D). We concluded that functionality of mETC complex I and mETC complex III is required for liver cancer cell survival.

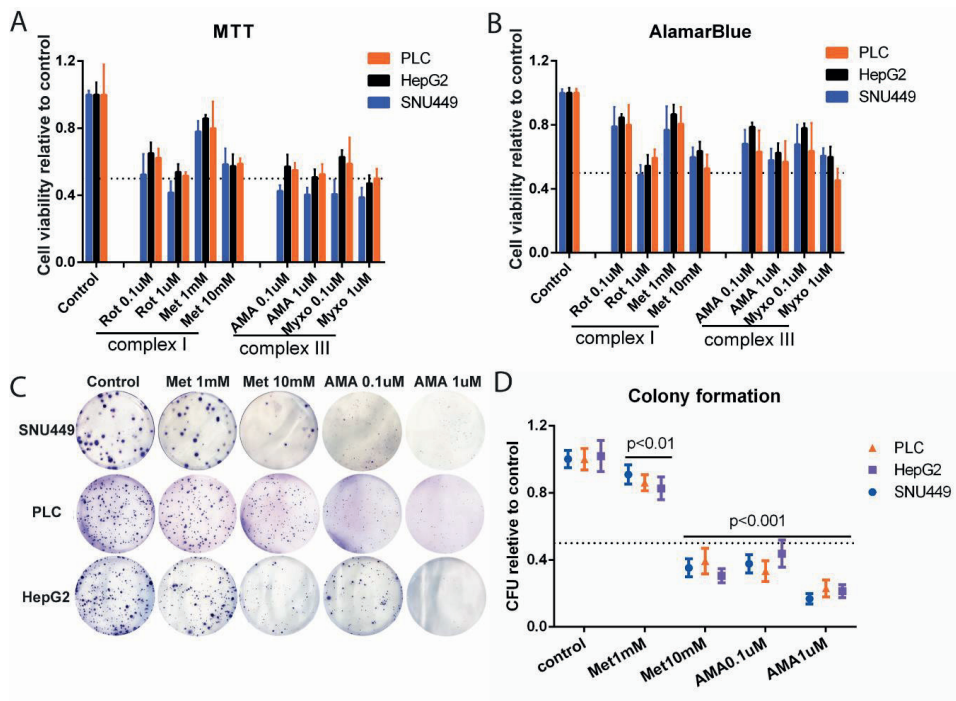


Figure 1. Complex I and III inhibitors of mitochondrial electron transport chain (mETC) inhibit the proliferation of HCC cells. (A, B) HepG2, PLC/PRF/5, and Snu-449 cells were treated for 48 hours with the mETC complex I inhibitors (Rotenone, ROT; Metformin, Met) and complex III inhibitors (Antimycin A, AMA; Myxothiazol, MYXO) at different concentrations. Cell viability was quantified by MTT and AlamarBlue (N = 9). (C, D) HepG2, PLC/PRF/5, and Snu-449 cells were treated with Met and AMA at different concentrations and the colony formation efficiency

was calculated (N = 9). P value was calculated by comparing with corresponding control. Histograms results are expressed as mean \pm SEM, with p values calculated by Mann-Whitney U Test.

Targeting mETC complex I and III inhibited growth of mouse liver tumor organoids.

Although cell line models allow for rapid screening of cancer drugs, they only partly capture the cancer process. Experimentation with cancer organoids is more cumbersome but more closely recapitulate the pathophysiological features of natural tumorigenesis and it was recently shown that such organoids are a useful approach for studying liver cancer [20]. Hence, we decided to study the effects of pharmacological inhibitors targeting mETC complex I and III in tumour organoids isolated from DEN-induced primary murine liver cancers [21] and contrasted results to those obtained in organoids derived from healthy liver. All the complex I and III inhibitors (ROT, Met, AMA and MYXO) limited the growth of both tumour organoids and untransformed organoids, but cancer organoids were more sensitive to such inhibition (Figure 2A and 2B). Thus, the effects of pharmacological complex I and III inhibitors seen in cell lines can be recapitulated in liver cancer organoids and liver cancer is more sensitive to mETC inhibition as untransformed liver-derived material.

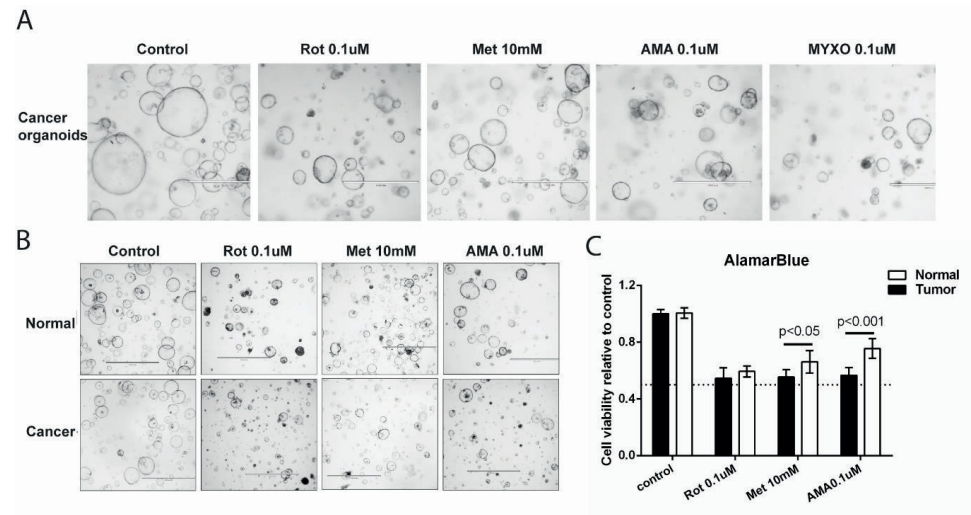


Figure 2. mETC complex I and III inhibitors impaired the growth of mouse liver tumor organoids. (A) Optical microscope images of liver tumor organoids after treating for 48 hours with the mETC complex I inhibitors (Rotenone, ROT; Metformin, Met) and complex III inhibitors (Antimycin A, AMA; Myxothiazol, MYXO) (N = 3). (B) Optical microscope images of liver tumor organoids and normal liver organoids after treating with AMA, Met and ROT for 48 hours (N = 9). (C) The growth rates of tumor and normal liver organoids measured by AlamarBlue assays (N=9). Histograms are mean \pm SEM, with p values by Mann-Whitney U Test.

Depletion of mitochondrial DNA or knock down of mETC constituting proteins counteracts liver cancer cell survival.

The importance of mETC integrity for liver cancer cell survival was confirmed in experiments in which two experimentally independent approaches were chosen to compromise such integrity. In the first approach, we depleted mitochondrial DNA from cells. Mitochondrial DNA encodes various proteins that are part of the mETC, the cytochrome c oxidase subunit I (COX I), cytochrome c oxidase subunit II (COX II) and cytochrome oxidase (CYTB). Thus mitochondrial DNA depletion should compromise mETC integrity. Depletion of mitochondrial DNA by exposing PLC/PRF/5 cultures to ethidium bromide (EB) strongly reduced expression of COX I, COX II and CYTB, whereas expression of cytochrome c oxidase subunit IV (COX IV; which is encoded by nuclear DNA) was not affected (Figure 3A-C). In the second approach, lentiviral vector-delivered shRNA was used to knockdown the mETC complex I subunit NDUF51 and Figure 3D-F documents the technical success of this strategy. Both approaches were used to determine the effect of comprised mETC integrity on liver cancer cell physiology.

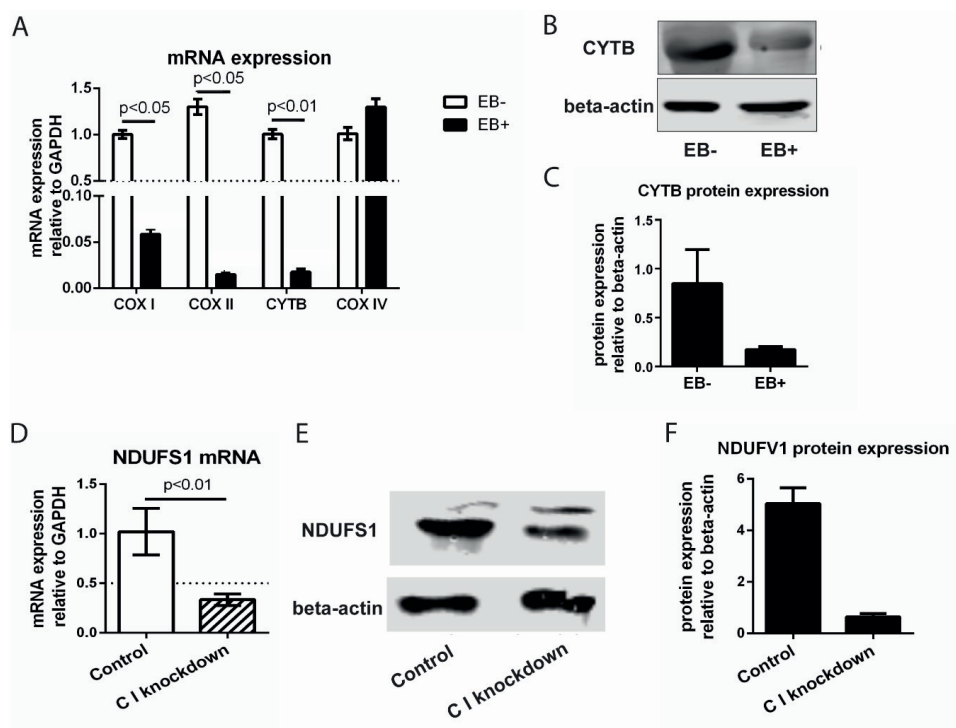


Figure 3. Establishing the mETC-deficient cell models. (A, B and C) Real-time PCR analysis of COX I, COX II, COX IV and CYTB mRNA (A) (N = 6) and Western blotting analysis of CYTB protein (B, C) (N = 3) in HCC cells after treatment with EB for 5 days. (D, E and F) Real-time PCR analysis of NDUF51 mRNA (D) (N = 6) and Western blotting analysis of NDUF51 protein (D, F) (N = 3) in HCC cells after transfected with NDUF51 lentivirus. Histograms are mean \pm SEM, with p values by Mann-Whitney U Test.

Importantly, both mETC targeting strategies provoke diminished proliferation (Figure 4A and 4B) and colony formation efficiency (Figure 4C). Importantly, pharmacological inhibitors of complex I were less effective in a background of mitochondrial DNA depletion or NDUFS1 knockdown, in apparent agreement with the specificity of the experimental approach chosen (Figure 4B). Upon subcutaneous engraftment in immunodeficient nude mice, cells with NDUFS1 knockdown were less capable of forming tumor *in vivo* compared with correspondence control (Figure 4D). We concluded that integrity of the mETC is essential for liver cancer cell growth.

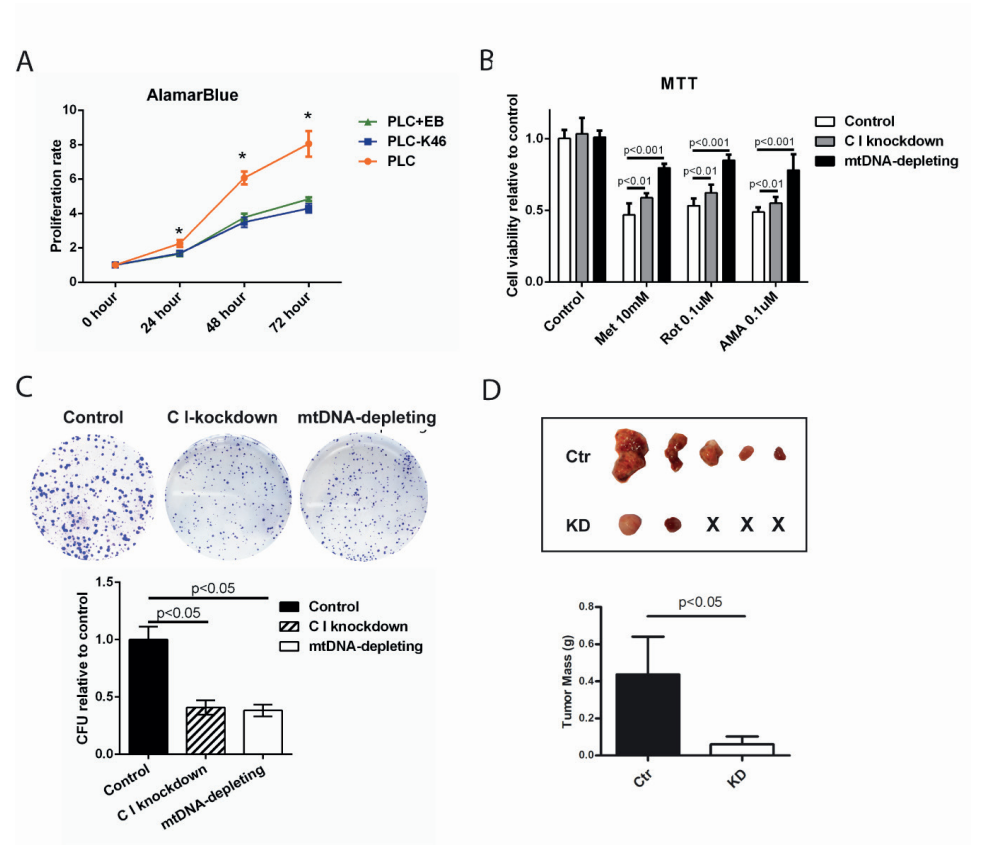


Figure 4. Compromising mETC integrity inhibits HCC cell growth *in vitro*. (A) AlamarBlue assays measure the cell growth rates in different liver cell lines (PLC/PRF/5, C I knockdown and mtDNA-depleting) were performed (N = 8). (B) MTT assays to test the mETC complex I and III inhibitors (Met, ROT and AMA) effect on the proliferation of the three cell lines (N = 9). (C) Representative images of colony formation assay of PLC/PRF/5, C I knockdown and mtDNA-depleting HCC cells and the colony formation units (CFU) was calculated. The results were normalized to the control (PLC/PRF/5), setting to 100% plating efficiency (N = 4). (D) Ctr (PLC/PRF/5 control group) and KD (PLC/PRF/5 C I knockdown group) cells were injected sub-cutaneously into nude mice. Tumors were harvested from nude mice and weighed (N = 5). Histograms are mean \pm SEM, with p values calculated by Mann-Whitney U Test and one-way ANOVA; *p<0.05.

Targeting mETC complex I and III induced cell apoptosis.

To further characterize the effects of targeting the mETC in liver cancer cells, we measured cellular apoptosis following treatment with complex I or complex III inhibitors. Programmed cell death can be studied using various approaches including measuring phosphatidylserine in the outer leaflet of the plasma membrane and the activation of caspases [22]. Following 48 hours treatment of PLC/prf/5 cells with mETC complex I inhibitors (ROT and Met) approximately 18%-20% of the cell displayed apoptosis, whereas cells that underwent depletion of mitochondrial DNA or knockdown of NDUFS1 showed the trend of less sensitive to inhibitor-induced apoptosis as measured I by FACS and Annexin V staining (Figure 5A and 5B). Similar results were obtained using caspase 3 activation as an approach (Figure 5C and 5D). We thus concluded that integrity of the mETC enables the liver cancer cell to counteract apoptosis.

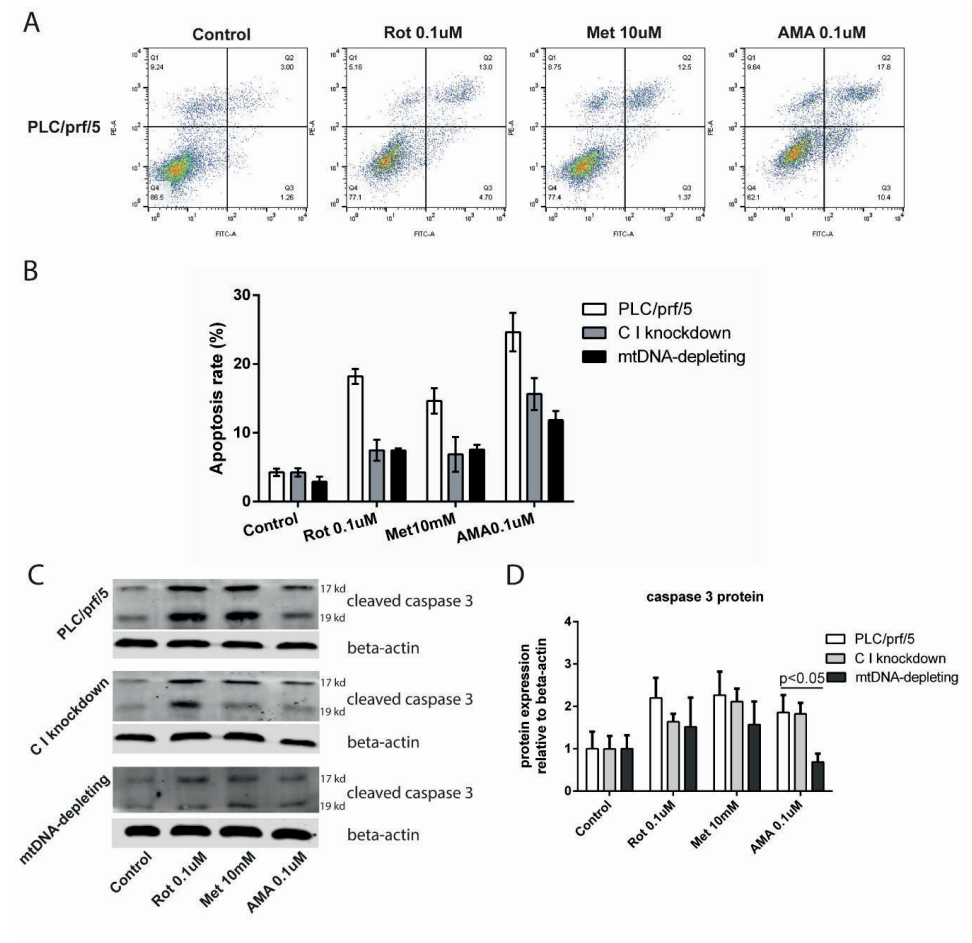


Figure 5. Inhibition of mETC complexes induces apoptosis. (A) Apoptotic cells were quantified by flow cytometry using Annexin V and propidium iodide co-staining in PLC/PRF/5 cells. The effects of 48 hours treatment with ROT, Met or AMA is shown (N = 3). (B) After treating cells with complex I and III inhibitors (ROT, Met and AMA) for 48 hours, the apoptotic rates of three HCC cell lines (PLC/PRF/5, C I knockdown and mtDNA-depleting) were quantified by flow cytometry. The histograms show mean \pm SEM (N = 3). (C and D) Three conditions (PLC/PRF/5, C I knockdown and mtDNA-depleted cells) are shown in presence or absence of ROT, Met and AMA, following a 48 hours incubation. The levels of cleaved-caspase 3 protein were measured by Western blotting analysis and quantified by Image J software. Histograms show mean \pm SEM, with p values calculated by Mann-Whitney U Test.

Inhibition of mETC complex I and III is associated with increased ROS production and decreased ATP generation.

The mETC is major source of mitochondrial ROS generation as up to 2% of electrons leak from the mETC before reaching complex IV and subsequently react with oxygen in a one-electron reduction to produce ROS instead of water molecules [23]. It is well-conceivable that a compromised mETC will result in excessive ROS generation. We measured cellular ROS levels of HCC cells in presence or absence of an mETC complex I inhibitor (ROT) and an mETC complex III inhibitor (AMA). In our experimental system H₂O₂ induced marked ROS production and thus served as a positive control. Our results show that both inhibition of complex I by ROT and complex III by AMA substantially increase cellular ROS levels. In the NDUFS1 knock down cells or cells depleted for mitochondrial DNA, pharmacological inhibitors of the mETC did not show this effect (Figure 6A). It thus appears that pharmacological inhibition of mETC complex I or mETC complex III is associated with increased ROS production.

To further characterise the functionality of the mETC in the physiology of liver cancer cells we also measured cellular ATP levels. As expected, inhibition of the mETC diminished cellular ATP levels (Figure 6B). In toto, our results show a pivotal role for the mETC complex I and mETC complex III in liver cancer cell physiology.

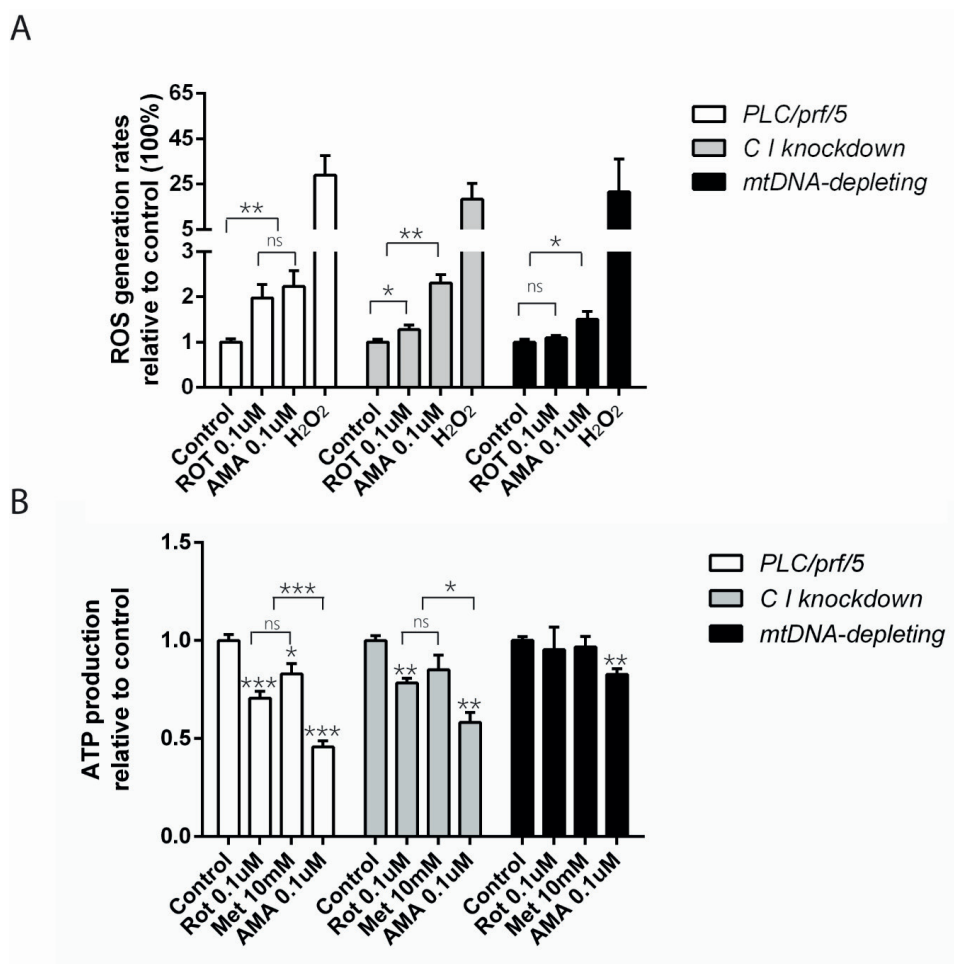


Figure 6. Inhibition of mETC affects cellular metabolism. (A) ROS production was measured after treating cells with ETC complex I (ROT) and III (AMA) inhibitors in three HCC cell lines (PLC/PRF/5 cells, C I knockdown and mtDNA-depletion) (N = 4). (B) After treating with ROT, Met and AMA for 48h respectively, ATP production of PLC/PRF/5 cells, C I knockdown and mtDNA-depletion HCC cells were measured. (N = 9). Histograms are mean \pm SEM, with p values being calculated by Mann-Whitney U Test. *p<0.05; ns, not significant.

Discussion

Liver cancer is a major challenge to global health and clinical options, especially for advanced disease remain highly unsatisfactory [24]. Liver cancer resistance to chemotherapeutic drugs makes is frustrating practitioners everywhere [25]. Increased understanding of liver cancer cell physiology may open novel therapeutic options and in the present study we focus on the role of the liver cancer cell mECT in this respect. We show that various strategies employing different mode of actions that target mETC complex I and III limit the proliferation of liver

cancer cells both in cell line models, in liver cancer organoids and in xenografts in vivo. Mechanistically this is probably linked to mECT inhibition-provoked cancer cell apoptosis, possibly provoked by increased ROS production following such inhibition. Our results provide a proof-of-concept that targeting mETC complex I or mETC complex III is a potential novel avenue for combating liver cancer.

Although intuitively targeting mitochondrial metabolism seems farfetched and potentially fraught with side effects, it is important to note that Metformin (which we also included in the present study) is an already clinically used complex I inhibitor [26]. Clinical experience with Metformin is especially extensive for patients with diabetes type I and its use is associated with a reduced propensity to contract liver cancer in apparent agreement with the effects observed with regard to mETC inhibition in the present study [27]. Generally speaking, the effects of Metformin in cancer are linked to AMPK/mTOR signalling and it should prove interesting to see to which extent the results of the current also relate to this signal transduction module [28]. In apparent support for this notion is the observation that inhibition of mETC complex I or mETC complex III is associated with substantially reduced ATP levels, which is well established to provoke activation of AMPK and inhibition of mTOR [29]. Also in agreement with this idea is that activating mutations upstream of mTOR in TSC are regularly detected in liver cancer, suggesting that this pathway is indeed important for liver cancer development. Intriguingly, however, in an unbiased kinome profiling study we found that the AMPK-provoked activation of TSC leads to the stimulation of p65PAK in addition to mTOR [30,31]. Thus these multiple effector pathways downstream of ATP generation that can mediate the effects observed in the present study.

Alternatively, the effects of mETC complex I and mETC complex III inhibition may relate to increased ROS generation. Increased ROS production as a mechanism counteracting cancer cell growth has now been described in various experimental systems [32-34]. Mechanistically, the role of ROS production in cancer cell physiology remains only partly understood, although ROS-mediated apoptosis appears mediated by apoptosis regulating mitochondrial protein cytochrome C [35,36]. Further experimentation is required to detail the exact mechanisms by which compromising the mETC pushes liver cancer cells into apoptosis. Disregarding the exact mechanisms involved, it is clear from the present study that targeting the mETC is a potential novel viable option for managing liver cancer and future studies should address its clinical promise.

Author Contributions: Q.Yang and M.Li contributed equally and share first authorship.

Funding: This research is supported by a KWF Young Investigator Grant (No. 10140) from the Dutch Cancer Society and a VIDI grant (No. 91719300) from the Netherlands Organization for

Scientific Research (NWO) to Q. Pan. This research is also financially supported by China Scholarship Council PhD fellowship (File No. 201506100033) to Meng Li.

Acknowledgments: We thank Ehsan Shokrollahi and Dr. Nicolaas J. H. Raat from Laboratory of Experimental Anesthesiology of Erasmus MC for facilitating mitochondrial metabolism measurements.

Conflicts of Interest: The author(s) declare no competing interests.

Reference

1. Sia, D.; Villanueva, A.; Friedman, S.L.; Llovet, J.M. Liver Cancer Cell of Origin, Molecular Class, and Effects on Patient Prognosis. *Gastroenterology* **2017**, *152*, 745-761, doi:10.1053/j.gastro.2016.11.048.
2. Forner, A.; Reig, M.; Bruix, J. Hepatocellular carcinoma. *Lancet* **2018**, *391*, 1301-1314, doi:10.1016/S0140-6736(18)30010-2.
3. Porporato, P.E.; Filigheddu, N.; Pedro, J.M.B.; Kroemer, G.; Galluzzi, L. Mitochondrial metabolism and cancer. *Cell Res* **2018**, *28*, 265-280, doi:10.1038/cr.2017.155.
4. Schwartz, L.; Supuran, C.T.; Alfarouk, K.O. The Warburg Effect and the Hallmarks of Cancer. *Anticancer Agents Med Chem* **2017**, *17*, 164-170, doi:10.2174/1871520616666161031143301.
5. Cui, Q.; Wen, S.; Huang, P. Targeting cancer cell mitochondria as a therapeutic approach: recent updates. *Future Med Chem* **2017**, *9*, 929-949, doi:10.4155/fmc-2017-0011.
6. Spinelli, J.B.; Haigis, M.C. The multifaceted contributions of mitochondria to cellular metabolism. *Nat Cell Biol* **2018**, *20*, 745-754, doi:10.1038/s41556-018-0124-1.
7. de Jongh, H.H.; Ritsema, T.; Killian, J.A. Lipid specificity for membrane mediated partial unfolding of cytochrome c. *FEBS Lett* **1995**, *360*, 255-260, doi:10.1016/0014-5793(95)00115-p.
8. Tielens, A.G.; Van Hellemond, J.J. The electron transport chain in anaerobically functioning eukaryotes. *Biochim Biophys Acta* **1998**, *1365*, 71-78, doi:10.1016/s0005-2728(98)00045-0.
9. Wheaton, W.W.; Weinberg, S.E.; Hamanaka, R.B.; Soberanes, S.; Sullivan, L.B.; Anso, E.; Glasauer, A.; Dufour, E.; Mutlu, G.M.; Budigner, G.S., et al. Metformin inhibits mitochondrial complex I of cancer cells to reduce tumorigenesis. *Elife* **2014**, *3*, e02242, doi:10.7554/eLife.02242.
10. Urra, F.A.; Weiss-Lopez, B.; Araya-Maturana, R. Determinants of Anti-Cancer Effect of Mitochondrial Electron Transport Chain Inhibitors: Bioenergetic Profile and Metabolic Flexibility of Cancer Cells. *Curr Pharm Des* **2016**, *22*, 5998-6008, doi:10.2174/1381612822666160719122626.
11. Urra, F.A.; Munoz, F.; Lovy, A.; Cardenas, C. The Mitochondrial Complex(I)ty of Cancer. *Front Oncol* **2017**, *7*, 118, doi:10.3389/fonc.2017.00118.
12. Valko, M.; Leibfritz, D.; Moncol, J.; Cronin, M.T.; Mazur, M.; Telser, J. Free radicals and antioxidants in normal physiological functions and human disease. *Int J Biochem Cell Biol* **2007**, *39*, 44-84, doi:10.1016/j.biocel.2006.07.001.
13. Qu, C.; Zhang, S.; Wang, W.; Li, M.; Wang, Y.; van der Heijde-Mulder, M.; Shokrollahi, E.; Hakim, M.S.; Raat, N.J.H.; Peppelenbosch, M.P., et al. Mitochondrial electron transport chain complex III sustains hepatitis E virus replication and represents an antiviral target. *FASEB J* **2019**, *33*, 1008-1019, doi:10.1096/fj.201800620R.

14. Wang, W.; Xu, L.; Liu, P.; Jairam, K.; Yin, Y.; Chen, K.; Sprengers, D.; Peppelenbosch, M.P.; Pan, Q.; Smits, R. Blocking Wnt Secretion Reduces Growth of Hepatocellular Carcinoma Cell Lines Mostly Independent of beta-Catenin Signaling. *Neoplasia* **2016**, *18*, 711-723, doi:10.1016/j.neo.2016.10.004.
15. Cao, W.; Chen, K.; Bolkestein, M.; Yin, Y.; Verstegen, M.M.A.; Bijvelds, M.J.C.; Wang, W.; Tuysuz, N.; Ten Berge, D.; Sprengers, D., et al. Dynamics of Proliferative and Quiescent Stem Cells in Liver Homeostasis and Injury. *Gastroenterology* **2017**, *153*, 1133-1147, doi:10.1053/j.gastro.2017.07.006.
16. Yin, Y.; Dang, W.; Zhou, X.; Xu, L.; Wang, W.; Cao, W.; Chen, S.; Su, J.; Cai, X.; Xiao, S., et al. PI3K-Akt-mTOR axis sustains rotavirus infection via the 4E-BP1 mediated autophagy pathway and represents an antiviral target. *Virulence* **2018**, *9*, 83-98, doi:10.1080/21505594.2017.1326443.
17. Hernanda, P.Y.; Pedroza-Gonzalez, A.; van der Laan, L.J.; Broker, M.E.; Hoogduijn, M.J.; Ijzermans, J.N.; Bruno, M.J.; Janssen, H.L.; Peppelenbosch, M.P.; Pan, Q. Tumor promotion through the mesenchymal stem cell compartment in human hepatocellular carcinoma. *Carcinogenesis* **2013**, *34*, 2330-2340, doi:10.1093/carcin/bgt210.
18. Li, M.; Wang, L.; Wang, Y.; Zhang, S.; Zhou, G.; Lieshout, R.; Ma, B.; Liu, J.; Qu, C.; Verstegen, M.M.A., et al. Mitochondrial Fusion Via OPA1 and MFN1 Supports Liver Tumor Cell Metabolism and Growth. *Cells* **2020**, *9*, doi:10.3390/cells9010121.
19. Zhou, X.; Wang, Y.; Metselaar, H.J.; Janssen, H.L.; Peppelenbosch, M.P.; Pan, Q. Rapamycin and everolimus facilitate hepatitis E virus replication: revealing a basal defense mechanism of PI3K-PKB-mTOR pathway. *J Hepatol* **2014**, *61*, 746-754, doi:10.1016/j.jhep.2014.05.026.
20. Broutier, L.; Mastrogianni, G.; Verstegen, M.M.; Francies, H.E.; Gavarro, L.M.; Bradshaw, C.R.; Allen, G.E.; Arnes-Benito, R.; Sidorova, O.; Gaspersz, M.P., et al. Human primary liver cancer-derived organoid cultures for disease modeling and drug screening. *Nat Med* **2017**, *23*, 1424-1435, doi:10.1038/nm.4438.
21. Cao, W.; Liu, J.; Wang, L.; Li, M.; Verstegen, M.M.A.; Yin, Y.; Ma, B.; Chen, K.; Bolkestein, M.; Sprengers, D., et al. Modeling liver cancer and therapy responsiveness using organoids derived from primary mouse liver tumors. *Carcinogenesis* **2019**, *40*, 145-154, doi:10.1093/carcin/bgy129.
22. Fiers, W.; Beyaert, R.; Declercq, W.; Vandenabeele, P. More than one way to die: apoptosis, necrosis and reactive oxygen damage. *Oncogene* **1999**, *18*, 7719-7730, doi:10.1038/sj.onc.1203249.
23. Scherz-Shouval, R.; Elazar, Z. ROS, mitochondria and the regulation of autophagy. *Trends Cell Biol* **2007**, *17*, 422-427, doi:10.1016/j.tcb.2007.07.009.
24. Wolter, K.; Zender, L. Therapy-induced senescence - an induced synthetic lethality in liver cancer? *Nat Rev Gastroenterol Hepatol* **2020**, *17*, 135-136, doi:10.1038/s41575-020-0262-3.
25. Zhu, Y.J.; Zheng, B.; Wang, H.Y.; Chen, L. New knowledge of the mechanisms of sorafenib resistance in liver cancer. *Acta Pharmacol Sin* **2017**, *38*, 614-622, doi:10.1038/aps.2017.5.

26. Foretz, M.; Guigas, B.; Viollet, B. Understanding the glucoregulatory mechanisms of metformin in type 2 diabetes mellitus. *Nat Rev Endocrinol* **2019**, *15*, 569-589, doi:10.1038/s41574-019-0242-2.
27. Yu, H.; Zhong, X.; Gao, P.; Shi, J.; Wu, Z.; Guo, Z.; Wang, Z.; Song, Y. The Potential Effect of Metformin on Cancer: An Umbrella Review. *Front Endocrinol (Lausanne)* **2019**, *10*, 617, doi:10.3389/fendo.2019.00617.
28. Korsse, S.E.; Peppelenbosch, M.P.; van Veelen, W. Targeting LKB1 signaling in cancer. *Biochim Biophys Acta* **2013**, *1835*, 194-210, doi:10.1016/j.bbcan.2012.12.006.
29. Saxton, R.A.; Sabatini, D.M. mTOR Signaling in Growth, Metabolism, and Disease. *Cell* **2017**, *168*, 960-976, doi:10.1016/j.cell.2017.02.004.
30. van Baal, J.W.; Diks, S.H.; Wanders, R.J.; Rygiel, A.M.; Milano, F.; Joore, J.; Bergman, J.J.; Peppelenbosch, M.P.; Krishnadath, K.K. Comparison of kinome profiles of Barrett's esophagus with normal squamous esophagus and normal gastric cardia. *Cancer Res* **2006**, *66*, 11605-11612, doi:10.1158/0008-5472.CAN-06-1370.
31. Alves, M.M.; Fuhler, G.M.; Queiroz, K.C.; Scholma, J.; Goorden, S.; Anink, J.; Spek, C.A.; Hoogeveen-Westerveld, M.; Bruno, M.J.; Nellist, M., et al. PAK2 is an effector of TSC1/2 signaling independent of mTOR and a potential therapeutic target for Tuberous Sclerosis Complex. *Sci Rep* **2015**, *5*, 14534, doi:10.1038/srep14534.
32. Corver, W.E.; Demmers, J.; Oosting, J.; Sahraeian, S.; Boot, A.; Ruano, D.; Wezel, T.V.; Morreau, H. ROS-induced near-homozygous genomes in thyroid cancer. *Endocr Relat Cancer* **2018**, *25*, 83-97, doi:10.1530/ERC-17-0288.
33. Teixeira, J.; Basit, F.; Swarts, H.G.; Forkink, M.; Oliveira, P.J.; Willems, P.; Koopman, W.J.H. Extracellular acidification induces ROS- and mPTP-mediated death in HEK293 cells. *Redox Biol* **2018**, *15*, 394-404, doi:10.1016/j.redox.2017.12.018.
34. Han, Y.H.; Park, W.H. Growth inhibition in antimycin A treated-lung cancer Calu-6 cells via inducing a G1 phase arrest and apoptosis. *Lung Cancer* **2009**, *65*, 150-160, doi:10.1016/j.lungcan.2008.11.005.
35. Kalpage, H.A.; Bazylanska, V.; Recanati, M.A.; Fite, A.; Liu, J.; Wan, J.; Mantena, N.; Malek, M.H.; Podgorski, I.; Heath, E.I., et al. Tissue-specific regulation of cytochrome c by post-translational modifications: respiration, the mitochondrial membrane potential, ROS, and apoptosis. *FASEB J* **2019**, *33*, 1540-1553, doi:10.1096/fj.201801417R.
36. Schulze-Osthoff, K.; Bakker, A.C.; Vanhaesebroeck, B.; Beyaert, R.; Jacob, W.A.; Fiers, W. Cytotoxic activity of tumor necrosis factor is mediated by early damage of mitochondrial functions. Evidence for the involvement of mitochondrial radical generation. *J Biol Chem* **1992**, *267*, 5317-5323.

Supplementary data for

The complex I and III of mitochondrial electron transport chain are therapeutically targetable in liver cancer

Meng Li *, Qin Yang *, Jiaye Liu, Changbo Qu, Yang Li, Maikel P. Peppelenbosch and Qiuwei Pan

Table of contents

Supplementary Figure 1

Supplementary Figure 2

Supplementary Table 1

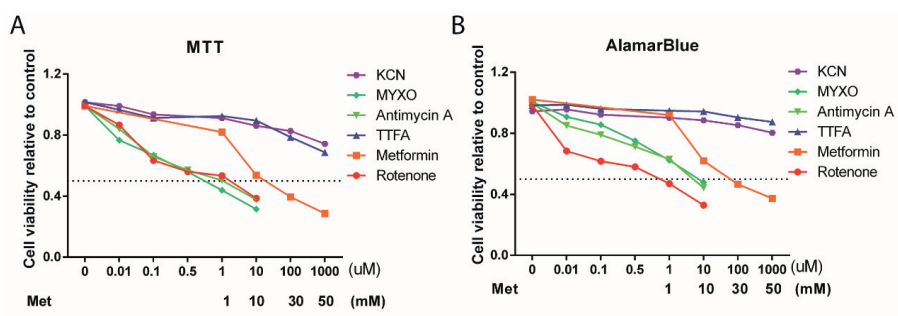


Figure S1. The half maximal inhibitory concentration curve of complex I and III inhibitors.

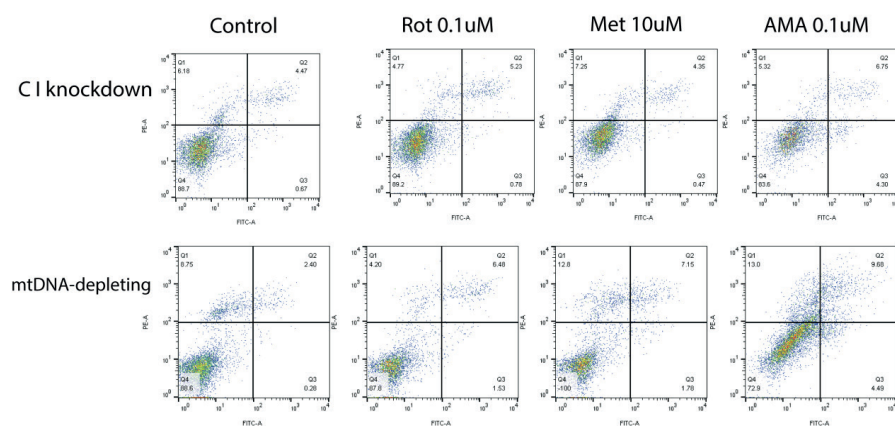


Figure S2. The apoptosis rate in complex I-knockdown and mtDNA-depleted cell lines.

Table S1 Primer sequences used for qRT-PCR

Gene	Forward sequence (5'-3')	Reverse sequence (5'-3')
NDUFS1	TGTGTGAGACGGTGCTGATGGA	CGATGGCTTTCACGATGTCCGT
COX I	CCTGACTGGCATTGTATTAG	GATAGGATGTTTCATGTGGTG
COX II	CATCCCTACGCATCCTTTAC	GGTTTGCTCCACAGATTTCA
COX IV	CAGAAGGCACTGAAGGAGAAG	TCATGTCCAGCATCCTCTTG
CYTB	CCCTAACAACTAGGAGGCG	TCTGCGGCTAGGAGTCAATA
GAPDH	GGAAATCCCATCACCATCT	GGACTCCACGACGTACTCA

CHAPTER 4

Cancer-associated fibroblasts provide a stromal niche for liver cancer organoids that confers trophic effects and therapy resistance

Jiaye Liu¹, Meng Li^{1*}, Pengfei Li^{1*}, Ling Wang^{1*}, Zhouhong Ge¹, Lisanne Noordam¹, Ruby Lieshout², Monique M. A. Verstegen², Buyun Ma¹, Junhong Su¹, Qin Yang^{1,3}, Ruyi Zhang¹, Guoying Zhou¹, Lucia Campos Carrascosa¹, Dave Sprengers¹, Ron Smits¹, Jaap Kwekkeboom¹, Luc J. W. van der Laan², Maikel P. Peppelenbosch¹, Qiuwei Pan¹, Wanlu Cao¹

¹Department of Gastroenterology and Hepatology, Erasmus MC University Medical Center Rotterdam, Rotterdam, The Netherlands.

²Department of Surgery, Erasmus MC University Medical Center Rotterdam, Rotterdam, The Netherlands.

³Department of general Surgery, The Third People's Hospital of Chengdu & the Affiliated Hospital of Southwest Jiaotong University & the Second Medical School of Chengdu affiliated to Chongqing Medical University, Chengdu, China.

In preparation

Background and Aims: Cancer associated fibroblasts (CAFs) play a key role in the cancer process, but progress is hampered by the paucity of preclinical models essential for mechanistic dissection of cancer cell – CAF interactions. Here, we aim to establish 3D organotypic co-cultures primary liver tumor-derived organoids with CAFs, and to establish the role of cancer cell – CAF interaction in liver cancer therapy resistance.

Method: Liver tumor organoids and CAFs were cultured from murine and human primary liver tumors and 3D co-culture models were contrasted to trans-well culture systems with only paracrine interaction between CAFs and cancer cells. A xenograft model was used to interrogate the cell-cell interactions *in vivo*.

Results: Gene expression analysis of CAF markers in tumors of our hepatocellular carcinoma (HCC) cohort and an online liver cancer database reveals reprogramming of liver cancer cell physiology by CAFs. In 3D co-culture models and transwell co-cultures of liver tumor organoids with murine or human CAFs, both effect CAFs mediate trophic effects on cancer cells both through paracrine signaling as well as through direct cell-cell interaction. and of mouse or human origin. *Vice versa*, cancer cells secrete paracrine factors regulating CAF physiology. Co-transplantation of CAFs with liver tumor organoids of mouse or human origin promotes tumor growth in xenograft models and confers therapy resistance to Sorafenib and Regorafenib.

Conclusion: Our results demonstrate the importance of CAF-liver cancer cell interaction for tumor growth and therapy resistance and show that 3D co-culture models allow mechanistic dissection of interactions involved facilitating development of novel rational liver cancer therapy.

Lay summary: Cancer associated fibroblasts (CAFs) are key components of the tumor microenvironment, and actively interact with cancer cells. Here, we developed a novel 3D co-culture model of primary liver tumor-derived organoids with the corresponding CAFs. This will enable the detailed study of the interactions between liver cancer cells with CAFs and help to develop new anti-cancer strategies.

Introduction

Liver cancer is one of the most common and deadly malignancies worldwide and is characterized with remarkable resistance to pharmacological and other therapy of as yet poorly understood origin. [1] A subpopulation of cancer cells within tumors, termed cancer stem cells (CSCs), have been recognized to possess capacity for both self-renewal but also the potential for differentiation and this population of cells appears responsible for resistance to treatment in addition to tumor initiation and progression. [2] Although liver cancer in general remains poorly understood, hopes for obtaining better understanding of this disease have been fostered by the recent development of 3D organoids culture technology. Such cultures, initially derived from tissue-resident stem/progenitor cells, embryonic stem cells (ESCs) or induced pluripotent stem cells (iPSCs), have emerged as technology-of-choice for stem cell research as they are capable of self-renewal and self-organization that recapitulates the functionality of the tissue-of-origin. It has now been successfully employed to culture a variety of primary cancer cells, providing insight into the role of CSCs in the cancer process. [3] For liver cancer, tumor organoids that resemble hepatocellular carcinoma (HCC) or cholangiocarcinoma (CCA) have been successfully cultured from human tumor [4] or mouse tumor models. [5] In general, organoids are much easier to be cultured from CCA than HCC.

Cancer cells, in particular CSCs, actively interact with the tumor microenvironment. This microenvironment contains numerous cell types, including immune cells, fibroblasts and endothelial cells, and various factors including signaling molecules and extracellular matrix (ECM). [6] Among these components, a specialized group of fibroblasts called cancer associated fibroblasts (CAFs) are considered to be of unusual importance to tumor development. Previous studies have identified a serial of CAF markers including alpha-smooth muscle actin (α -SMA), fibroblast associated protein (FAP), Vimentin, fibroblast specific protein 1 (FSP1), CD29, Caveonin 1 (CAV1), Desmin, platelet-derived growth factor receptor alpha (PDGFRA), platelet-derived growth factor receptor beta (PDGFRB), Gremlin1, Collagen, type I, alpha 1 (COL1A1), Periostin and C-X-C motif chemokine 12 (CXCL12). [7-14] CAFs can directly interact with cancer cells, but also secrete a panel of factors and nutrients to support tumor growth, metastasis and formation of cancer stem cell niches, and mediate immunosuppression and drug resistance. [15, 16] More than 80% of HCC patients have the background of liver cirrhosis, [17] and these livers are enriched with activated fibroblasts due to the chronic inflammation that characterizes this disease. Thus, CAFs are assumed to play a prominent role in liver cancer even in the absence of formal proof.

In this study, we first develop a 3D co-culture system of primary liver tumor-derived organoids with CAFs of mouse or human origin. By using this system, we investigated the reciprocal interactions of cancer cells and CAFs, and the role that the CAF niche provides with respect to the nurturing of cancer cells and their importance for treatment resistance of liver cancer cells.

Results

Evidence for clinical significance of CAFs in liver cancer

We first examined the potential clinical relevance of CAFs in liver cancer patients. We quantified the mRNA expression of three well-recognized CAF markers including FAP, CD29 and Periostin in our HCC patient cohort. Their expression is significantly elevated in tumors compared to adjacent liver tissues of the same patients (n=75, Fig. S1A-C). We next analyzed the expression of these CAF markers using the large online TCGA database. Consistently, FAP, CD29 and Periostin are upregulated in tumor compared to tumor free liver tissues (n=400, 364 HCC and 36 CCA, Fig. S1D, G, J). This upregulation is more apparent in late stage of liver cancer (Fig. S1E, H, K). Importantly, high expression of FAP, CD29 or Periostin in tumor tissues is significantly associated with poor overall survival of the patients (Fig. S1F, I, L), although the cancer-specific survival of our HCC patients are not fully in accordance with TCGA database (Fig. S2). Analysis of additional CAF markers revealed the upregulation of several other markers in tumor, although their expression is not associated with patient survival (Fig. S3). These results provided strong evidence for the clinical relevance of CAFs in liver cancer and promoted us to establish experimental models for further investigation.

Construction of 3D co-culture systems of liver tumor organoids with CAFs

For studying the interaction between cancer cells and CAFs, we first explored the construction of 3D organotypic co-culture systems of liver tumor organoids with CAFs. We established 6 mouse tumor organoids from carcinogen N-nitrosodiethylamine (DEN) induced mouse liver tumors and 4 human CCA tumor organoids from resected patient CCA tumors as previously described. [4, 5] CAFs were isolated and cultured from DEN-induced liver tumors of RFP-expression Rosa-mT mice (Fig. S4A), and tumors of HCC and CCA patient (Fig. 1A). As a result, 2 mouse CAFs (2 out of 6 mice), 6 human CAFs (2 out of 3 CCA and 4 out of 10 HCC) were established. CAFs were enriched by plastic adherence and propagated in culture. Both mouse and human CAFs display an elongated, spindle-like morphology (Fig. 1B). Immunofluorescence staining confirmed that most CAFs were positive for α -SMA and FAP (Fig. 1C). We excluded the presence of other cell types including cancer cells, immune cells and endothelial cells by staining with the corresponding makers AFP, EpCAM, CD45 and CD31 (Fig. S4B).

We have successfully established the 3D co-culture of mouse liver tumor organoids with CAFs of mouse origin (Fig. 1D), and co-culture model of patient-derived CCA organoids and CAFs (Fig. 1E, S5). However, the co-cultured organoids and CAFs were not derived from same mice or patients. After three days in co-culture, CAFs become further elongated and gradually formed net-like structure which encircled organoids (Fig. 1F; Fig. S5). Corresponding immunofluorescence images of the culture system of mouse origin are displayed, as these CAFs were derived from RFP expression murine liver tumor (Fig. 1G). By using immunofluorescence staining and 3D reconstructing the Z-stack of confocal images, we further confirmed that CAFs closely surrounded the organoids (Fig. S6A, B).

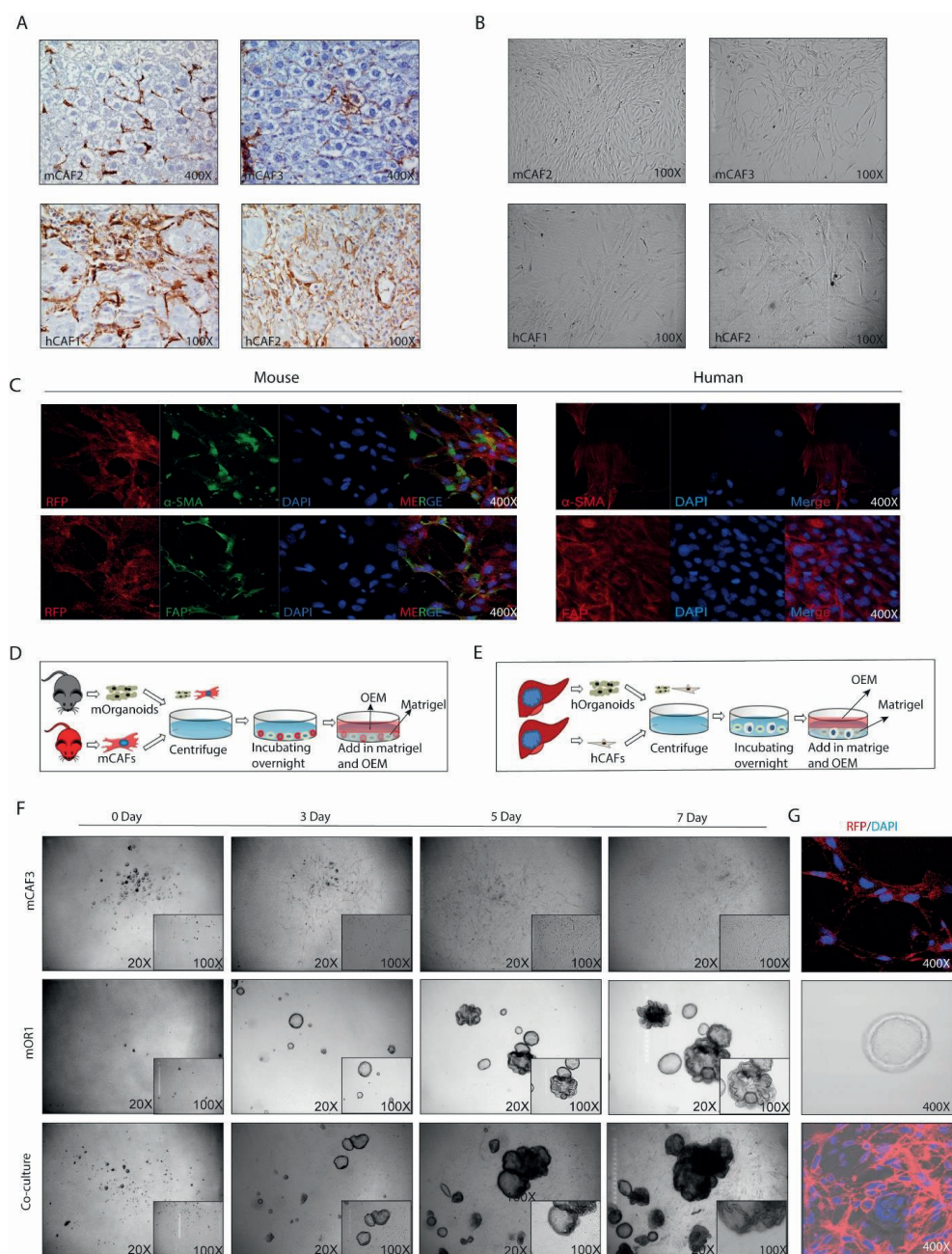


Figure 1. Establishment of cancer associated fibroblasts and liver tumor organoids co-culture models. (A) Representative immunohistochemical (IHC) staining of alpha-SMA in mouse and human primary tissue (Upper image magnification 400X; Lower image 100X). (B) Representative image of established human and mouse CAFs (magnification 50X). (C) Representative immunofluorescence (IF) staining of Alpha-SMA and FAP in mouse and human CAFs (magnification 400X). (D-E) Schematic illustration of the co-culture model of mouse and human origin. (F) Representative image of mouse CAFs, mouse organoids and co-cultures from day 0 to day 7 (magnification 20X, inset magnification 100X). (G) Representative IF staining of mouse CAFs, mouse organoids and co-cultures (magnification 400X).

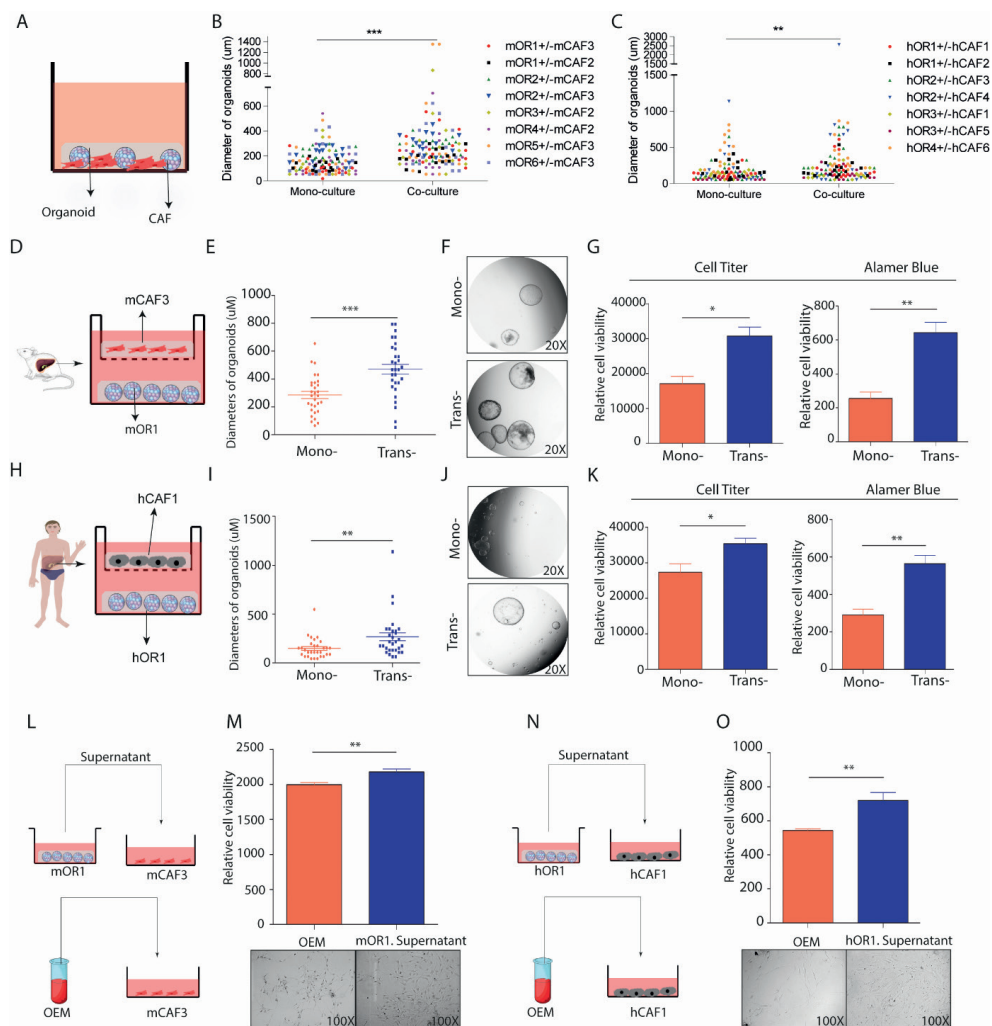


Figure 2. The reciprocal effects of tumor organoids and CAFs. (A) Mouse or human tumor organoids cultured with or without corresponding CAFs. (B) Diameters of mouse organoids cultured with or without mouse CAFs (n=8 with three replicates. Every replicate with diameters of five organoids). (C) Diameters of human organoids cultured with or without human CAFs (n=7 with three replicates. Every replicate with diameters of five organoids). (D) Schematic illustration of trans-well culture platform for mouse cells. (E) Diameters of mouse organoids in trans-well platform with or without CAFs. (F) Representative images of mono-, co-cultured mouse organoids. (G) Growth of mouse liver tumor organoids determined by CellTiter and Alamar Blue Assay. (H) Schematic illustration of trans-well culture platform for human cells. (I) Diameters of human organoids in trans-well platform with or without CAFs. (J) Representative images of mono-, co-cultured human organoids in trans-well platform. (K) Growth of human organoids determined by CellTiter and Alamar Blue Assay. (L-M) Growth of mouse CAFs in the presence or absence of organoids conditioned medium. (N-O) Growth of human CAFs in the presence or absence of organoids conditioned medium. (E, I) Three independent experiments with two replicates. Each replicate contained diameters of five randomly measured organoids in each well. Data were presented as mean \pm SEM, Non-parametric Mann-Whitney *U* tests were used for statistical analysis. ***p*<0.01, ****p*<0.001. (G, K, M, O) Three independent experiments with two replicates. Data were presented as mean \pm SEM, Non-parametric Mann-Whitney *U* tests were used for statistical analysis. **p*<0.05, ***p*<0.01.

CAFs promote the growth of organoids in co-culture

After co-culturing digested single organoid cells with CAFs of mouse origin for 7 days and those of human origin for 14 days, we counted the number of formed organoids and randomly measured the diameter of five organoids in each well (Fig. S7A). We verified the accuracy of our measurement by measuring the diameter both under immunofluorescence and bright field vision (Fig. S7B). We found that co-culturing CAFs did not affect the number (Fig. S8A, S9A), but enlarged the size of formed organoids (Fig. 2A-C; Fig. S8B-G, S9B-G). This effect was already apparent at a 1:1 ratio input of organoid and CAF cells, but was not enhanced by further increasing the input of CAFs (Fig. S10A, B). Therefore, these results suggest that CAFs may not regulate the efficiency of organoid initiation, but promote the growth of formed organoids in the co-culture system.

Reciprocal enhancement of CAFs and tumor organoids growth through paracrine signaling

The aforementioned results were demonstrated in a co-culture system, but this does not exclude the possibility of paracrine effects. To investigate this, we established a trans-well system in which CAFs were seeded on the top and organoids on the bottom layer (Fig. 2D). After incubation for 10 days, we found that CAFs did not affect the number (Fig. S12G, H), but, reminiscent to co-cultures, increased the diameter of formed organoids in the setting of cells of mouse origin (Fig. 2E, F). Cell Titer Assay and Alamar Blue Assay further confirmed these results (Fig. 2G). Same results were observed in the setting of other combination of mouse cells as well as cells of human origin (Fig. 2H-K, Fig. S11-12). Interestingly, several stem cell markers including Lrig1, Muc5ac, CD133, TERT, NANOG were upregulated in mouse organoids by the paracrine effect of CAFs (Fig. S13). But this was not observed in human organoids (Fig. S14).

Next, we examined the reverse effect by exposing CAFs to the conditioned medium of tumor organoids (Fig. 2L, N). We found that education with soluble factors from tumor organoids significantly promoted the growth of CAFs (Fig. 2M, O). Profiling a panel of potential CAFs makers revealed that Gremlin1 was upregulated in both mouse and human CAFs (Fig. S15, 16). Previous studies documented that gremlin1 suppresses the function of BMPs, which may help maintaining the tumor stemness. [18] Thus, CAFs and organoids reciprocally facilitate their growth -at least partially- through paracrine signaling.

CAFs promote the growth of organoids-formed tumors in mice

We have previously demonstrated that liver tumor organoids are capable of forming tumors upon subcutaneous transplantation in immunodeficient mice.[5] We thus investigated the effects of CAFs on organoids-based tumor formation and growth *in vivo* (Fig. 3A). We found that co-transplantation of organoids with CAFs lead to more efficient tumor formation (12/12) than transplanting mouse organoids alone (9/12) (Fig. 3B). More importantly, co-transplantation resulted in much larger tumors compared to transplanting organoids alone (tumor weight $0.60 \pm 0.31g$, $n=12$, VS. $0.33 \pm 0.13g$, $n=9$, $p<0.05$, Fig. 3C). Immunohistochemistry

and immunofluorescence staining confirmed the presence of CAFs in the tumor tissue of mice co-transplanted with CAFs (Fig. 3D-F). Interestingly, CAFs are also abundantly present in the tumors of control mice transplanted with organoids alone (Fig. 3D-F), suggesting that tumor organoids and the formed tumors can efficiently recruit endogenous CAFs. As the transplanted CAFs express RFP, we were able to separate the transplanted CAFs and endogenous CAFs by using FACS. Their expression patterns of the CAF markers are indeed substantially different (Fig. S17).

Consistently, co-transplantation with human CAFs also promoted tumor formation and growth of patient CCA organoids in mice (Fig. 4A-C). Immunohistochemistry and immunofluorescence staining confirmed the presence of CAFs in the tumors (Fig. 4D-F). We next isolated the *in vivo* educated human CAFs from the tumors and compared their gene expression with *in vitro* cultured CAFs. We found a distinct expression pattern of the CAF markers (Fig. S18). Taken together, CAFs support organoids-based tumor formation and growth *in vivo*.

CAFs protect tumor organoids from drug treatment

We next examined the effects of CAFs on the response of tumor organoids to the anti-HCC drug Sorafenib and Regorafenib. Mouse liver tumor organoids were treated with Sorafenib or Regorafenib in the presence or absence of CAFs (Fig. 5A). Although the number of formed organoids are not significantly different, the diameters of organoids are significantly larger when co-culture with CAFs compared with organoids alone (Fig. 5B-F). Of note, most of the organoids that survived from the treatment were surrounded by CAFs (Fig. 5G, H). These results were further confirmed in human liver tumor organoids, treated with Sorafenib or Regorafenib in the presence or absence of human CAFs (Fig. 5I-N).

To investigate whether these effects are related to paracrine signaling, both mouse and human organoids were exposed to conditioned medium of pretreated-CAFs and treated with Sorafenib or Regorafenib (Fig. 6A, H). Interestingly, organoids in the presence of educated-CAF conditioned medium are more resistant to the treatment, as shown by higher half maximal inhibitory concentrations (IC₅₀) (Fig. 6B, E, I, L), and the morphological appearance (Fig. 6C, F, J, M). A dynamic response of treatment at different time points revealed similar pattern of resistance in the presence of CAF conditioned medium (Fig. 6D, G, K, N). Taken together, these findings demonstrate that CAFs protect tumor organoids from anti-cancer treatment.

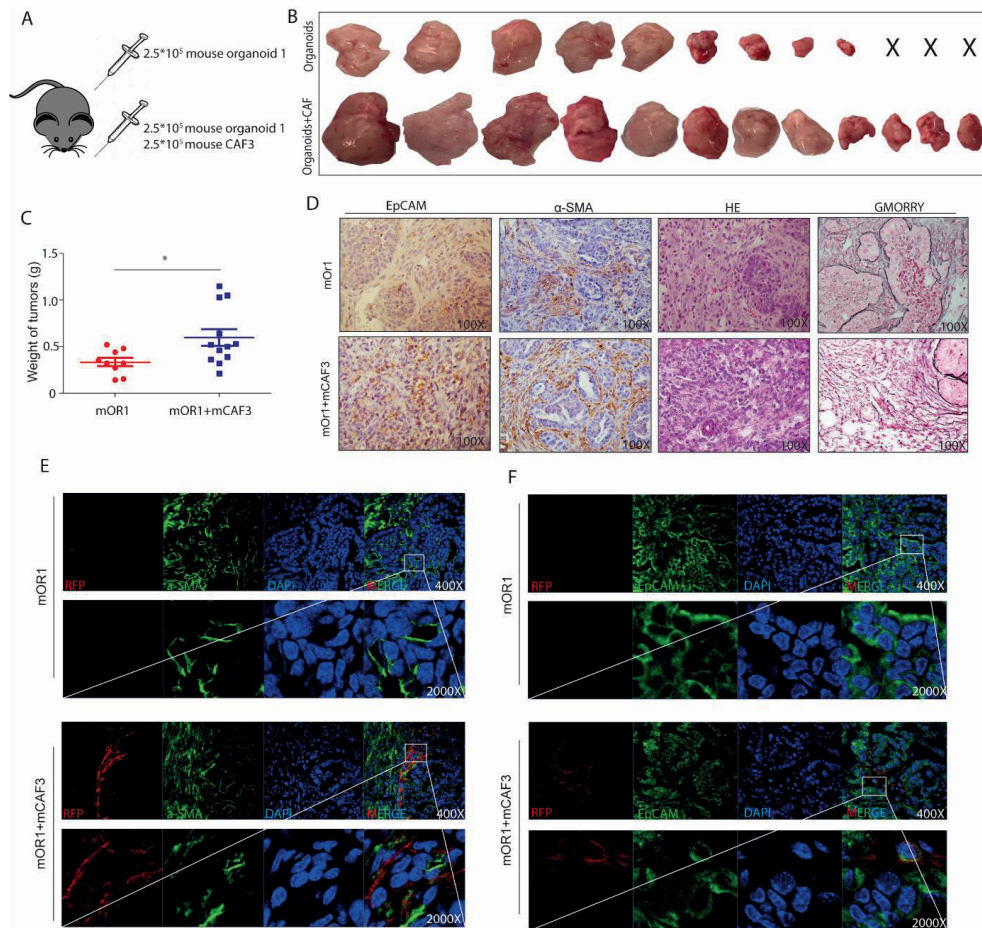


Figure 3. Mouse CAFs promote the growth of mouse organoids formed tumors *in vivo*. (A) 2.5×10^5 mouse tumor organoids together with or without 2.5×10^5 mouse CAFs were transplanted into NSG mouse. (B) Representative pictures showed the tumors from mono- and co-transplantation. (C) The weight of tumors from mono- or co-transplantation ($n=9$, data were presented as mean \pm SEM, Non-parametric Mann-Whitney U tests were used for statistical analysis, * $P < 0.05$). (D) The representative IHC staining of EpCAM, α -SMA, H&E and Gmorry for tumors from mono- or co-transplantation (magnification 100X). (E) The representative confocal image of α -SMA expression for tumors from mono- or co-transplantation (magnification 400X, inset magnification 2000X). (F) The representative confocal image of EpCAM expression for tumors from mono- or co-transplantation (magnification 400X, inset magnification 2000X).

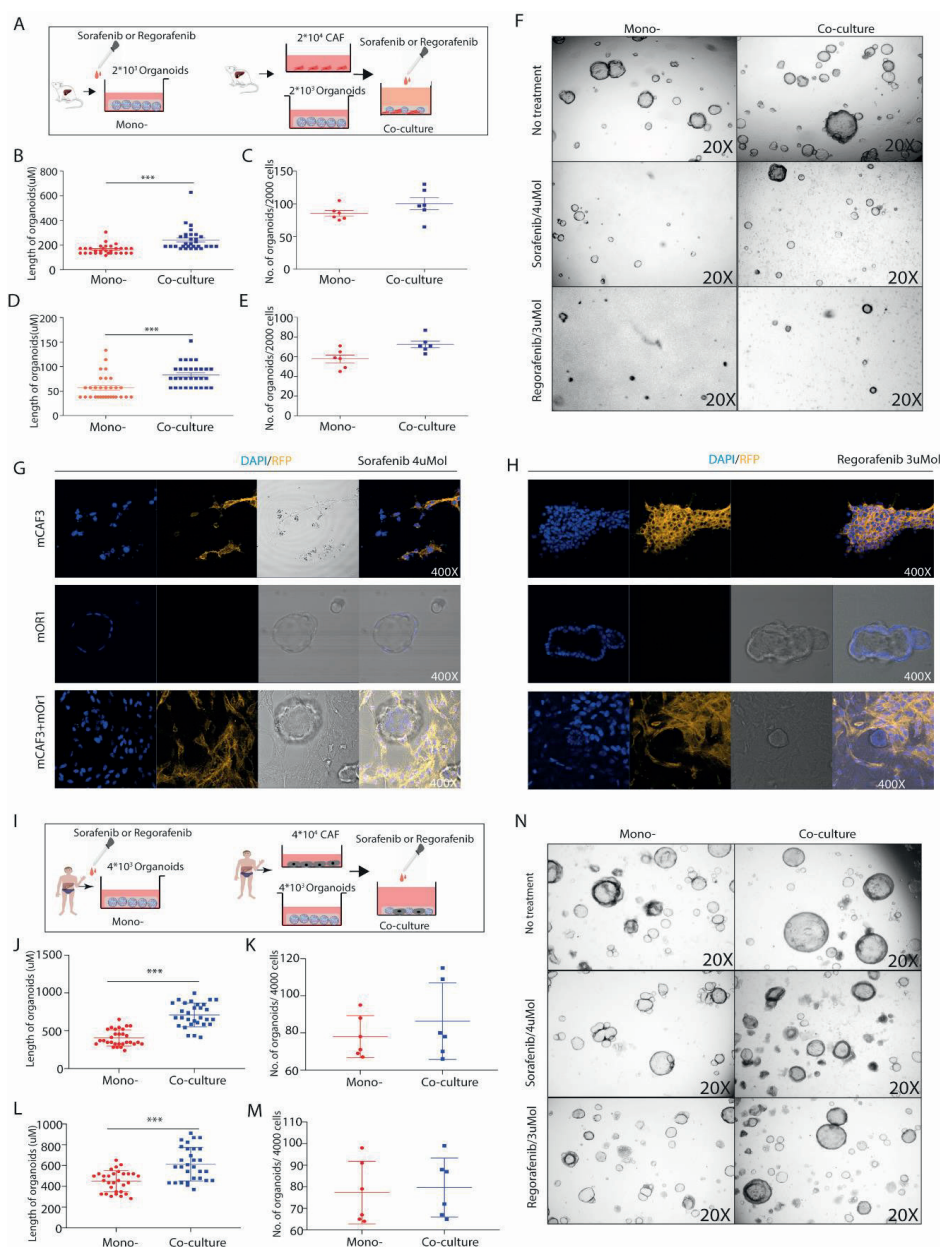


Figure 5. Organoids in the presence or absence of CAFs in response to anti-HCC drugs. (A) An outline of the experimental strategy used to illustrate the drug administration on tumor organoids with or without CAFs. (B-E) Mouse organoids in response to treatment of Sorafenib (4 uM/ml) or Regorafenib (3.5 uM/ml) with or without CAFs. (F) Representative image of treatment for mouse mono-culture and co-culture. (G-H) Representative confocal image of mouse CAFs, organoids and co-cultures in response to treatment of Sorafenib and Regorafenib. (I) An outline of the experimental strategy used to illustrate the drug treatment on tumor organoids with or without CAFs. (J-M) Human organoids in response to treatment of Sorafenib (4 uM/ml) or Regorafenib (3.5 uM/ml) with or without CAFs. (N) Representative image of human mono-culture and co-culture with or without treatment. (B, D, J, L) Three independent experiments with two replicates, each replicate contained diameters of five randomly measured organoids in each well. Data were presented as mean ± SEM, Non-parametric Mann-Whitney U

tests were used for statistical analysis.***P<0.001. (C, E, K, M) Three independent experiments with two replicates. Data were presented as mean \pm SEM, Non-parametric Mann-Whitney *U* tests were used for statistical analysis.

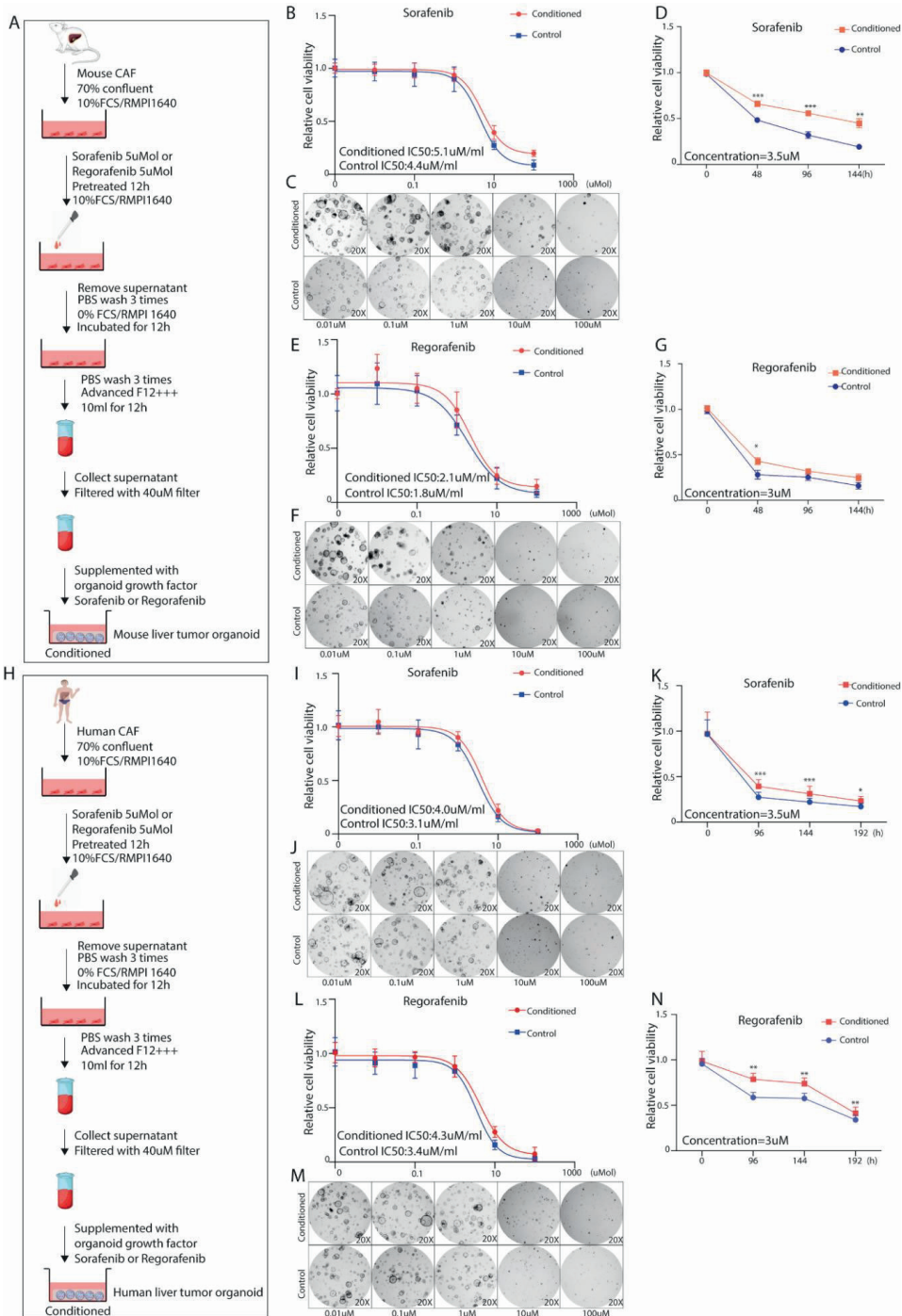


Figure 6. Organoids in the presence or absence of conditioned medium of educated CAFs in response to the anti-HCC treatment. (A, H) An outline of the experimental strategy used to illustrate drug treatment on tumor organoids with or without conditioned medium of educated CAFs. (B, E, I, L) Organoids in the presence or absence of conditioned medium of educated CAFs were treated with a serial concentration of Sorafenib or Regorafenib, and the half maximal inhibitory concentration (IC50) was determined. (C, F, J, M) Representative image of mouse or human tumor organoids in the presence or absence of conditioned medium of educated CAFs, treated with a serial concentration of Sorafenib or Regorafenib for 10 days of mouse cells and 14 days of human cells. (D, G, K, N) Cell viability assays were performed and measured at the indicated times, using mouse or human tumor organoids incubated with indicated anti-cancer drugs and parenthesized concentration in the presence or absence of conditioned medium of educated CAFs. Three independents with two replicates. Graphs show means \pm SEM of data normalized to $t=0$. Non-parametric Mann-Whitney *U* tests were used for statistical analysis, **P*<0.05, ***P*<0.01, ****P*<0.001.

Materials and methods

Mouse liver tumor organoid culture

Mouse liver tumor organoids were cultured from DEN-treated LGR5-DTR mice with histologically verified liver tumors. Tumor tissue was minced and digested with a digestion solution: Collagenase type XI (0.5mg/ml, Sigma Aldrich), Dispase (0.2mg/ml, Gibco), 1% fetal bovine serum in Dulbecco's modified Eagle's medium (DMEM, Lonza) (37°C, 30mins). The tissue debris was allowed to settle, and the dissociated cells were pelleted and washed in Advanced DMEM/F12 (Invitrogen) and seeded in Matrigel (BD bioscience). After the Matrigel became solid, expansion medium was slowly added in. Mouse organoid expansion medium (OEM) was based on mouse organoid basic medium (OBM, Advanced DMEM/F12 supplemented with 1% Penicillin/Streptomycin, 1% Glutamax, 10 mM HEPES), B27(2% vol/vol), N2 (1%, vol/vol, Invitrogen), N-acetylcysteine (1.25 μ M, Sigma–Aldrich), gastrin (10 nM, Sigma Aldrich), epidermal growth factor (EGF, 50 ng/ml, PeproTech), R-spondin 1 (10% vol/vol, conditioned medium produced by 293T-H-Rspol-Fc cell line), fibroblast growth factor 10 (FGF10, 100 ng/ml, PeproTech), nicotinamide (10 mM, Sigma–Aldrich) and hepatocyte growth factor (HGF, 50 ng/ml, PeproTech). For the initial 3 days, the organoids were cultured with organoid initiation medium (OIM) supplemented with Noggin (10% vol/vol, conditioned medium produced by 293T-HA-Noggin cell line), Wnt3a (10% vol/vol, conditioned medium produced by L-Wnt3a cell line), and Y-27632 (10.5 μ M, Sigma-Aldrich).

To passage, cold OBM was used to collect the organoids. Organoids were mechanically dissociated into small pieces by pipetting, and then seeded back into fresh Matrigel again. Passaging was performed at a ratio from 1:6~1:10 per week according to the growth of the organoids. To create frozen stocks, organoids were passaged and mixed with Freeze medium (90% FBS supplemented with 10% DMSO) using standard procedures. Cultures were thawed using standard thawing procedures, washed once with OBM, and seeded in Matrigel with OIM for the first passage.

Isolation and culture of mouse CAFs

Mouse CAFs were isolated from DEN-induced Rosa26-mT mice with histologically verified liver tumors. CAFs were isolated by using an outgrowth isolation. Tissue from tumor edge was minced and digested with a digestion solution: Collagenase type XI (0.5mg/ml, Sigma Aldrich), Dispase (0.2mg/ml, Gibco), 1% fetal bovine serum in Dulbecco's modified Eagle's medium (DMEM, Lonza) for 30mins to 2 hours at 37 °C in a water bath. Then the sample was filtered by using a filter tip and subsequently quenched in 10% FCS RPMI 1640 medium. The pellet that contained tumor debris was plated in a T25 flask and fibroblast was allowed to grow out and attached to the wall of the flask. To avoid cancer cell contamination, established cell culture was passed at least 3 generations. The medium was changed every 2 days. CAFs were sub-cultured when 80% confluent, banked and used for experimental studies at passages 4-8. The fibroblasts were checked by using immunofluorescence of staining of the fibroblast markers α -SMA and FAP and negative staining for the HCC cell, epithelial cell marker (AFP and EpCAM), endothelial marker (CD31) and immune cell marker (CD45) to exclude contamination of other cells types before subjected to experiments.

Human CCA organoids and CAF culture

OEM for culturing human CCA organoids was based upon OBM, B27(2% vol/vol), N2 (1% vol/vol, Invitrogen), N-acetylcysteine (1.25 μ M, Sigma–Aldrich), gastrin (10 nM, Sigma Aldrich), Rspo-1 conditioned medium(10% vol/vol), 10mM nicotinamide, recombinant human EGF (50ng/ml), recombinant human FGF10 (100ng/ml), recombinant human HGF (25ng/ml), 10 μ M Forskolin, 5 μ M A8301, and 10 μ M Y27632. Upon attainment of dense tumor-derived organoids (2-3 weeks after isolation), they were passaged by mechanical dissociation into small fragments via trituration with pipet, and transferred to fresh Matrigel in the previously defined OEM. Medium was refreshed every 2–3 days and organoids were passaged in 1:2–1:10 split ratio according to the growth of the organoids.

For isolation and culture of human CAFs from HCC and CCA tumors, the protocol was similar as isolation and culture of mouse CAFs. The study was approved by the medical ethical committee of Erasmus Medical Center. In addition, the study protocol conforms to the ethical guidelines of the 1975 Declaration of Helsinki.

Co-culture of tumor organoids and CAFs

Cold OBM was used to collect the organoids. Organoids were mechanically dissociated into small pieces by pipetting (20-30 times) and further digested into single cells by Trypsin-EDTA (gibco, 37°C, 2 min). Fluorescence-activated cell sorting sorter (BD FACS Aria™ II) was used to further isolate the single living cells. Propidium iodide staining was used to exclude dead cells. Forward scattered light-width (FSC-Width) with FSC-Area and then side scattered light-width (SSC-Width) with SSC-Area gates were used to select the single cells. CAFs were collected when they were 80% fluent in the flask. After digesting into single cell, fluorescence-activated cell sorting sorter was used to further isolate the single living cells. For co-cultures, different concentrations between CAFs and tumor organoids cells were sorted into 48 wells

or 96 wells plates with OBM contained 1% Matrigel. Then the cells were centrifuged in 1000rpm for three minutes and incubated in the plate overnight. The supernatant was removed on the second day and coated plastic surface of the cells with Matrigel to provide biomatrix for 3-D organoid growth. When Matrigel became solid, mouse OEM or human OEM were added. After co-culturing for 7-14 days, the diameters of organoids was performed on confocal microscope (Leica Sp5) by using a scale tool.

Statistics analysis

Prism software (GraphPad Software) was used for all statistical analysis. For statistical significance of the differences between groups, we used Mann-Whitney U-test. For Differences were considered significant at a *P* value less than 0.05.

For additional methods, please refer to supplementary file.

Discussion

CAFs as a vital component of the tumor microenvironment have been extensively demonstrated to support cancer development and progression, and to promote treatment resistance. [19, 20] The clinical significance of CAFs in disease progression, therapeutic response and patient outcome has been widely reported in various types of cancer. [21-23] In this study, we found that enhanced expression of CAF markers in liver tumors are associated with poor patient outcome. Contemporary, a major challenge is how to dissect the interactions of cancer cells with CAFs in robust experimental models. We successfully established 3D co-culture systems of liver tumor organoids and CAFs of both mouse and human origins to study the interactions between these two cell types.

A prominent role of CAFs is thought to shape the stem cell niche to nurture CSCs, whereas the conventional 2D culture of immortalized cancer cell lines is far from satisfactory in recapitulating the properties of CSCs. [24, 25] The recent development of organoids technology that grows embryonic or adult mammalian stem cells-derived 3D organotypic structures *in vitro* has greatly facilitated stem cell research. This now has been extended to the culture of primary cancer cells that recapitulates the genomic and structural architecture of the tumor-of-origin, and especially CSC compartment. [26] Tumor organoids have been successfully established across variety of cancer types, including liver cancer. [4, 5] The co-culture model of organoids with CAFs was first pioneered in pancreatic cancer, as pancreatic cancer has the most extensive stromal reaction accounting for up to 90% of the tumor volume. [27, 28] In this study, we established the co-culture of liver tumor organoids with CAFs. We first cultured organoids and CAFs from DEN-induced mouse liver tumors. We have recently shown that these organoids can recapitulate the heterogeneity of patient liver cancer types to some extent. [5] For patient liver cancer, organoids are much easier to be cultured from CCA compared to HCC, [4] and therefore we used CCA organoids for establishing the model. Our model systems shall enable the detailed study of interactions between liver cancer cells, especially CSCs, with CAFs.

CAFs secrete a variety of cytokines, chemokines and growth factors to create a tumor-permissive microenvironment. [29] Many factors like CCL-5, CXCL12, TGF β , insulin-like growth factors (IGF), epidermal growth factors (EGF), FGF, IL-6, IL-8, IL-10 and IL-11 secreted by CAFs have an essential role in regulating cancer development. [21, 24, 30-36] In addition to biochemical crosstalk, direct contact between CAFs and cancer cells also play a critical role in tumor progression. By ECM remodeling, CAFs facilitate the migration of cancer cells. [37] On the other hand, CAFs directly exert a pulling force on cancer cells through epithelial to mesenchymal transition (EMT) by mediating N-cadherin and E-cadherin expression. [38] These results are in accordance with our findings that CAFs confer growth advantages of tumor organoids in co-culture with cell-cell contact and in a trans-well system via paracrine signaling. Furthermore, co-transplantation with CAFs promotes organoids-based tumor formation and growth in mice. In pancreatic tumor organoids, a Wnt-non-producing subtype requires Wnt

ligands from CAFs. [27] CAF-derived HGF has been reported to regulate liver tumor initiating cells via activation of FRAI in an Erk1, 2-dependent manner. [39] In our model, the exact contribution of paracrine signaling and physical interaction, and the underline molecular mechanisms, remain to be further

Development of drug-resistance is a relentless clinical challenge for cancer treatment. [40] This re-enables tumor growth, cancer cell dissemination and early onset of metastasis. Studies on the mechanisms of therapy resistance have primarily focused on the intrinsic properties of tumor cells. Emerging evidence has redirected to the role of the organ/tumor-specific microenvironment for developing drug resistance. CAFs contribute to treatment resistance mainly through impaired drug delivery and biochemical signaling. Remodeled ECM by CAFs acts as a physical barrier to inhibit the uptake of anti-cancer drugs by increasing intratumoral interstitial fluid pressures and inducing vascular collapse. [41, 42] CAFs-derived soluble factors including IL-6, IL-17A, IGF1, IGF2 and nitric oxide can indirectly mediate the development of cancer treatment resistance. [41, 43-45] Our study revealed that co-culture with CAFs confer resistance of liver tumor organoids to the clinically used anti-cancer drug Sorafenib and Regorafenib. This effect was recapitulated by adding conditioned medium from Sorafenib or Regorafenib pre-educated CAFs. However, whether this effect occurs *in vivo* and the involved molecular mechanisms remain to be further studied.

A recent study has shown that the CAF population is implicated in immune dysregulation and associated with immunotherapy outcome in melanoma patients. [46] Interestingly, cultured CAFs from colon tumor, as well as lung cancer, have been reported to express immune checkpoint molecule programmed death 1 ligand 1/2 (PDL-1 /2), which strongly induce T cell exhaustion. [47, 48] CAFs may also indirectly regulate the immune response through ECM remodeling by acting as a barrier which block the access of immune cells to cancer cells. [49] A co-culture model with human pancreatic cancer organoids, matched stromal and immune cells has been recently developed. Thus, we call the further advance of our models by incorporating immune cells that shall enable the study of tumor-stroma and tumor immune interaction and the assessment of immunotherapeutic such as checkpoint inhibitors in the context of T-cell infiltration. [50] Because the clinical benefits of immune-based therapies for HCC are evident, and ongoing clinical trials will soon establish their role in management of HCC patients. [51]

In summary, we have successfully established 3D co-culture models of liver tumor organoids with CAFs of mouse or human origin. We have revealed the robust effects of CAFs in liver cancer nurturing and treatment resistance. These model systems will be helpful for future research on the interactions of liver cancer cells with the stromal compartment and facilitate therapeutic development.

Author Contributions: P Li, L Wang and M Li contributed equally and share co-second authorship.

Conflicts of Interest: The author(s) declare no competing interests.

References

- [1] Liu J, Dang H, Wang XW. The significance of intertumor and intratumor heterogeneity in liver cancer. *Exp Mol Med* 2018;50:e416.
- [2] Batlle E, Clevers H. Cancer stem cells revisited. *Nat Med* 2017;23:1124-1134.
- [3] Tuveson D, Clevers H. Cancer modeling meets human organoid technology. *Science* 2019;364:952-955.
- [4] Broutier L, Mastrogiorganni G, Verstegen MM, Francies HE, Gavarro LM, Bradshaw CR, et al. Human primary liver cancer-derived organoid cultures for disease modeling and drug screening. *Nat Med* 2017;23:1424-1435.
- [5] Cao W, Liu J, Wang L, Li M, Verstegen MMA, Yin Y, et al. Modeling liver cancer and therapy responsiveness using organoids derived from primary mouse liver tumors. *Carcinogenesis* 2019;40:145-154.
- [6] Giraldo NA, Becht E, Remark R, Damotte D, Sautes-Fridman C, Fridman WH. The immune contexture of primary and metastatic human tumours. *Current Opinion in Immunology* 2014;27:8-15.
- [7] Kalluri R. The biology and function of fibroblasts in cancer. *Nature Reviews Cancer* 2016;16:582-598.
- [8] Arnold JN, Magiera L, Kraman M, Fearon DT. Tumoral immune suppression by macrophages expressing fibroblast activation protein-alpha and heme oxygenase-1. *Cancer Immunology Research* 2014;2:121-126.
- [9] Weissmueller S, Manchado E, Saborowski M, Morris JPt, Wagenblast E, Davis CA, et al. Mutant p53 drives pancreatic cancer metastasis through cell-autonomous PDGF receptor beta signaling. *Cell* 2014;157:382-394.
- [10] Cadamuro M, Nardo G, Indraccolo S, Dall'olmo L, Sambado L, Moserle L, et al. Platelet-derived growth factor-D and Rho GTPases regulate recruitment of cancer-associated fibroblasts in cholangiocarcinoma. *Hepatology* 2013;58:1042-1053.
- [11] Koliarakis V, Pallangyo CK, Greten FR, Kollias G. Mesenchymal Cells in Colon Cancer. *Gastroenterology* 2017;152:964-979.
- [12] Sugimoto H, Mundel TM, Kieran MW, Kalluri R. Identification of fibroblast heterogeneity in the tumor microenvironment. *Cancer Biol Ther* 2006;5:1640-1646.
- [13] Record Owner NLM. Fibroblast-specific protein 1 identifies an inflammatory subpopulation of macrophages in the liver.
- [14] Liu AY, Zheng H, Ouyang G. Periostin, a multifunctional matricellular protein in inflammatory and tumor microenvironments. *Matrix Biol* 2014;37:150-156.

- [15] Multhaupt HA, Leitingner B, Gullberg D, Couchman JR. Extracellular matrix component signaling in cancer. *Advanced Drug Delivery Reviews* 2016;97:28-40.
- [16] Record Owner NLM. CD10 GPR77 Cancer-Associated Fibroblasts Promote Cancer Formation and Chemoresistance by Sustaining Cancer Stemness.
- [17] Fattovich G, Stroffolini T, Zagni I, Donato F. Hepatocellular carcinoma in cirrhosis: incidence and risk factors. *Gastroenterology* 2004;127:S35-50.
- [18] Ren J, Smid M, Iaria J, Salvatori DCF, van Dam H, Zhu HJ, et al. Cancer-associated fibroblast-derived Gremlin 1 promotes breast cancer progression. *Breast Cancer Res* 2019;21:109.
- [19] Xiong S, Wang R, Chen Q, Luo J, Wang J, Zhao Z, et al. Cancer-associated fibroblasts promote stem cell-like properties of hepatocellular carcinoma cells through IL-6/STAT3/Notch signaling. *Am J Cancer Res* 2018;8:302-316.
- [20] Fang T, Lv H, Lv G, Li T, Wang C, Han Q, et al. Tumor-derived exosomal miR-1247-3p induces cancer-associated fibroblast activation to foster lung metastasis of liver cancer. *Nature communications* 2018;9:191.
- [21] Chen WJ, Ho CC, Chang YL, Chen HY, Lin CA, Ling TY, et al. Cancer-associated fibroblasts regulate the plasticity of lung cancer stemness via paracrine signalling. *Nature communications* 2014;5:3472.
- [22] Ebbing EA, van der Zalm AP, Steins A, Creemers A, Hermsen S, Rentenaar R, et al. Stromal-derived interleukin 6 drives epithelial-to-mesenchymal transition and therapy resistance in esophageal adenocarcinoma. *Proc Natl Acad Sci U S A* 2019;116:2237-2242.
- [23] Hu G, Wang S, Xu F, Ding Q, Chen W, Zhong K, et al. Tumor-Infiltrating Podoplanin+ Fibroblasts Predict Worse Outcome in Solid Tumors. *Cell Physiol Biochem* 2018;51:1041-1050.
- [24] Su S, Chen J, Yao H, Liu J, Yu S, Lao L, et al. CD10(+)/GPR77(+) Cancer-Associated Fibroblasts Promote Cancer Formation and Chemoresistance by Sustaining Cancer Stemness. *Cell* 2018;172:841-856 e816.
- [25] Lenos KJ, Miedema DM, Lodestijn SC, Nijman LE, van den Bosch T, Romero Ros X, et al. Stem cell functionality is microenvironmentally defined during tumour expansion and therapy response in colon cancer. *Nat Cell Biol* 2018;20:1193-1202.
- [26] Clevers H. Modeling Development and Disease with Organoids. *Cell* 2016;165:1586-1597.
- [27] Seino T, Kawasaki S, Shimokawa M, Tamagawa H, Toshimitsu K, Fujii M, et al. Human Pancreatic Tumor Organoids Reveal Loss of Stem Cell Niche Factor Dependence during Disease Progression. *Cell Stem Cell* 2018;22:454-467 e456.
- [28] Ohlund D, Handly-Santana A, Biffi G, Elyada E, Almeida AS, Ponz-Sarvisé M, et al. Distinct populations of inflammatory fibroblasts and myofibroblasts in pancreatic cancer. *J Exp Med* 2017;214:579-596.

- [29] Yamamura Y, Asai N, Enomoto A, Kato T, Mii S, Kondo Y, et al. Akt-Girdin signaling in cancer-associated fibroblasts contributes to tumor progression. *Cancer Res* 2015;75:813-823.
- [30] Orimo A, Gupta PB, Sgroi DC, Arenzana-Seisdedos F, Delaunay T, Naeem R, et al. Stromal fibroblasts present in invasive human breast carcinomas promote tumor growth and angiogenesis through elevated SDF-1/CXCL12 secretion. *Cell* 2005;121:335-348.
- [31] Record Owner NLM. Hepatic myofibroblasts promote the progression of human cholangiocarcinoma through activation of epidermal growth factor receptor.
- [32] Neufert C, Becker C, Tureci O, Waldner MJ, Backert I, Floh K, et al. Tumor fibroblast-derived epiregulin promotes growth of colitis-associated neoplasms through ERK. *Journal of Clinical Investigation* 2013;123:1428-1443.
- [33] Vaquero J, Lobe C, Tahraoui S, Claperon A, Mergey M, Merabtene F, et al. The IGF2/IR/IGF1R Pathway in Tumor Cells and Myofibroblasts Mediates Resistance to EGFR Inhibition in Cholangiocarcinoma. *Clin Cancer Res* 2018;24:4282-4296.
- [34] Grivennikov S, Karin E, Terzic J, Mucida D, Yu GY, Vallabhapurapu S, et al. IL-6 and Stat3 are required for survival of intestinal epithelial cells and development of colitis-associated cancer. *Cancer Cell* 2009;15:103-113.
- [35] Record Owner NLM. Interleukin-11 is the dominant IL-6 family cytokine during gastrointestinal tumorigenesis and can be targeted therapeutically.
- [36] Calon A, Espinet E, Palomo-Ponce S, Tauriello DV, Iglesias M, Cespedes MV, et al. Dependency of colorectal cancer on a TGF-beta-driven program in stromal cells for metastasis initiation. *Cancer Cell* 2012;22:571-584.
- [37] Gaggioli C, Hooper S, Hidalgo-Carcedo C, Grosse R, Marshall JF, Harrington K, et al. Fibroblast-led collective invasion of carcinoma cells with differing roles for RhoGTPases in leading and following cells. *Nat Cell Biol* 2007;9:1392-1400.
- [38] Labernadie A, Kato T, Brugues A, Serra-Picamal X, Derzsi S, Arwert E, et al. A mechanically active heterotypic E-cadherin/N-cadherin adhesion enables fibroblasts to drive cancer cell invasion. *Nat Cell Biol* 2017;19:224-237.
- [39] Lau EY, Lo J, Cheng BY, Ma MK, Lee JM, Ng JK, et al. Cancer-Associated Fibroblasts Regulate Tumor-Initiating Cell Plasticity in Hepatocellular Carcinoma through c-Met/FRA1/HEY1 Signaling. *Cell Reports* 2016;15:1175-1189.
- [40] Chen X, Song E. Turning foes to friends: targeting cancer-associated fibroblasts. *Nat Rev Drug Discov* 2019;18:99-115.
- [41] Meads MB, Gatenby RA, Dalton WS. Environment-mediated drug resistance: a major contributor to minimal residual disease. *Nature Reviews Cancer* 2009;9:665-674.
- [42] Paraiso KH, Smalley KS. Fibroblast-mediated drug resistance in cancer. *Biochem Pharmacol* 2013;85:1033-1041.

- [43] Kumari N, Dwarakanath BS, Das A, Bhatt AN. Role of interleukin-6 in cancer progression and therapeutic resistance. *Tumour Biol* 2016;37:11553-11572.
- [44] Roodhart JM, Daenen LG, Stigter EC, Prins HJ, Gerrits J, Houthuijzen JM, et al. Mesenchymal stem cells induce resistance to chemotherapy through the release of platinum-induced fatty acids. *Cancer Cell* 2011;20:370-383.
- [45] Lotti F, Jarrar AM, Pai RK, Hitomi M, Lathia J, Mace A, et al. Chemotherapy activates cancer-associated fibroblasts to maintain colorectal cancer-initiating cells by IL-17A. *J Exp Med* 2013;210:2851-2872.
- [46] Wong PF, Wei W, Gupta S, Smithy JW, Zelterman D, Kluger HM, et al. Multiplex quantitative analysis of cancer-associated fibroblasts and immunotherapy outcome in metastatic melanoma. *J Immunother Cancer* 2019;7:194.
- [47] Nazareth MR, Broderick L, Simpson-Abelson MR, Kelleher RJ, Jr., Yokota SJ, Bankert RB. Characterization of human lung tumor-associated fibroblasts and their ability to modulate the activation of tumor-associated T cells. *J Immunol* 2007;178:5552-5562.
- [48] Pinchuk IV, Saada JI, Beswick EJ, Boya G, Qiu SM, Mifflin RC, et al. PD-1 ligand expression by human colonic myofibroblasts/fibroblasts regulates CD4+ T-cell activity. *Gastroenterology* 2008;135:1228-1237, 1237 e1221-1222.
- [49] Joyce JA, Fearon DT. T cell exclusion, immune privilege, and the tumor microenvironment. *Science* 2015;348:74-80.
- [50] Tsai S, McOlash L, Palen K, Johnson B, Duris C, Yang Q, et al. Development of primary human pancreatic cancer organoids, matched stromal and immune cells and 3D tumor microenvironment models. *BMC Cancer* 2018;18:335.
- [51] Villanueva A. Hepatocellular Carcinoma. *N Engl J Med* 2019;380:1450-1462.

Supplementary data for

Cancer-associated fibroblasts provide a stromal niche for liver cancer organoids that confers trophic effects and therapy resistance

Jiaye Liu¹, Meng Li^{1*}, Pengfei Li^{1*}, Ling Wang^{1*}, Zhouhong Ge¹, Lisanne Noordam¹, Ruby Lieshout², Monique M. A. Verstegen², Buyun Ma¹, Junhong Su¹, Qin Yang^{1,3}, Ruyi Zhang¹, Guoying Zhou¹, Lucia Campos Carrascosa¹, Dave Sprengers¹, Ron Smits¹, Jaap Kwekkeboom¹, Luc J. W. van der Laan², Maikel P. Peppelenbosch¹, Qiuwei Pan¹, Wanlu Cao¹

Table of contents

Supplementary Figure 1

Supplementary Figure 2

Supplementary Figure 3

Supplementary Figure 4

Supplementary Figure 5

Supplementary Figure 6

Supplementary Figure 7

Supplementary Figure 8

Supplementary Figure 9

Supplementary Figure 10

Supplementary Figure 11

Supplementary Figure 12

Supplementary Figure 13

Supplementary Figure 14

Supplementary Figure 15

Supplementary Figure 16

Supplementary Figure 17

Supplementary Figure 18

Supplementary methods

Trans-well culture

For Trans-well culture, 1000 CAF cells were seeded on top of the trans-well membrane (1 µm pore size, Greiner Bio-One) and 500 single organoid cells growing in the lower compartment in 24-well plates for 10 days for mouse cells and 14 days for human cells.

Alamar blue assay

CAFs or organoids were incubated with Alamar Blue (Invitrogen, 1:20 in DMEM) for two to four hours (37°C), and then medium was collected for analysis of the metabolic activity of the cells. Absorbance was determined by using fluorescence plate reader (CytoFluor Series 4000, Perseptive Biosystems) at the excitation of 530/25nm and emission of 590/35. Matrigel with medium only was used as blank control.

Cell titer assay

After culturing organoids with either mouse or human OEM for 10 days for mouse cells or 14 days for human cells in trans-well, a volume of CellTiter-Glo 3D reagent (Promega, G9681) equal to the volume of cell culture medium was added in each well. The contents were mixed vigorously for 5 minutes to induce cell lysis. The plate was incubated at room temperature for an additional 25 minutes to stabilize the luminescent signal, then luminescence was recorded.

Quantitative real-time RT-PCR

Total RNA was isolated using Macherey-Nagel NucleoSpin RNA II kit (Bioke, Leiden, Netherlands) and quantified using a Nanodrop ND-1000 (Wilmington, DE, USA). Quantification was measured with Nanodrop ND-1000 (Wilmington). RNA was then converted to cDNA by using a cDNA Synthesis kit (TAKARA BIO INC.). Real-time PCR reactions were performed with SYBRGreen-based real-time PCR (Applied Biosystems®) and amplified in a thermal cycler (GeneAmp PCR System 9700). For cells collected from murine tissues, glyceraldehyde 3-phosphate dehydrogenase (*Gapdh*) gene was used as reference. All qRT-PCR primers are listed in Supplementary Table 1.

Organoid-based tumor formation assay in NSG mice

Five to six weeks old NSG mice were used for in vivo tumorigenesis assay. 2.5×10^5 mouse or human organoids together with or without 2.5×10^5 CAFs in 100 µl Matrigel subcutaneously inoculated into the flanks of the mice. Tumor formation and tumor weight were examined and determined after 1-2 months. Mice were housed in a room maintained on a 12h light/dark cycle (light on at 6 a.m.) with food and water provided ad libitum. All animal experiments were approved by the Committee on the Ethics of Animal Experiments of the Erasmus Medical Center.

Flow cytometry assay and cell sorting

For FACS analysis, single cells derived from liver and organoids were suspended in DMEM plus 2% FBS. Cell suspensions were analyzed using a BD FACSCalibur or BD FACSaria™ II. For FACS sort, a BD FACSaria™ II cell sorter was used to isolate the target cell population. Single cell suspensions of tumor cells were labelled with PE anti-human CD140a (PDGFRα) Antibody (Biolegend, 323506), Pacific Blue

anti-human CD31 Antibody (Biolegend, 102422), FITC anti-human CD326 (EpCAM) Antibody (Biolegend, 324204), Alexa Fluor 700 anti-human CD45 Antibody (Biolegend, 135906) and PE anti-mouse CD140a (PDGFR α) Antibody (Biolegend, 135906). For cell sorting, two populations EpCAM+ for epithelial cells and PDGFR α + for CAFs were collected and processed for RNA extraction and qRT-PCR.

Immunofluorescence

CAFs were fixed in 4% paraformaldehyde (PFA) for 1 h and permeabilised by incubation in PBS 0.2% Triton 100 (Sigma) at room temperature for 20 min. Samples were blocked for 1 h at room temperature in blocking buffer: 5% BSA PBS 0.05% Tween 20 (Sigma). Then cells were incubated with primary antibody in blocking solution in a wet chamber overnight at 4°C. After three washes of 15 min in PBS, the samples were mounted and analyzed by using a Zeiss Axioskop 20 microscope.

Tissue histology, immunohistology and immunofluorescence

For histological analysis, tumors were dissected into 10% neutral buffered formalin, embedded in paraffin blocks and serial sections were taken. Paraffin-embedded tissue sections were rehydrated before antigen retrieval using pH 6 sodium citrate buffer. After blocking endogenous peroxidase (DAKO peroxidase block), sections were incubated with primary antibodies overnight. Then sections were incubated with second antibody for 1 h at room temperature. The slides were placed in DAB substrate (ab64238) and incubated until desired color is achieved (30s-3min). Consequently, the slides were counterstained with haematoxylin. Images were acquired with a Zeiss Axioskop 20 microscope.

For immunofluorescence, samples were further dehydrated with 30% sucrose (Sigma-Aldrich, 4°C, overnight), stored at -80°C and then sectioned at 8 μ m for further analysis. Images were acquired with a Zeiss LSM510META confocal microscope.

Drug treatment

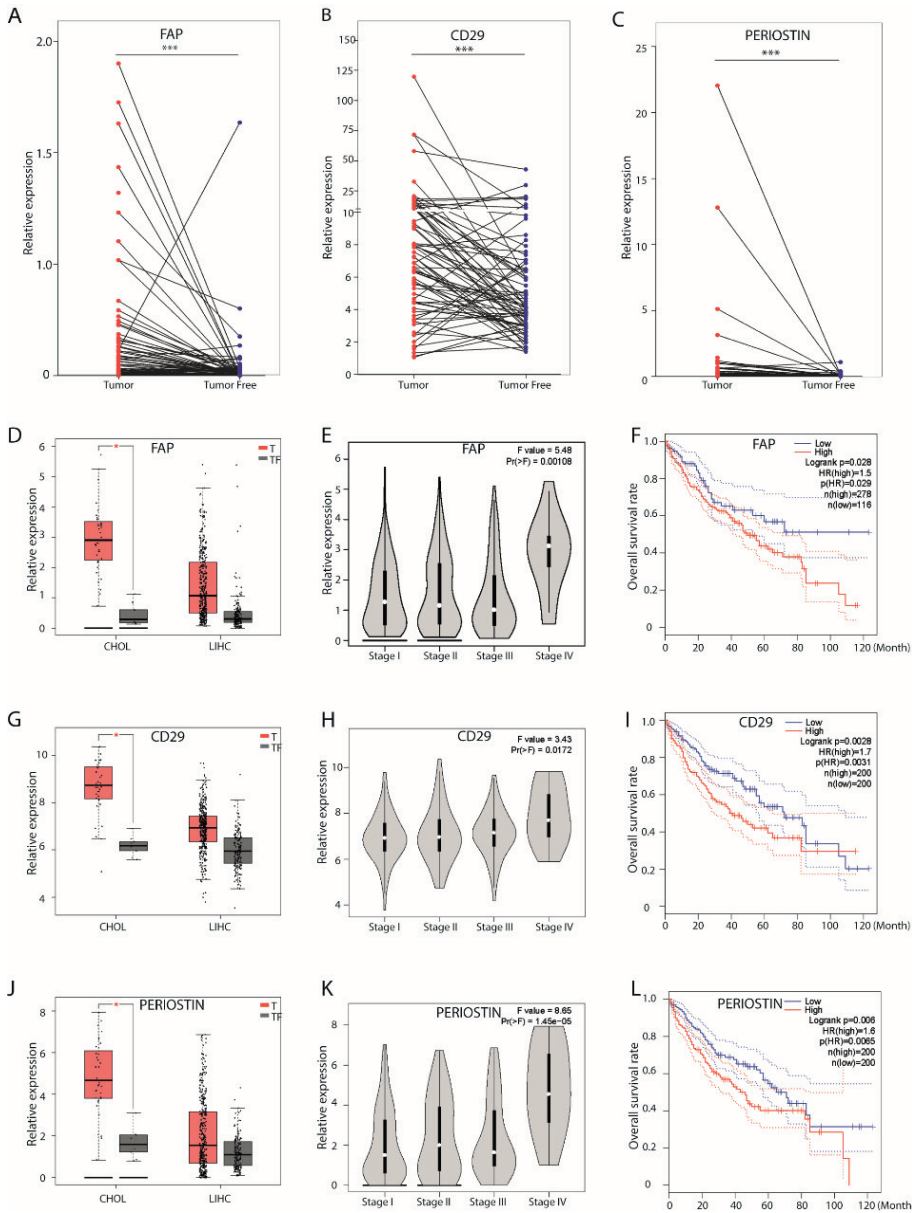
Organoids and CAFs were digested by using trypsin-EDTA into single cells. By using FACS sorting, 2000 mouse organoids or 4000 human organoids cells with or without CAFs in a 1:10 ratio were seeded and treated with Sorafenib (4 μ Mol/ml) or Regorafenib (3 μ Mol/ml) for 7 days. The number of formed organoids were counted and their diameters were measured.

To investigate the paracrine effect of CAFs on tumor organoids, conditioned medium human or mouse CAFs were prepared. CAFs with 70% confluent were pretreated with 5 μ M Sorafenib or 5 μ M Regorafenib in 10% FCS RPMI1640 medium for 12 h. Then the supernatant was removed and the cells were washed by PBS for three times. CAFs were then cultured in 0% FCS RPMI 1640 medium for another 12 h. After removing medium and washing three times with PBS, 10 ml OBM was added and conditioned for 12 h. The supernatant were then collected and filtered by a 40 μ m filter.

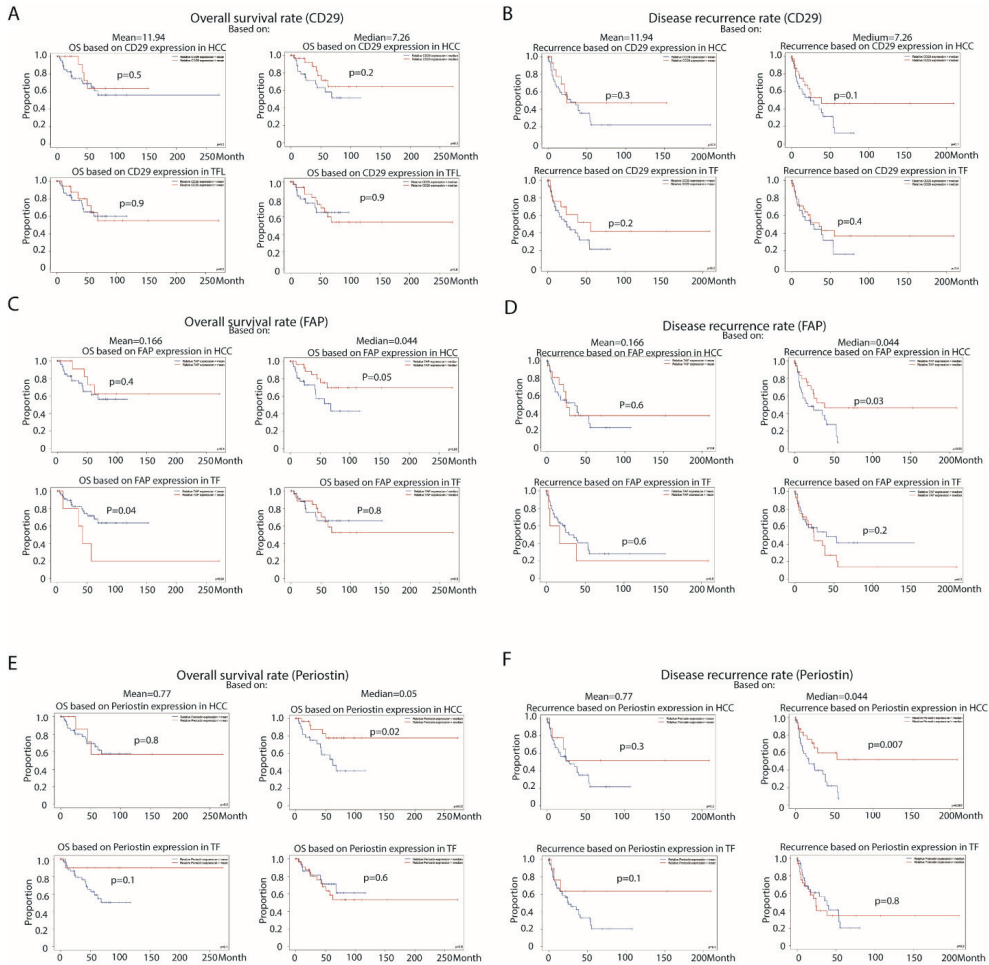
For IC50 analysis, 5000 mouse organoids or 10000 human organoids cells were cultured with conditioned or unconditioned medium with a series of concentrations of Sorafenib or Regorafenib for 10 days of mouse cells and 14 days of human cells. Cell viability was measured by Alamar blue assay. To study the dynamic response of treatment at different time points, 5000 mouse or human organoids cells were cultured with conditioned or unconditioned medium with Sorafenib (3.5 μ Mol/ml) or Regorafenib (3 μ Mol/ml) for 0-192 h. Alamar blue assay was used to determine cell viability.

Online database

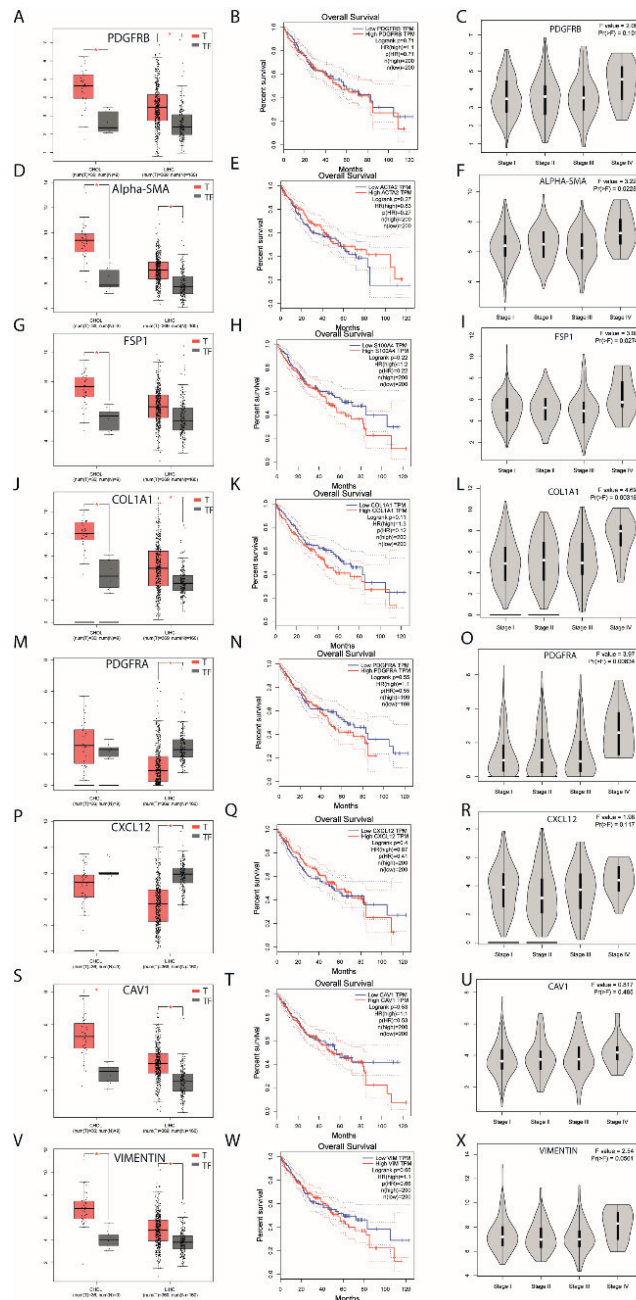
We used a database of GEPIA gene expression profiling interactive analysis (<http://gepia.cancer-pku.cn/>) to evaluate the association of patient overall survival with the expression of target genes in tumor and tumor surrounding tissue as well as at different stages of tumors.



Supplementary Figure1. Bioinformatics analysis between FAP, CD29 and Periostin gene expression and clinical relevance in liver cancer. (A-C) Gene expression of CAF markers FAP, CD29 and Periostin in tumors compared to paired adjacent tissues in our HCC cohort (n=75). (D, G, J) Gene expression of CAF markers FAP, CD29 and Periostin in tumors compared to paired adjacent tissues in an online TCGA database (n=400, 364 HCC and 36 CCA). (E, H, K) The expression of FAP, CD29 and Periostin in different tumor stage (n=400). (F, I, L) Overall survival assessed using the online TCGA database at www.gepia.com. The difference in survival related to CAFs markers alpha-SMA, FAP and Periostin mRNA expression were compared in each group involving in all patients (n=400). (A-C, D, G, J) *P<0.05, ***P<0.001.

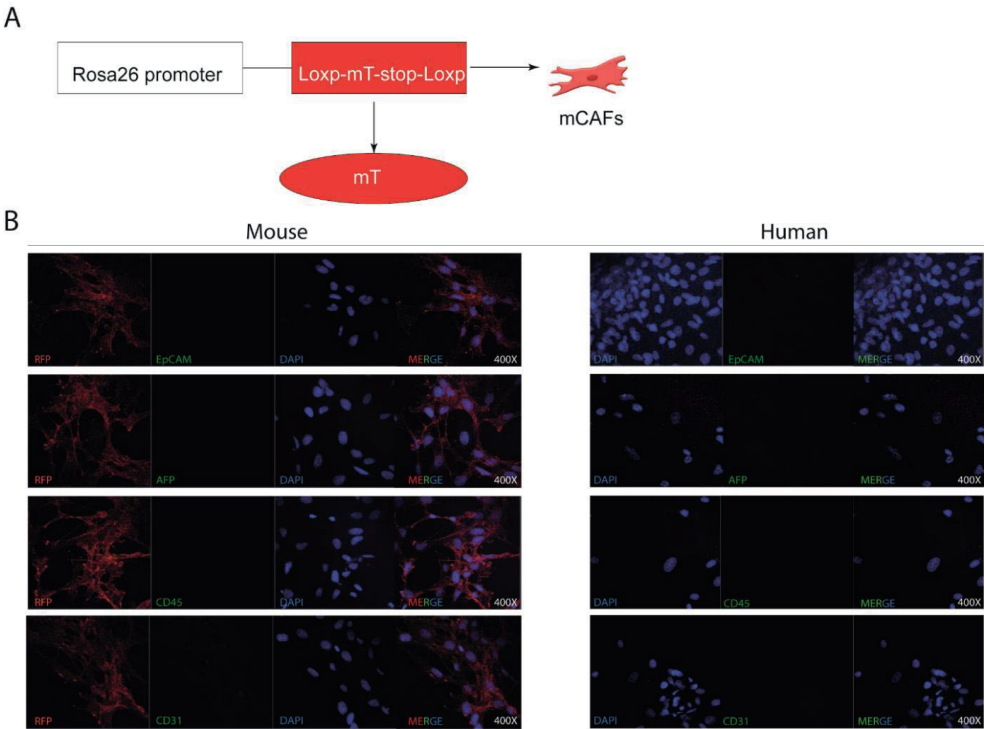


Supplementary figure 2. Overall survival and disease free rate based on the gene expression of CD29, FAP and Periostin in tumor tissue or tumor free tissue of our HCC patients (n=79).

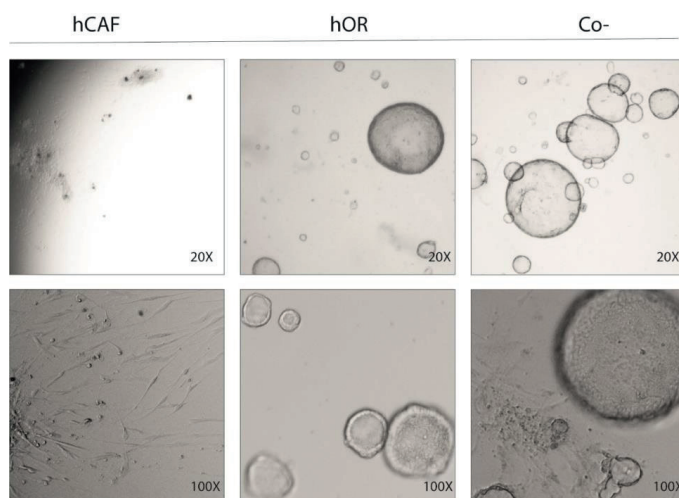


Supplementary Figure3. Additional CAFs markers like PDGFRB, Alpha-SMA, FSP1, COL1A1, PDGFRA, CXCL12, CAV1 and Vimentin gene expression in patients with liver cancer through online database. (A, D, G, J, M, P, S, V) The gene expression of PDGFRB, Alpha-SMA, FSP1, COL1A1, PDGFRA, CXCL12, CAV1 and Vimentin in tumor and adjacent tissue. (B, E, H, K, N, Q, T, W) Overall survival rate between high

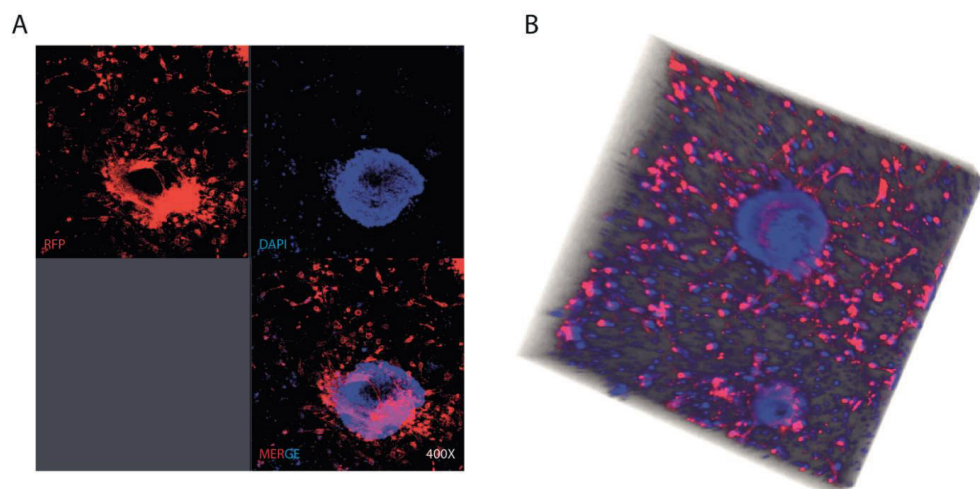
expression and low expression of these genes. (C, F, I, L, O, R, U, X) The gene expression of PDGFRB, Alpha-SMA, FSP1, COL1A1, PDGFRA, CXCL12, CAV1 and Vimentin in different stage of liver tumors.



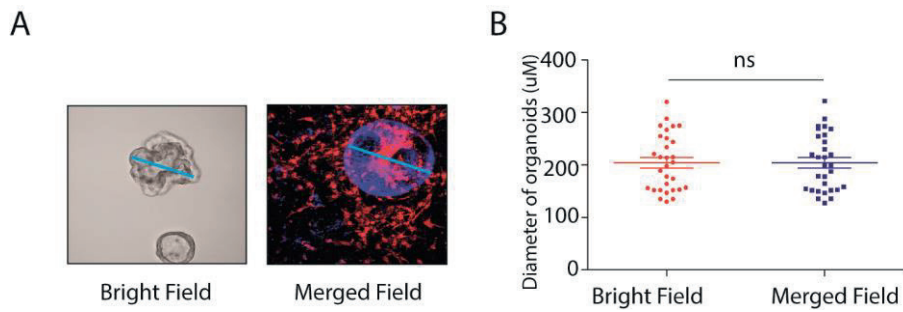
Supplementary Figure4. Establishment of CAFs. (A) Rosa26-mT mouse treated with DEN for 17 weeks, then waited 30 weeks for tumor formation. Then mouse CAFs were culture according to our protocol. (B) Representative confocal image of EpCAM, AFP, CD45 and CD31 expression in mouse CAF and human CAF (magnification 400X).



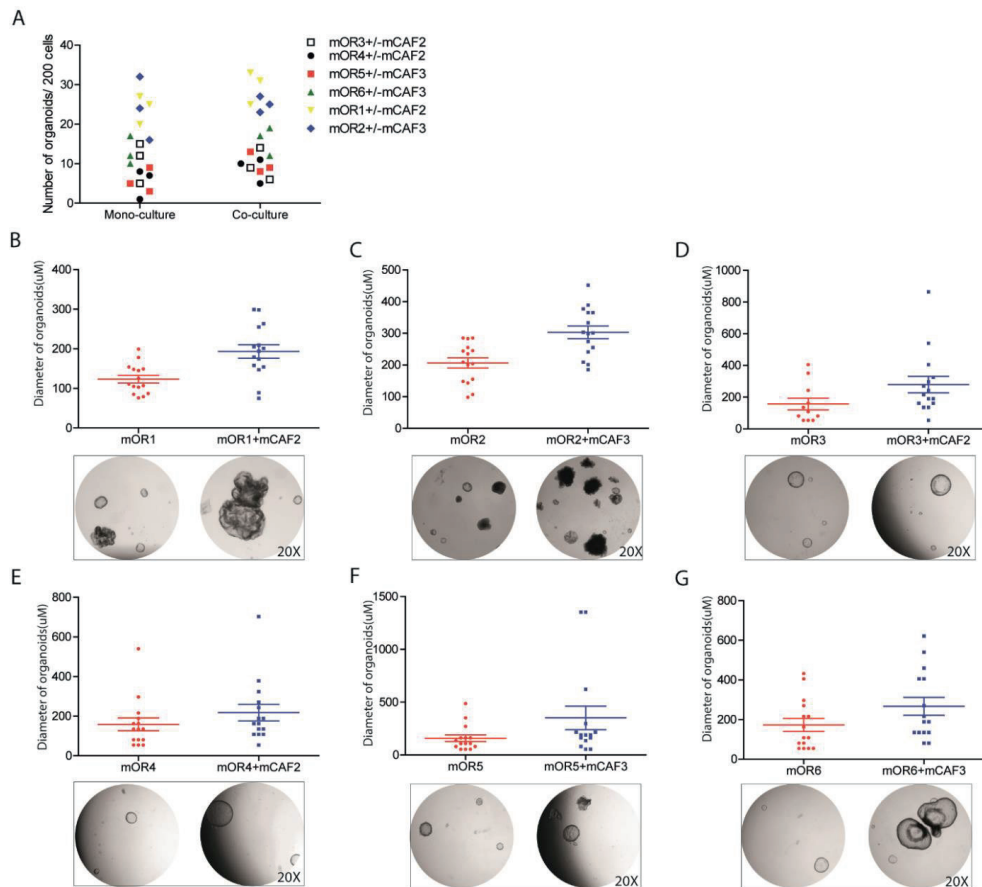
Supplementary Figure5. Human organoids cultured with or without CAFs.



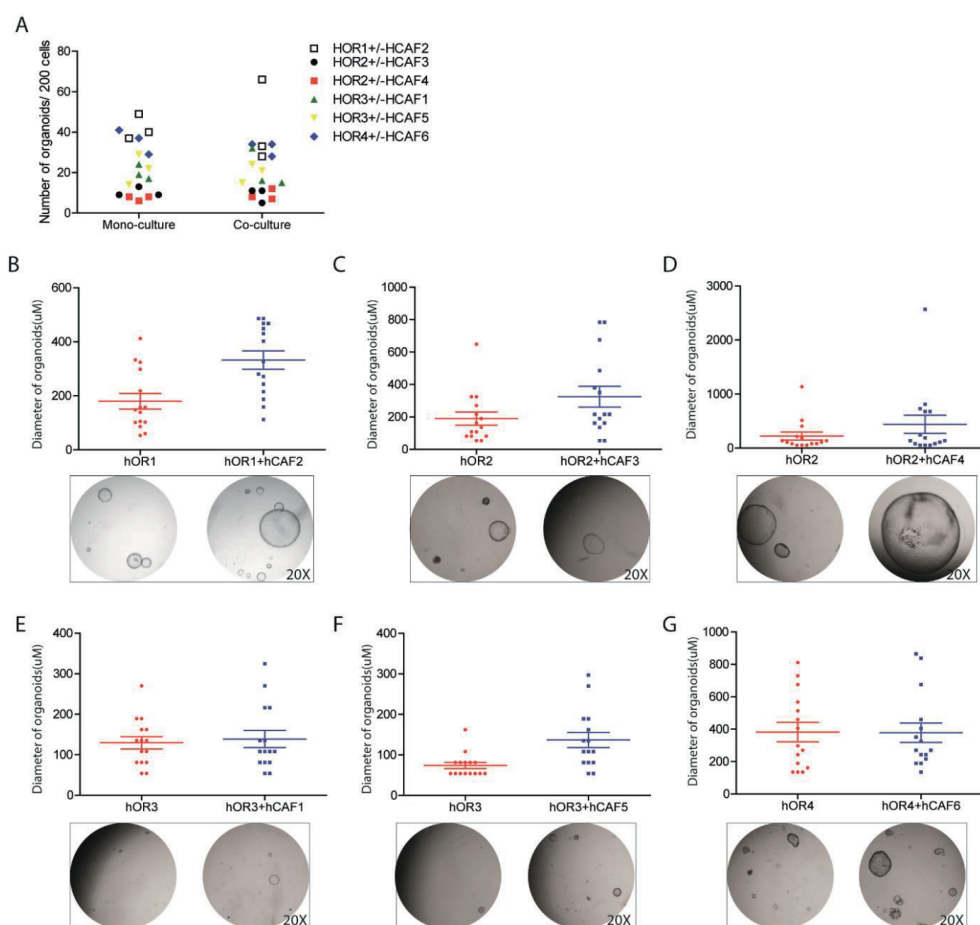
Supplementary Figure 6. Representative of mouse co-culture model and reconstruction. (A) Representative confocal image of mouse co-culture model (magnification 400X). (B) Representative 3D reconstruction of Z-stack of mouse co-culture model.



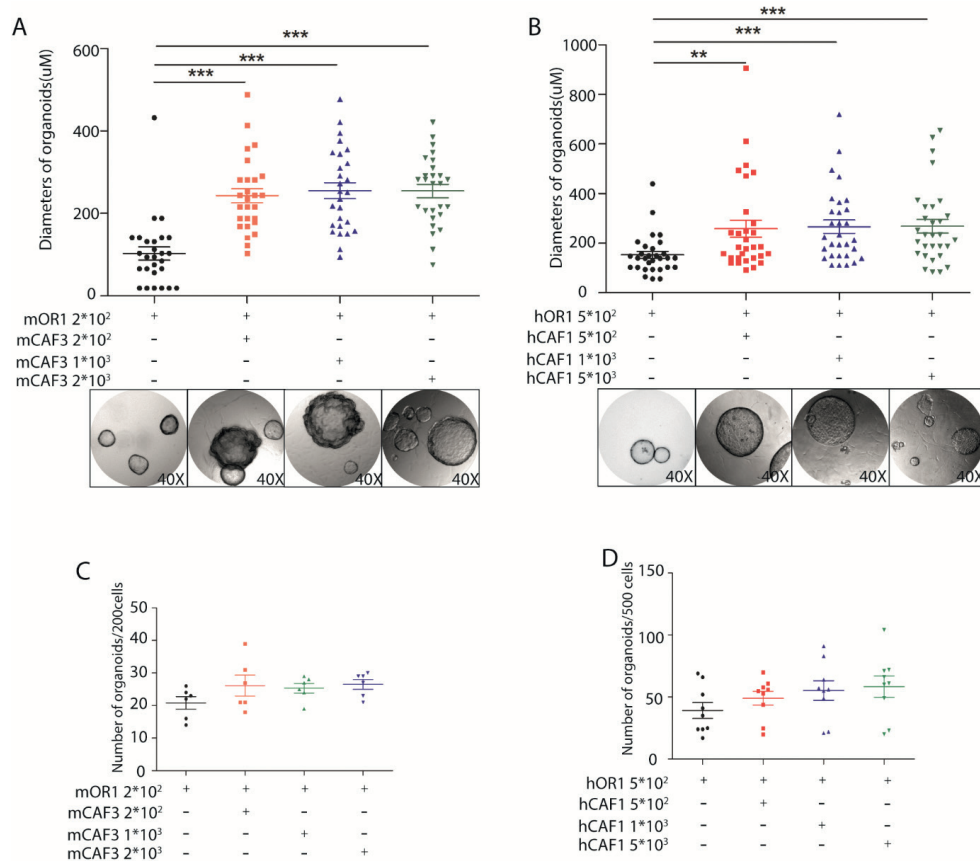
Supplementary Figure7. The accuracy of our measurement by measuring the diameter was verified under immunofluorescence and bright field vision.



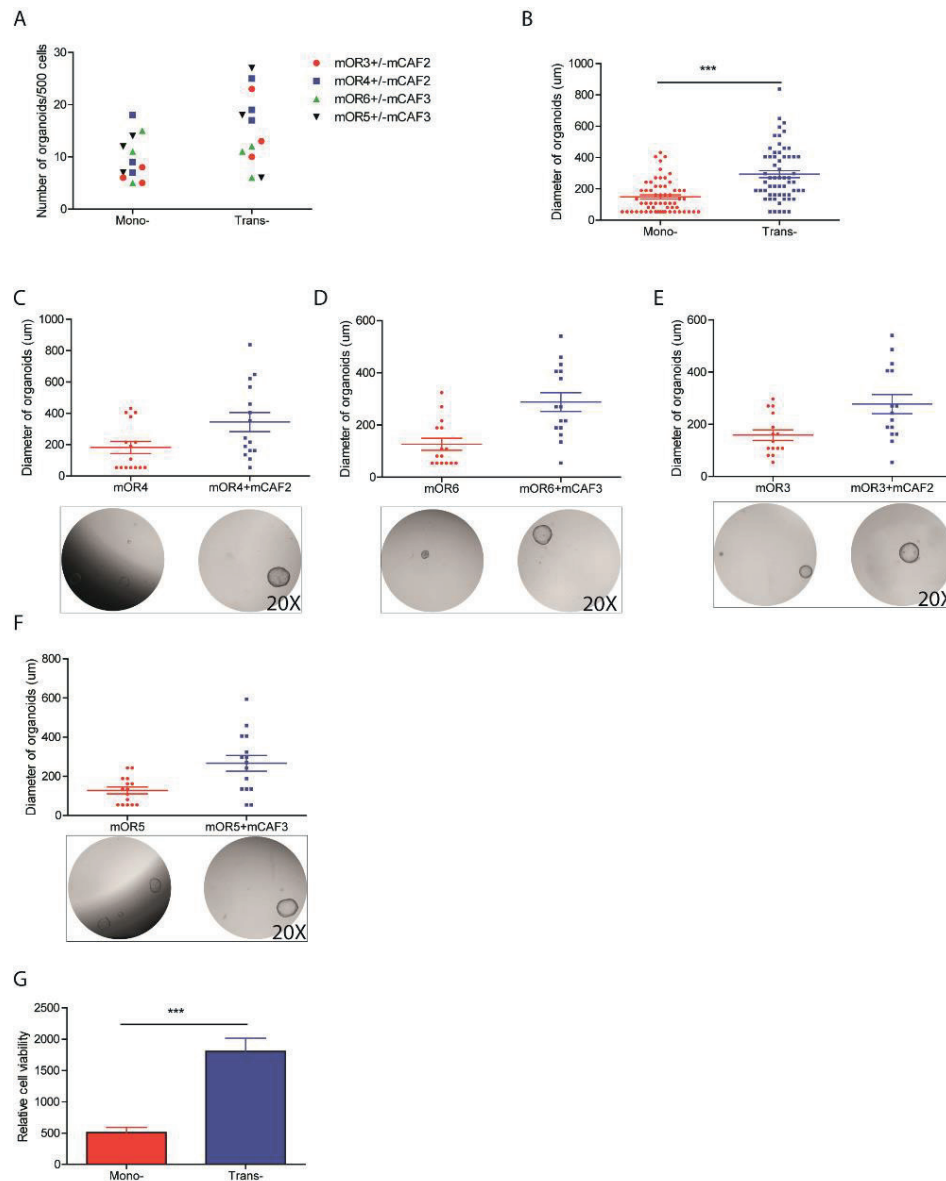
Supplementary figure 8. The reciprocal effects of mouse tumor organoids and mouse CAFs. A. The number of formed mouse tumor organoids in mono- or co-cultures ($n=6$ with three replicates). (B-G) The size of formed mouse tumor organoids in mono- or co-cultures ($n=3$ with three replicates, each replicate contained diameters of five randomly measured organoids in each well).



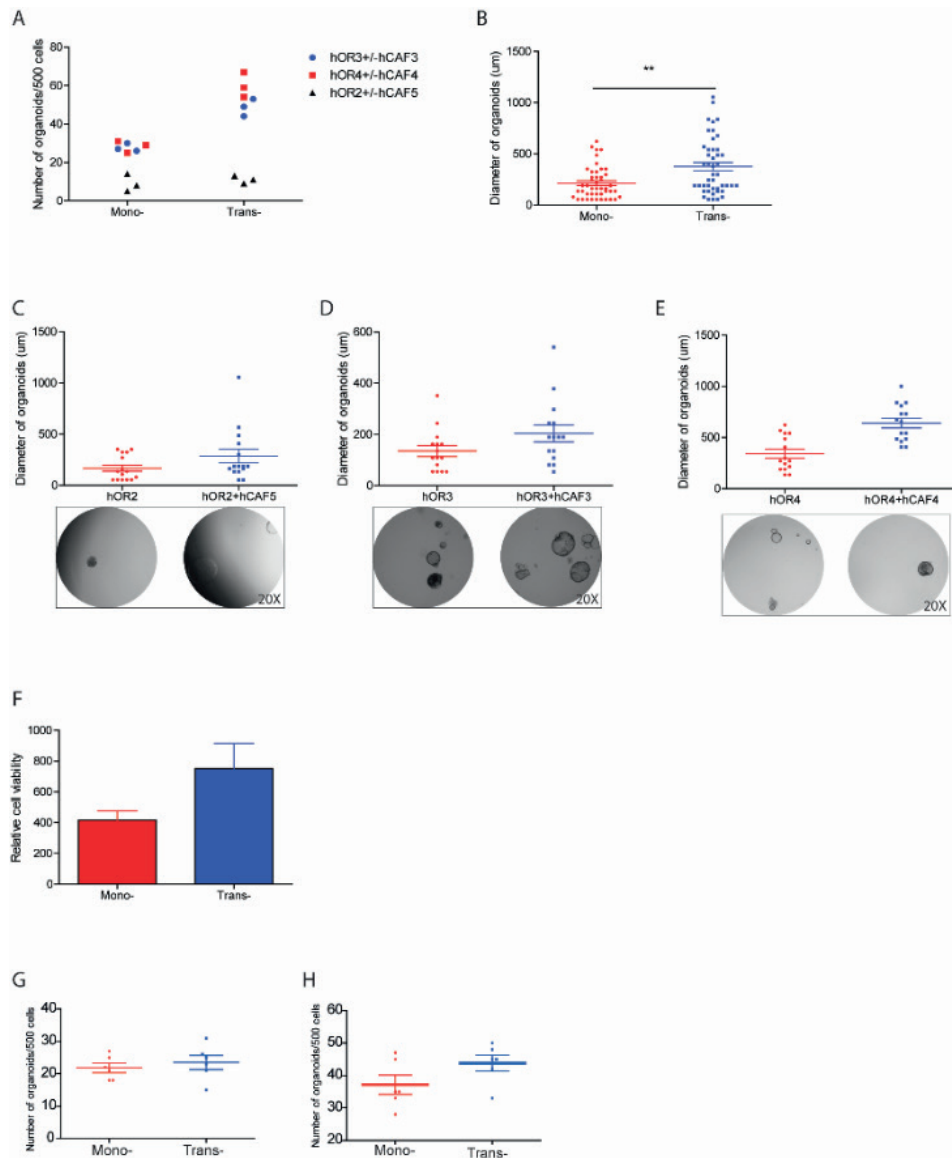
Supplementary figure 8. The reciprocal effects of human tumor organoids and human CAFs. A. The number of formed human tumor organoids in mono- or co-cultures (n=6 with three replicates). (B-G) The size of formed human tumor organoids in mono- or co-cultures (n=3 with three replicates, each replicate contained diameters of five randomly measured organoids in each well).



Supplementary figure 10. The reciprocal effects of tumor organoids and CAFs. (A, B) The size of formed organoids in mono- or co-cultures with different concentration between organoids and CAFs ($n=3$ with two replicate, each replicate contained diameters of five randomly measured organoids in each well. Non-parametric Mann-Whitney U tests were used for statistical analysis. ** $p<0.01$; *** $p<0.001$). (C, D) The number of formed organoids in mono- or co-cultures with different concentration between organoids and CAFs ($n=3$ with two replicates).

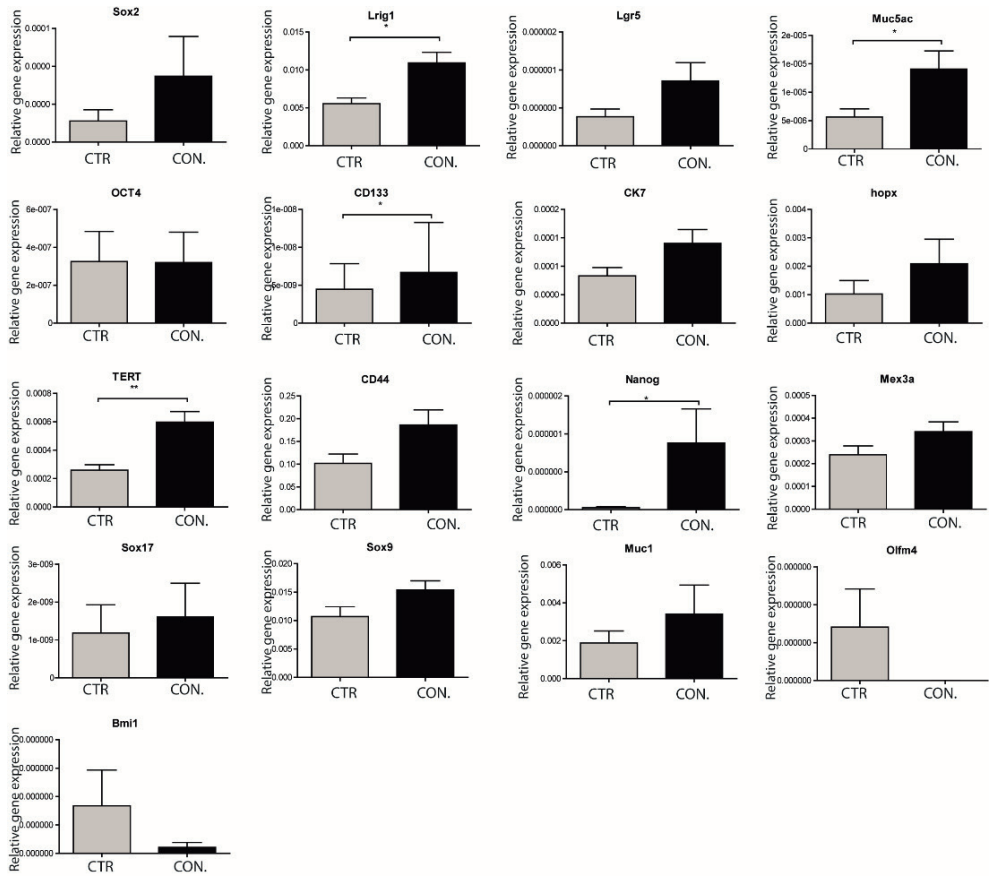


Supplementary Figure 11. The reciprocal effects of mouse tumor organoids and mouse CAFs in a trans-well system. (A) The number of formed mouse tumor organoids in the presence or absence of CAFs in a trans-well system (n=4). (B) The size of formed mouse tumor organoids in the presence or absence of CAFs in a trans-well system (n=4 with three replicate, each replicate contained diameters of five randomly measured organoids in each well. Non-parametric Mann-Whitney *U* tests were used for statistical analysis. ***p<0.001). (C-F) The size of formed mouse tumor organoids in the presence or absence of CAFs in a trans-well system. (G) Growth of mouse liver tumor organoids determined by Alamar Blue Assay (n=4 with three replicate, Non-parametric Mann-Whitney *U* tests were used for statistical analysis. ***p<0.001).

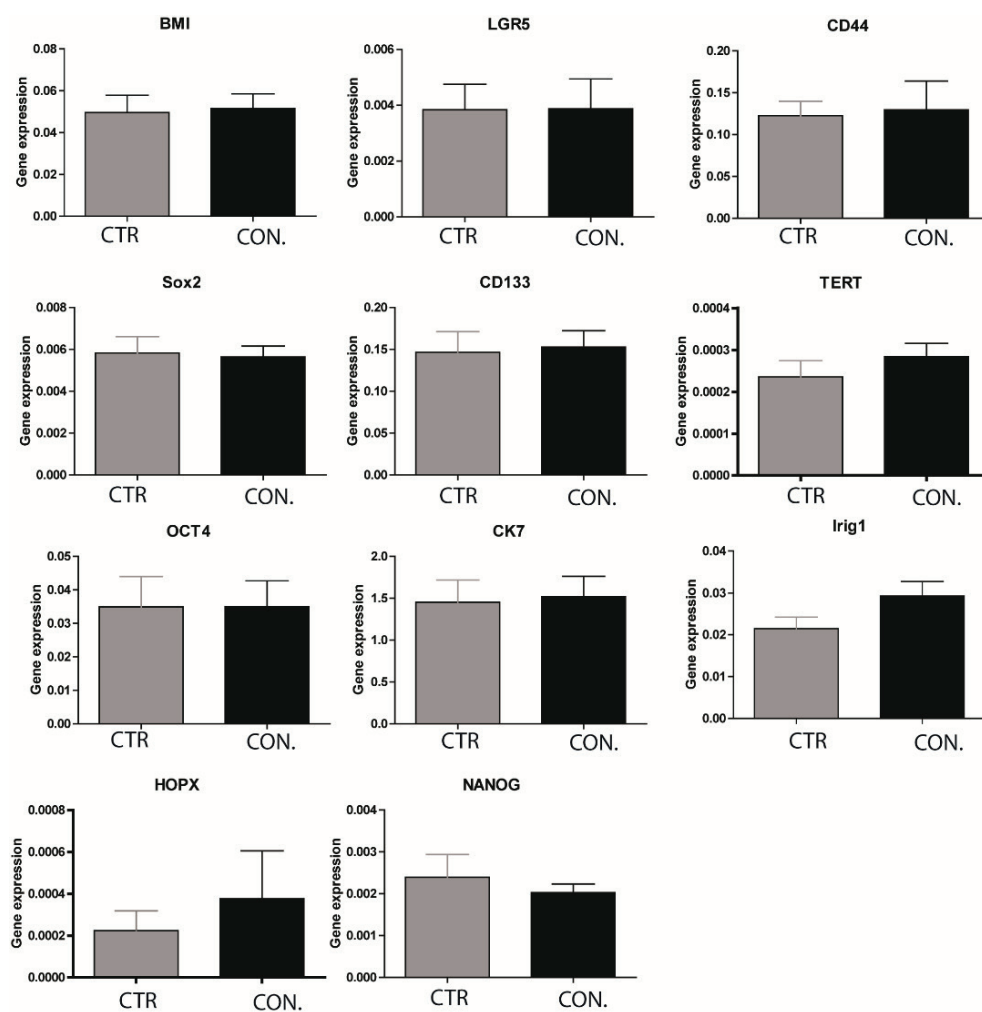


Supplementary Figure 12. The reciprocal effects of human tumor organoids and human CAFs in a trans-well system. (A) The number of formed human tumor organoids in the presence or absence of CAFs in a trans-well system (n=3). (B) The size of formed human tumor organoids in the presence or absence of CAFs in a trans-well system (n=3 with three replicate, each replicate contained diameters of five randomly measured organoids in each well. Non-parametric Mann-Whitney *U* tests were used for statistical analysis. ***p<0.001). (C-E) The size of formed human tumor organoids in the presence or absence of CAFs in a trans-well system. (F) Growth of human liver tumor organoids determined by Alamar Blue Assay (n=3 with three replicate, Non-parametric Mann-Whitney *U* tests were used for statistical analysis). (G) The number of formed mouse organoids in a trans-well system (n=3 with two

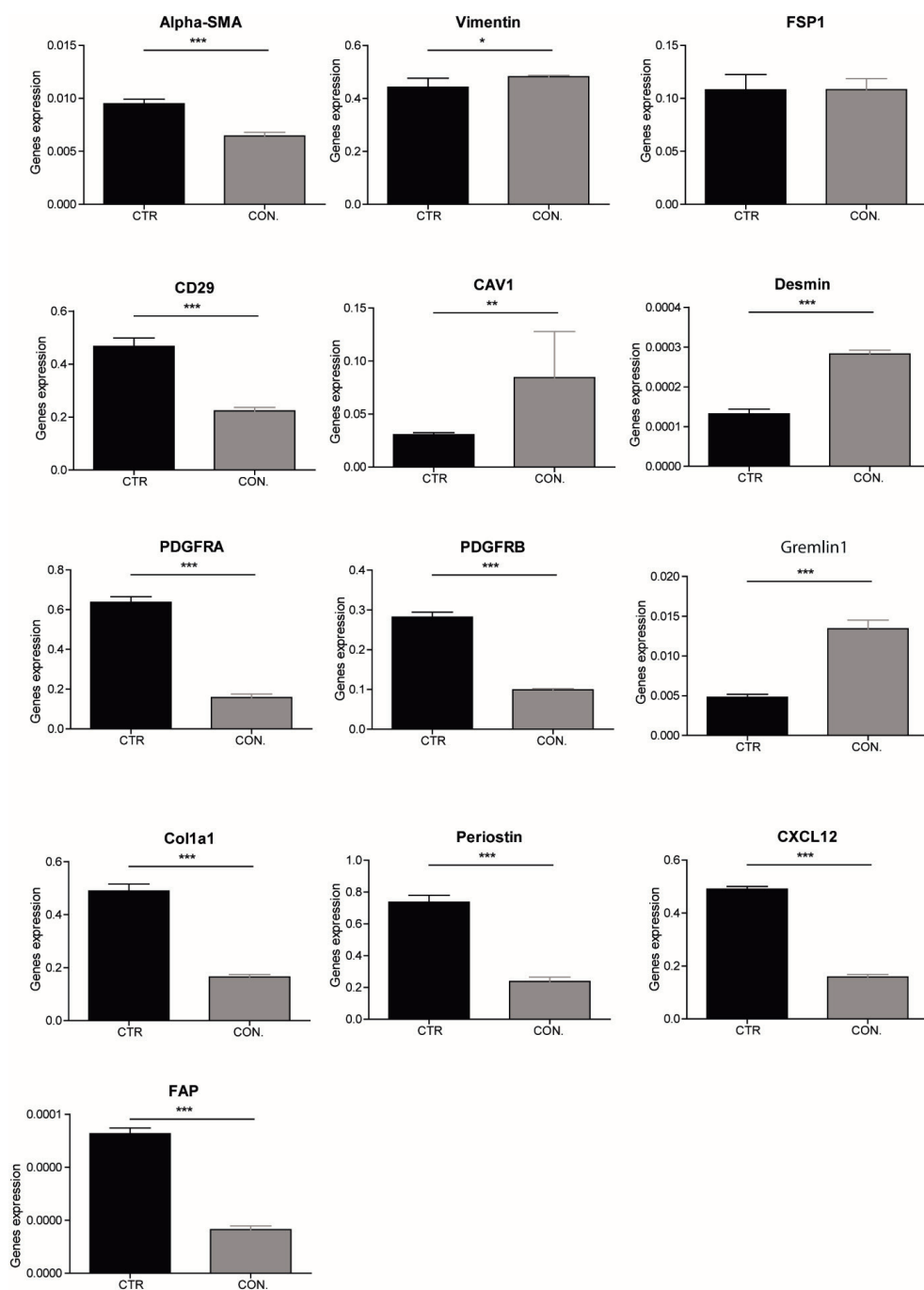
replicates). (H) The number of formed human organoids in a trans-well system (n=3 with two replicates).



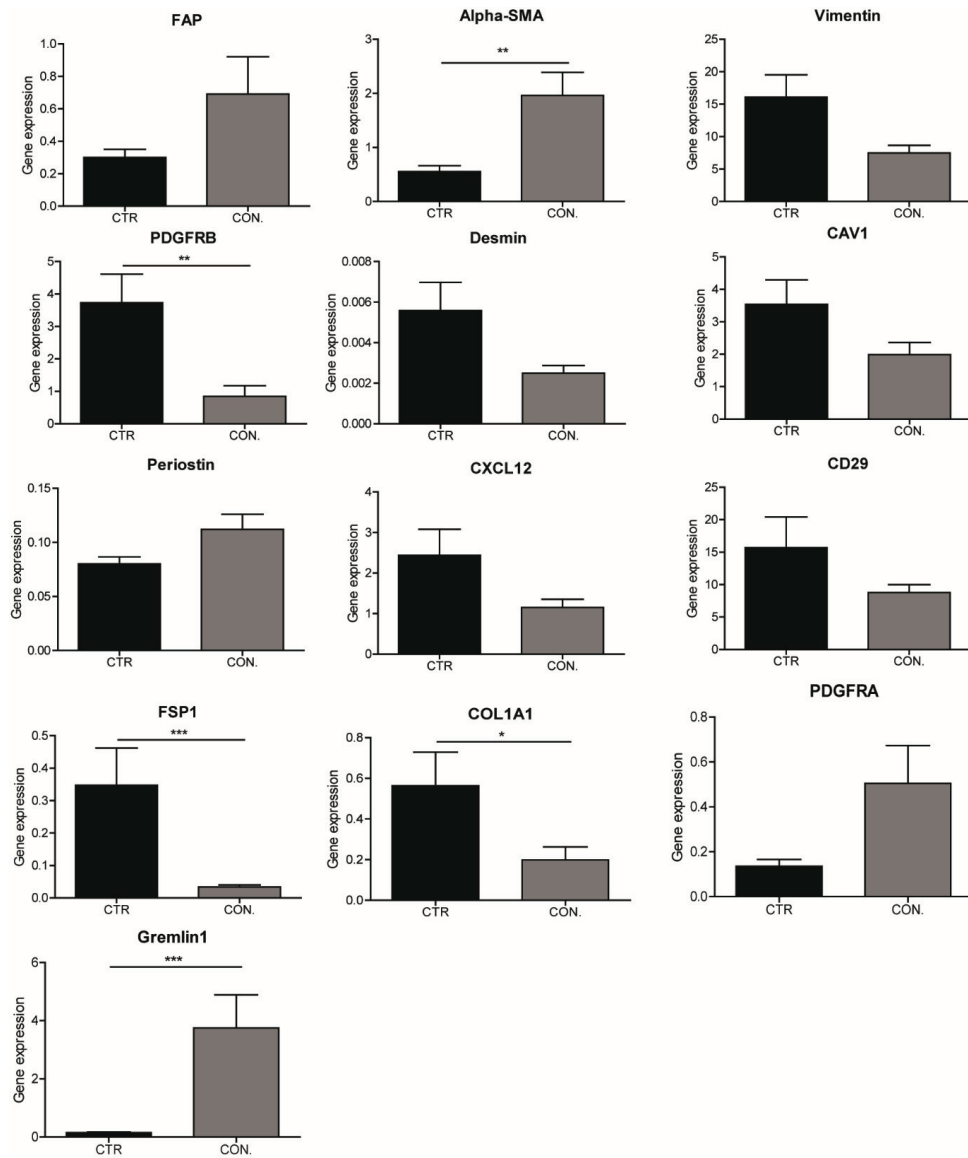
Supplementary Figure 13. Stem cell markers expression profiling for mouse organoids in the presence or absence of CAFs conditioned medium. (n=8, Non-parametric Mann-Whitney *U* tests were used for statistical analysis, *p<0.05)



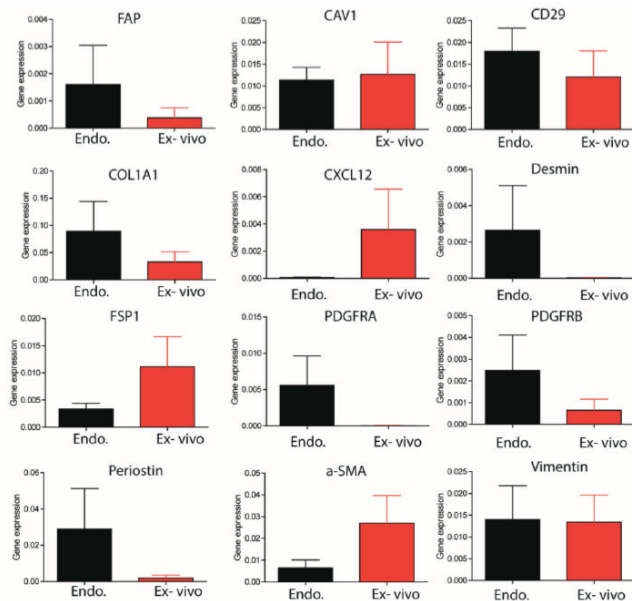
Supplementary Figure 14. Stem cell markers expression profiling for human organoids in the presence or absence of CAFs conditioned medium. (n=8, Non-parametric Mann-Whitney *U* tests were used for statistical analysis).



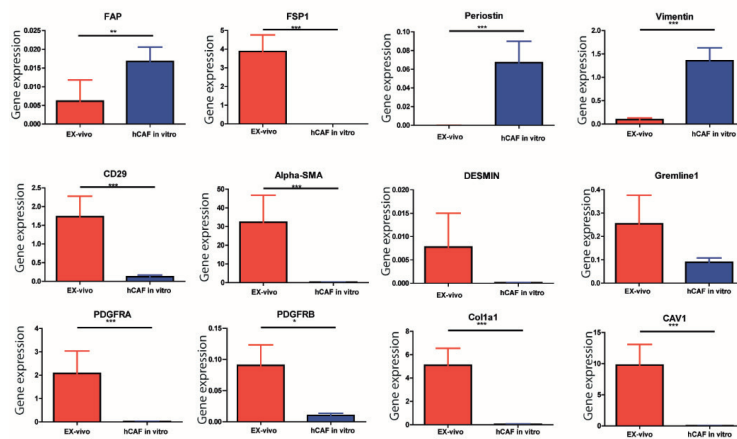
Supplementary Figure 15. CAFs markers expression profiling for mouse CAFs in the presence or absence of organoids conditioned medium. (n=8, Non-parametric Mann-Whitney *U* tests were used for statistical analysis, *p<0.05, ** P<0.01, ***P<0.001)



Supplementary Figure 16. CAFs markers expression profiling for human CAFs in the presence or absence of organoids conditioned medium. (n=8, Non-parametric Mann-Whitney *U* tests were used for statistical analysis, **p*<0.05, ** *P*<0.01, ****P*<0.001)



Supplementary Figure 17. Expression patterns of the CAF markers for the transplanted and the endogenous mouse CAFs (Endo, n=4; Ex-vivo, n=8).



Supplementary Figure 18. Expression patterns of the CAF markers for *in vivo* educated human CAFs from the tumors compare to *in vitro* cultured CAFs (n=8, Non-parametric Mann-Whitney *U* tests were used for statistical analysis, *p<0.05, **p<0.01, ***p<0.001).

CHAPTER 5

Modeling liver cancer and therapy responsiveness using organoids derived from primary mouse liver tumors

Wanlu Cao¹, Meng Li^{1*}, Jiaye Liu^{1*}, Ling Wang^{1*}, Monique M.A. Verstegen², Yuebang Yin¹, Buyun Ma¹, Kan Chen³, Michiel Bolkestein^{2,4}, Dave Sprengers¹, Luc J. W. van der Laan², Michael Doukas⁵, Jaap Kwekkeboom¹, Ron Smits¹, Maikel P. Peppelenbosch¹ and Qiuwei Pan¹

¹Department of Gastroenterology and Hepatology, Erasmus MC-University Medical Center, Rotterdam, The Netherlands.

²Department of Surgery, Erasmus MC-University Medical Center, Rotterdam, The Netherlands.

³College of Life Sciences, Zhejiang Sci-Tech University, Hangzhou, China.

⁴Department of Cell Biology, Erasmus MC-University Medical Center, Rotterdam, The Netherlands.

⁵Department of Pathology, Erasmus MC-University Medical Center, Rotterdam, The Netherlands.

Carcinogenesis. 2019 Mar 12;40(1):145-154.

Abstract

The current understanding of cancer biology and development of effective treatments for cancer remain far from satisfactory. This in turn heavily relies on the availability of easy and robust model systems that resemble the architecture/physiology of the tumors in patients to facilitate research. Cancer research *in vitro* has mainly been based on the use of immortalized 2D cancer cell lines for, which deviate in many aspects from the original primary tumors. The recent development of the organoid technology allowing generation of organ-buds in 3D culture from adult stem cells has endowed the possibility of establishing stable culture from primary tumors. Although culturing organoids from liver tumors is thought to be difficult, we now convincingly demonstrate the establishment of organoids from mouse primary liver tumors. We have succeeded in culturing 91 lines from 129 liver tissue/tumors. These organoids can be grown in long-term cultures *in vitro*. About 20% of these organoids form tumors in immunodeficient mice upon (serial) transplantation, confirming their tumorigenic and self-renewal properties. Interestingly, single cells from the tumor organoids have high efficiency of organoid initiation, and a single organoid derived from a cancer cell is able to initiate a tumor in mice, indicating the enrichment of tumor-initiating cells in the tumor organoids. Furthermore, these organoids recapitulate, to some extent, the heterogeneity of liver cancer in patients, with respect to phenotype, cancer cell composition and treatment response. These model systems shall provide enormous opportunities to advance our research on liver cancer (stem cell) biology, drug development and personalized medicine.

Keywords:

Tumor organoid, Liver tumor, Mouse, Anti-cancer research

Introduction

Liver cancer is one of the most common cause of cancer-related death worldwide with limited treatment options available (1). Better understanding of the biology of liver cancer is urgently needed for facilitating the development of new therapies. However, this in turn heavily relies on the availability of easy and robust model systems that resemble the architecture and physiology of the tumors in patients. So far, the cancer research society has mainly used immortalized cancer cell lines that have been propagated in 2D culture as *in vitro* model for decades. Obviously, these cell lines behave very different from the original tumor in many aspects and cost long time to establish (2). Primary cell culture of liver cancer cells from either human or mouse has proven to be very difficult (3). Thus, innovative approaches enabling *in vitro* propagation of primary liver cancer cells that maximize the modeling capacity of the patient disease and treatment response will be of particular importance.

The recent development of the organoid technology has driven the stem cell research field moving forward (4,5). Organoids are initiated *in vitro* from one or a few adult Lgr5⁺ stem cells of a particular tissue/organ and self-organize into 3D structures (6,7). They recapitulate the tissue architecture and lineage hierarchy, allow self-renewal and expansion of the stem cell population and empower different types of experimental manipulation (8). Many types of cancers are believed to harbor a subset of cells, termed as tumor-initiating cells (TIC). Thus, it is conceivable that organoids could be cultured from tumor tissues, if sophisticated 3D cell culture techniques/conditions are employed. Indeed, tumor organoid models have been established from primary tumors of colorectal (9), pancreatic (10,11), prostate (12) and liver cancer (13) patients. This technology is now used to explore many aspects of cancer research, including studying oncogenic transformation, cancer stem cells, drug development and personalized treatment (14,15). Our study has presented the successful establishment of malignant organoid models from mouse primary liver tumors, performed extensive characterization and demonstrated their applications in liver cancer research.

Method and material

Tumor/healthy organoid culture

Single cells were isolated from liver tumor tissues using a digestion solution: Collagenase type XI (0.5 mg/ml, Sigma-Aldrich), Dispase (0.2 mg/ml, Gibco), 1 % FBS in DMEM medium (Lonza) (37 °C, 30 min), then centrifuged (600 rpm, 10 min) to collect the cell pellets. Cells were directly mixed with matrigel (BD Bioscience), seeded on 24/48 well plates and kept at 37 °C for at least 30 min. After the matrigel formed a solid gel, medium was slowly added. Organoid culture medium was based on advanced DMEM/F12 (Invitrogen), which is supplemented with B27 (2% vol/vol) and N2 (1% vol/vol, Invitrogen), N-acetylcysteine (1.25 μM, Sigma-Aldrich), gastrin (10 nM, Sigma-Aldrich), EGF (50 ng/ml, Peprotech), R-spondin 1 (10% vol/vol, conditioned medium produced by 293T-H-Rspol-Fc cell line), FGF10 (100 ng/ml, Peprotech), nicotinamide (10 mM, Sigma-Aldrich) and HGF (50 ng/ml, Peprotech), as described previously (5). For the initial 3 days, the organoids also need to be supplemented with Noggin (10% vol/vol, conditioned medium produced by 293T-HA-Noggin cell line) Wnt3a (30% vol/vol, conditioned medium produced by L-Wnt3a cell line) (5). Medium was refreshed every 2-3 days and organoids were passaged in 1:2-1:10 split ratio once per week, or according to the growth of the organoids. The healthy liver-derived organoids were also isolated and cultured by using the same methodology as tumor organoid culture (stemness-keeping culture condition, without further differentiation).

Organoid allograft

Cold advanced DMEM/F12 medium was used to collect the organoids. Organoids were mechanically dissociated into pieces by pipetting (5-10 times) (collect enough amount of organoids from an entire 24-well plate, averagely 1×10^6 - 1×10^7). After centrifuging, organoids pellets (broken organoid pieces) were re-suspended in cold advanced DMEM/F12 medium and then mixed directly with matrigel in the ratio of 1:1 with a total volume of 100-200ul. 4-6 weeks old female NOG/JicTac (CIEA NOD.Cg-Prkdc-scid Il2rg-tm1Sug) mice were purchased from Taconic, and subcutaneously injected with the collected tumor organoids. Tumor formation was monitored weekly and mice were sacrificed to harvest tumor after visualizing the tumor (the tumor size reached 1cm). Tumor tissues were stored or cultured as described above. All animal experiments were approved by the Committee on the Ethics of Animal Experiments of the Erasmus Medical Center.

Single organoid formation assay and allograft assay

Cold advanced DMEM/F12 medium was used to collect the organoids. Organoids were mechanically dissociated into small pieces by pipetting (20-30 times) and further digested into

single cells by TrypLE (Gibco, 37°C, 5-10 min). FACS sorter (BD FACSARIA™ II) was used to further isolate the single living cells. Propidium iodide (PI) staining was used to exclude dead cells; FSC-Width with FSC-Area and then SSC-Width with SSC-Area gates were used to select the single cells. After mixing one single cell with matrigel, a droplet with in total volume of 5 µl was seeded in a well of 96-well plate for organoid initiation. After 1-3 weeks, single organoids were formed. Cold advanced DMEM/F12 medium was used to collect the single organoids. After removing the supernatant, matrigel was mixed with the organoid pellet and transplanted subcutaneously into the NOG mice directly. Tumor formation was monitored as described above.

Metabolic activity analyses for drug treatment

Different organoid lines were seeded separately in a 24/48-well plate. Sorafenib (1 µM) and Regorafenib (1 µM) was added to the organoid culture since the initial day. Drugs were refreshed every 2 days. At the day 7, organoids were incubated with Alamar Blue (Invitrogen, 1:20 in DMEM) for four hours, and then medium was collected for analysis of the metabolic activity of the cells. Absorbance was determined by using fluorescence plate reader (CytoFluor® Series 4000, Perseptive Biosystems) at the excitation of 530/25 nm and emission of 590/35. Each treatment condition was repeated for four times and matrigel only was used as blank control.

Karyotyping

Karyotyping was performed as previously described (16). Briefly, cultures were incubated with 0.1 µg/ml Karyomax Colcemid (Gibco, 152120-012) for 24 h. Organoids were harvested by cold organoid basic medium and then kept on ice for 10 min. Then, TrypLE (Gibco) were added for digesting organoids into single cells. Cells were then incubated with KCL 0.0075 M hypotonic solution for 10 min in 37°C incubator. Methanol: acetic acid (3:1, freshly prepared) was used for further fixation. Cells were dropped onto a microscope slide for visualization. Nuclei were mounted and stained using Vectashield with DAPI (Vector Labs). A minimum of 15 metaphases per sample were counted.

Statistical Analysis

Prism software (GraphPad Software) was used for all statistical analysis. For statistical significance of the differences between the means of two groups, we used Mann-Whitney U-test. For comparing two paired groups, we used Paired T-test. Differences were considered significant at a p value less than 0.05.

Results

Successful culture of organoids from mouse primary liver tumors

Diethylnitrosamine (DEN) is widely used as a carcinogen in experimental animal models, in particular for inducing liver tumors in mice. Similar to the gender disparity in patients, DEN also preferentially induce liver tumors in male mice (17). Thus, we have mainly used male mice (53 male; 3 female) to induce liver tumor by DEN (Supplementary Figure 1 and Supplementary Figure 2). The livers were harvested for organoid culture (Figure 1A and Supplementary Figure 3). The numbers of visible tumors vary among the harvested mouse livers, ranging from zero to multiple tumors per liver (Supplementary Figure 1 and Supplementary Figure 4A). In total, we obtained 129 individual tissue/tumors from these mice, which were subjected to organoid culture (Figure 1A and Supplementary Figure 3). In general, small organoids could be visualized since post day 2-7 and passage was required around 7-14 days. We have succeeded in establishing organoid culture from 91 out of the 129 tumors, representing an efficiency of 70.5% (Supplementary Figure 2 and Supplementary Figure 4). The initiation efficiency varied from 0% to 100% among individual livers (Supplementary Figure 4B). For the rest 38 tissues that failed to form into organoids, 12 samples did initiate organoids but stopped proliferation at an early stage (maintained less than 3-4 weeks, 1-3 passages); whereas the other tumors had extensive necrosis and did not initiate any organoid from the start.

The successfully established lines could be maintained and propagated in 3D culture for at least 3 months, by passaging in the ratio of 1:2-1:4 for every 7 days. We further demonstrated that these tumor-derived organoids can be frozen, stored and re-cultured again without affecting their growth rate. With respect to the morphology, we (Figure 1C) and others (5) have observed that organoids derived from the healthy liver have a uniform bubble-like structure. In contrast, organoids derived from liver tumors presented diverse morphologies, ranging from bubble-like to condensed and flower-like, as well as an irregular sheet-like structure (Figure 1D-H). Interestingly, some cultures contained a mixture of organoids with different morphology (Supplementary Figure 5), which may reflect the heterogeneity of cell types within the tumors.

Tumorigenicity of expanded organoids in immunodeficient mice

To functionally assess whether these tumor-derived organoids are malignant, we performed the allograft assay in NOG immunodeficient mice as described previously (Figure 1A and Supplementary Figure 3) (18). We have subcutaneously engrafted all the established 91 organoid lines and assessed their tumor formation ability *in vivo*. Within 4-16 weeks, 18 out of 91 (20%) lines initiated tumor formation in NOG mice (Figure 1A and Supplementary Table 1: The upper panel).

Organoids could be cultured again from these allograft tumors (Figure 1A-B and Supplementary Figure 3). These tumor organoids needed to be passaged every 5 days in the ratio of 1:5-1:10, indicating an increased speed of growth. Importantly, when engrafting into NOG mice, these organoids are capable to initiate tumors again, with relatively shorter time compared to engraftment of the primary tumor organoids (Figure 1B and Supplementary Table 1, allograft tumor vs. primary tumor: 35 days vs 40.6 days). These results firmly demonstrated that liver tumor derived organoids are malignant and tumorigenic with self-renewal capability. Furthermore, we have performed karyotyping for the organoid strains (Figure 2). The majority of the strains from the primary tumors and all the strains derived from allograft showed irregular chromosome numbers. In contrast, organoids from healthy livers stably maintain diploid/tetraploid/octoploid chromosome numbers in culture.

A single organoid derived from a single cancer cell is able to initiate tumor formation in mice

To further consolidate the ability to initiate tumor growth of the organoids, we performed an organoid formation assay with isolated single cells. We found that isolated single cells from the tumor organoids can efficiently re-initiate organoids (Figure 1A). More importantly, subcutaneous transplantation of a single tumor organoid derived from a single cell into immunodeficient NOG mice rapidly initiated tumor around two weeks, confirming their malignant property (Figure 1B and Supplementary Table 1: the lower panel). Furthermore, organoids can be re-cultured from those allograft tumors and exhibited progressive expansion for over 4 months. These results indicate that 3D tumor organoid system enriches the cells with the capacity of tumor initiating.

Classically, stem cell markers have been widely used to identify potential TIC, although it is an ever debating issue of defining qualified TIC markers (19). Based on previous studies (19,20), we have profiled a panel of potential TIC markers, in comparison with organoids from normal liver stem cells. We found that the expression profile for stem cell/tumor stem cell markers varied from different strains (Supplementary file 1). Several markers, including *Bmi1*, *Lgr5*, *Oct4*, *Cd133*, *Hopx* and *Sox2* were upregulated in allograft strains compared to normal organoid or primary tumor-derived organoid strains (Figure 3). CD44 and *Tert* were downregulated in allograft strains. By paired analysis of the available paired strains, we observed the upregulation of *Bmi1*, *Lgr5* and *Muc5ac* and the downregulation of *Sox9* and *Ck7* (Supplementary Figure 6).

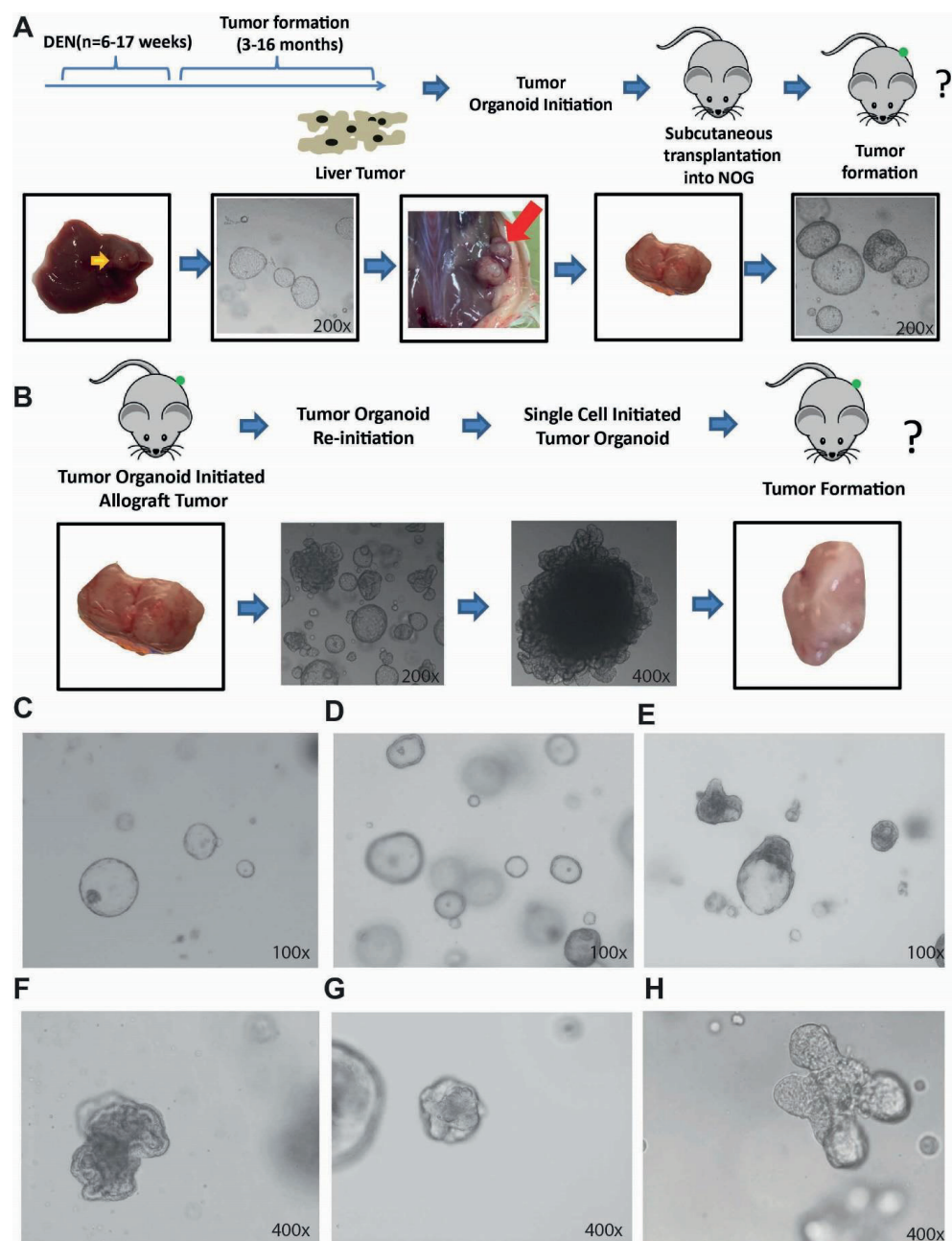


Figure 1. Establishment and characterization of organoid cultures from mouse liver tumors. (A) The upper panel: An outline of the experimental strategy used to establish primary tumor organoids. The lower panel: Representative pictures showing tumor organoids cultured from mouse primary liver tumors, and the formation of allograft tumor in NOG mice. The allograft tumors can be cultured into tumor organoids again. (B) The upper panel: An outline of the experimental strategy used to investigate single tumor organoid. The lower panel: Representative pictures showing that allograft tumor can initiate tumor organoids again. A single cell isolated from the tumor organoid can initiate a single organoid and then initiate tumor in NOG mice. (C) Example of normal liver organoids. (D-H) Liver tumor organoids with different morphologies.

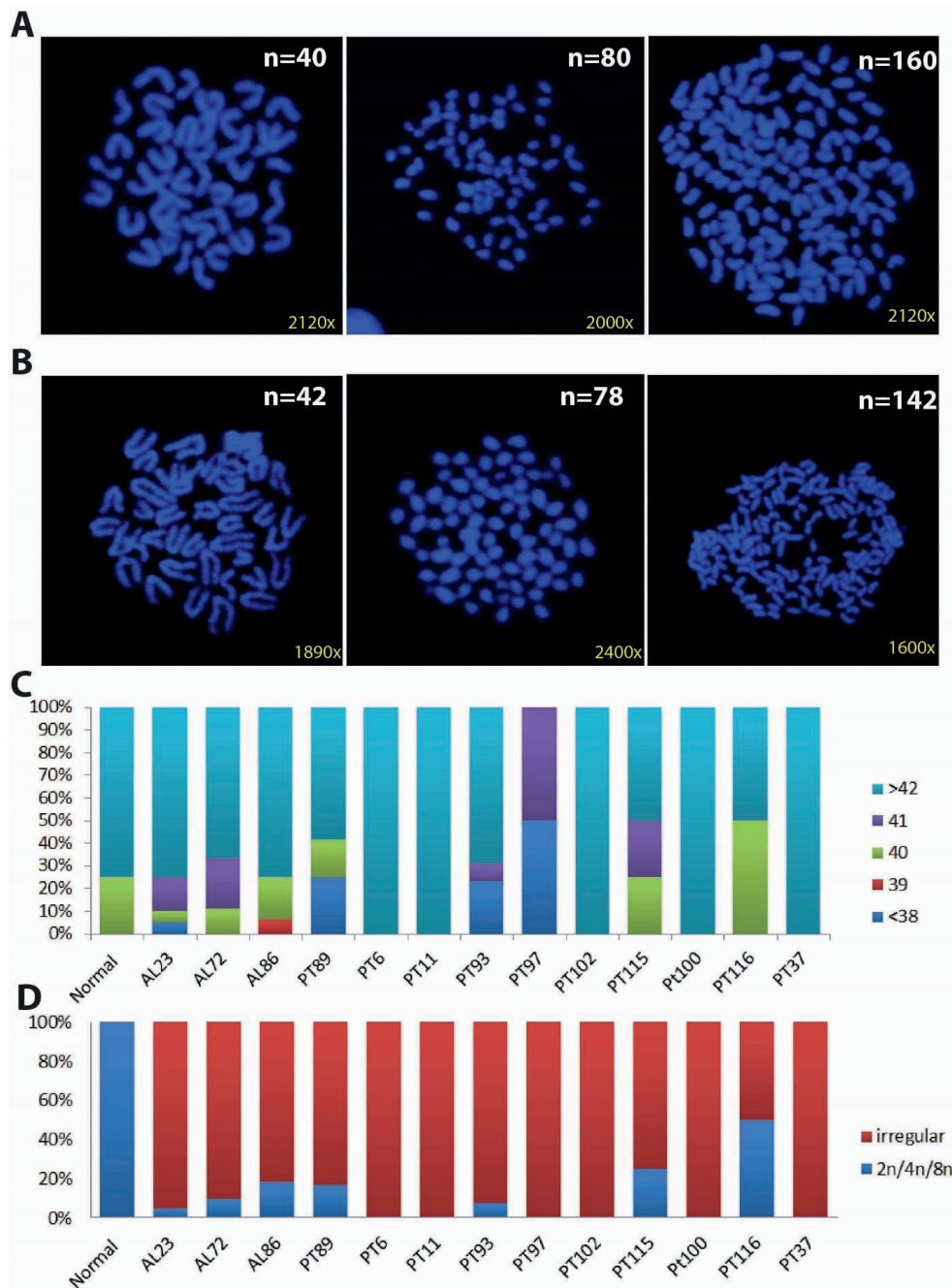


Figure 2. Karyotyping of normal and tumor organoids. (A-B) Representative images of organoid metaphases used for the ploidy analysis (A: normal chromosome number B: irregular chromosome number; Original magnification for organoids were 2800 \times). (C-D) Different analysis methods showing the percentage of ploidy per number of metaphases counted (at least 15 total), for normal organoid (N), allograft organoid (AL) and primary organoid (PT).

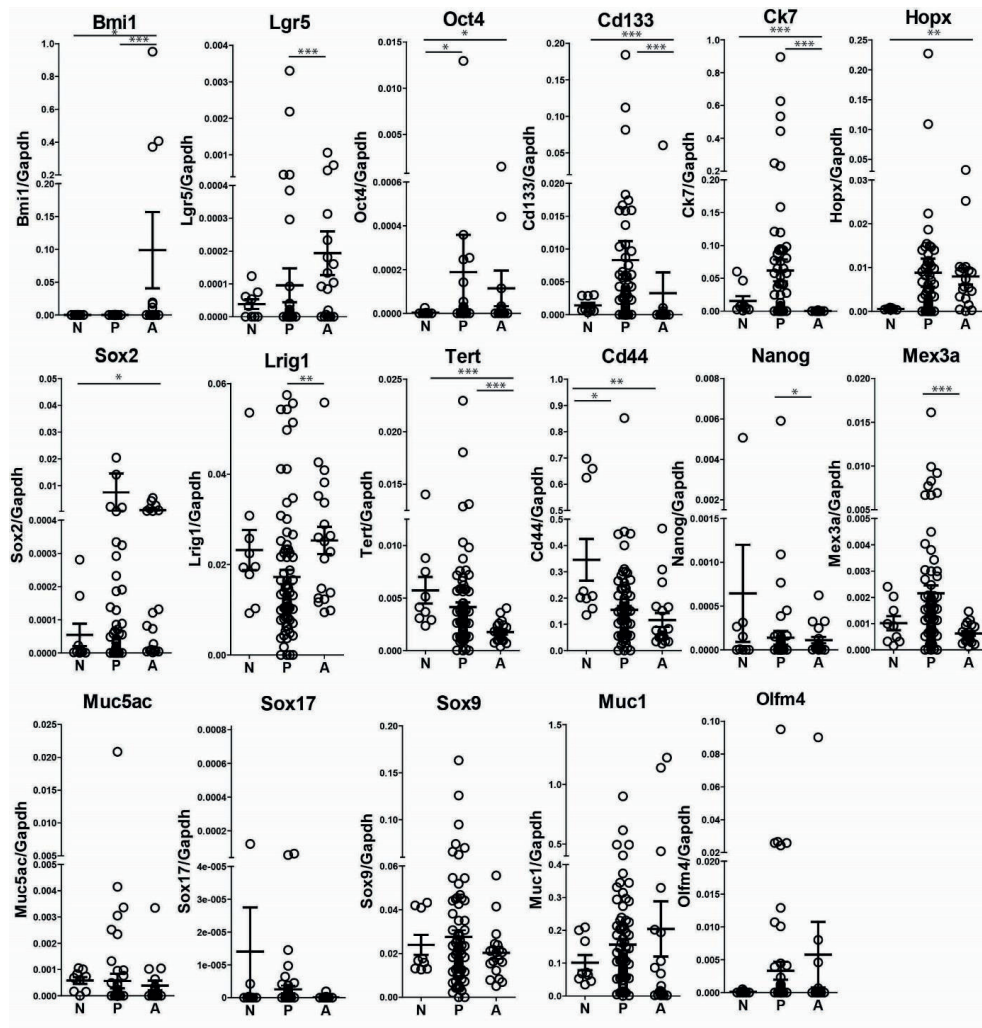


Figure 3. Comparison of the expression of progenitor/stem cell markers. N: normal liver organoid strains; P: strains from primary liver tumors; A: strains from allograft liver tumors (*P < .05; **P < .01; ***P < .001).

Tumor organoids express cholangiocyte and/or hepatocyte markers

In patients, primary liver cancer has been traditionally classified into three main types based on the tumor cell type. These are hepatocellular carcinoma (HCC), cholangiocarcinoma (CC) and hepatocellular-cholangiocarcinoma (CHCs). Although it remains a challenge to differentiate these types, hepatocyte (e.g. AFP, HNF4a) or/and cholangiocyte (e.g. CEA, CK19, C-KIT, EpCAM) markers are often used as one of the approaches to distinguish these types of liver cancer (21). In this respect, we have characterized the established tumor organoids and corresponding tissues by staining with HCC (AFP/HNF4a), CC (EpCAM/CK19) marker, H&E

staining and Gomori's reticulin staining respectively (Figure 4, supplementary file 1-3). Among the 91 strains which were transplanted into the NOG mice, 25 were lost due to infection in culture or storage issue later on (Supplementary Figure 4, marked by yellow). Thus, we mainly focused on the rest 66 strains, as well as the 18 allograft strains. We found distinct expression patterns among different lines of established tumor organoids. Some with a subset of cells express AFP and Hnf4a, some express EpCAM and CK19, and others express both markers (Supplementary file 1). More importantly, some allograft strains maintained the expression profile as well as the histology, compared to the primary tissue/strains (Figure 5A); whereas the other strains did not (Figure 5B). These data indicate that murine tumor organoids may recapitulate the heterogeneity of liver cancer types in patients to some extent. Of note, given that the etiology of liver is diverse, DEN induced liver tumors in mice do not fully represent liver cancer in patients (17).

Assessment of anti-cancer drugs in the tumor organoid model

Current treatment options, in particular for advanced liver cancer, are very limited. Sorafenib is the only FDA-approved first-line systemic therapy for patients with advanced HCC, with improvement of patient survival for only 3 months (1). Regorafenib is now emerging as a potential second-line therapy for HCC patients (22). To explore the potential of using liver tumor organoid models for future drug development, we assessed the feasibility by testing the effects of Sorafenib and Regorafenib.

We used organoid lines established from nine allograft tumors, as well as four primary-tumor derived organoid strains. Overall, these two targeted therapies inhibited the growth of the organoids (Figure 6 and Supplementary figure 7). However, we also observed clear variations of the responsiveness among these organoids. Thus, we have classified the organoid strains into three groups. Group 1 is sensitive to both (Figure 6A and Supplementary figure 7A); whereas Group 2 is only sensitive to Sorafenib but not Regorafenib (Figure 6B and Supplementary figure 7B); and Group 3 is not sensitive to both (Figure 6C and Supplementary figure 7C). We further compared the expression profile of stem cell/tumor stem cell markers between Group 1 with the rest strains. We have observed low expression of Oct4 and high expression of Sox9 in Group 1 (Supplementary Figure 8).

AL23

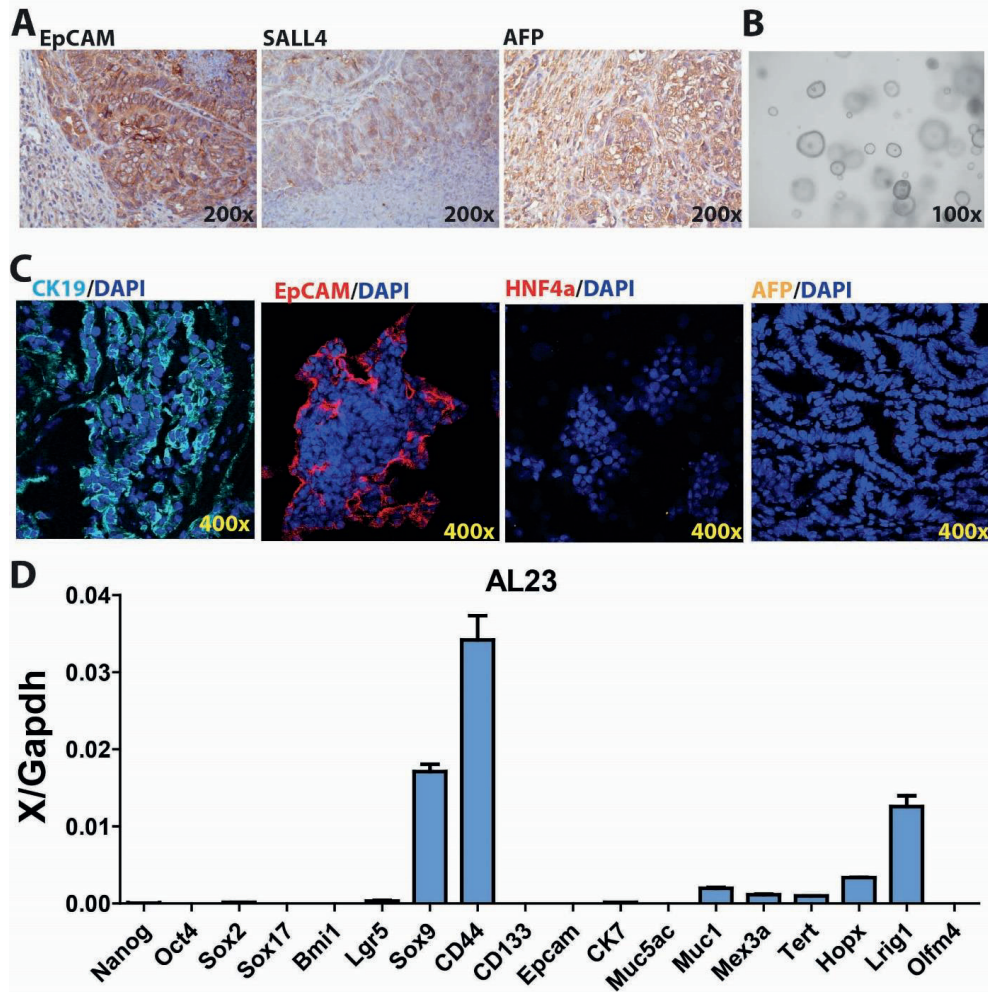


Figure 4. An example of the characterization of an organoid strain. (A) IHC straining for the allograft tissue of EpCAM (CC marker), SALL4 (poorly differentiated tumor marker) and AFP (HCC marker). (B) The morphology of organoid. (C) IF straining for the allograft organoid strain of CK19 (CC), EpCAM (CC), HNF4a(HCC) and AFP (HCC). (D) The expression profile for stem cell/tumor stem cell markers of the allograft organoid strains (n=3).

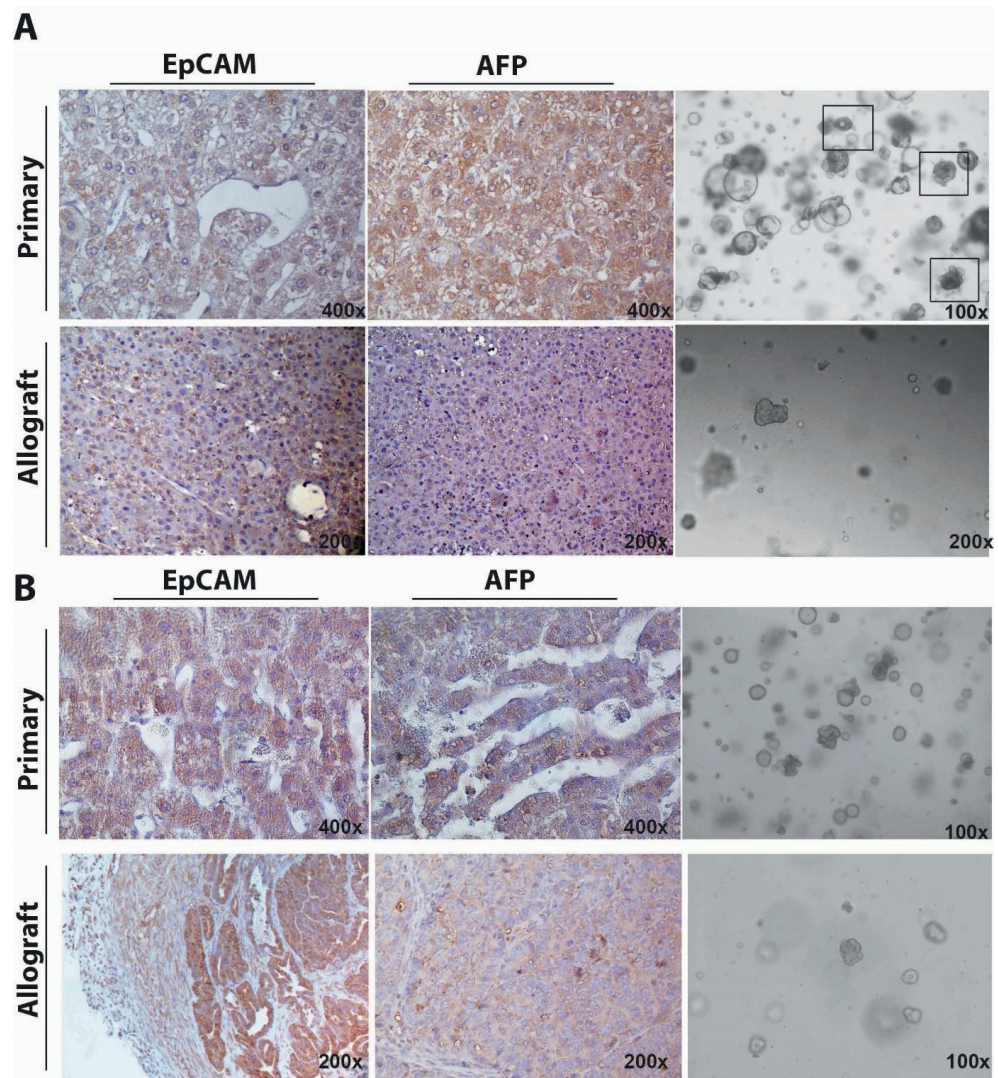


Figure 5. The characterization of organoid strains and corresponding tissue. (A) The tumor initiated by organoids showed similar histology and expression patterns of EpCAM and AFP compared to the primary tissue. Black box: the tumor organoid. (B) The tumor initiated by organoids showed different histology and expression profile of patterns of EpCAM and AFP compared to the primary tissue.

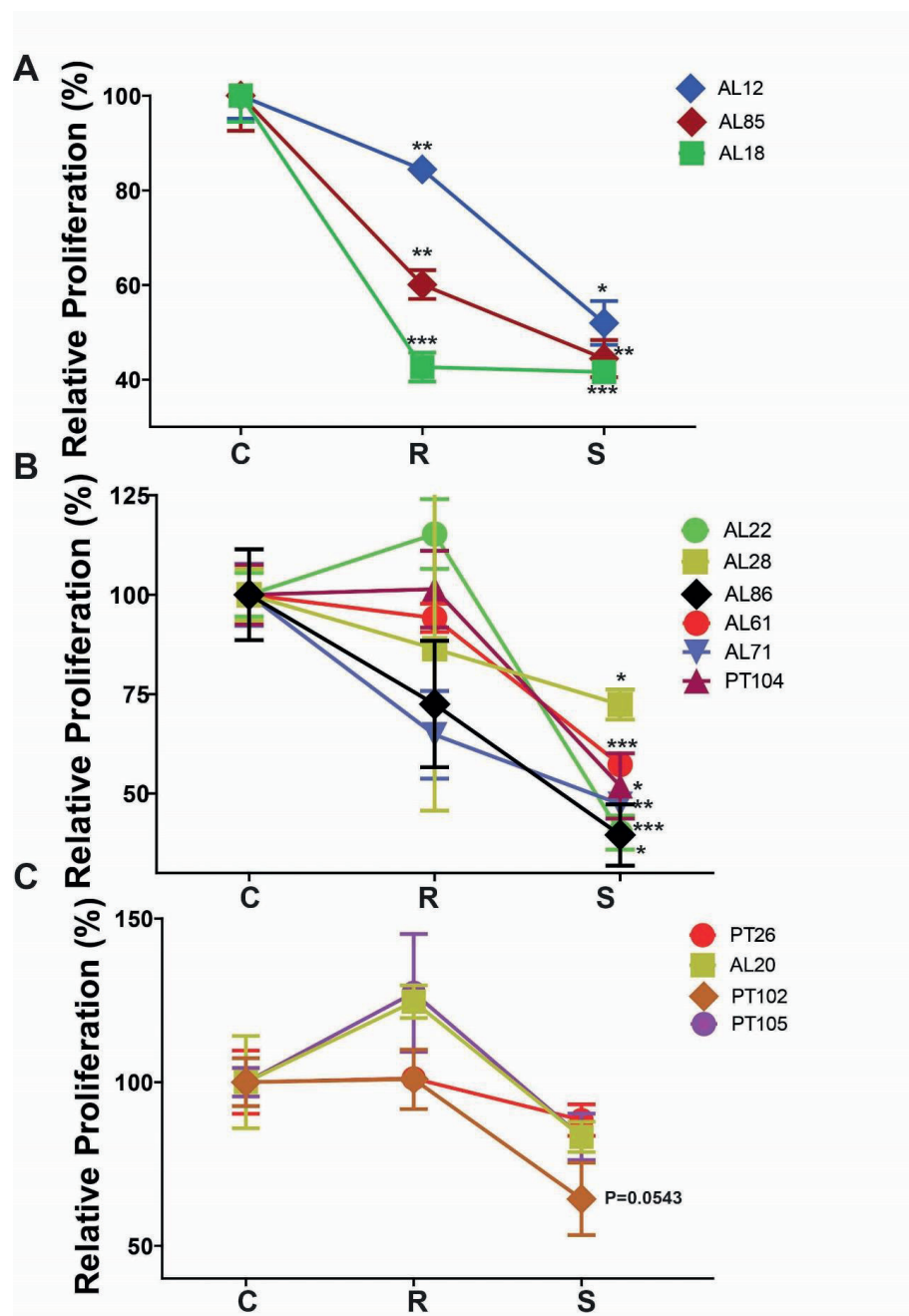


Figure 6. Tumor organoids in response to the treatment of the targeted therapeutics Sorafenib or Regorafenib. 13 tumor organoid lines (AL12, AL18, AL20, AL22, AL26, AL28, AL61, AL71, AL85, AL86, PT102, PT104 and PT105) were analyzed. At day 7, the Alamar blue assay was used to measure the growth of organoids. (* $P < .05$; ** $P < .01$; *** $P < .001$, $n=4$). (A) Group 1: organoid strains which were both sensitive to Sorafenib and Regorafenib. (B) Group 2: organoid strains which were only sensitive to Sorafenib, but not Regorafenib. (C) Group 3: organoid strains which were not sensitive to both Sorafenib and Regorafenib.

Discussion

This study has demonstrated the establishment of organoids from primary mouse liver tumors. These organoids can be expanded in long-term cultures and initiate tumors in immunodeficient mice. Importantly, these organoids recapitulate, to some extent, the heterogeneity of liver cancer as seen in patients, with respect to phenotype, cancer cell composition and treatment response.

Classically, the *in vitro* investigation of liver cancer is based on cell lines, which have the following limitations: 1) limited number of established cell lines; 2) low efficiency of establishing new lines from primary tissues; 3) only aggressive tumors have high chance to establish *in vitro* culture successfully. Thus, the majority of primary tissue (>90%) cannot be successfully culture *in vitro*, especially the benign or less aggressive tumors, which also should be further investigated. Except the traditional cell line culture model, several other methods have also been explored to model liver cancer *in vitro*. The rotating wall vessel bioreactor has been reported to be used to culture HCC cell lines. This system was further used to co-culture the liver tumor cells with colon carcinoma cells to form liver-tumor hybrid, as a model to mimic liver metastasis. In addition, 2D or 3D spheroid culture has been applied to culture HCC cell lines. However, the majority of those *in vitro* system focus on immortalized cell lines, rather than primary tissue.

We here adopted matrigel based 3D organoid culture system. This model allows investigation of healthy adult stem cells, as well as various types of diseases, in particular cancer. Successful examples have been reported in establishing organoids from colon, pancreas and prostate tumor tissues. A very recent study has reported the culture of organoids from a few liver cancer patients (13). Here we reported that we have succeeded in establishing 91 lines from 128 mouse liver tissues/tumors. These organoids are capable of long-term culture and expansion *in vitro*. They are capable of initiating tumors in immunodeficient mice upon (serial) transplantation, confirming their tumorigenic, malignant and self-renewal properties. However, a subset of the tumor organoid strains did not initiate tumor in the current allograft transplantation model. First of all, we cannot exclude the possible existence of normal organoids among these organoid lines established from primary tumors. Secondly, the mouse model used for allograft transplantation retains part of the immune system which may inhibit tumor initiation (23).

There is substantial heterogeneity among different organoid strains, in respect to organoid morphology, tissue histology and marker expression. The diversity of morphology has previously also been observed in other types of tumor organoids, such as those derived from colorectal (9), pancreatic (10,11) and prostate (12) cancer. Interestingly, the tumor histology of the allograft and the corresponding primary tumor is not always matched (Supplementary Table 2, Supplementary Table 3 and Supplementary figure 9). One possible explanation is that the current liver organoid culture protocol more favors the growth of stem cell/cholangiocyte like cells (5,13,24). Secondly, trans-differentiation between hepatocyte and cholangiocyte has

been well-recognized (25). We speculate that with the current organoid culture approach we may drive the trans-differentiation of primary HCC cells into cholangiocarcinoma cells. Last but not the least, in case of a small tumor, tissue was prioritized for organoid culture, left no representative primary tumor tissue for histology evaluation.

Our results also support the notion that liver tumors contain TIC, and organoids may represent an innovative model system for studying these cancer cells. TIC is a rare cancer cell population, but is thought to be the engine of tumor formation, relapse, metastasis and chemo-resistance in many cancer types (19), including in liver cancer (26). We envision that these tumor organoid models have potential to circumvent a major bottleneck in the TIC field as these cells are usually not able to be cultured *in vitro*. The current research is largely based on phenotypic description and tumor formation assays in immunodeficient mice (26). Sophisticated *in vitro* culture of liver tumor organoids that are capable of long-term propagation *ex vivo*, as demonstrated in our study, provides a unique tool for the research field to advance in-depth research of liver TIC.

We further reveal the heterogeneity of individual lines as well as the differences in responsiveness between treatments. This provides proof-of-concept that organoids have the potential to be used as an *in vitro* model to study anti-cancer drug development in general, as well as for personalized medicine in cancer treatment. Furthermore, TIC have been proposed as attractive anti-cancer targets and recent studies have demonstrated the possibility and efficacy of targeting TIC in animal models. Different allograft organoid strains showed different expression patterns for the stem cell/tumor stem cell markers, which may be useful for further investigation of the specific tumor initiating cell/cancer stem cell populations (Supplementary figure 10). We believe that tumor organoid models have particular privileges as a platform for facilitating the development of TIC targeted therapies, given that these cells can be *ex vivo* cultured from primary tumor tissues.

Organoid model system shall provide enormous opportunities to advance the research on liver cancer/stem cell biology, drug development and personalized medicine. Of note, organoid systems do not mutually exclude the use of the classical cancer cell lines, but in fact complement each other. Finally, more efforts are urgently required to establish robust organoid models from patient liver tumors.

Acknowledgments

We thank S.A. van der Heide-Mulder and R. Lieshout for technical assistance. This research is supported by the KWF (Dutch Cancer Society) Young Investigator Grant 10140 (to Q.P.), the Daniel den Hoed Foundation for a Centennial Award fellowship (to Q. Pan) and the China Scholarship Council for funding PhD fellowships to W. Cao (201307060013), Y. Yin (201307720045), M. Li (201506100033), B. Ma (201508330291) and J. Liu (201606240079).

Authors' Contributions

J.L, L.W and M.L contributed equally and share co-second authorship.

Reference

1. Llovet, J.M., *et al.* (2008) Sorafenib in advanced hepatocellular carcinoma. *N Engl J Med*, **359**, 378-90.
2. Voskoglou-Nomikos, T., *et al.* (2003) Clinical predictive value of the in vitro cell line, human xenograft, and mouse allograft preclinical cancer models. *Clin Cancer Res*, **9**, 4227-39.
3. Llovet, J.M., *et al.* (2016) Hepatocellular carcinoma. *Nat Rev Dis Primers*, **2**, 16018.
4. Michalopoulos, G.K., *et al.* (2001) Histological organization in hepatocyte organoid cultures. *Am J Pathol*, **159**, 1877-87.
5. Huch, M., *et al.* (2013) In vitro expansion of single Lgr5+ liver stem cells induced by Wnt-driven regeneration. *Nature*, **494**, 247-50.
6. Sato, T., *et al.* (2009) Single Lgr5 stem cells build crypt-villus structures in vitro without a mesenchymal niche. *Nature*, **459**, 262-5.
7. Clevers, H. (2016) Modeling Development and Disease with Organoids. *Cell*, **165**, 1586-1597.
8. Bredenoord, A.L., *et al.* (2017) Human tissues in a dish: The research and ethical implications of organoid technology. *Science*, **355**.
9. van de Wetering, M., *et al.* (2015) Prospective derivation of a living organoid biobank of colorectal cancer patients. *Cell*, **161**, 933-45.
10. Li, X., *et al.* (2014) Oncogenic transformation of diverse gastrointestinal tissues in primary organoid culture. *Nat Med*, **20**, 769-77.
11. Boj, S.F., *et al.* (2015) Organoid models of human and mouse ductal pancreatic cancer. *Cell*, **160**, 324-38.
12. Gao, D., *et al.* (2014) Organoid cultures derived from patients with advanced prostate cancer. *Cell*, **159**, 176-87.
13. Broutier, L., *et al.* (2017) Human primary liver cancer-derived organoid cultures for disease modeling and drug screening. *Nat Med*, **23**, 1424-1435.
14. Schutte, M., *et al.* (2017) Molecular dissection of colorectal cancer in pre-clinical models identifies biomarkers predicting sensitivity to EGFR inhibitors. *Nat Commun*, **8**, 14262.
15. Lancaster, M.A., *et al.* (2014) Organogenesis in a dish: modeling development and disease using organoid technologies. *Science*, **345**, 1247125.
16. Huch, M., *et al.* (2015) Long-term culture of genome-stable bipotent stem cells from adult human liver. *Cell*, **160**, 299-312.
17. He, L., *et al.* (2015) Mouse models of liver cancer: Progress and recommendations. *Oncotarget*, **6**, 23306-22.

18. Pan, Q., *et al.* (2014) Detection of spontaneous tumorigenic transformation during culture expansion of human mesenchymal stromal cells. *Exp Biol Med (Maywood)*, **239**, 105-15.
19. Peitzsch, C., *et al.* (2017) Cancer stem cells: The root of tumor recurrence and metastases. *Semin Cancer Biol.*
20. La Porta, C.A., *et al.* (2017) Complexity in cancer stem cells and tumor evolution: Toward precision medicine. *Semin Cancer Biol.*
21. Kim, H., *et al.* (2004) Primary liver carcinoma of intermediate (hepatocyte-cholangiocyte) phenotype. *J Hepatol*, **40**, 298-304.
22. Bruix, J., *et al.* (2013) Regorafenib as second-line therapy for intermediate or advanced hepatocellular carcinoma: multicentre, open-label, phase II safety study. *Eur J Cancer*, **49**, 3412-9.
23. Shultz, L.D., *et al.* (2012) Humanized mice for immune system investigation: progress, promise and challenges. *Nat Rev Immunol*, **12**, 786-98.
24. Cao, W., *et al.* (2017) Dynamics of Proliferative and Quiescent Stem Cells in Liver Homeostasis and Injury. *Gastroenterology*, **153**, 1133-1147.
25. Schaub, J.R., *et al.* (2018) De novo formation of the biliary system by TGFbeta-mediated hepatocyte transdifferentiation. *Nature*, **557**, 247-251.
26. Yamashita, T., *et al.* (2013) Cancer stem cells in the development of liver cancer. *J Clin Invest*, **123**, 1911-8.

Supplementary data for

Modeling liver cancer and therapy responsiveness using organoids derived from primary mouse liver tumors

Wanlu Cao¹, Meng Li^{1*}, Jiaye Liu^{1*}, Ling Wang^{1*}, Monique M.A. Verstegen², Yuebang Yin¹, Buyun Ma¹, Kan Chen³, Michiel Bolkestein^{2,4}, Dave Sprengers¹, Luc J. W. van der Laan², Michael Doukas⁵, Jaap Kwekkeboom¹, Ron Smits¹, Maikel P. Peppelenbosch¹ and Qiuwei Pan¹

Table of contents

Supplementary Figure 1

Supplementary Figure 2

Supplementary Figure 3

Supplementary Figure 4

Supplementary Figure 5

Supplementary Figure 6

Supplementary Figure 7

Supplementary Figure 8

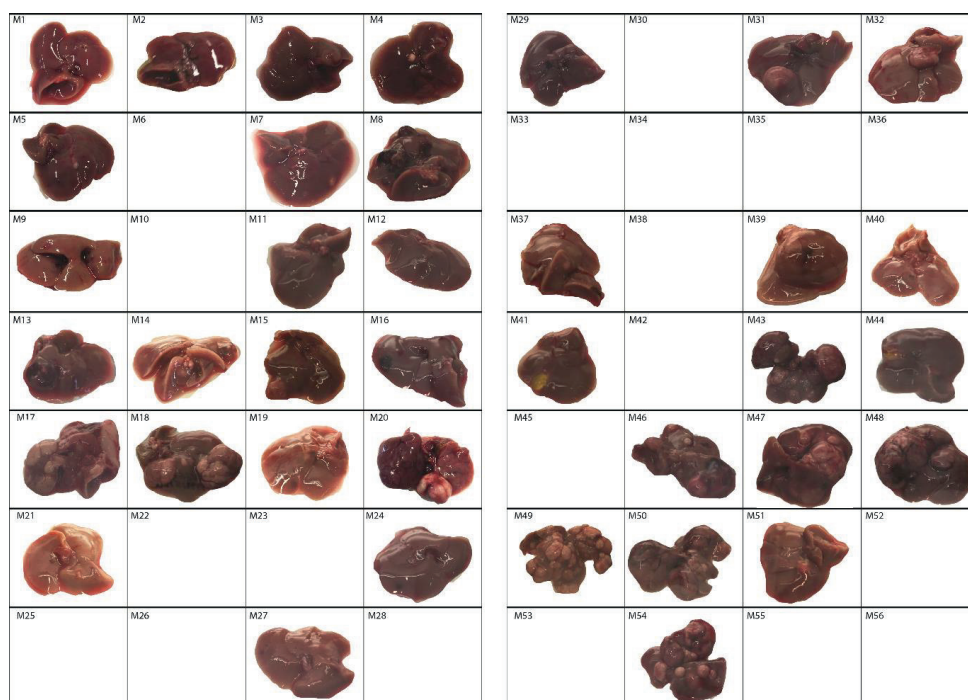
Supplementary Figure 9

Supplementary Figure 10

Supplementary Table 1

Supplementary Table 2

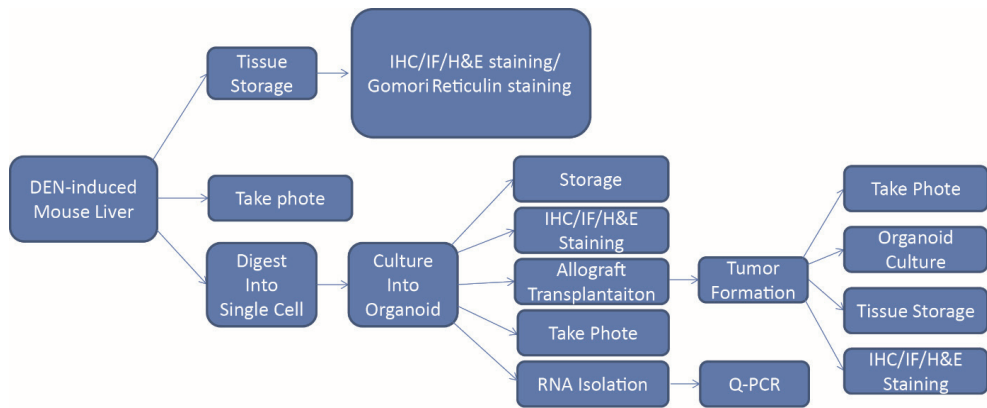
Supplementary Table 3



Supplementary Figure 1. The livers. The black squares are pictures of the corresponding livers which missed due to technical issue.

	Organoid Code	Mice Background	M/F	Primary Tumor Formation Time(Month)		Organoid Code	Mice Background	M/F	Primary Tumor Formation Time(Month)
1	PT1	B6	M	7	47	PT57	B6	M	10
2	PT2	B6/CD1	M	7	48	PT59	B6/CD1	M	14
3	PT3	B6/CD1	M	7	49	PT61	B6	M	14
4	PT6	B6	M	7	50	PT62	B6/CD1	M	15
5	PT7	B6	M	7	51	PT63	B6/C3H	M	8
6	PT8	B6	M	7	52	PT68	B6	M	8
7	PT9	B6	M	7	53	PT69	B6	M	8
8	PT10	B6	M	13	54	PT70	B6	M	8
9	PT11	B6	M	12	55	PT71	B6	M	15
10	PT12	B6/CD1	M	14	56	PT72	B6/C3H	M	7
11	PT13	B6/CD1	F	12	57	PT77	B6/CD1	M	14
12	PT14	B6/CD1	M	12	58	PT78	B6	M	8
13	PT15	B6/CD1	F	12	59	PT79	B6/C3H	M	8
14	PT16	B6	M	13	60	PT80	B6/C3H	M	7
15	PT17	B6	M	10	61	PT81	B6	M	15
16	PT18	B6	M	13	62	PT82	B6/C3H	M	7
17	PT19	B6	M	9	63	PT85	B6/C3H	M	7
18	PT20	B6/CD1	M	16	64	PT86	B6/C3H	M	8
19	PT21	B6/CD1	M	16	65	PT87	B6	M	15
20	PT22	B6	M	9	66	PT88	B6/C3H	M	8
21	PT23	B6/C3H	M	5	67	PT89	B6	M	15
22	PT24	B6	M	7	68	PT90	B6	M	15
23	PT25	B6/CD1	M	15	69	PT92	B6/CD1	M	15
24	PT26	B6	M	9	70	PT91	B6	M	15
25	PT27	B6	M	13	71	PT93	B6/CD1	M	15
26	PT28	B6	M	13	72	PT94	B6	M	15
27	PT29	B6	M	9	73	PT96	B6	M	15
28	PT30	B6	M	9	74	PT97	B6	M	15
29	PT31	B6	M	9	75	PT98	B6	M	15
30	PT32	B6	M	14	76	PT99	B6	M	15
31	PT35	B6	M	13	77	PT100	B6/C3H	M	8
32	PT36	B6	M	12	78	PT101	B6/C3H	M	8
33	PT37	B6	M	13	79	PT102	B6/CD1	M	14
34	PT38	B6	M	6	80	PT103	B6	M	13
35	PT39	B6/C3H	M	3	81	PT104	B6	M	13
36	PT40	B6	F	15	82	PT105	B6	M	13
37	PT41	B6	M	9	83	PT107	B6	M	15
38	PT42	B6	M	13	84	PT108	B6/CD1	M	15
39	PT43	B6	M	13	85	PT109	B6/CD1	M	15
40	PT44	B6	M	13	86	PT110	B6/CD1	M	16
41	PT45	B6	M	13	87	PT111	B6/C3H	M	7
42	PT46	B6	M	13	88	PT112	B6	M	15
43	PT47	B6	M	16	89	PT113	B6/CD1	M	15
44	PT49	B6	M	13	90	PT115	B6	M	15
45	PT51	B6	M	14	91	PT116	B6&C3H	M	8
46	PT52	B6/CD1	M	14					

Supplementary Figure 2. Tumor organoid lines. All the 91 tumor organoid lines, for the genetic background, gender and primary tumor formation time (counted since the time of first Den injection until the time to sacrifice the mice).



Supplementary Figure 3. The flowchart of the experimental design.

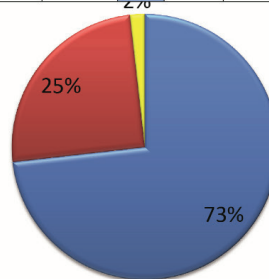
A

Mice Code	Organoid Code	Number of Initiated Organoid Stain	Tissue Number from each Mice	Initiation Efficiency(%)	Mice Code	Organoid Code	Number of Initiated Organoid Stain	Tissue Number from each Mice	Initiation Efficiency(%)	Mice Code	Organoid Code	Number of Initiated Organoid Stain	Tissue Number from each Mice	Initiation Efficiency(%)
M1	PT1	1	1	100		PT34				M39	PT68	4	4	100
M2	PT2	2	4	50		PT122					PT69			
	PT3					PT123					PT70			
	PT4					PT124					PT78			
	PT5				M20	PT32	1	1	100	M40	PT71	1	1	100
M3	PT6	2	2	100	M21	PT112	1	1	100	M41	PT72	1	1	100
	PT7				M22	PT116	1	1	100	M42	PT73	3	5	60
M4	PT8	3	3	100	M23	PT35	1	1	100		PT74			
	PT9				M24	PT36	1	1	100		PT92			
	PT24				M25	PT38	1	1	100		PT94			
M5	PT10	2	2	100	M26	PT39	1	1	100		PT115			
	PT16				M27	PT40	1	1	100	M43	PT75	3	8	37.5
M6	PT11	1	1	100	M28	PT42	1	6	16.7		PT76			
M7	PT12	1	5	20		PT125					PT81			
	PT53					PT126					PT90			
	PT54					PT127					PT95			
	PT55					PT128					PT107			
	PT56					PT60					PT117			
M8	PT13	2	2	100	M29	PT43	2	3	66.7		PT118			
	PT15					PT67				M44	PT88	1	1	100
M9	PT14	1	1	100		PT77				M45	PT113	1	1	100
M10	PT17	2	2	100	M30	PT96	1	1	100	M46	PT80	2	2	100
	PT57				M31	PT45	3	4	75		PT82			
M11	PT18	1	2	50		PT58				M47	PT85	1	1	100
	PT84					PT46				M48	PT87	3	3	100
M12	PT19	2	2	100		PT108					PT97			
	PT41				M32	PT47	2	2	100		PT98			
M13	PT20	2	2	100		PT44				M49	PT93	1	1	100
	PT21				M33	PT48	0	1	0	M50	PT99	1	1	100
M14	PT22	3	3	100	M34	PT49	2	2	100	M51	PT100	2	2	100
	PT26					PT51					PT101			
	PT31				M35	PT50	2	3	66.7	M52	PT102	1	1	100
M15	PT23	1	4	25		PT52				M53	PT103	3	3	100
	PT65					PT59					PT104			
	PT66				M36	PT61	1	2	50		PT105			
	PT83					PT114				M54	PT109	1	1	100
M16	PT25	1	1	100	M37	PT62	1	4	25	M55	PT110	1	1	100
M17	PT27	2	2	100		PT119				M56	PT111	1	1	100
	PT37					PT120								
M18	PT28	3	3	100		PT121								
	PT89				M38	PT63	3	5	60					
	PT91					PT64								
M19	PT29	2	7	28.6		PT79								
	PT30					PT86								
	PT33					PT106								

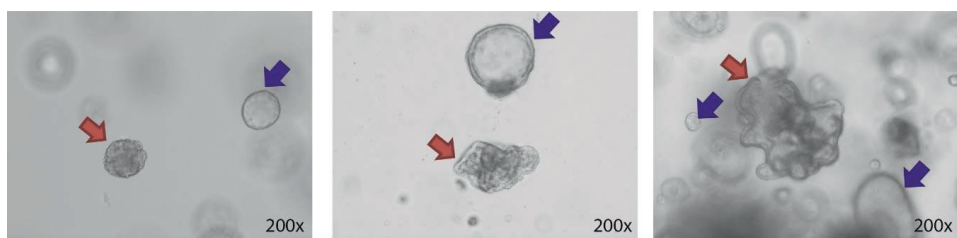
B

Organoid initiation efficiency from individual mouse

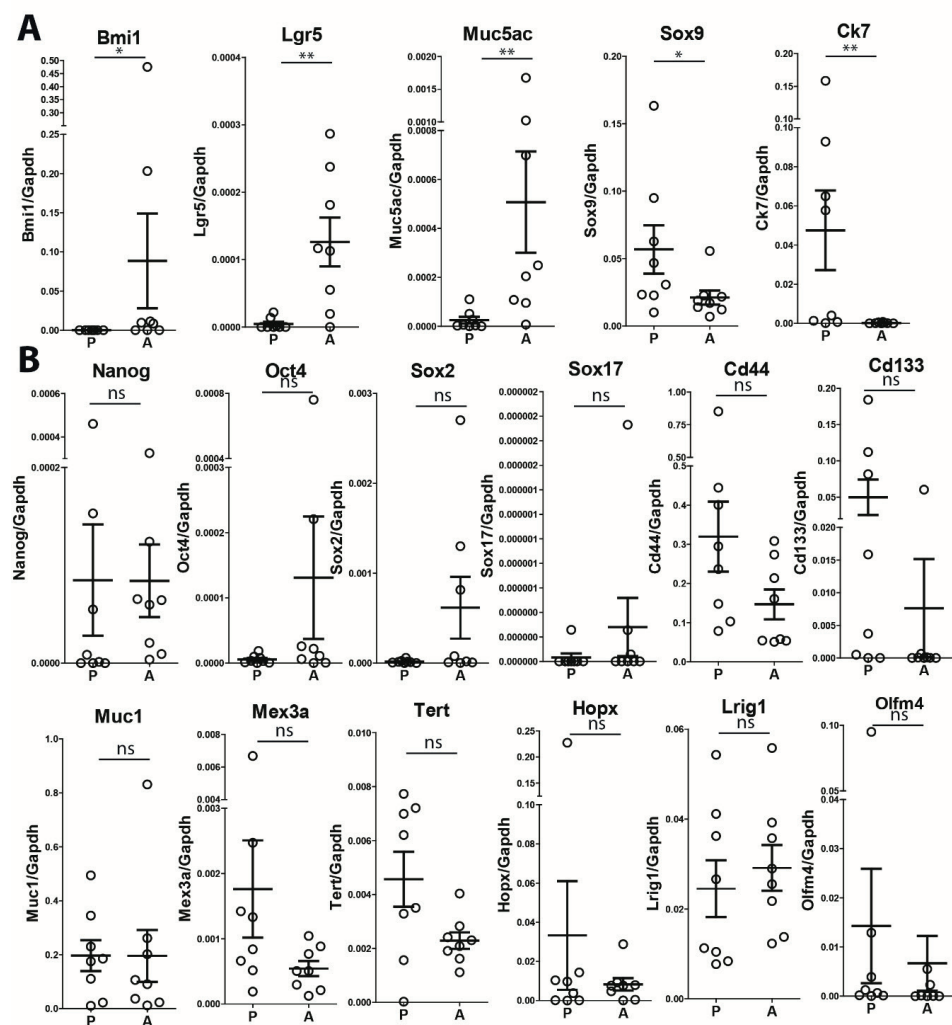
■ 100% ■ 1%-99% ■ 0%



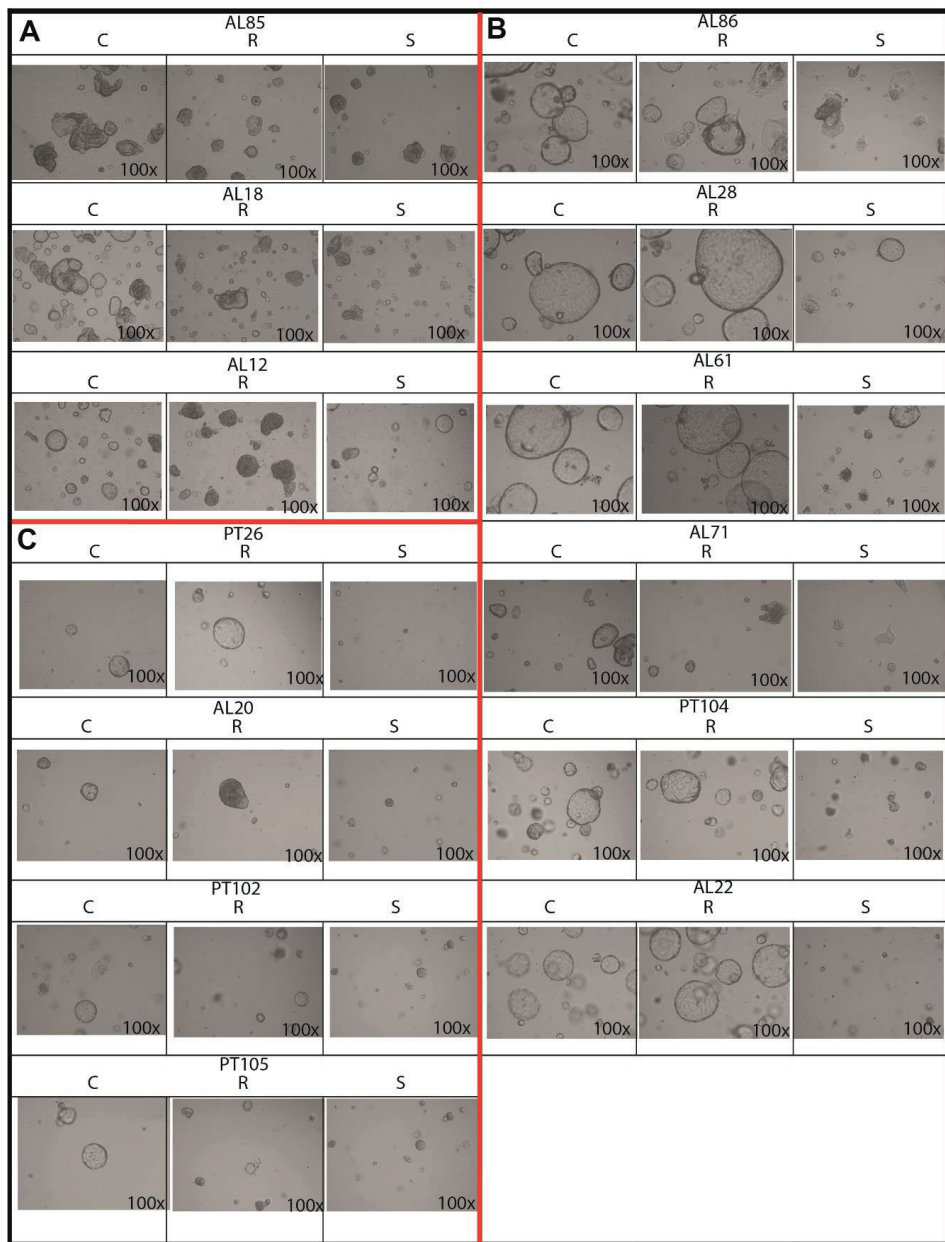
Supplementary Figure 4. The organoid strains grouped according to the mice. (A) The organoid strains which were successfully initiated and maintained are marked by green; The organoid strains which were successfully initiated (maintained over 3 months), transplanted into NOG mice for tumor initiation but lost afterward due to storage issue/infection are marked by yellow. (B) The distribution of the organoid initiation efficiency for individual mouse liver.



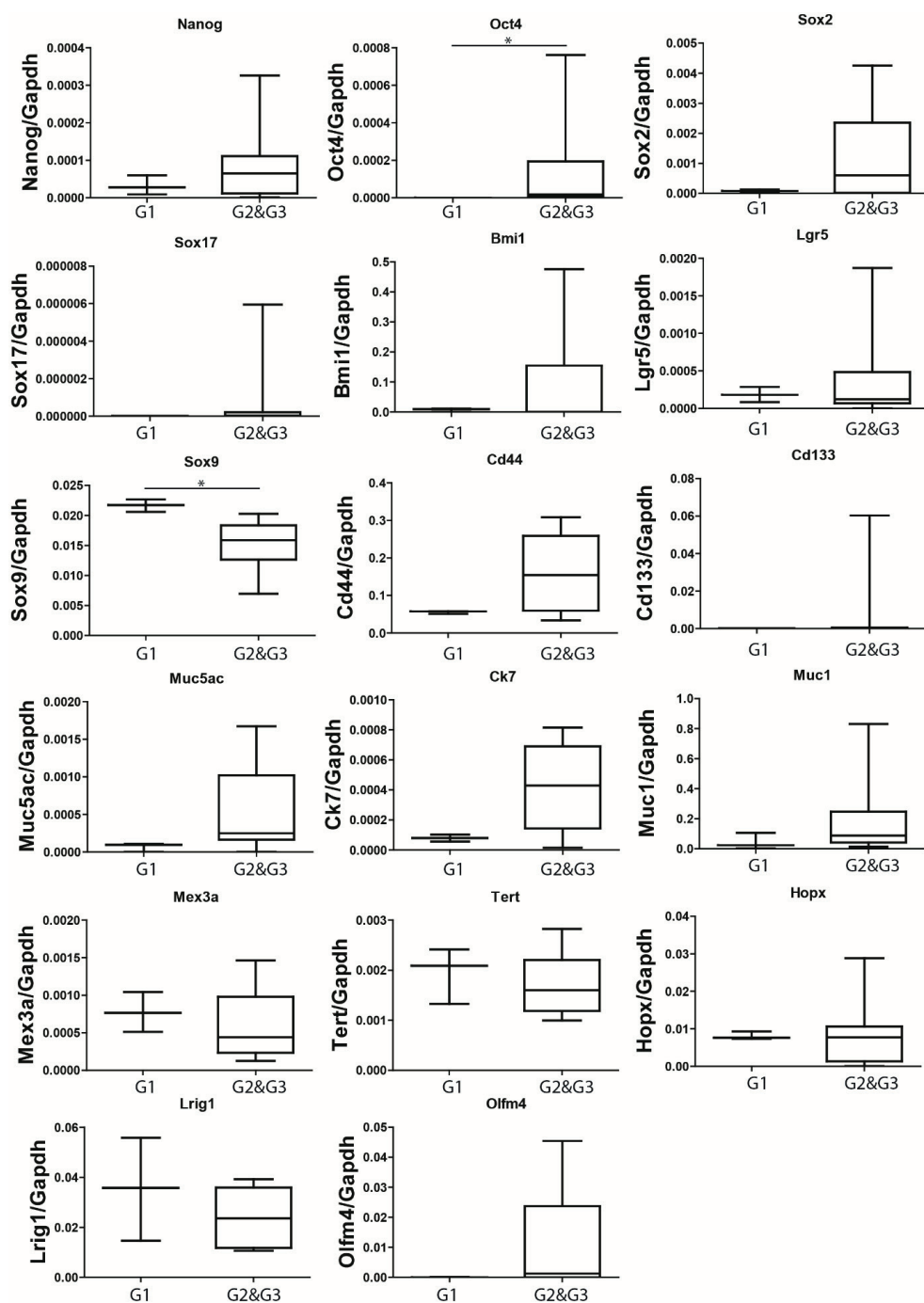
Supplementary Figure 5. Tumor organoids show mixed morphology. Red arrow: “tumor organoid” morphology; Blue arrow: “normal organoid” morphology.



Supplementary Figure 6. The panel of progenitor cell markers which compared between paired primary organoid strains and corresponding allograft organoid strains (* $P < .05$; ** $P < .01$; $n = 8$).

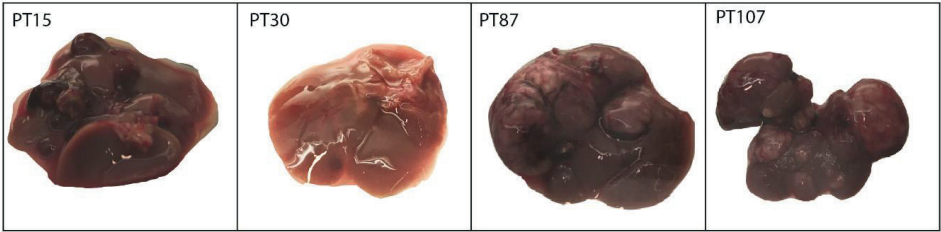


Supplementary Figure 7. Tumor organoids in response to the treatment of the targeted therapeutics Sorafenib or Regorafenib. (A) Representative pictures taken at day 7, showing that tumor organoids respond differently to the treatment (n=4). (A) Group 1: organoid strains which were both sensitive to Sorafenib and Regorafenib. (B) Group 2: organoid strains which were only sensitive to Sorafenib, but not Regorafenib. (C) Group 3: organoid strains which were not sensitive to both Sorafenib and Regorafenib.

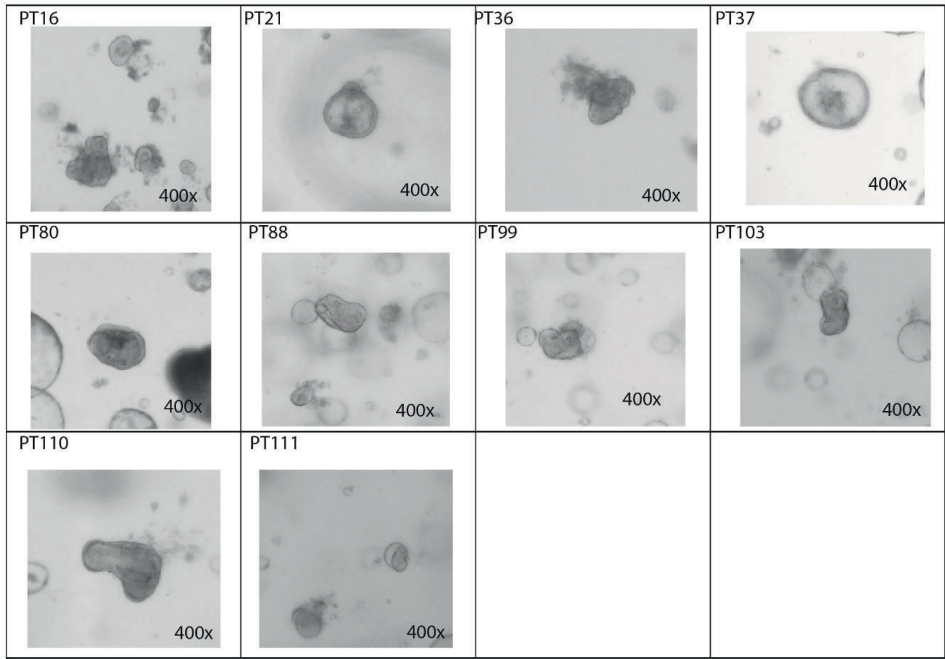


Supplementary figure 8: The panel of progenitor cell markers which compared between Group 1 (organoid strains which were sensitive to both treatment) and the rest strains (* $P < .05$; ** $P < .01$).

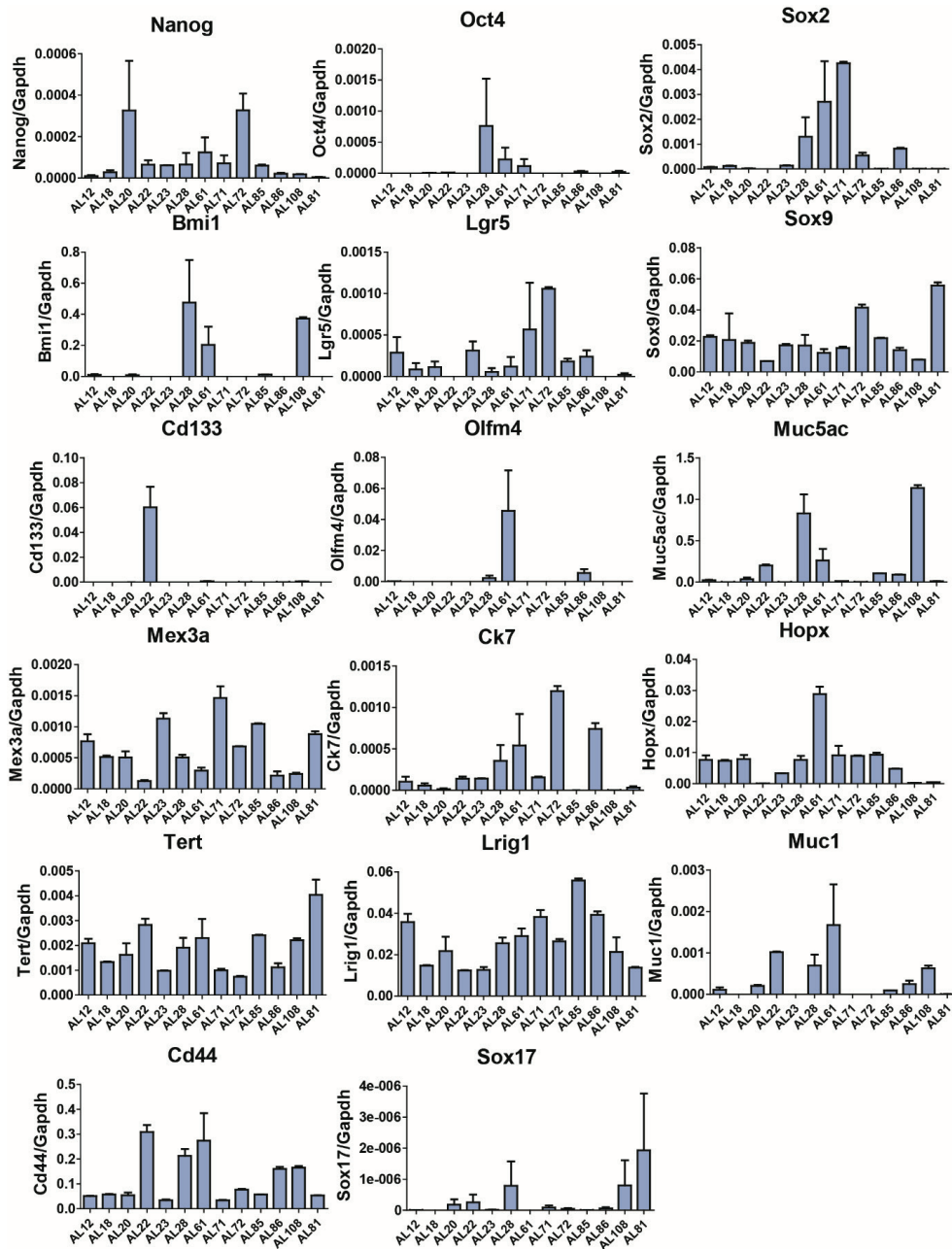
Group 3: Tumor liver



Group 5: Tumor organoid



Supplementary figure 9: (A) Group 3: The organoid strains showed normal organoid morphology, normal tissue histology but liver tumor morphology. (B) Group 5: The organoid strains showed tumor organoid morphology but with normal histology.



Supplementary figure 10: Allograft organoid strains have different profiles of stem cell/tumor stem cell expression.

Tumor Organoid Lines				
	Organoid Code	Primary Tumor Harvesting Time(Month)	Mice Background	Allograft Tumor Harvesting Time(Day)
1 2 3 4 5 6 7 8 9 10 11 12 13 14 15 16 17 18	PT12	14	B6/CD1	24
	PT18	13	B6	58
	PT20	16	B6/CD1	41
	PT22	9	B6	58
	PT23	5	B6/C3H	58
	PT26	9	B6	58
	PT28	13	B6	58
	PT61	14	B6	36
	PT71	15	B6	22
	PT72	7	B6/C3H	22
	PT81	15	B6	66
	PT85	7	B6/C3H	40
	PT86	8	B6/C3H	40
	PT102	14	B6/CD1	33
	PT104	13	B6	33
	PT105	13	B6	33
	PT108	13	B6	16
	PT109	14	B6	36
Tumor Re-initiation From Allograft Tumor Derived Organoids				
	Organoid Code	2nd Allograft Tumor Harvesting Time (Day)		
1 2 3 4	AT65	28		
	AT66	28		
	AT83	42		
	AT84	42		
Tumor Initiation Of Single Organoids				
	Organoid Code	2nd Allograft Tumor Harvesting Time (Day)		
1 2 3	AT50	14		
	AT53	22		
	AT54	22		

Supplementary Table 1. Liver tumor organoid can initiate tumor. The upper panel: The primary tumor organoid lines which formed tumor in the NOG mice, and the corresponding information of tumor harvesting time and mouse strain; The middle panel: Tumor organoids derived from the allograft (1st allograft) can re-initiate tumor again (2nd allograft) in the NOG mice; The lower panel: The corresponding tumor harvesting time of single cell formed organoid derived allograft tumors.

Primary strain		Allograft strain	
PT12	Normal, Extramedullary hematopoiesis	AL12	CC or d/d mixed type
PT18	Normal	AL18	Cc with complex papillary structures
PT20	HCC, possibly also with an hemangioma	AL20	CC with complex papillary structures/villi structure.
PT22	HCC, possibly also with an vascular tumor	AL22	Not sure tumor type
PT23	HCC	AL23	CC
PT26	Hemangioma	AL26	Not sure tumor type
PT28	HCC	AL28	CC
PT61	Small HCC	AL61	CC
PT71	Normal	AL71	CC
PT72	Normal	AL72	CC or mixed type
PT81	HCC	AL81	HCC
PT85	HCC	AL85	CC or mixed type
PT86	HCC	AL86	CC
PT102	Normal	AL102	Maybe CC
PT104	CC	AL104	CC
PT105	HCC, with hemangioma	AL105	Not sure tumor type
PT108	HCC	AL108	Not sure tumor type
PT109	HCC tumor	AL109	Not sure tumor type

Supplementary Table 2: The histology for paired primary organoid strain (PT) and allograft organoid strain (AL). The green mark: the strains which showed consistent histology between primary and allograft tissues.

Group 1: Normal		Group 2: Tumor histology	
Organoid code	Tissue Histology	Organoid code	Tissue Histology
PT1	Normal	PT8	HCC d/d mixed type
PT2	Normal	PT9	Mixed type
PT3	Normal	PT11	HCC(?), No obvious Portal traid
PT6	Normal		
PT7	Normal		
PT10	Normal		
PT14	Normal	PT13	Necrosis, HCC
PT19	Normal	PT32	Necrosis, HCC
PT24	Normal	PT68	HCC
PT25	Normal	PT79	HCC
PT35	Normal	PT82	HCC
PT39	Normal	PT90	HCC
PT57	Normal	PT93	HCC
PT89	Normal	PT97	HCC With pale bodies (fibrinogen), Mallory hyaline
PT91	Normal		
PT96	Normal	PT98	HCC, steatosis, pale bodies
PT112	Normal	PT100	HCC
Group 3: Tumor liver		PT101	HCC
Organoid code	Tissue Histology	PT115	HCC
PT15	Normal	PT116	HCC
PT30	Normal	Group 4: Other diseases	
PT87	Normal	Organoid code	Tissue Histology
PT107	Normal	PT27	Necrosis, Fat liver
Group 5: Tumor organoid		PT29	Hemangioma
Organoid code	Tissue Histology	PT31	A possible tumor
PT16	Normal	PT38	Gland structure, could be maglinant, cholangiocyte direction differentiation
PT21	Normal		
PT36	Normal	PT40	Steatosis liver
PT37	Fat liver	PT49	Fat liver
PT80	Necrosis	PT92	Necrosis
PT88	Normal	PT113	Necrosis tumor
PT99	Normal		
PT103	Normal		
PT110	Normal		
PT111	Normal		

Supplementary Table 3: Different groups of organoids which grouped by liver morphology, histology, organoid morphology. Group 1: 17 out of 55 strains showed normal for all three aspect, thus considering as “Normal group” (30.9%); Group 2: 16 out of 55 showed tumor organoid morphology with tumor/”normal” histology, considering as tumor organoid group (29.1%). Group 3: 4 out of 55 showed normal organoid morphology with tumor liver morphology (7.3%); Group 4: 8 out of 55 showed “normal” organoid

morphology but with normal/other disease histology (14.5%); Group 5: 10 out of 55 showed tumor organoid morphology but with normal/other disease histology (18.2%);

CHAPTER 6

LGR5 marks targetable tumor-initiating cells in liver cancer

Wanlu Cao¹, Meng Li^{1*}, Jiaye Liu^{1*}, Shaoshi Zhang¹, Lisanne Noordam¹, Monique M. A. Verstegen², Ling Wang¹, Buyun Ma¹, Shan Li¹, Wenshi Wang¹, Michiel Bolkestein^{2,3}, Michael Doukas⁴, Kan Chen^{1,5,6}, Zhongren Ma⁵, Marco Bruno¹, Dave Sprengers¹, Jaap Kwekkeboom¹, Luc J. W. van der Laan², Ron Smits¹, Maikel P. Peppelenbosch¹ and Qiuwei Pan¹

¹Department of Gastroenterology and Hepatology, Erasmus MC-University Medical Center, Rotterdam, The Netherlands.

²Department of Surgery, Erasmus MC-University Medical Center, Rotterdam, The Netherlands.

³Department of Cell Biology, Erasmus MC-University Medical Center, Rotterdam, The Netherlands.

⁴Department of Pathology, Erasmus MC-University Medical Center, Rotterdam, The Netherlands.

⁵Biomedical Research Center, Northwest Minzu University, Lanzhou, China.

⁶College of Life Sciences, Zhejiang Sci-Tech University, Hangzhou, China.

***Nat Commun.* 2020 Apr 23;11(1):1961.**

Abstract

Cancer stem cells (CSCs) or tumor-initiating cells (TICs) are thought to be the main drivers for disease progression and treatment resistance across various cancer types. Identifying and targeting these rare cancer cells, however, remains challenging and unproven with respect to therapeutic benefit. Here, we report the enrichment of LGR5 expressing cells, a well-recognized stem cell marker, in mouse liver tumors, and the upregulation of LGR5 expression in human hepatocellular carcinoma. Isolated LGR5 expressing cells from mouse liver tumors are superior in initiating organoids in 3D culture and forming tumors in immunodeficient mice upon engraftment compared to LGR5⁻ cells, featuring candidate TICs. These cells are resistant to conventional treatment including sorafenib and 5-FU. Importantly, LGR5 lineage ablation significantly inhibits organoid initiation and tumor growth. The combination of LGR5 ablation with 5-FU, but not sorafenib, further augments the therapeutic efficacy *in vivo*. Thus, we have identified the LGR5⁺ compartment as an important TIC population, representing a viable therapeutic target for combating liver cancer.

Keyword: LGR5; Tumor-initiating cells, Liver cancer; Anti-cancer target.

Introduction

The key concept underlying the cancer stem cell (CSC) or tumor-initiating cell (TIC) theory is that tumors are maintained through a hierarchical structure in which different cell populations have different functionalities in pathophysiology¹. The bulk of a tumor is thought to consist of CSCs/TICs as well as rapidly proliferating cells. CSCs/TICs are responsible for tumor initiation, resistance to conventional treatment and distant metastasis. Rapidly proliferating cancer cells, thought to be derived from the tumor stem cell pool, are responsible for volume increment of the tumor². A prediction based on this model is that ablation of the relatively small CSC compartment would ultimately result in cessation of tumor growth and metastasis, and provoke sensitization of the tumor to conventional treatment as well.

Within the framework of this theory, CSCs/TICs would be characterized by a large capacity for self-renewal, a potential for differentiation into different cell types that constitute the tumor, and a resistance to conventional treatment¹. These key features largely overlap with those of normal stem cells, making it extremely difficult to specifically identify CSCs/TICs, but on the other hand would allow techniques traditionally used for identifying normal stem cells also to be applied for CSCs/TICs³. LGR5 (leucine-rich repeat-containing G protein-coupled receptor 5) evokes special interest as a potential marker for the CSC/TIC compartment in this respect. LGR5 is a well-characterized stem cell marker in several tissues/organs, including the small intestine, the colon and the liver⁴⁻⁶. In colon and intestine, the LGR5 stem cell pool constantly proliferates and differentiates into mature cell types to compensate for the loss of functional epithelial cells. Interestingly, these LGR5 stem cells also participate in the process of oncogenesis, acting as the cells-of-origin of intestinal cancer⁷. Importantly, LGR5 marks CSCs in colon cancer⁸⁻¹⁰, intestinal cancer¹¹ and basal cell carcinoma¹². In intestinal adenoma as well as malignant carcinoma, LGR5 cells account consistently for a ratio of 5-10% of tumor cells and fuel tumor growth^{8,13}. Proof-of-concept showing that specific elimination of LGR5 cells delays tumor growth in colon cancer has been provided⁹. Given the essential role of CSCs/TICs, these cells are attractive targets for anti-cancer treatment, whereas their resistance to conventional therapies impedes the therapeutic development.

In contrast to the colon and intestine, LGR5 stem cells are absent in the homeostatic liver, but emerge upon tissue injury^{4,14}. These liver LGR5 cells are likely to be an intermediate stem/progenitor cell population that responds to injury but they may have a limited contribution to tissue repair¹⁴. Whether an LGR5⁺ compartment exists in liver cancer remains obscure and the possible importance of such a compartment in this disease is unexplored. Nevertheless, research into this possibility is urgently needed as liver cancer is one of the most common forms of malignancy worldwide, with nearly 800,000 cases reported yearly and it is characterized by a depressing lack of treatment options¹⁵. Hepatocellular carcinoma (HCC) and cholangiocarcinoma (CC) are the two main types of primary liver cancer. Currently, surgery remains the only potentially curative therapeutic strategy available but is well-known for its high recurrence rate following tumor resection. Chemotherapy and targeted treatment are

generally ineffective, with sorafenib providing some extension of life expectancy to HCC patients. The unusual treatment resistance of liver cancer is thought to be associated with the presence of CSCs/TICs, but this notion remains largely unproven¹⁶. Thus, we aimed to investigate whether LGR5 marks CSCs/TICs in liver cancer, and to explore the potential for therapeutic targeting of these cells. Our results show that in liver cancer an LGR5⁺ compartment exists that is superior in tumor initiation and mediates therapy resistance. Targeting this compartment constitutes a rational novel avenue for combating this disease.

Results

Enrichment of LGR5 expressing cells in primary liver tumors

Homeostatic livers are reported to be devoid of LGR5⁺ cells, but injury does induce such cells¹⁴. Whether LGR5⁺ cells are present in liver cancer is largely unknown. By adopting *Lgr5-DTR-GFP* knock-in mice (**Fig. 1a**), we first investigated the presence of LGR5⁺ cells (GFP co-expressing cells) in the healthy and injured liver, and during carcinogenesis. Carbon tetrachloride (CCl₄) was used to trigger liver injury. Diethylnitrosamine (DEN) was used to induce primary liver tumor formation (**Fig. 1b**, and **Supplementary Fig. 1**). Although LGR5 cells are absent in the homeostatic liver (**Fig. 1c**), either a single course or repeated administration of DEN can rapidly trigger the emergence of LGR5-GFP⁺ cells (post DEN induction day 7; relative size of the LGR5-GFP⁺ compartment following 1 X DEN: $0.025 \pm 0.05\%$, $n = 3$ [mean \pm SEM]; **Supplementary Fig. 2a-b**). Animals were monitored for liver tumor formation from 4 to 14 months post DEN induction (**Supplementary File. 1**). Analysis of the resulting hepatic neoplasms revealed stable presence of an LGR5⁺ compartment in these liver tumors (**Fig. 1c**). The relative abundance of LGR5 cells in the tumors (**Supplementary File. 1** and **Supplementary Fig. 2c-d**) are significantly higher as compared to those in the tumor surrounding tissues (**Fig. 1d**) or as detected in CCl₄ injured livers (**Fig. 1c**). The LGR5 expression levels in the tumor cells show substantial variation, but are substantially and significantly higher compared to that in injured liver (**Fig. 1e**). Immunohistochemistry (IHC) and immunofluorescence (IF) staining of GFP expression further confirms the presence of an LGR5⁺ compartment and enables detailed analysis of spatial distribution of LGR5-GFP⁺ cells in the liver (IF: **Fig. 1f**; IHC: **Supplementary Fig. 2e-f**). Co-staining with hepatocyte marker (HNF4 α) or cholangiocyte marker (CK19) revealed that a proportion of LGR5 cells in the tumor express HNF4 α or CK19 (**Fig. 1g-h**), suggesting that LGR5⁺ cells may give rise to both a HCC-like and a CC-like phenotype, the two main types of primary liver cancer. Thus, these data have demonstrated the presence of an LGR5⁺ compartment in primary murine liver cancer.

To examine the clinical relevance, we investigated *LGR5* expression in human HCC tumors from our patient cohort (Erasmus MC cohort). We found that *LGR5* expression is significantly elevated in tumor tissues compared to the paired tumor free liver tissues (**Fig. 2a**), and also in some subpopulations of patients with specific etiologies of HCC (**Fig. 2b**). Survival analysis by predicting Kaplan-Meier curves revealed a tendency towards worse clinical outcome in patients with higher *LGR5* expression (**Fig. 2c**). Further analysis of online publically available datasets confirmed the upregulation of *LGR5* expression in HCC (**Supplementary Fig. 3a**), and possible association with clinical outcome especially in subpopulations of specific patients (**Supplementary Fig. 3b**). Interestingly, with data from the TCGA database and International Cancer Genome Consortium-France (LICA-FR) and International Cancer Genome Consortium-Japan (LIRI-JP), we found that the upregulation of *LGR5* expression is more pronounced in HCC tumors with β -catenin mutation (**Supplementary Fig. 4**). This is in line with LGR5 being a β -

catenin target gene both in the intestine and liver^{5,17}. Taken together, *LGR5* cells are enriched in both mouse and human liver tumors, and bear substantial clinical relevance.

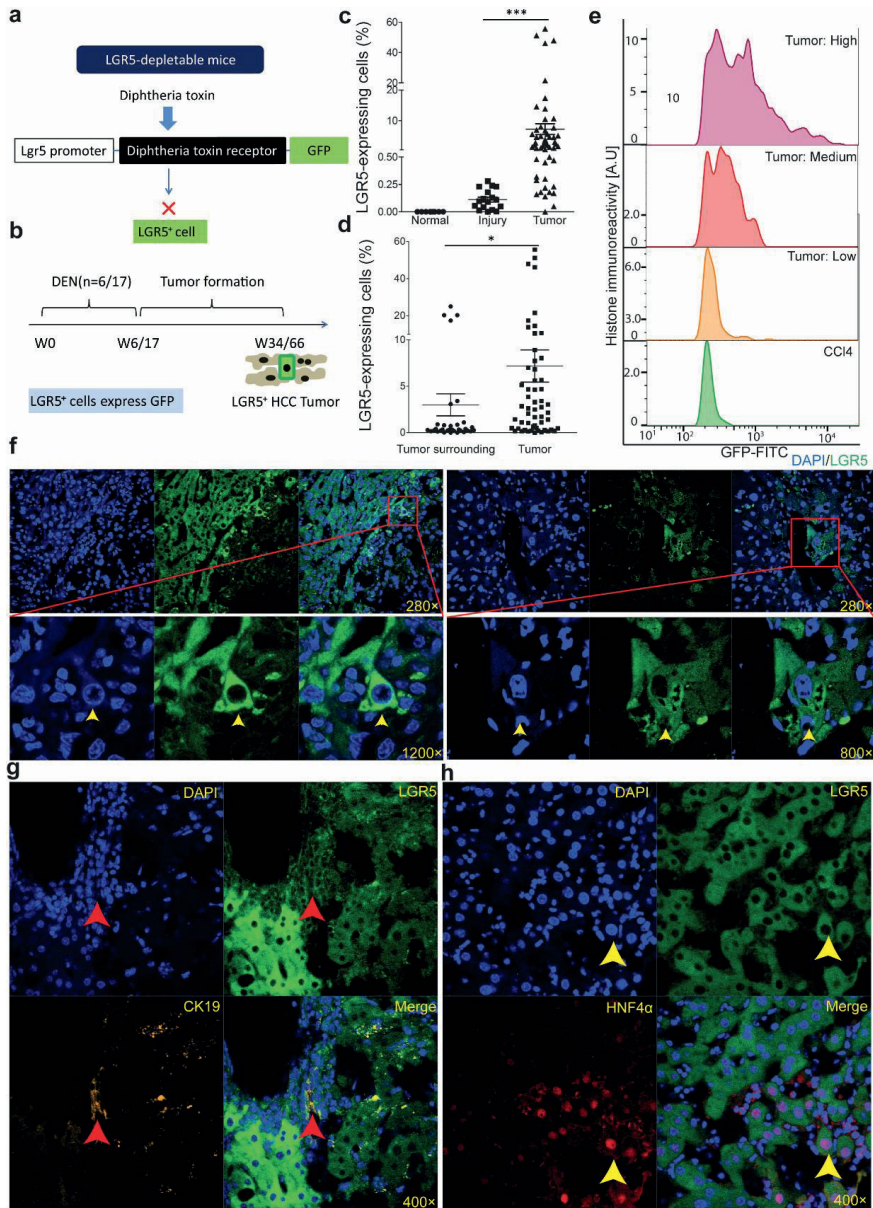


Fig. 1 Primary murine liver tumors are enriched with LGR5 expressing cells. **a** Principle of *Lgr5*-DTR-GFP transgenic mouse strategy used in this study. **b** Principle of the experimental strategy used to induce primary murine tumors in the context of this study. **c** The percentage of LGR5⁺ cells, as determined by flow cytometry, is significantly higher in liver tumors from DEN-treated ($7.29 \pm 1.76\%$, $n = 55$) as compared to livers from untreated animals ($0 \pm 0\%$, $n = 8$) or injured livers from CCl₄-treated

animals ($0.11 \pm 0.022\%$, $n = 17$) (Welch test, $P = 0.0001$). **d** The percentage of LGR5-GFP⁺ cells is significantly increased in liver tumors ($7.29 \pm 1.76\%$, $n = 55$) as compared to the tumor-surrounding tissues ($2.93 \pm 1.15\%$, $n = 34$) of the same mice (Welch test, $P = 0.0407$). **e** Liver tumor-derived LGR5-GFP⁺ cells showed increased fluorescence intensity when compared to LGR5-GFP⁺ cells derived from CCl₄-injured livers. **f** Representative images showing LGR5-GFP⁺ cells as present in liver tumors. Yellow arrow: LGR5-GFP⁺ cell. DAPI: blue. **g-h** Representative confocal images showing the expression of the cholangiocyte marker (**g**, CK19, yellow) and the hepatocyte-specific marker (**h**, HNF4 α , red) in LGR5-GFP expressing cells. Source data are provided as a Source Data file.

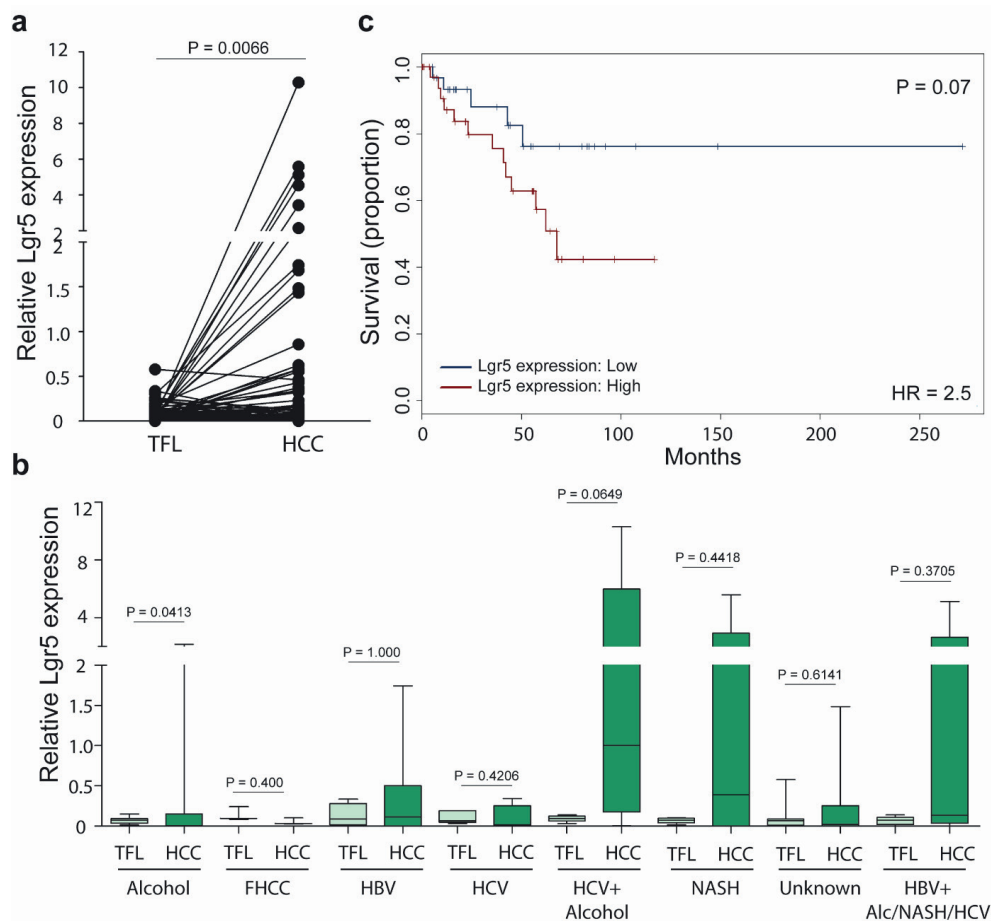


Fig. 2 The expression of *LGR5* is upregulated in human HCC tissues. **a** Upregulation of *LGR5* expression in HCC tissues ($n = 74$) compared with tumor free liver tissues (TFL, $n = 75$) from the Erasmus MC cohort (Paired T-test, $P = 0.0066$). *GUSB* (Beta-glucuronidase), *HPRT1* (hypoxanthine phosphoribosyltransferase 1) and *PMM1* (phosphomannomutase 1) were used as reference genes for normalization. **b** The expression of *LGR5* in HCC tissues compared with TFL stratified based on the etiologies of HCC (Paired T-test). FHCC: Fibrolamellar carcinoma; HBV: Hepatitis B virus; HCV: Hepatitis C virus; NASH: Non-alcoholic steatohepatitis. Alc: Alcohol. Patient number: Alcohol ($n = 16$); FHCC ($n = 3$); HBV ($n = 9$); HCV ($n = 5$); HCV + Alcohol ($n = 6$); NASH ($n = 8$); Unknown ($n = 21$); HBV + Alc/NASH/HCV ($n = 5$). **c** Kaplan-Meier curve of HCC patient survival with high ($n = 37$) and low ($n = 37$) *LGR5* expression (cut-off value based on median value – 0.047). Source data are provided as a Source Data file.

Preservation of LGR5 cells in liver tumor-derived organoids and allograft tumors

3D organoid cultures are robust model systems for studying the properties of (cancer) stem cells¹⁸⁻²⁰. We have successfully established routine procedures²¹ for creating organoid cultures from primary liver tumors of DEN-induced mice (**Supplementary Fig. 1**). In total, 89 tissues were obtained from 41 individual murine livers (**Supplementary File. 1**). 63 out of 89 (70.8%) tumor/tumor surrounding tissues successfully initiated organoids (8 out of 34 tumor surrounding tissues did not initiate organoid, 23.5%; 18 out of 55 tumor tissues did not initiate organoids, 32.7%). These organoids can be maintained and propagated in 3D culture for at least 5 months. Staining for CK19 and HNF4 α demonstrates that these organoids either display a CC or HCC-like phenotype (**Fig. 3a-b**). Importantly, these cultured organoids maintain a population of LGR5 positive cells (**Fig. 3c**).

To investigate whether these organoid lines are malignant, we transplanted all the 63 strains into immunodeficient NOG mice (**Fig. 3d**). One to six months after allografting, eleven out of 63 organoid-strains formed palpable tumors in the immune deficient mice (17.5%). All contained an LGR5-GFP⁺ compartment as determined by FACS analysis of the tumors (**Fig. 3e**).

Following re-culture of cells obtained from these allograft tumors as organoids, we observed substantial diversity of the morphology (**Supplementary Fig. 5a-c**) and CK19/HNF4 α expression in the corresponding allograft tumors (**Fig. 3f** and **Supplementary File. 2**). A population of LGR5-expressing cells were again observed in these organoid cultures (**Supplementary Fig. 5d**), in line with the existence of such a compartment in the allograft tumors from which these organoid cultures originated (IF: **Supplementary Fig. 5e**; IHC: **Supplementary Fig. 5f** and **Supplementary File. 2**). In addition, genome-wide transcriptomic analysis revealed a distinct gene expression signature between LGR5⁺ and LGR5⁻ cells, including TATA-box binding protein associated factor 7 like (Taf7l), Sialophorin (Spn), SRY-box 2 (Sox2), Nidogen-1(Nid1), Paralemmin 3 (Palm3), Alpha-1-microglobulin/bikunin precursor (Ambp), Membrane bound O-acyltransferase domain containing 4 (Mboat4) and Chymase 1 (Cma1), which had higher expression levels in LGR5⁺ compared with LGR5⁻ population. Kaplan-Meier curve analysis revealed that all these genes are associated with the survival of liver cancer patients (**Supplementary Fig. 6** and **Supplementary File. 3-4**). Especially, Sox2 as a transcription factor is essential for maintaining self-renewal or pluripotency of undifferentiated embryonic stem cells, and has been reported as a marker for cancer stem cells in breast cancer and squamous-cell carcinoma²². Gene enrichment analysis of the 196 differentially expressed genes further revealed the involvement of metabolism-related pathways, including "Oxidation by Cytochrome P450", "Calcium Regulation", "Metapathway biotransformation" and "Purine metabolism". There are also differentially expressed genes involved in immune regulation, including "Macrophage markers pathway", "Kit Receptor Signaling Pathway" and "IL-6 signaling Pathway". Furthermore, LGR5⁺ cells had significantly differentially expressed genes involved in cell proliferation/migration, including "Chemokine signaling pathway", "Matrix Metalloproteinases" and "PPAR signaling pathway". Interestingly,

there are differentially expressed genes enriched in “Wnt Signaling Pathway” and “G Protein Signaling Pathways”. Subsequent experiments were initiated to assess the exact functionality of LGR5 expressing cells.

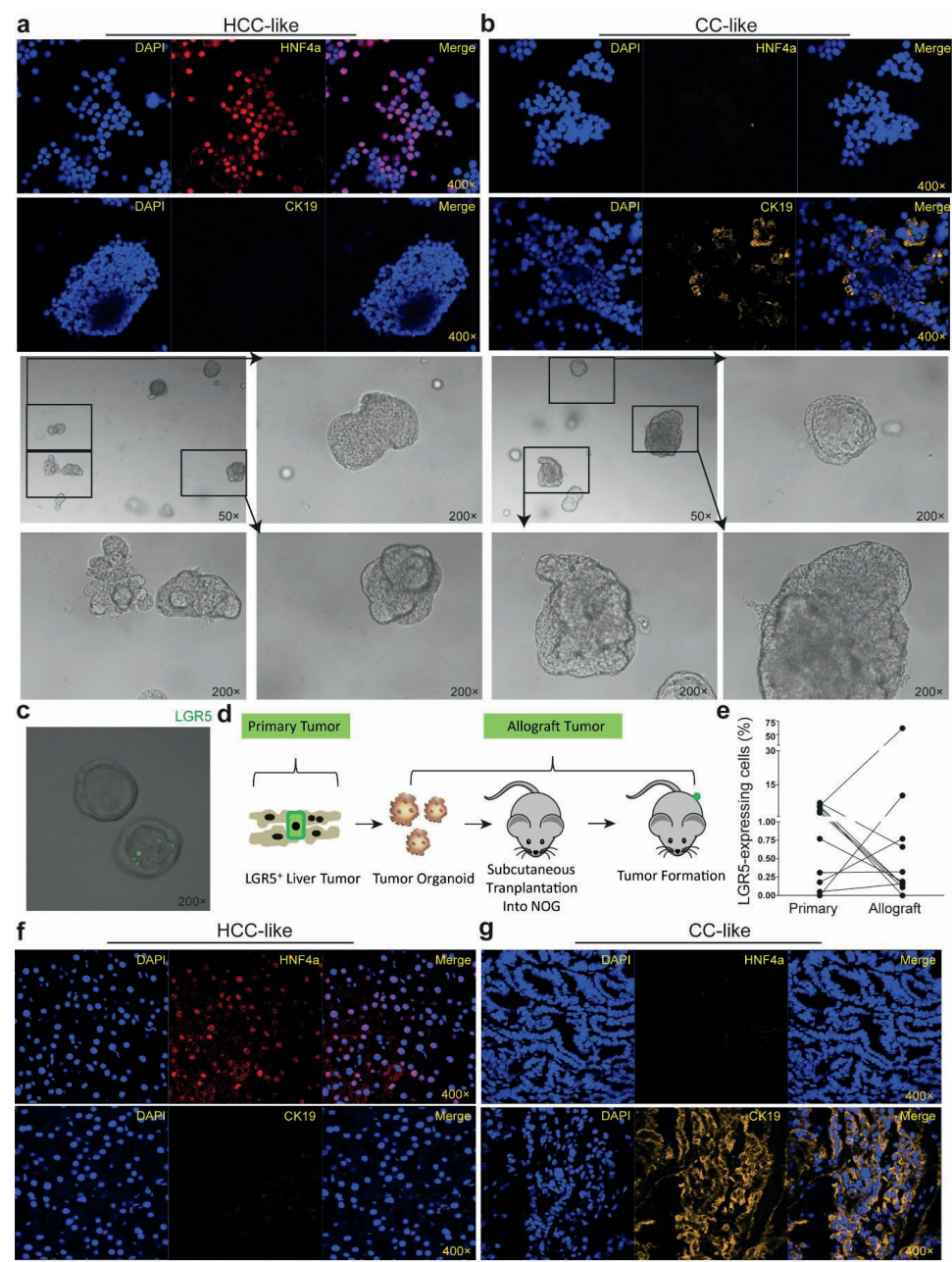


Fig. 3 Maintenance of LGR5 expressing cells in liver tumor organoids and allograft tumors. **a-b** Representative pictures showing organoid lines that predominately express the hepatocyte marker HNF4 α (**a**) or the cholangiocyte marker CK19 (**b**) (Upper panels: IF staining; lower panels bright-field microscopic pictures). **c** Representative pictures showing the presence of LGR5 expressing cells in organoids. LGR5-driven GFP: Green. **d** An outline of the experimental strategy used to transplant tumor organoid lines into immunodeficient mice. **e** The percentages of LGR5 expressing cells in allograft tumors and the corresponding primary tumors (Primary vs. Allograft: $2.8 \pm 0.8\%$ vs. $6.8 \pm 5.6\%$, $n = 11$, $P = 0.3577$). **f-g** Representative pictures of allograft tumors that mainly express either the hepatocyte marker HNF4 α (**f**) or the cholangiocyte marker CK19 (**g**). Source data are provided as a Source Data file.

Dissociated LGR5⁺ cells from liver tumors are superior in organoid and tumor initiation compared to LGR5⁻ cells

For functional comparison of LGR5⁺ and LGR5⁻ liver cancer cells, we first assessed their relative clonogenic ability using an organoid initiation assay. Employing FACS (the sorting strategy: **Supplementary Fig. 7a**), LGR5-GFP⁺ and LGR5-GFP⁻ cells were collected from 71 individual primary murine liver tissues, and cultured in 3D matrigel (**Fig. 4a** and **Supplementary File. 5**). After 2-3 weeks, we observed organoid formation from single cells (**Fig. 4b-d**). Importantly, LGR5-GFP⁺ cells have stronger organoid formation ability compared to LGR5-GFP⁻ cells ($2.13 \pm 0.67\%$ vs. $0.07 \pm 0.02\%$, $n = 30$) (**Supplementary File. 5**: detailed organoid initiation efficiency). In addition, we also observed that the initiation ability of LGR5⁺ cells showed close correlation to collected cell number. The average numbers of LGR5⁺ cells collected from tissues that did initiate organoid (1906 ± 442 , $n = 25$) were significantly higher compared to the number that did not (171 ± 47 , $n = 46$). This was not the case for LGR5⁻ cells (28350 ± 8914 , $n = 60$ vs. 13860 ± 3654 , $n = 11$) (**Supplementary Fig. 7b-d**). This indicates that a sufficient cell number (>1000) is essential for successful organoid initiation of LGR5 expressing cells from liver tumors.

We next performed organoid initiation for cells derived from the allograft tumors (**Fig. 4e**). Similar as observed with primary tumors, LGR5⁺ cells of allograft tumors initiate more organoids as compared to LGR5⁻ cells ($40.5 \pm 10.2\%$ vs. $9.8 \pm 3.9\%$, $n = 10$) (**Fig. 4f**). Compared to cells isolated from primary tissues, allograft tumor cells are more potent with respect to their potential for organoid initiation (**Supplementary Fig. 7e-g**). Interestingly, organoids formed from a single LGR5-GFP⁺ or LGR5-GFP⁻ cell produce both LGR5 positive and negative offspring, suggesting possible self-formation of a hierarchical organization sustaining organoid growth and differentiation (**Supplementary Fig. 7h**).

The ultimate measure of potential functionality of LGR5⁺ cells in pathophysiology is their capacity to form allograft tumors *in vivo* (**Fig. 4g**). Hence identical numbers of FACS sorted LGR5-GFP⁺ and LGR5-GFP⁻ cells derived from primary liver tumors were subcutaneously engrafted into NOG mice and tumor formation was monitored (**Supplementary File. 6**). As expected, LGR5⁺ cells display a stronger capacity for tumor initiation as compared to LGR5⁻ cells (LGR5⁺ vs LGR5⁻: 33.3% vs 11.1%) (**Fig. 4h**, **Supplementary File. 6**). Moreover, tumors initiated from LGR5⁺ cells contain both LGR5 positive and negative populations (**Fig. 4i-n**). Additionally, we have performed a tumor formation assay for the cells that were derived from

the allograft tumors (**Fig. 4o**). Again the LGR5⁺ compartment proved markedly more potent in this respect relative to the LGR5-GFP⁻ compartment (**Fig. 4p-q** and **Supplementary Table. 1**). Collectively, our results are best interpreted that liver tumor-derived LGR5⁺ cells constitute a *bona fide* TIC compartment.

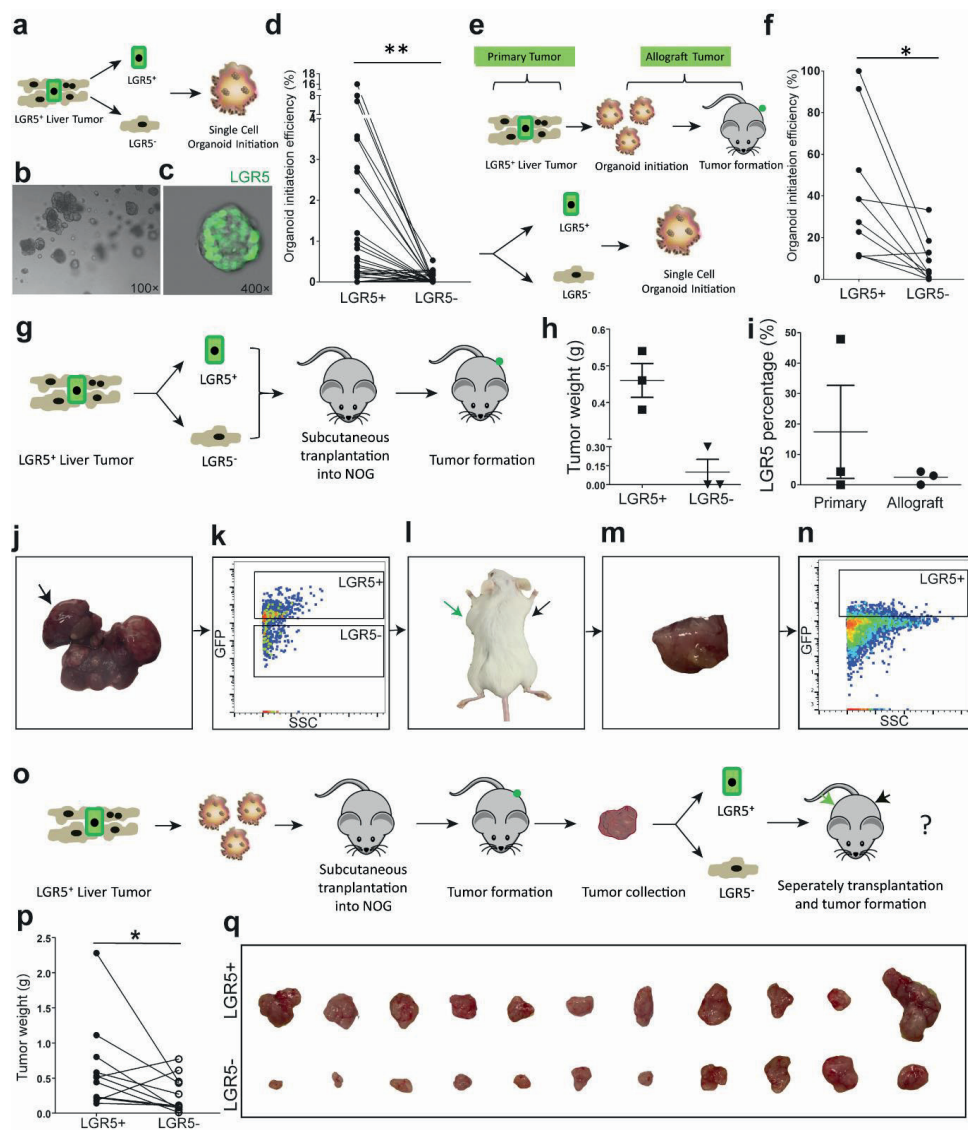


Fig. 4 Single LGR5⁺ cells from liver tumors are superior in organoid and tumor initiation. **a** An outline of the experimental strategy for studying *ex vivo* organoid initiation of cells derived from primary murine liver tumors. **b** A representative picture of organoids derived from single LGR5⁺ cells. **c** Representative confocal micrograph of a single LGR5⁺ cell-initiated organoid dominated by LGR5 expressing cells. LGR5-driven GFP: Green. **d** Organoid initiation efficiency of LGR5-GFP⁺ and LGR5-GFP⁻ cells, isolated from primary liver tumors (LGR5⁺ cells: 25 out of 71 tissues, 35.2%; LGR5⁻ cells: 11 out of 71 tissues, 15.5%)

(Paired T test, $2.13 \pm 0.67\%$ vs. $0.065 \pm 0.023\%$, $n = 30$, $P = 0.0048$). **e** An outline of the experimental strategy used to study *ex vivo* organoid initiation of allograft tumor-derived cells. **f** Efficiency of organoid initiation by allograft liver tumor-derived LGR5-GFP⁺ and LGR5-GFP⁻ cells (Paired T test, $40.46 \pm 10.19\%$ vs. $9.84 \pm 3.93\%$, $n = 10$, $P = 0.0187$). **g** Outline of the experimental strategy used to assess *in vivo* tumor initiation of cells isolated from primary murine liver tumors. **h** Weight of tumors initiated by LGR5⁺ and LGR5⁻ cells (LGR5⁺ vs. LGR5⁻: 0.46 ± 0.046 g vs. 0.10 ± 0.10 g, $n = 3$) (Formed tumor number: LGR5⁺ cells--3 out of 9; LGR5⁻ cells--1 out of 9). **i** LGR5 expression in single LGR5⁺ cell-derived allograft tumors and corresponding primary tumors ($17.42 \pm 15.29\%$ vs. $2.47 \pm 1.27\%$, $n = 3$). **j-n** Representative pictures showing that LGR5-GFP⁺ and LGR5-GFP⁻ cells (**k**) were isolated from DEN-induced primary liver tumors (**j**). Then, LGR5-GFP⁺ cells (green arrow) initiated allograft tumors in immunodeficient mouse (**l-n**). The initiated allograft tumors sustained LGR5 expression (**n**). **o** An outline of the experimental strategy for *in vivo* tumor initiation assay of cells isolated from allograft murine liver tumors. **p** Tumor weight of allografts initiated by LGR5-GFP⁺ cells and LGR5-GFP⁻ cells (isolated from allograft tumors). (0.64 ± 0.19 g vs. 0.27 ± 0.08 g, $n = 11$, $P = 0.0418$). **q** Macroscopic aspect of the tumors initiated by LGR5-GFP⁺ cells and LGR5-GFP⁻ cells (isolated from allograft tumors). Source data are provided as a Source Data file.

Anti-cancer treatment enriches LGR5 expressing cells

CSCs or TICs are presumed to be relatively resistant to conventional anti-cancer treatment. A prediction would thus be that in liver cancer the LGR5⁺ cells would be more resistant to anti-cancer treatment as compared to the LGR5⁻ cells. Hence we challenged tumor organoids with sorafenib, the FDA-approved drug for treating advanced HCC, and compared the relative potential of LGR5-GFP⁺ and LGR5-GFP⁻ cells to withstand such treatment (**Fig. 5a**). Treatment of tumor organoids with sorafenib significantly increased the percentage of LGR5 positive cells in the population (**Fig. 5b-d**). This effect became even more profound when the organoids were treated with the chemotherapeutic agent, 5-fluoro-uracil (5-FU) (**Fig. 5a-d**).

Subsequently the relative size of the LGR5⁺ compartment following *in vivo* treatment with these therapeutic agents was assessed (**Fig. 5e**). Treatment with either sorafenib or 5-FU to mice bearing allograft tumors, formed by engrafting tumor organoids, substantially increased the fraction of the LGR5-GFP⁺ cells in the tumors (**Fig. 5f**). Also when LGR5-GFP⁺ and LGR5-GFP⁻ cells were isolated from tumor organoids and used for organoid re-initiation, while subsequently being treated with 5-FU, the resulting cultures were dominated by LGR5-GFP⁺ expressing cells, independent from whether LGR5-GFP⁺ or LGR5-GFP⁻ were used as starting material (**Fig. 5g**). Of note, LGR5⁺ cells isolated from 5-FU-treated tumors retained the ability of organoid and tumor initiation (**Supplementary Fig. 8**). Interestingly, 5-FU treatment effectively rewired the transcriptome of LGR5⁺ cells (**Fig. 5h**; **Supplementary Fig. 6 and 9**). Gene enrichment analysis of the 1464 differentially expressed genes between 5-FU treated compared to untreated LGR5⁺ cells revealed the involvement of stem cell-related pathways, including “Wnt Signaling”, “Notch Signaling Pathway”, “ErbB signaling pathway”, “Hedgehog Signaling Pathway” and “BMP Signaling Pathway” (**Fig. 5i** and **Supplementary File. 3**). These pathways are commonly activated in many types of solid tumors, associated with cancer initiation, progression and metastasis²³. Interestingly, there are several pathways, including “TGF Beta Signaling Pathway”, “EGFR1 Signaling Pathway”, “PPAR signaling pathway”, “G1 to S cell cycle control”, “Mismatch repair”, “p53 signaling” and “Apoptosis Modulation/Apoptosis pathway”, are known to be implicated in anti-cancer treatment response and DNA damage

response²⁴. These results may partially explain the enrichment of LGR5 expressing cells upon 5-FU treatment. In conclusion, besides resistance, conventional anti-cancer treatment also triggers the generation and propagation of LGR5 expressing cells.

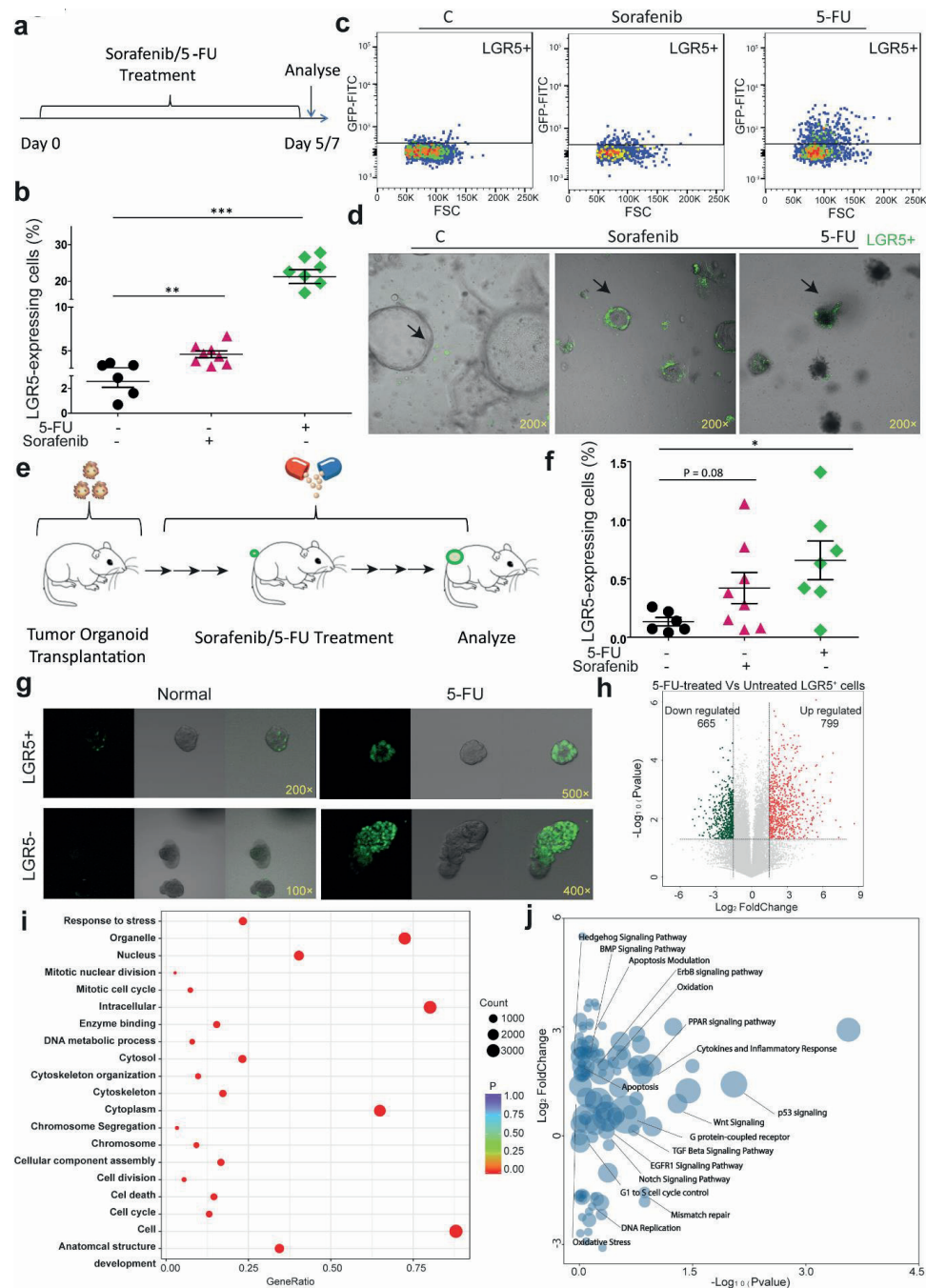


Fig. 5 Anti-cancer treatment selects for LGR5⁺ cells. **a** Outline of the *ex vivo* experimental strategy used to assess the effects of drug treatment on the size of the LGR5⁺ compartment. **b** The fraction of LGR5-GFP⁺ cells is significantly increased upon treatment with sorafenib or 5-FU (vehicle control vs. 10 μ M sorafenib vs. 10 μ M 5-FU: $2.6 \pm 0.5\%$ vs. $4.6 \pm 0.4\%$ vs. $21.3 \pm 1.9\%$). **c-d** Representative FACS plots (**c**) and confocal pictures (**d**) demonstrating that the fraction of LGR5-GFP⁺ cells is increased upon treatment with sorafenib or 5-FU. **e** An outline of the experimental strategy used for testing the effects of drug administration *in vivo*. **f** The percentages of LGR5-GFP⁺ cells is increased upon administration of sorafenib or 5-FU to allografted animals (vehicle control vs. sorafenib vs. 5-FU: $0.13 \pm 0.04\%$, $n = 6$ vs. $0.42 \pm 0.13\%$, $n = 8$ vs. $0.66 \pm 0.17\%$, $n = 7$). **g** Representative confocal pictures showing that both single LGR5-GFP⁺ and LGR5-GFP⁻ cell-initiated organoids contain LGR5 expressing cells and the relative fraction of LGR5 expressing cells is increased in treatment resistant organoids. LGR5-driven GFP: Green. **h** A Volcano plot showing the most significantly differentially expressed genes between 5-FU treated/untreated LGR5⁺ cells. **i** Gene enrichment analysis (with the library of Wiki2019) within the differentially expressed genes. Source data are provided as a Source Data file.

LGR5 lineage ablation inhibits organoid and tumor growth

From the results described above, we inferred that ablation of the LGR5⁺ compartment should impair liver cancer growth. To experimentally test this notion, we exploited the co-expression of the diphtheria toxin receptor (DTR) in the *Lgr5-DTR-GFP* mice. This would allow us to specifically deplete the *Lgr5-DTR-GFP*⁺ compartment through diphtheria toxin (DT) administration (**Fig. 1a**). We have previously optimized the concentrations of DT treatment (1-10 ng/ml) for LGR5 depletion, with organoids derived from healthy *Lgr5-DTR-GFP* mice¹⁴. Accordingly, we evaluated the effects on organoid initiation and proliferation (**Fig. 6a-b**), and sorafenib treatment served as a positive control. DT treatment inhibited the growth of tumor organoids in an effect that showed close correlation as to the effects on the numbers of LGR5-GFP⁺ cells (**Fig. 6c-e**). DT treatment did not influence the growth of tumor organoids of genetically wild type (**Fig. 6c**: left panel).

We further assessed therapeutic targeting of LGR5 liver cancer cells *in vivo*. We first evaluated the effect of DT treatment after formation of visible tumors, following transplantation of tumor organoids into immunodeficient mice (**Supplementary Fig. 10a**). 5-FU and sorafenib served as the positive controls. The effects of LGR5 cell depletion on the growth of formed tumors was minor (**Supplementary Fig. 10c**: right panel and **10d**: right panel). In contrast, administration of DT immediately after transplantation of tumor organoids (**Fig. 6f**) efficiently delayed tumor initiation and inhibited their growth (**Fig. 6h**; **Supplementary Fig. 10c**: left panel and **10d**: left panel). Further analysis of the tumors confirmed the depletion of the LGR5-GFP⁺ compartment in the DT treated animals (**Fig. 6g**). Also using absolute tumor size as a measure, DT-mediated depletion of the LGR5⁺ compartment impaired tumor growth (**Fig. 6i**). The enrichment of stem cell markers also differed in control and DT-treated LGR5^{+/−} cells (**Supplementary Fig. 11**). Interestingly, there was an inverse correlation between tumor size and the relative size of the LGR5-GFP⁺ compartment at the end of the experiment (**Supplementary Fig. 10e-f**), indicating that LGR5 expressing cells are probably more active in the tumor initiation period. As control, DT treatment did not influence initiation and growth of tumors formed from the wild type tumor organoids (**Supplementary Fig. 12a-b**). Thus, LGR5 lineage ablation impedes organoid and tumor initiation and further growth.

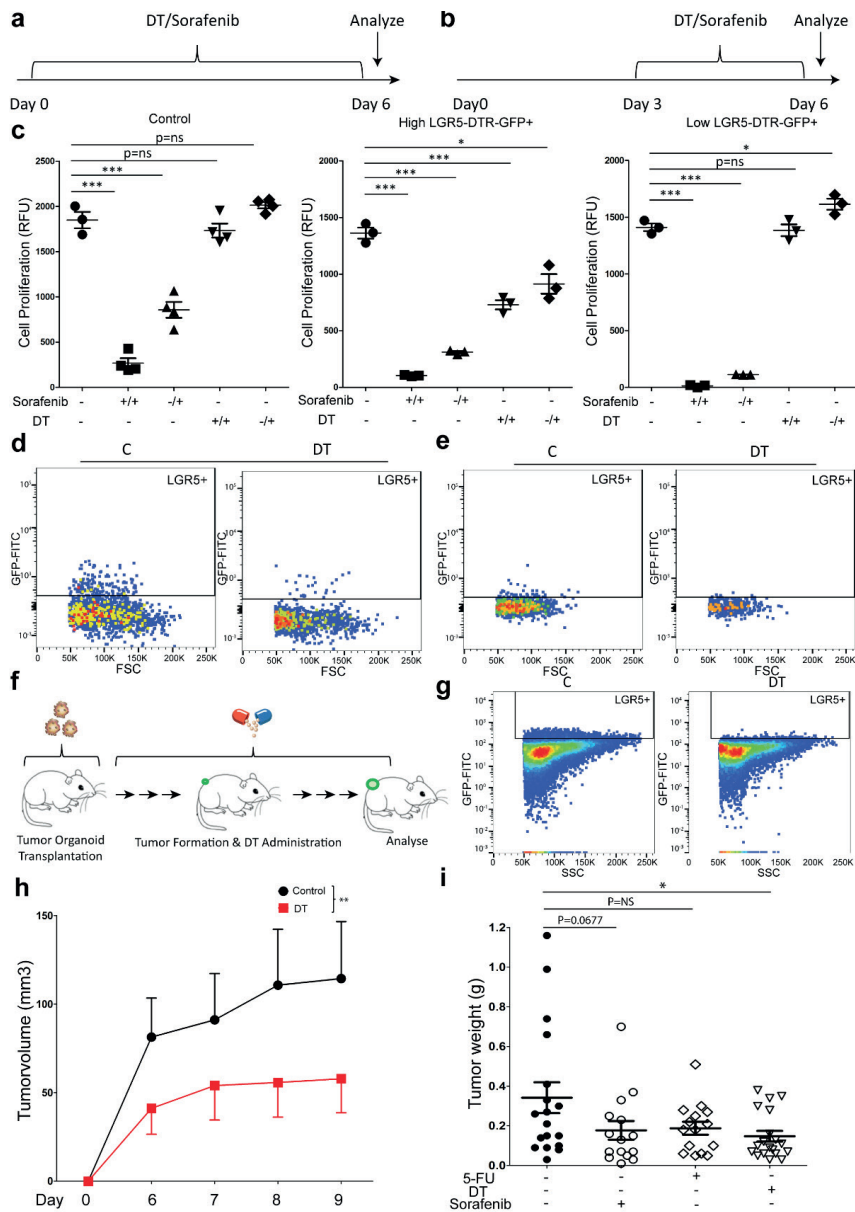


Fig. 6 LGR5 lineage ablation inhibits organoid and tumor growth. **a-b** The outlines of the *ex vivo* experimental strategy to assess the effects of anti-cancer drug treatment on organoid initiation and delineate its temporal aspect (**a**) or during organoid expansion (**b**). **c** The response of wild type tumor organoids (Left) and Lgr5-DTR-GFP mice derived tumor organoids, with relatively high LGR5 expression (the percentage of LGR5 expression is higher than 1%)(Middle) or low LGR5 expression (the percentage of LGR5 expression is lower than 1%)(Right) during regular expansion, to DT/sorafenib treatment. -/+ : drug treatment during the expansion period; +/+ : DT treatment since the initial culture day. **d-e** Representative FACS plots showing that LGR5-GFP⁺ cells are depleted by DT treatment, for high LGR5 expression organoid strains (**d**) and low LGR5 expression organoid strains (**e**). **f** Outlines of the experimental strategy used to assess the efficacy of DT/sorafenib/5-FU administration on allograft tumors in mice. **g** Representative FACS plots from experiments validating the strategy to deplete LGR5⁺ cells. **h** A representative growth curve showing the volumes of tumors derived from the vehicle control group and the DT-administrated

group ($n = 8$). i, The weight of tumors from vehicle control, DT, 5-FU or sorafenib-treated groups, on the day of mice sacrifice (Control vs. sorafenib vs. 5-FU vs. DT: 0.34 ± 0.078 g, $n = 18$ vs. 0.18 ± 0.047 g, $n = 15$ vs. 0.19 ± 0.033 g, $n = 15$ vs. 0.15 ± 0.027 g, $n = 19$). Source data are provided as a Source Data file.

Combination of LGR5 lineage ablation with chemotherapy enhances the anti-cancer efficacy

As LGR5⁺ cells appear to mediate resistance against conventional anti-cancer treatment, it is rational to evaluate the combination of LGR5⁺ lineage ablation with conventional anticancer treatment.

To experimentally test this notion, we first combined DT with sorafenib treatment. However, with different strategies of combination therapy, no enhanced anti-tumor activity was observed on allografted tumors (**Fig. 7**). We next tested the combination of 5-FU and DT. Allograft tumor-bearing mice were first subjected to 5-FU (which increases the relative size of the LGR5⁺ compartment) followed by cessation of 5-FU therapy and start of DT treatment as to kill the LGR5⁺ cells (**Fig. 8a** and **Supplementary Fig. 13a-c**). Indeed this approach is effective in combating allograft tumor formation (**Fig. 8b**) and is substantially superior to monotherapy with 5-FU, stand-alone DT treatment (**Fig. 8c-d** and **Supplementary Fig. 14a**) or initial treatment with DT followed by 5-FU therapy (**Supplementary Fig. 13d-h**). Simultaneous administration of 5-FU and DT (**Fig. 8e**) also resulted in robust anti-cancer effects (**Fig. 8f-h** and **Supplementary Fig. 14b**). Thus targeting the LGR5⁺ compartment markedly enhances efficacy of conventional treatment aimed at combating liver cancer.

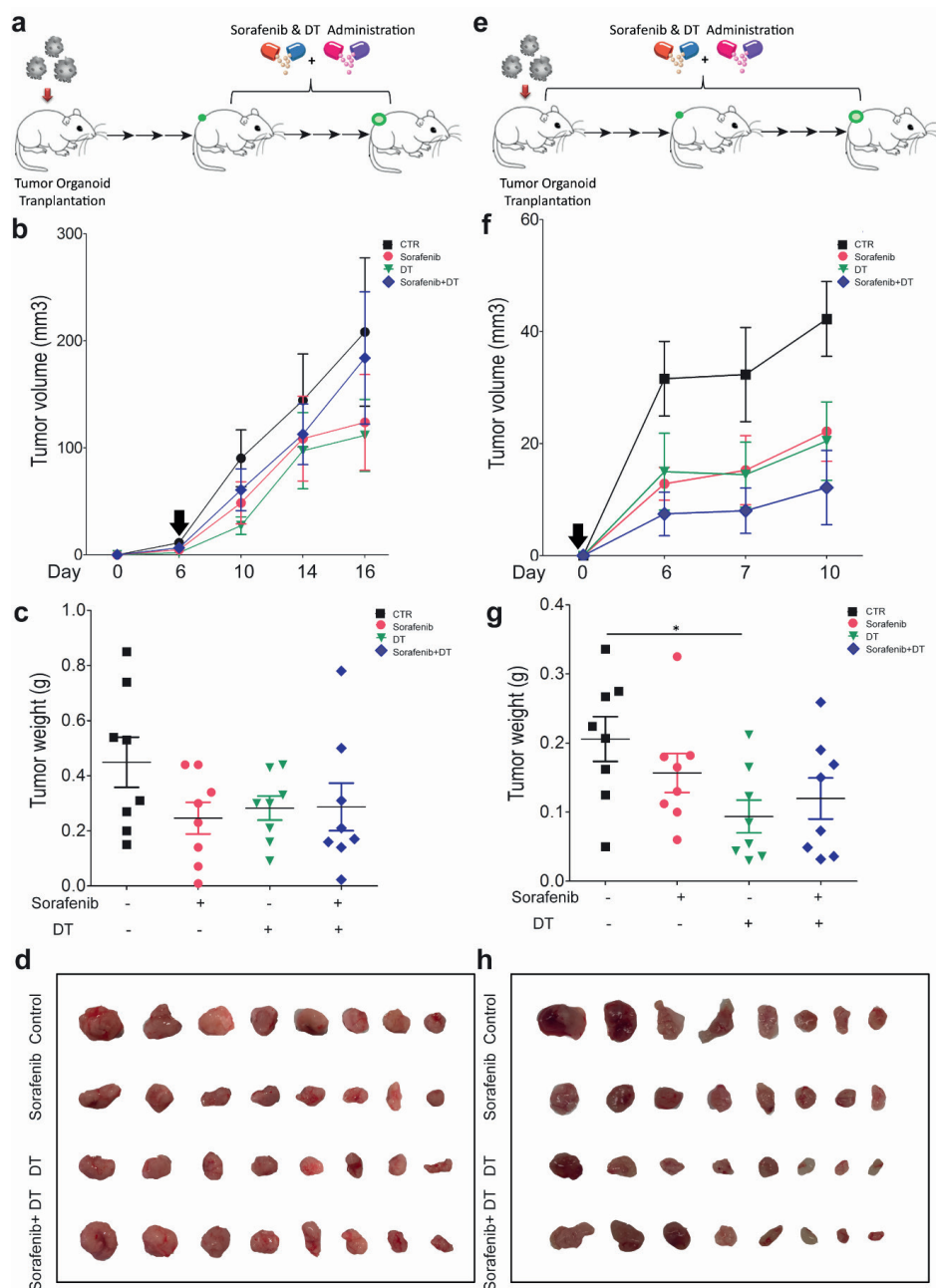


Fig. 7 Combination of LGR5 lineage ablation with sorafenib does not enhance the anti-cancer efficacy. **a** Outline of the experimental strategy to assess the combinatory effect of LGR5 lineage ablation with sorafenib. sorafenib and DT were administrated every other day for in total 10 days since visualization of tumor formation after organoid engraftment. **b** Representative growth curves showing tumor volumes in the vehicle control (CTR), sorafenib, DT, and sorafenib + DT treated groups. Black arrow: onset of administration. **c** Tumor masses from these four groups (CTR vs. sorafenib vs. DT. vs. sorafenib + DT: 0.45 ± 0.09 g, $n = 8$, vs. 0.25 ± 0.06 g, $n = 8$ vs. 0.28 ± 0.043 g, $n = 8$ vs. 0.29 ± 0.09 g, $n = 8$). **d** Images showing tumors from these four groups. **e** Outlines of the experimental strategy for assessing the effects of combining LGR5 lineage ablation and

sorafenib treatment. sorafenib, DT or the combination were administered immediately since transplantation of the organoids every other day, for in total ten days. **f**, Representative growth curves showing tumor volumes of the four groups. Black arrow: onset of administration. **g** The tumor masses of these four groups (CTR vs. sorafenib vs. DT vs. sorafenib + DT: 0.21 ± 0.03 g, $n = 8$ vs. 0.16 ± 0.02 g, $n = 8$ vs. 0.09 ± 0.02 g, $n = 8$ vs. 0.12 ± 0.03 g, $n = 8$). **h** Images showing the tumors from the different groups. Source data are provided as a Source Data file.

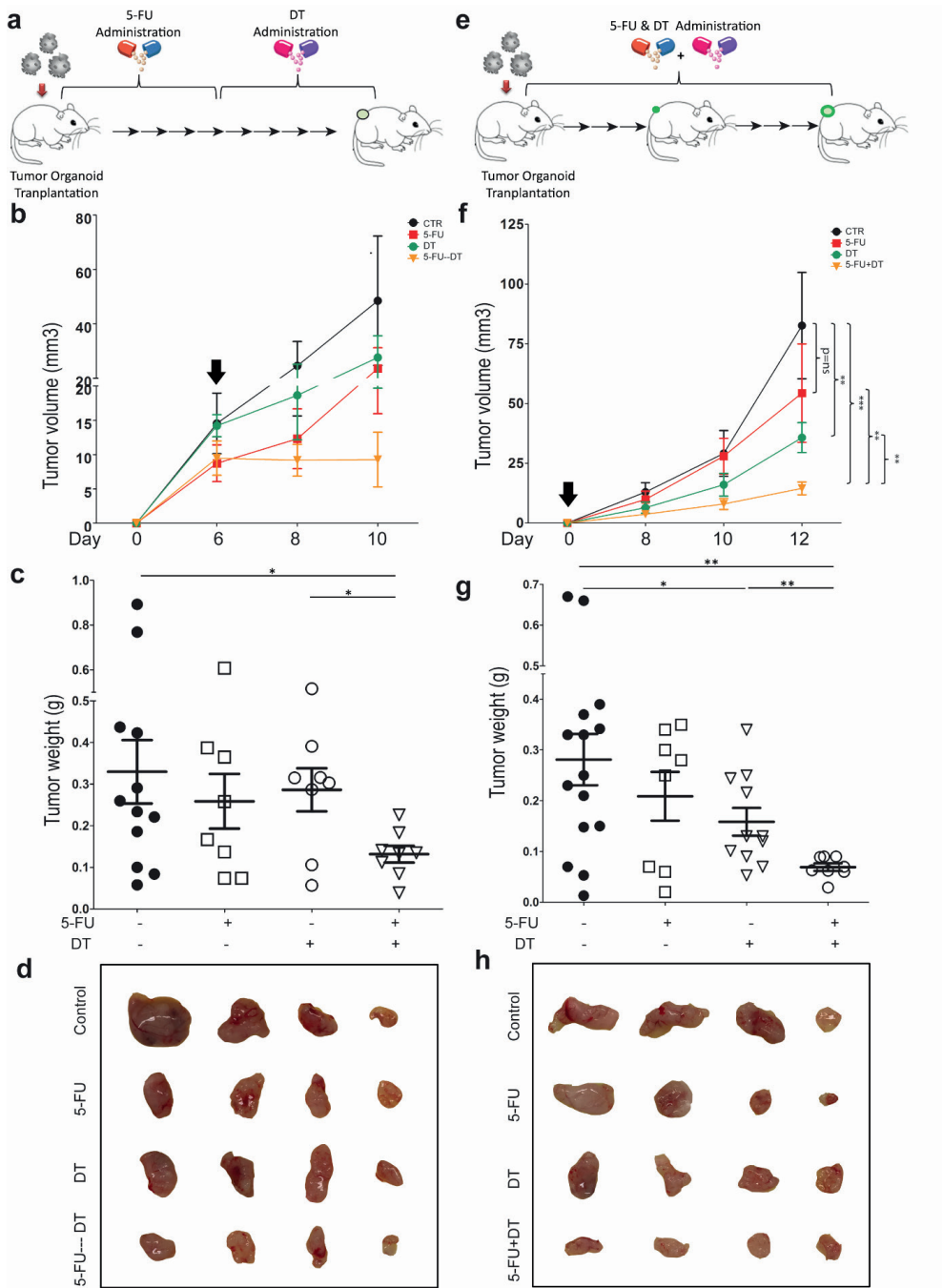


Fig. 8 Combination of LGR5 lineage ablation with 5-FU results in enhanced anti-cancer efficacy. **a** Outline of the experimental strategy to assess the combinatory effect of LGR5 lineage ablation with 5-FU. Following tumor organoid allografting, 5-FU was administrated for the first half of the experiment (every other day, for in total six days). DT was administrated for the second half of the experiment (every other day, for in total 6 days). **b** Representative growth curves showing tumor volumes in the vehicle control group (CTR), the 5-FU monotherapy group, the DT administration-only group, and the hybrid 5-FU/DT group. Black arrow: onset of administration. **c** Tumor masses from these four groups (Control vs. 5-FU vs. DT. vs. 5-FU-DT: 0.33 ± 0.076 g, $n = 12$ vs. 0.25 ± 0.066 g, $n = 8$ vs. 0.29 ± 0.052 g, $n = 8$ vs. 0.13 ± 0.020 g, $n = 8$). **d** Representative images showing tumors from these four groups. **e** Outlines of the experimental strategy for assessing the effects of combined LGR5 lineage ablation and 5-FU treatment. 5-FU, DT or the combination were administered since organoid engraftment every other day, for in total twelve days. **f** Representative growth curves showing tumor volumes of the four groups. Black arrow: onset of administration. **g** The tumor masses of these four groups (Control vs. 5-FU vs. DT. vs. 5-FU+DT: 0.28 ± 0.050 g, $n = 15$ vs. 0.21 ± 0.048 g, $n = 8$ vs. 0.16 ± 0.027 g, $n = 11$ vs. 0.069 ± 0.007 g, $n = 8$). **h** Representative images showing the tumors from the different groups. Source data are provided as a Source Data file.

Discussion

This study has demonstrated that liver cancer contains an LGR5⁺ compartment that has various hallmarks of TICs/CSCs, including an increased capacity for tumor organoid formation in culture and allograft formation in mice as well as resistance against conventional anti-cancer therapy. Functionally, these cells seem more important in tumor initiation, whereas the LGR5⁻ compartment appears to bear the proliferative burden. Simultaneously targeting both compartments as demonstrated in this study by 5-FU treatment in combination with DT-mediated ablation of the LGR5⁺ compartment was effective in combating experimental liver cancer. Thus, combining conventional therapy and LGR5⁺-targeted therapy deserve to be further explored for the treatment of liver cancer in the clinic. Conceivably, this approach could be more effective for subset of patients with high levels of LGR5 expression, such as CTNNB1 mutated or alcohol-related HCC patients^{25,26}. Although LGR5⁺-targeting therapies are still largely in their infancy, the analogy with neuroendocrine tumors, which are successfully combated by radioactive somatostatin analogues (e.g. ¹⁷⁷Lu-Dotate) that target receptors with homology to LGR5²⁷, suggests that radioactive drugs (e.g. R-spondin) may be an option for treating liver cancer²⁸. Our results, however, indicate that such therapy will be more effective when combined with particular conventional anti-cancer therapies.

Overexpression of LGR5 has been previously reported in patient HCC¹⁷, and we confirmed that this is more pronounced in β -catenin mutated liver tumors. Although the elevation of LGR5 expression and potential association with clinical outcome have been observed in HCC patients, whether it can serve as an independent prognostic biomarker remains to be further investigated in specifically designed tumor marker prognostic studies in patients²⁹.

Of note, these early observations are based on mRNA expression, due to the lack of a reliable anti-LGR5 antibody. We now used transgenic mice in which LGR5-expressing cells co-express GFP and we can conditionally ablate these cells with the DT-DTR system³⁰. This model allows for the identification and direct visualization of LGR5 expressing cells based on GFP expression,

as well as isolation of LGR5-GFP⁺ cells for further functional analyses and detailed characterization.

In intestinal adenomas, LGR5 marks 5-10% of the cells, which keep fueling the growth of established mouse adenomas¹³. We found that the percentages of LGR5-GFP⁺ cells in murine liver tumors vary from 0.1% up to 55% ($7.3 \pm 1.8\%$, $n = 55$). Over 32% of the primary liver tumors harbor relatively high percentages (over 5%) (**Supplementary Fig. 2c**). In colon cancer, the percentage of LGR5 expressing cells has been reported to be associated with different background of the tumors, especially the accumulation of certain oncogenic mutations⁸. Thus, we speculate that the large variation of the abundance of LGR5 cells in liver tumors may also be related to different types of oncogenic mutations, although this hypothesis requires further investigation. Of note, DEN was used to induce primary liver cancer in this study and this compound is associated with the accumulation of liver β -catenin mutations³¹. Therefore, it is possible that our results are mainly relevant to liver cancers with deregulated Wnt/ β -catenin signaling and their importance requires future investigation in other mutational backgrounds (*e.g.* deregulated TSC/mTOR signaling)³² as well.

Through a series of functional assays, in particular *in vitro* organoid initiation and *in vivo* tumor formation, we have demonstrated the importance of these LGR5 TICs in liver cancer. To define the potential for therapeutic targeting, we have performed LGR5 lineage ablation in organoids *in vitro* and in the tumor-bearing mouse model. Of note, the presence of LGR5 cells in tumors is likely dynamic. We observed large variations of their percentages among different primary liver tumors and allograft tumors generally contain lower numbers of LGR5 cells (less than 1%). In colorectal cancer, advanced stages compared to the early stages contain less LGR5 cells³³. A speculative explanation could be that the tumors are derived from LGR5-positive stem cells, yet these cells are suppressed thereafter during tumor progression³³. The dynamics could be essential for determining at which stage to target LGR5 TICs. When we performed LGR5 ablation in established tumors, we only observed a minor effect, probably due to a low percentage of LGR5 cells as well as their dispensable function at that stage, while depletion at the early stage yielded optimal anti-tumor effects. This result is in line with previous findings showing that LGR5 cells play distinct roles in primary and metastatic colon cancer⁸.

Although we have demonstrated the feasibility and value of targeting LGR5 TICs in liver cancer, therapeutic ablation of these cells remains challenging. Resistance to conventional therapy is a common feature of CSCs². We found that treatment with sorafenib or 5-FU enriches LGR5 cells, consistent with the findings in gastric³⁴ and colorectal cancer³⁵. Different mechanisms may contribute to treatment resistance. Although LGR5 stem cells are generally fast-cycling in the intestine³⁶, the existence of quiescent LGR5 cells have been reported in basal cell carcinoma, which mediate relapse after treatment¹². Cell plasticity could be one of the potential mechanisms of treatment resistance. The loss of LGR5 stem cells in the intestine can be compensated by trans-differentiation from other stem cell pools³⁰, or through plasticity of their enterocyte-lineage daughters³⁷. Cancer cell plasticity, shifting dynamically between a

differentiated and a stemness state, has also been proposed as an important feature contributing to tumor progression, metastasis and therapeutic response³⁸. We now have observed the induction of LGR5⁺ from LGR5⁻ liver cancer cells. This may implicate cell plasticity of LGR5 CSCs, but there could also be other mechanisms regulating the origin and expansion of LGR5 cells. Eventually, these LGR5 liver cancer cells may partially contribute to treatment resistance.

Currently, several innovative scenarios are being explored to therapeutically target CSCs, including antibody-drug conjugates⁹, targeting quiescent CSCs³⁹ and inhibiting CSC-related pathways². However, as discussed, different mechanisms could lead to treatment resistance⁸. Thus, combined therapies are likely necessary for this respect. With the intention to fully expand the stem cell pool, cetuximab has been used to first trigger the LGR5 population, followed by the ablation of these CSCs. This combined therapy has resulted in potent efficacy against colorectal cancer¹⁰. Similarly, we have observed that the combination of LGR5 lineage ablation with 5-FU chemotherapy can also lead to enhanced anti-liver cancer activity. However, combination of LGR5 lineage ablation with sorafenib did not yield enhanced anti-tumor activity. This is probably related to the mild effect of sorafenib in triggering the LGR5 CSC pool.

Lastly, a potential concern of such strategies is the possible harmful effects on normal LGR5 stem cells. In intestine, colon and skin, although LGR5 stem cells essentially contribute to tissue renewal at a daily basis^{5,6}, their loss can be compensated by trans-differentiation from other reserve stem cell pools^{30,40} or through plasticity of their daughter cells³⁷. Importantly, antibody conjugated drug targeting LGR5 CSCs in colon cancer has no major impact on the function of normal LGR5 stem cells⁹. In liver, LGR5 stem cells are absent during homeostasis, but only transiently activated upon injury likely without major contribution towards tissue repair^{4,14}. Thus, we envision that our identification of targetable LGR5 TICs in liver cancer bears important implications for future therapeutic development.

Materials and Methods

Primary liver tumor model

Lgr5-DTR-GFP transgenic mice (kindly provided by Genentech) specifically co-express the diphtheria toxin (DT) receptor (DTR) and green fluorescent protein (GFP) under the control of the *Lgr5* promoter³⁰. Thus, LGR5⁺ cells can be identified by GFP expression, and LGR5-GFP⁺ cells can be specifically depleted by DT administration. *Lgr5-DTR-GFP* transgenic mice (3-4 weeks) were administered with Diethylnitrosamine (DEN) by intraperitoneal injection (Sigma-Aldrich, i.p., 100 mg/kg) weekly for 6-17 weeks⁴¹. DEN is used to induce liver tumor in *Lgr5-DTR-GFP* transgenic mice and wild type mice, which could cause liver disease from basophilic foci, hyperplastic nodules, hepatocellular adenoma and finally lead to HCC^{31,42,43}. Mice were sacrificed 3-16 months after the last DEN injection and livers/tumors were collected for further experiments (**Supplementary File. 1**: In total, 41 mice were monitored; 80.5%, 33 out of 41, mice formed liver tumors; the expression of LGR5 in each tumor/tumor surrounding tissues were also listed; **Supplementary Fig. 2g-h**). For each liver, biopsies were taken from the tumor and tumor surrounding tissue. If livers contain more than one tumors, individual tumors were collected and analyzed separately. For CCl₄ induced liver injury, *Lgr5-DTR-GFP* transgenic mice were weekly repeated administered with (6 or 17 weeks) intraperitoneal CCl₄ injection (10 µl/20 g body weight of 10% CCl₄ solution in corn oil or corn oil as control). All animal experiments were approved by the Committee on the Ethics of Animal Experiments of the Erasmus Medical Center.

HCC specimens and patient information

HCC specimens (paired tumor tissue and adjacent tumor free liver tissue) were collected from HCC patients undergoing tumor resection at the Erasmus Medical Center, The Netherlands. Samples were stored at -80°C and then used for RNA extraction. 74 specimens were obtained from HCC patients and the corresponding clinical-pathological data are summarized in **Supplementary Table. 2**. HCC-specific survival was assessed in all patients and patients were stratified according to relative LGR5 expression (below and above median – 0.047). The Kaplan-Meier method was used to estimate survival outcome curves and the log-rank test was used to compare the survival between the two groups. The hazard ratio (HR) for HCC-specific survival was estimated using the Cox proportional hazards regression model. The study was approved by the medical ethical committee of Erasmus Medical Center. In addition, the study protocol conforms to the ethical guidelines of the 1975 Declaration of Helsinki.

Online database

For analysis of Lgr5 mRNA expression, data were retrieved from three independent HCC cohorts including The Cancer Genome Atlas (TCGA), Wurbach⁴⁴, and Roessler⁴⁵. For survival analysis based on Lgr5 mRNA expression, the TCGA cohort was used. For analysis of the relationship between gene mutation and Lgr5 expression, three independent cohorts were investigated, including TCGA, International Cancer Genome Consortium-France (LICA-FR) and International Cancer Genome Consortium-Japan (LIRI-JP).

Tumor organoid culture

Digestion solution II (37°C, 30 min, 500 µg/ml of collagenase type XI, 200 µg/ml of Dnase-1, 1% FBS in DMEM medium) (collagenase type XI: Sigma-Aldrich; Dnase-1: Sigma-Aldrich) was used to digest liver or tumor tissues into single cell suspension. Single cell suspension was directly mixed with matrigel (Corning BV) and then used for culturing, or sorted for further experiments. Sorted cells were also mixed with matrigel and seeded for organoid initiation. Cells were cultured in organoid culture medium as previously described^{4,14}. For the first 8-12 days, organoids were supplemented with 10 µM Y-27632 (Sigma-Aldrich), Noggin and Wnt3a conditioned medium. Medium was refreshed every 2 days and passage was performed in split ratios of 1:2-1:15 weekly. The proposed tumor organoid phenotypes is based on the expression of EpCAM/CK19 positive for CC-like and HNF4a/AFP positive for HCC-like phenotype.

Histology, immunohistochemistry and immunofluorescence

Liver or tumor was fixed in 4% paraformaldehyde (PFA) overnight at 4 °C. For immunofluorescence, samples were further dehydrated with 30% sucrose (Sigma-Aldrich, 4 °C, overnight), stored at -80 °C and then sectioned at 8 µm for further analysis. Images were acquired with a Zeiss LSM510META confocal microscope. For histology and immunohistochemistry, materials were dehydrated with 70% ethanol, embedded with paraffin, and sectioned at 4 µm for staining. Images were acquired with a Zeiss Axioskop 20 microscope. All antibodies are listed in **Supplementary Table. 3**.

Organoid-based allograft tumor model

Cold advanced DMEM/F12 medium was used to collect the organoids. After centrifuging, supernatant was discarded and organoid pellets (organoid fragmentation size: range from 5 ~ 150 µm) were mixed directly with matrigel in a ratio of 1:1 with a total volume of 200 µl. 4-6 weeks old female NOD.Cg-PrkdcSCIDIl2rgtm1Wjl/SzJ (NSG) mice, NOG/JicTac (CIEA NOD.Cg-Prkdc-scid Il2rg-tm1Sug) mice or nude mice (NMRI:BomTac-Nude) were purchased from Taconic, and subcutaneously injected with the collected tumor organoids. The

characterization of phenotypes for murine allograft tumor is based on the expression of EpCAM/CK19 for CC-like and HNF4 α /AFP for HCC-like phenotype (**Supplementary File 2**). Tumor dimensions were measured using calipers and tumor volume was calculated as $0.523 \times \text{length} \times \text{width} \times \text{width}^9$. Tumor formation was monitored every other day and mice were sacrificed to harvest tumors after the tumor diameter reached approximately 2 cm. Tumor tissues were stored or cultured as described above.

Cell ablation by diphtheria toxin and treatment of 5-FU/sorafenib

To ablate LGR5⁺ cells in organoids, DT (Calbiochem, 1-10 ng/ml) was added to organoid expansion/initiation medium, followed by further analysis¹⁴. For *in vivo* ablation, DT was administrated via intraperitoneal injection every other day (50 μ g per kg body weight). If mice suffering from weight loss $\geq 10\%$, compared to the previous injection, the injection was omitted. 5-FU/sorafenib were also administrated via intraperitoneal injection every other day (5-FU/sorafenib: 30 mg per kg body weight) (sorafenib: Bio-Connect BV; 5-FU: Sigma-Aldrich).

qRT-PCR

For freshly FACS-sorted cells and HCC specimens, RNeasy Micro Kit (QIAGEN) was used to isolate RNA. For organoids, Machery-NucleoSpin RNA II kit (Bioké) was used. Quantification was measured with Nanodrop ND-1000 (Wilmington). RNA was then converted to cDNA by using a cDNA Synthesis kit (TAKARA BIO INC.). Real-time PCR reactions were performed with SYBRGreen-based real-time PCR (Applied Biosystems®) and amplified in a thermal cycler (GeneAmp PCR System 9700). For cells collected from murine tissues, glyceraldehyde 3-phosphate dehydrogenase (*Gapdh*) gene was used as reference. For quantification of LGR5 mRNA in human tumors and tumor-free liver tissues, *Gusb* (Beta-glucuronidases), *Hprt1* (hypoxanthine phosphoribosyltransferase 1) and *Pmm1* (phosphomannomutase 1) were used as reference genes. All primers are listed in **Supplementary Table. 4**.

RNA sequencing

Total RNA was isolated using RNeasy Micro Kit (QIAGEN). The quantity of RNA was measured by a NanoDrop 2000. The collected RNA was further amplified by using SMARTer kit. Then, RNA sequencing was performed by Novogene with the paired-end 150bp (PE 150) sequencing strategy. Gene expression was analyzed. The identification of differentially expressed genes is based on $P < 0.05$ and absolute values of $\log Fc > 1.5$. GSEA with the library of Wiki2019 was performed to reveal the alteration of signaling pathways.

FACS analysis

For FACS analysis, single cells derived from liver tumors/tumor surrounding tissues or organoids were suspended in DMEM plus 2% FBS. Cell suspensions were analyzed using a BD FACSCalibur or BD FACSARIA™ II. For FACS sorting, a BD FACSARIA™ II cell sorter was used to isolate the target cell population. Propidium iodide (PI) staining was performed to exclude dead cells and CD45 staining was adopted for excluding leucocytes.

Metabolic activity analysis of organoids

Different organoid lines were seeded separately in a 24/48-well plate. sorafenib (10 μ M) or 5-FU (10 μ M) was added to the organoid culture since the initial day or post-initiation day 3, respectively. Drugs were refreshed every other day. At the day 6-7, organoids were incubated with Alamar Blue (Invitrogen, 1:20 in DMEM) for four hours (37 °C), and then medium was collected for analysis of the metabolic activity of the cells. Absorbance was determined by using fluorescence plate reader (CytoFluor® Series 4000, Perseptive Biosystems) at the excitation of 530/25 nm and emission of 590/35. Each treatment condition was repeated for four times and matrigel with medium only was used as blank control.

Statistical analysis.

Prism software (GraphPad Software) was used for all statistical analysis. For statistical significance of the differences between the means of groups, we used Mann-Whitney U-test; For statistical significance of the differences between groups with inequivalent sample sizes, we used Welch test (indicated in the legends); For statistical significance of the differences between paired samples, we used Paired T-test (indicated in the legends); For statistical significance of the differences between multiple independent groups, we used two-way ANOVA. Differences were considered significant at a *P* value less than 0.05.

Acknowledgements

We gratefully thank Genentech for providing the *Lgr5-DTR-GFP* mouse strains. We thank R. Lieshout, S.A. van der Heide-Mulder for discussion and technical assistance. We also thank Prof. R. Fodde for discussing the project. This study was supported by the Dutch Cancer Society for funding a KWF Young Investigator Grant (10140) and the Netherlands Organization for Scientific Research (NWO) for a VIDI grant (No. 91719300) to Q. Pan.

Author contributions

M.L. and J.L. contributed equally and share co-second authorship.

Competing interests

The authors declare no competing interests.

References

- 1 Clevers, H. The cancer stem cell: premises, promises and challenges. *Nat Med* **17**, 313-319, doi:nm.2304 [pii]10.1038/nm.2304 (2011).
- 2 Batlle, E. & Clevers, H. Cancer stem cells revisited. *Nat Med* **23**, 1124-1134, doi:nm.4409 [pii]10.1038/nm.4409 (2017).
- 3 Ebben, J. D. *et al.* The cancer stem cell paradigm: a new understanding of tumor development and treatment. *Expert Opin Ther Targets* **14**, 621-632, doi:10.1517/14712598.2010.485186 (2010).
- 4 Huch, M. *et al.* In vitro expansion of single Lgr5+ liver stem cells induced by Wnt-driven regeneration. *Nature* **494**, 247-250, doi:nature11826 [pii]10.1038/nature11826 (2013).
- 5 Barker, N. *et al.* Identification of stem cells in small intestine and colon by marker gene Lgr5. *Nature* **449**, 1003-1007, doi:nature06196 [pii]10.1038/nature06196 (2007).
- 6 Haegbarth, A. & Clevers, H. Wnt signaling, lgr5, and stem cells in the intestine and skin. *Am J Pathol* **174**, 715-721, doi:S0002-9440(10)60932-7 [pii]10.2353/ajpath.2009.080758 (2009).
- 7 Barker, N. *et al.* Crypt stem cells as the cells-of-origin of intestinal cancer. *Nature* **457**, 608-611, doi:nature07602 [pii]10.1038/nature07602 (2009).
- 8 de Sousa e Melo, F. *et al.* A distinct role for Lgr5+ stem cells in primary and metastatic colon cancer. *Nature* **543**, 676-680, doi:nature21713 [pii]10.1038/nature21713 (2017).
- 9 Junttila, M. R. *et al.* Targeting LGR5+ cells with an antibody-drug conjugate for the treatment of colon cancer. *Sci Transl Med* **7**, 314ra186, doi:7/314/314ra186 [pii]10.1126/scitranslmed.aac7433 (2015).
- 10 Shimokawa, M. *et al.* Visualization and targeting of LGR5+ human colon cancer stem cells. *Nature* **545**, 187-192, doi:nature22081 [pii]10.1038/nature22081 (2017).
- 11 Yanai, H. *et al.* Intestinal cancer stem cells marked by Bmi1 or Lgr5 expression contribute to tumor propagation via clonal expansion. *Sci Rep* **7**, 41838, doi:srep41838 [pii]10.1038/srep41838 (2017).
- 12 Sanchez-Danes, A. *et al.* A slow-cycling LGR5 tumour population mediates basal cell carcinoma relapse after therapy. *Nature* **562**, 434-438, doi:10.1038/s41586-018-0603-310.1038/s41586-018-0603-3 [pii] (2018).
- 13 Schepers, A. G. *et al.* Lineage tracing reveals Lgr5+ stem cell activity in mouse intestinal adenomas. *Science* **337**, 730-735, doi:science.1224676 [pii]10.1126/science.1224676 (2012).
- 14 Cao, W. *et al.* Dynamics of Proliferative and Quiescent Stem Cells in Liver Homeostasis and Injury. *Gastroenterology* **153**, 1133-1147, doi:S0016-5085(17)35907-3 [pii]10.1053/j.gastro.2017.07.006 (2017).

- 15 Bosch, F. X., Ribes, J., Diaz, M. & Cleries, R. Primary liver cancer: worldwide incidence and trends. *Gastroenterology* **127**, S5-S16, doi:S0016508504015902 [pii] (2004).
- 16 Yamashita, T. & Wang, X. W. Cancer stem cells in the development of liver cancer. *J Clin Invest* **123**, 1911-1918, doi:66024 [pii]10.1172/JCI66024 (2013).
- 17 Yamamoto, Y. *et al.* Overexpression of orphan G-protein-coupled receptor, Gpr49, in human hepatocellular carcinomas with beta-catenin mutations. *Hepatology* **37**, 528-533, doi:10.1053/jhep.2003.50029S0270913902141437 [pii] (2003).
- 18 Broutier, L. *et al.* Human primary liver cancer-derived organoid cultures for disease modeling and drug screening. *Nat Med*, doi:nm.4438 [pii]10.1038/nm.4438 (2017).
- 19 Drost, J. & Clevers, H. Organoids in cancer research. *Nat Rev Cancer* **18**, 407-418, doi:10.1038/s41568-018-0007-610.1038/s41568-018-0007-6 [pii] (2018).
- 20 Nuciforo, S. *et al.* Organoid Models of Human Liver Cancers Derived from Tumor Needle Biopsies. *Cell Rep* **24**, 1363-1376, doi:S2211-1247(18)31078-7 [pii]10.1016/j.celrep.2018.07.001 (2018).
- 21 Cao, W. *et al.* Modeling liver cancer and therapy responsiveness using organoids derived from primary mouse liver tumors. *Carcinogenesis* **40**, 145-154, doi:5115755 [pii]10.1093/carcin/bgy129 (2019).
- 22 Boumahdi, S. *et al.* SOX2 controls tumour initiation and cancer stem-cell functions in squamous-cell carcinoma. *Nature* **511**, 246-250, doi:nature13305 [pii]10.1038/nature13305 (2014).
- 23 Nwabo Kamdje, A. H. *et al.* Developmental pathways associated with cancer metastasis: Notch, Wnt, and Hedgehog. *Cancer Biol Med* **14**, 109-120, doi:10.20892/j.issn.2095-3941.2016.0032CBM-2016-0032-R2 [pii] (2017).
- 24 Nussinov, R., Tsai, C. J. & Jang, H. A New View of Pathway-Driven Drug Resistance in Tumor Proliferation. *Trends Pharmacol Sci* **38**, 427-437, doi:S0165-6147(17)30026-3 [pii]10.1016/j.tips.2017.02.001 (2017).
- 25 Boyault, S. *et al.* Transcriptome classification of HCC is related to gene alterations and to new therapeutic targets. *Hepatology* **45**, 42-52, doi:10.1002/hep.21467 (2007).
- 26 Zucman-Rossi, J., Villanueva, A., Nault, J. C. & Llovet, J. M. Genetic Landscape and Biomarkers of Hepatocellular Carcinoma. *Gastroenterology* **149**, 1226-1239 e1224, doi:10.1053/j.gastro.2015.05.061 (2015).
- 27 Strosberg, J. *et al.* Phase 3 Trial of (177)Lu-Dotatate for Midgut Neuroendocrine Tumors. *N Engl J Med* **376**, 125-135, doi:10.1056/NEJMoa1607427 (2017).
- 28 Koo, B. K. *et al.* Tumour suppressor RNF43 is a stem-cell E3 ligase that induces endocytosis of Wnt receptors. *Nature* **488**, 665-669, doi:nature11308 [pii]10.1038/nature11308 (2012).

- 29 Sauerbrei, W., Taube, S. E., McShane, L. M., Cavenagh, M. M. & Altman, D. G. Reporting Recommendations for Tumor Marker Prognostic Studies (REMARK): An Abridged Explanation and Elaboration. *J Natl Cancer Inst* **110**, 803-811, doi:5032903 [pii]10.1093/jnci/djy088 (2018).
- 30 Tian, H. *et al.* A reserve stem cell population in small intestine renders Lgr5-positive cells dispensable. *Nature* **478**, 255-259, doi:nature10408 [pii]10.1038/nature10408 (2011).
- 31 Connor, F. *et al.* Mutational landscape of a chemically-induced mouse model of liver cancer. *J Hepatol* **69**, 840-850, doi:S0168-8278(18)32162-7 [pii]10.1016/j.jhep.2018.06.009 (2018).
- 32 van Veelen, W., Korsse, S. E., van de Laar, L. & Peppelenbosch, M. P. The long and winding road to rational treatment of cancer associated with LKB1/AMPK/TSC/mTORC1 signaling. *Oncogene* **30**, 2289-2303, doi:onc2010630 [pii]10.1038/onc.2010.630 (2011).
- 33 Zhou, X. *et al.* R-Spondin1/LGR5 Activates TGFbeta Signaling and Suppresses Colon Cancer Metastasis. *Cancer Res* **77**, 6589-6602, doi:0008-5472.CAN-17-0219 [pii]10.1158/0008-5472.CAN-17-0219 (2017).
- 34 Xi, H. Q. *et al.* Increased expression of Lgr5 is associated with chemotherapy resistance in human gastric cancer. *Oncol Rep* **32**, 181-188, doi:10.3892/or.2014.3207 (2014).
- 35 Osawa, H. *et al.* Full-length LGR5-positive cells have chemoresistant characteristics in colorectal cancer. *Br J Cancer* **114**, 1251-1260, doi:bjc2016112 [pii]10.1038/bjc.2016.112 (2016).
- 36 Basak, O. *et al.* Mapping early fate determination in Lgr5+ crypt stem cells using a novel Ki67-RFP allele. *EMBO J* **33**, 2057-2068, doi:embj.201488017 [pii]10.15252/embj.201488017 (2014).
- 37 Tetteh, P. W. *et al.* Replacement of Lost Lgr5-Positive Stem Cells through Plasticity of Their Enterocyte-Lineage Daughters. *Cell Stem Cell* **18**, 203-213, doi:S1934-5909(16)00002-3 [pii]10.1016/j.stem.2016.01.001 (2016).
- 38 da Silva-Diz, V., Lorenzo-Sanz, L., Bernat-Peguera, A., Lopez-Cerda, M. & Munoz, P. Cancer cell plasticity: Impact on tumor progression and therapy response. *Semin Cancer Biol* **53**, 48-58, doi:S1044-579X(18)30024-5 [pii]10.1016/j.semcancer.2018.08.009 (2018).
- 39 Pascual, G. *et al.* Targeting metastasis-initiating cells through the fatty acid receptor CD36. *Nature* **541**, 41-45, doi:nature20791 [pii]10.1038/nature20791 (2017).
- 40 Buczacki, S. J. *et al.* Intestinal label-retaining cells are secretory precursors expressing Lgr5. *Nature* **495**, 65-69, doi:nature11965 [pii]10.1038/nature11965 (2013).
- 41 Tolba, R., Kraus, T., Liedtke, C., Schwarz, M. & Weiskirchen, R. Diethylnitrosamine (DEN)-induced carcinogenic liver injury in mice. *Lab Anim* **49**, 59-69, doi:49/1_suppl/59 [pii]10.1177/0023677215570086 (2015).
- 42 Brown, Z. J., Heinrich, B. & Greten, T. F. Mouse models of hepatocellular carcinoma: an overview and highlights for immunotherapy research. *Nat Rev Gastroenterol Hepatol* **15**, 536-554, doi:10.1038/s41575-018-0033-610.1038/s41575-018-0033-6 [pii] (2018).

- 43 Dow, M. *et al.* Integrative genomic analysis of mouse and human hepatocellular carcinoma. *Proc Natl Acad Sci U S A* **115**, E9879-E9888, doi:1811029115 [pii]10.1073/pnas.1811029115 (2018).
- 44 Wurmbach, E. *et al.* Genome-wide molecular profiles of HCV-induced dysplasia and hepatocellular carcinoma. *Hepatology* **45**, 938-947, doi:10.1002/hep.21622 (2007).
- 45 Roessler, S. *et al.* A unique metastasis gene signature enables prediction of tumor relapse in early-stage hepatocellular carcinoma patients. *Cancer Res* **70**, 10202-10212, doi:70/24/10202 [pii]10.1158/0008-5472.CAN-10-2607 (2010).

Supplementary Information for:

LGR5 marks targetable tumor-initiating cells in mouse liver cancer

Cao et al

Table of contents

Supplementary Figure 1

Supplementary Figure 2

Supplementary Figure 3

Supplementary Figure 4

Supplementary Figure 5

Supplementary Figure 6

Supplementary Figure 7

Supplementary Figure 8

Supplementary Figure 9

Supplementary Figure 10

Supplementary Figure 11

Supplementary Figure 12

Supplementary Figure 13

Supplementary Figure 14

Supplementary Table 1

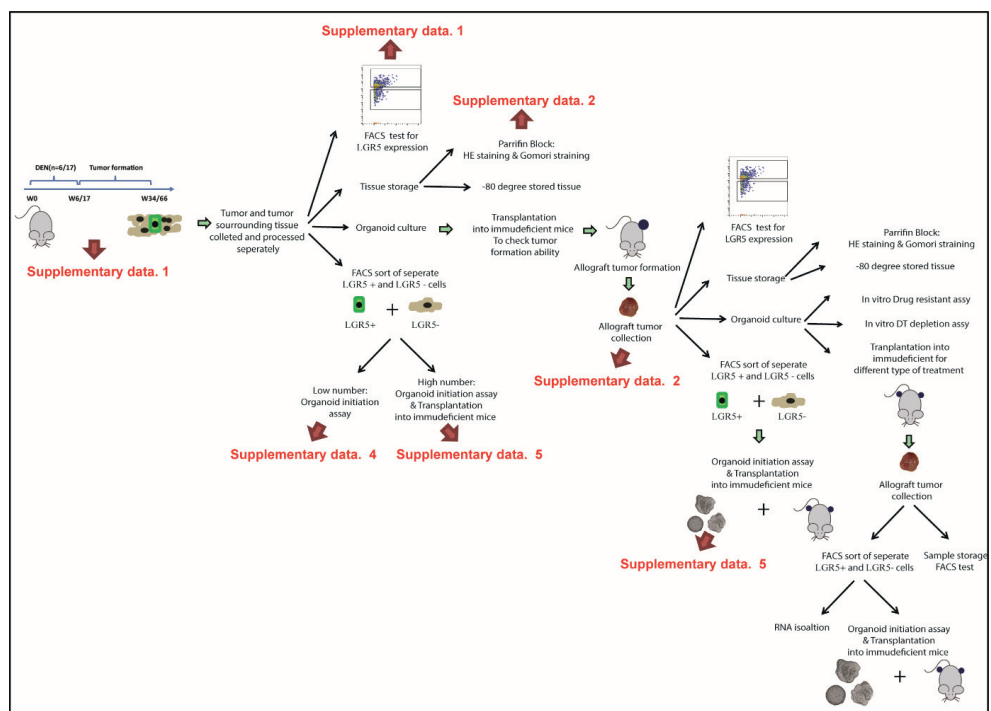
Supplementary Table 2

Page | 170

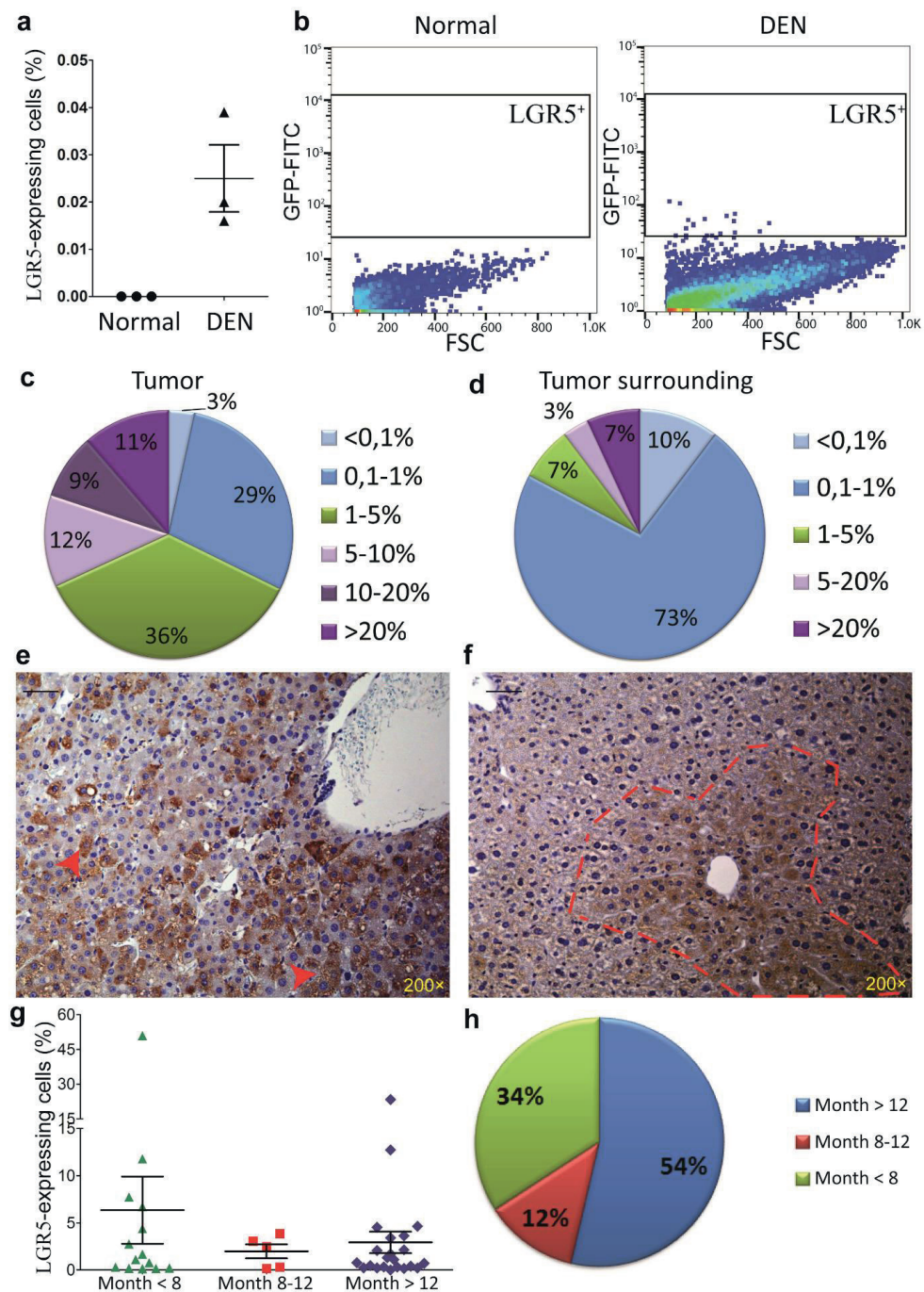
Supplementary Table 3

Supplementary Table 4

Supplementary Note



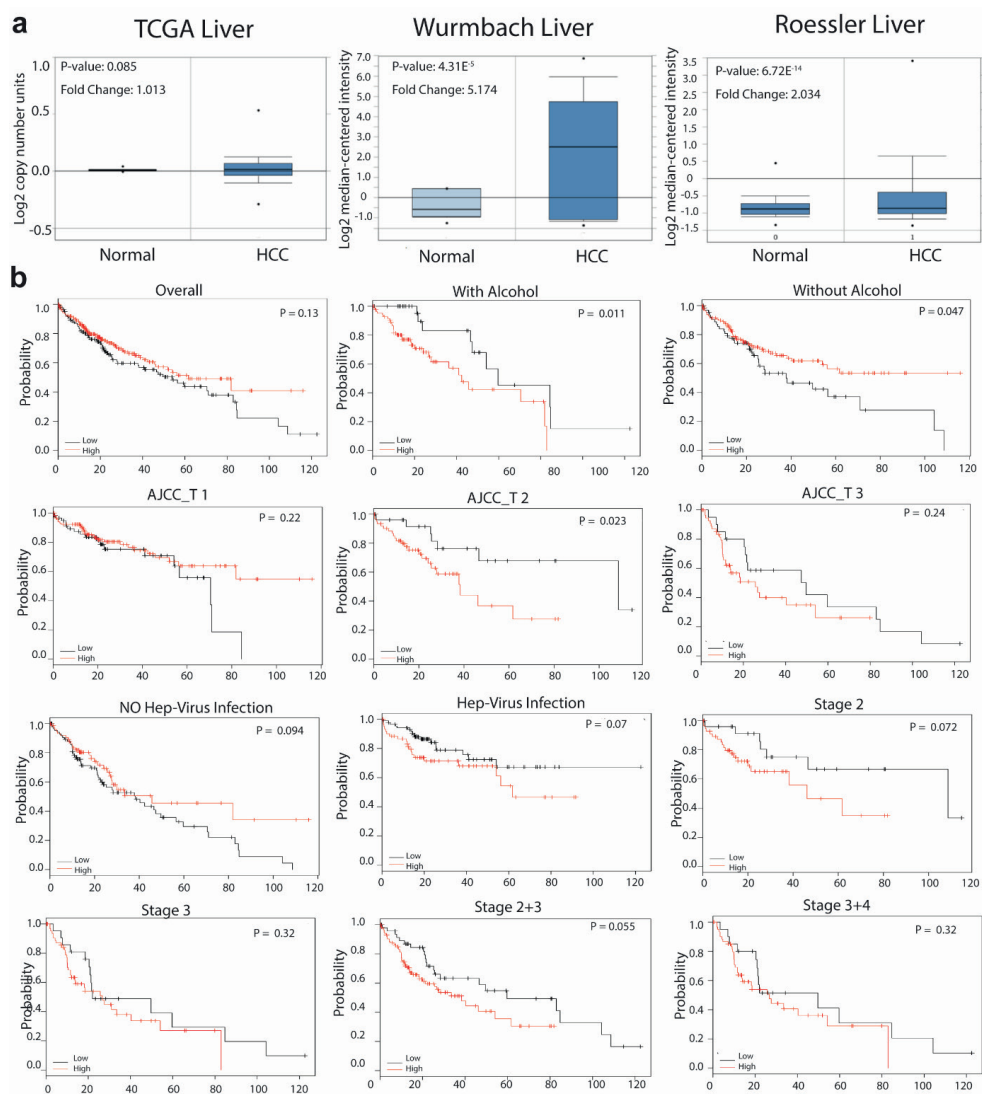
Supplementary Figure 1 | General flowchart of the experimental design.



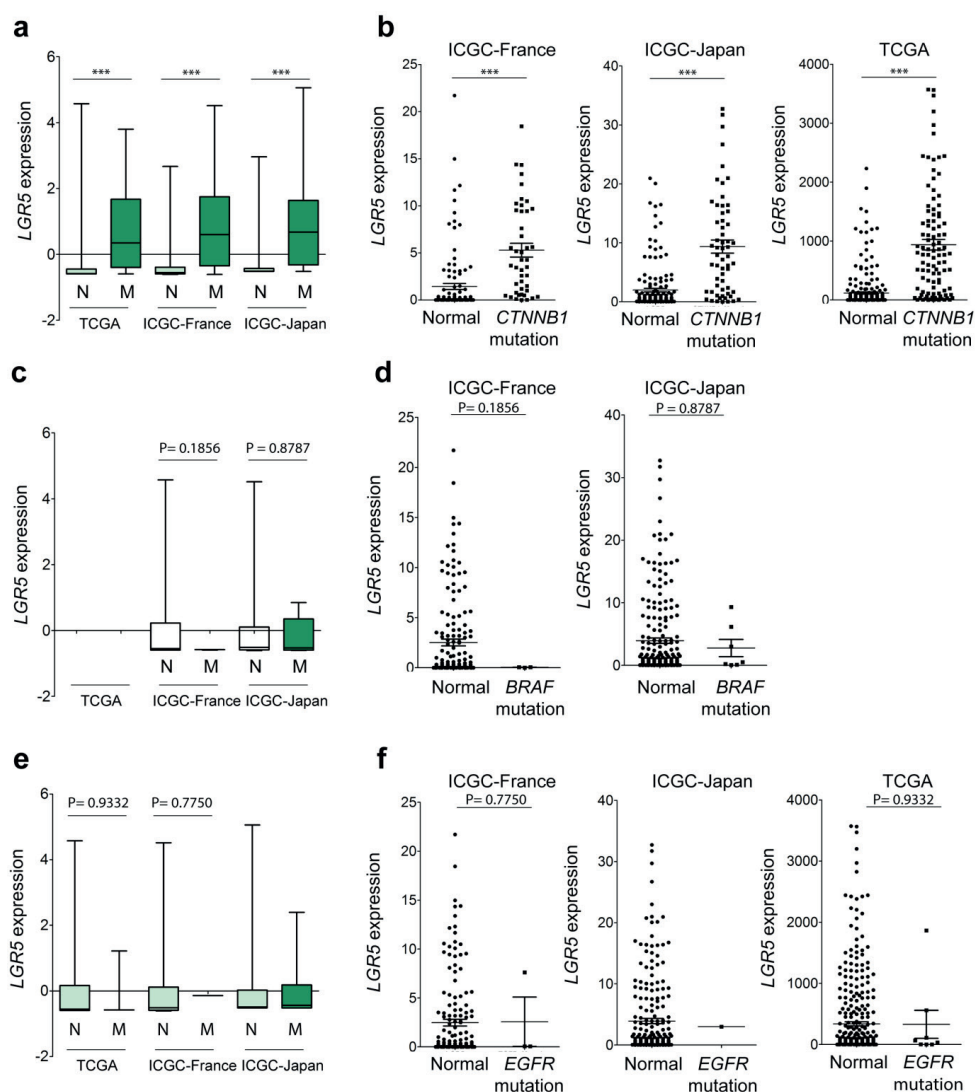
Supplementary Figure 2 | LGR5 expressing cells are present in the DEN-induced primary liver tumor.

a, LGR5⁺ cells are present in the liver upon DEN administration (Post DEN induction day 7). **b**,

Representative FACS plots showing that LGR5⁺ cells are present in the liver following DEN administration (Post DEN induction day 7). **c**, Relative LGR5⁺ fraction in DEN-induced liver tumors. **d**, Relative LGR5⁺ fraction in tissue bordering the DEN-induced liver tumors (denominated as surrounding). **e-f**, Representative immunohistochemistry pictures showing the microscopic aspect of the LGR5⁺ cells in liver cancer. Two types of LGR5⁺ cell distribution patterns are apparent, scattered LGR5⁺ cell distribution (**e**) and LGR5⁺ island-like clusters (**f**). The pictures show an anti-GFP immunohistochemistry staining in which LGR5⁺ cells are brown and nuclei are blue. Scale bar = 50μm. **g**, The percentage of LGR5-expressing cells within each tissue, grouped by tumor collection month (the month is counted since the first administration of DEN). Mean ± SEM. **(h)** Relative mice number fraction in all DEN-induced mice, grouped by tumor collection month. Source data are provided as a Source Data file.

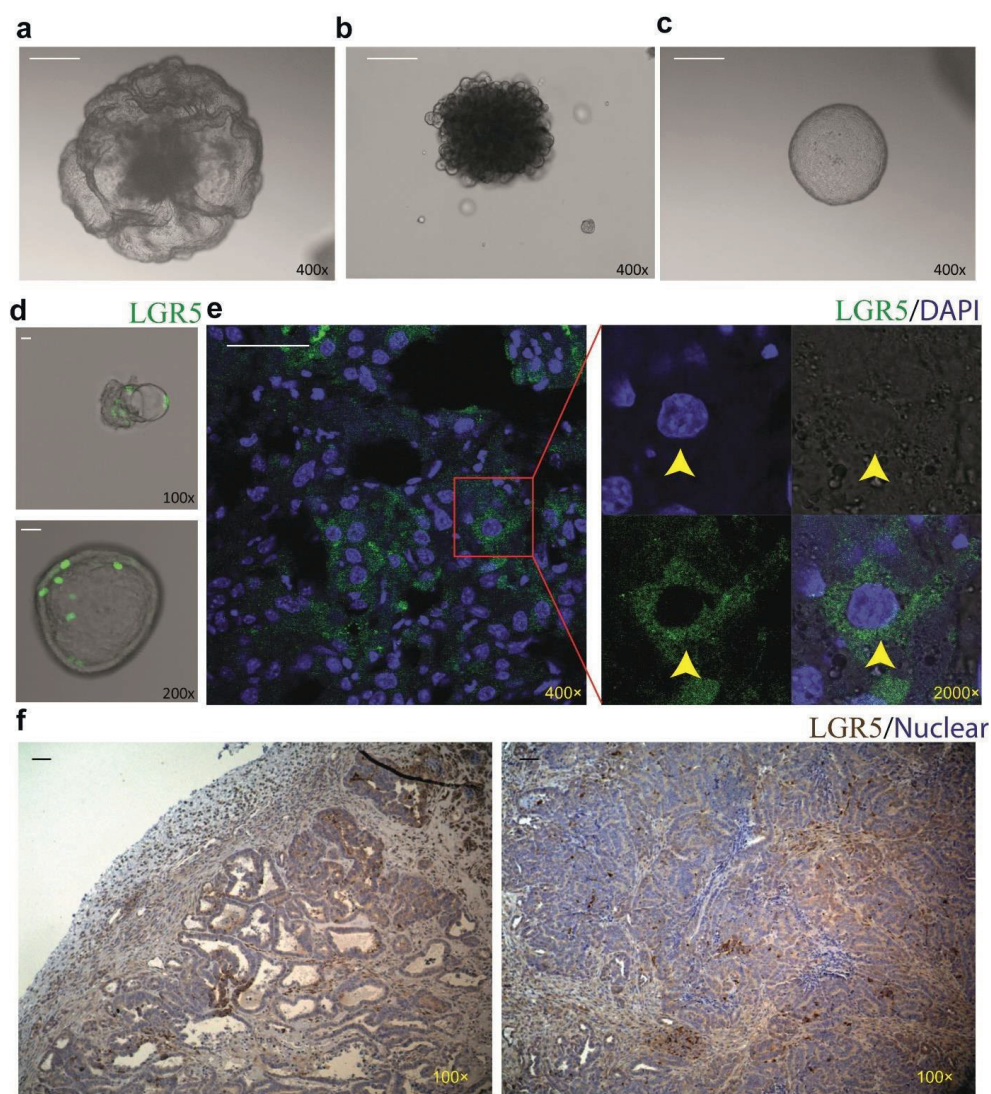


Supplementary Figure 3 | *LGR5* expression in HCC tissues and relation to patient outcome. **a**, The upregulated expression of *LGR5* in HCC tissues compared with normal tissues from TCGA Liver cohort (Normal vs. HCC: $n = 115$ vs. $n = 97$, $P = 0.085$, Fold change: 1.013), Wurmbach liver cohort (Normal vs. HCC: $n = 10$ vs. $n = 35$, $P = 4.31E^{-5}$, Fold change: 5.174) and Roessler liver cohort (Normal vs. HCC: $n = 200$ vs. $n = 225$, $P = 6.72E^{-14}$, Fold change: 2.034). **b**, Kaplan-Meier curve for HCC of patients based on different etiology/tumor stage of HCC from TCGA Liver cohort. AJCC_T: American Joint Committee on Cancer (AJCC) tumor staging system; Stage: Barcelona Clinic Liver Cancer (BCLC) tumor staging system. Source data are provided as a Source Data file.



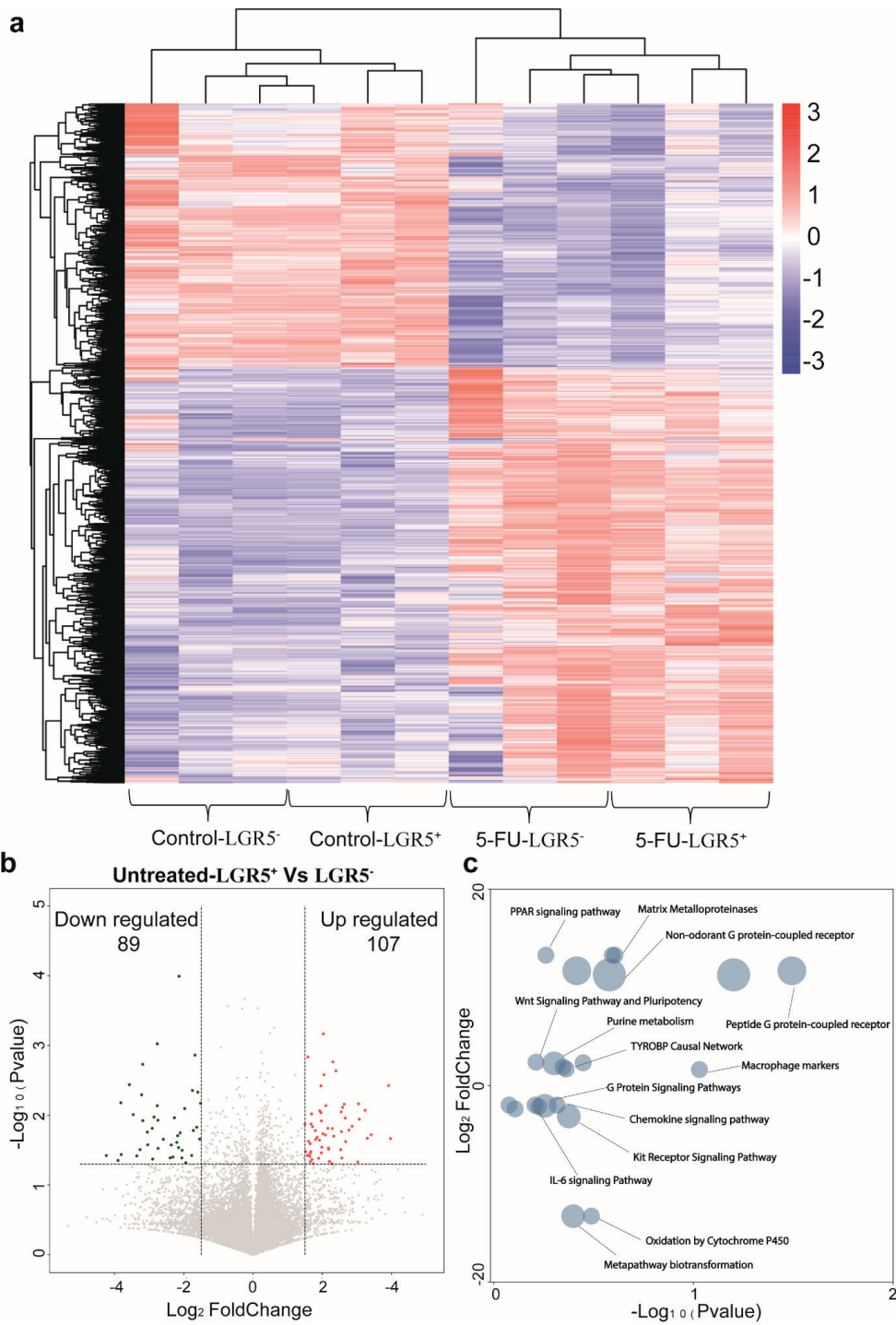
Supplementary Figure 4 | The expression level of *LGR5* is upregulated in *Cttnb1* mutated HCC tumors.

a-b, Upregulation of *LGR5* expression in *Cttnb1* mutated compared to non-*Cttnb1* mutated patient HCC tumors, in ICGC-France, ICGC-Japan and TCGA cohort. **c-d,** No significant difference of *LGR5* expression in *Braf* mutated compared to non-*Braf* mutated HCC tumors, in ICGC-France and ICGC-Japan cohort. **e-f,** No significant difference of *LGR5* expression in *Egfr* mutated compared to non-*Egfr* mutated HCC tumors, in ICGC-France, ICGC-Japan and TCGA cohort. Mean \pm SEM. Source data are provided as a Source Data file.

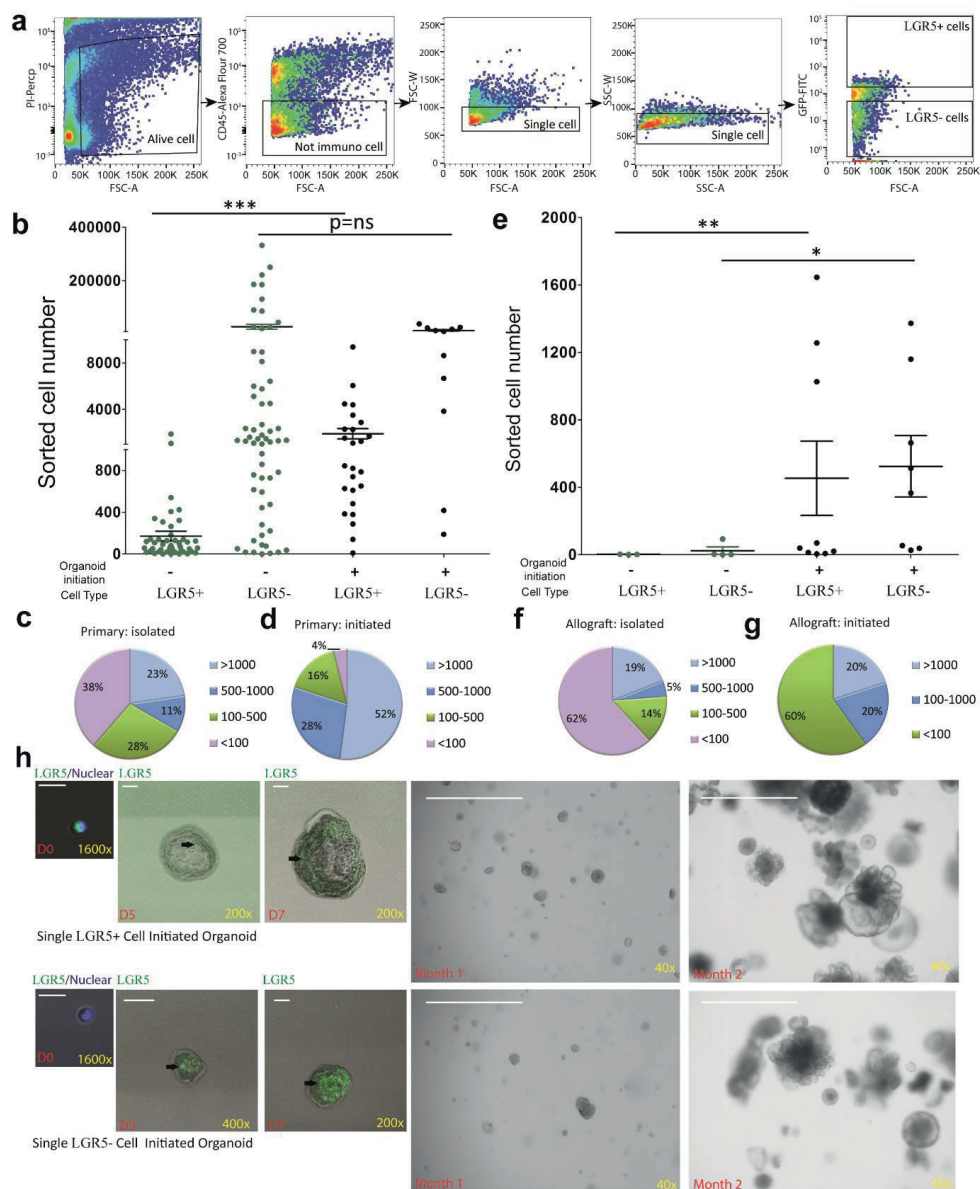


Supplementary Figure 5 | Allograft liver tumors maintain an LGR5⁺ compartment. a-c, 3-7 days after initiation of allograft tumor-derived cultures, small organoids were observed and subsequently passage was performed every 4-7 days, employing splitting ratios ranging from 1:4 to 1:10 as appropriate. Representative pictures show the different morphologies of the tumor organoids obtained, which include but also flower-like, irregular sheet-like structures (a), and grape-like, condensed phenotypes (b), and relative normal hollow sphere-like aspects (c). d, Representative confocal pictures showing the maintenance of an LGR5⁺ compartment in tumor organoids (LGR5-driven GFP: green). e, Representative immunofluorescent pictures showing an LGR5⁺ compartment

in allograft tumors (*LGR5*-driven GFP: green; DAPI: blue). **f**, Representative immunohistochemistry pictures showing expression of *LGR5* promotor-driven GFP in allograft tumors (anti-GFP immunohistochemistry: brown; nuclei: blue). Scale bar = 50µm.

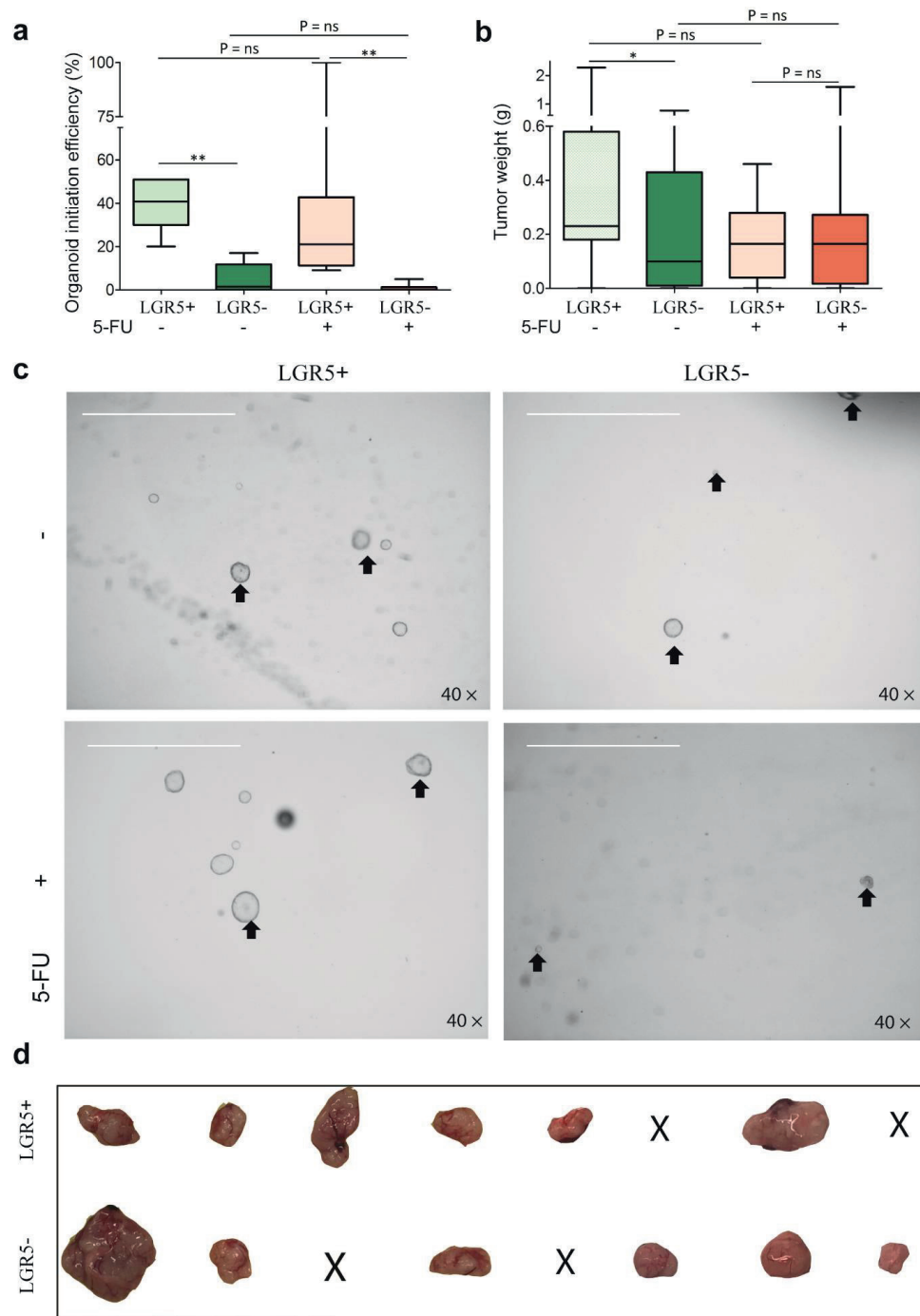


Supplementary Figure 6 | Genome-wide transcriptomic analysis of LGR5⁺ and LGR5⁻ cells by RNA-Seq. **a**, Hierarchical clustering showed a separation of all four different groups (Untreated LGR5⁺ cells, Untreated LGR5⁻ cells, 5-FU-treated LGR5⁺ cells, 5-FU-treated LGR5⁻ cells). **b**, A Volcano plot showing the most significantly differentially expressed genes between untreated LGR5⁺ and LGR5⁻ cells. **c**, GSEA with the library of Wiki2019 was performed to reveal the alteration of signaling pathways between untreated LGR5⁺ and LGR5⁻ cells. Source data are provided as a Source Data file.

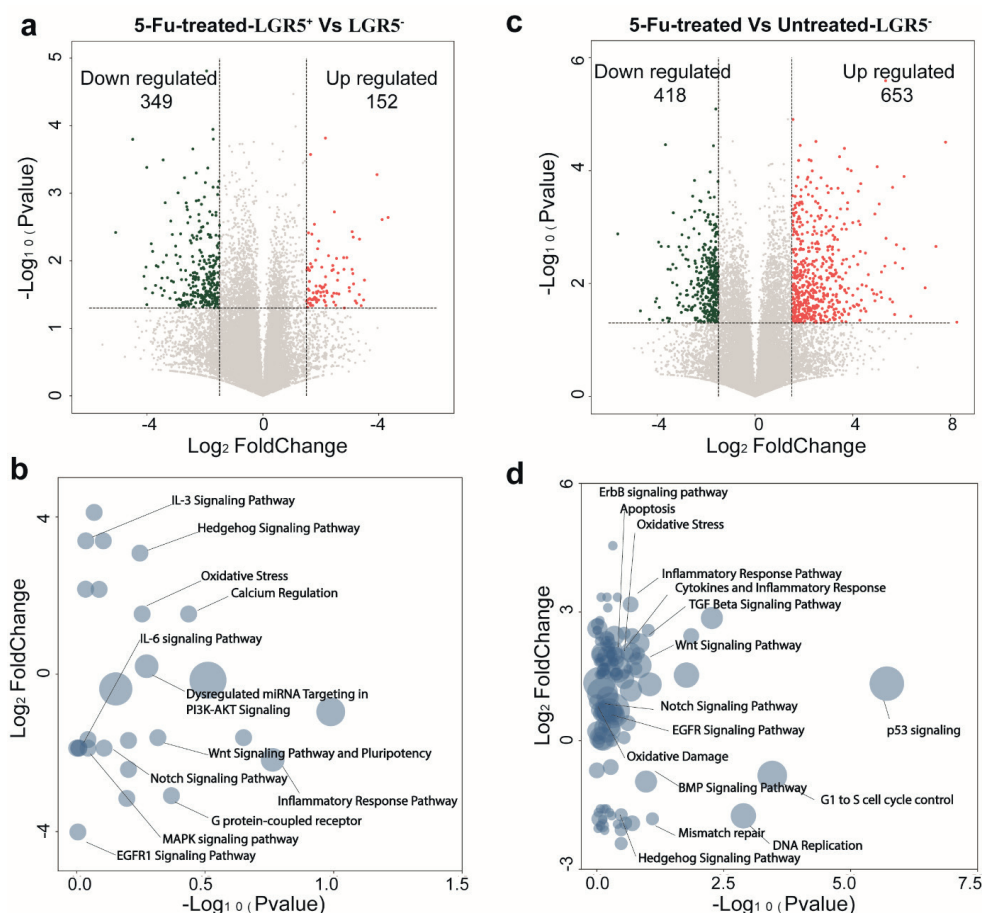


Supplementary Figure 7 | LGR5⁺ cells have stronger organoid initiation ability. **a**, The FACS test/sort strategy for isolating LGR5-GFP⁺ and LGR5-GFP⁻ cells obtained from liver/allograft tumors/organoids. **b**, The numbers of sorted LGR5-GFP⁺ and LGR5-GFP⁻ cells yielding successful (black dots) or failure of organoid initiation (green dots), employing material obtained from DEN-induced murine livers (LGR5⁺-non-initiation vs. LGR5⁻-non-initiation vs. LGR5⁺-initiation vs. LGR5⁻-initiation: 171.4 ± 47.1, n = 46 vs. 28350 ± 8914, n = 60 vs. 1906 ± 441.6, n = 25 vs. 13860 ± 3654, n = 11, Mean ± SEM). **c**, The

distribution showing the percentage of the number of LGR5⁺ cells which were isolated from primary liver tumors. **d**, The cell number distribution for the sorted LGR5⁺ cells which can initiate organoid, from primary tumors. **e**, The exact sorted numbers for LGR5⁺ cells and LGR5⁻ cells , for organoid initiated (black dots) and non-organoid initiated (green dots), from allograft tumors (LGR5⁺-non-initiated vs. LGR5⁻-non-initiated vs. LGR5⁺-initiated vs. LGR5⁻-initiated: 2.0 ± 0.6 , $n = 3$ vs. 24.3 ± 22.9 , $n = 4$ vs. 453.7 ± 220.3 , $n = 9$ vs. 524.3 ± 182.9 , $n = 8$). **f**, Frequency distribution of the relative number of LGR5⁺ cells obtained from allograft liver tumors. **g**, Frequency distribution of the number of LGR5⁺ cells that display successful organoid initiation from material obtained from allograft tumors. **h**, Representative pictures tracing organoids initiation and growth from LGR5⁺ or LGR5⁻ cells. Black arrow: LGR5 expressing cells. Day0/5/7: Scale bar = 50 μ m; Month1/2: Scale bar = 1000 μ m. Source data are provided as a Source Data file.

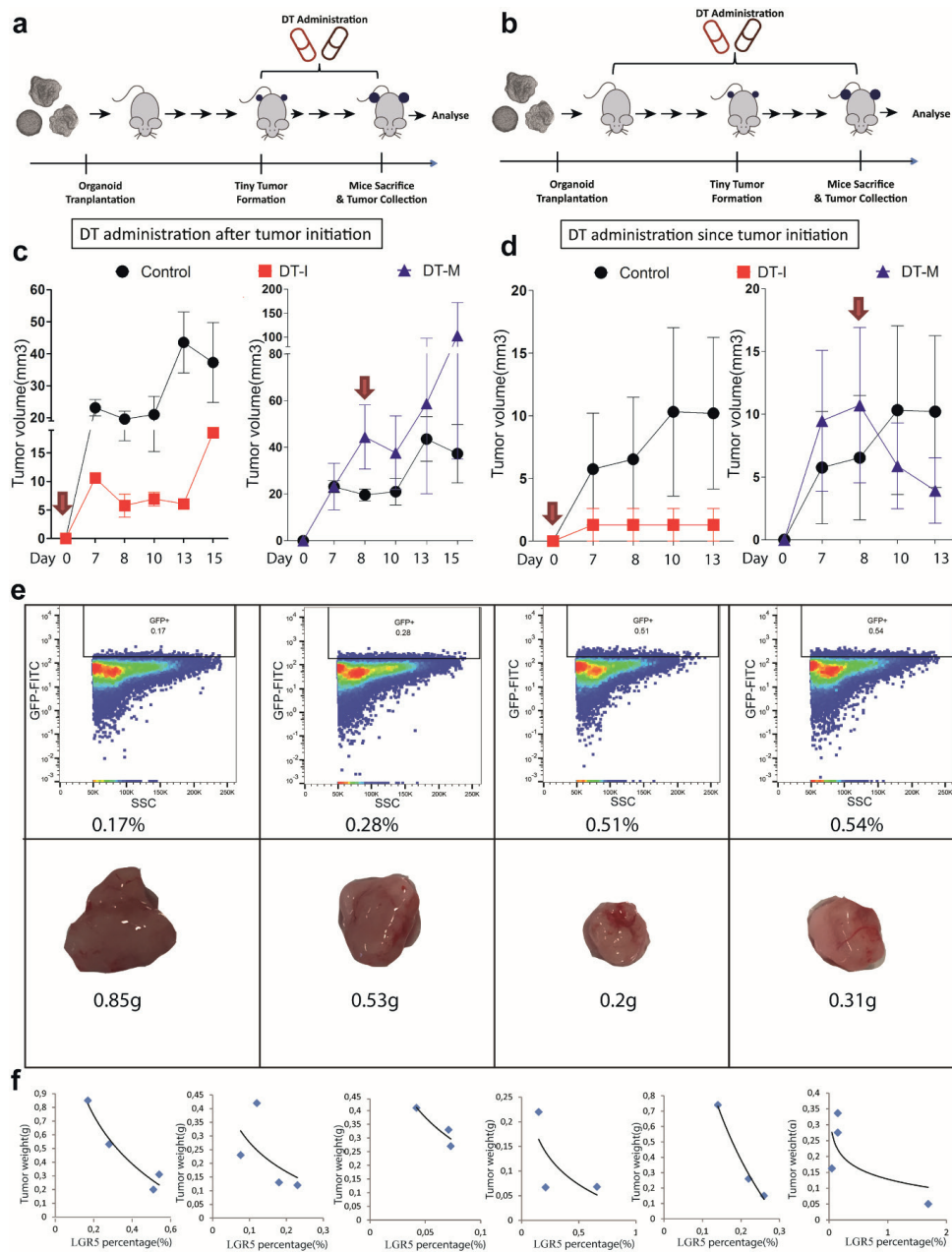


Supplementary Figure 8 | LGR5⁺ cells from 5-FU treated tumors can initiate organoid and tumor. a, The organoid initiation ability of untreated LGR5⁺ cells ($39.5 \pm 4.8 \%$, $n = 6$, Mean \pm SEM), untreated LGR5⁻ cells ($5.0 \pm 2.9 \%$, $n = 6$), 5-FU-treated LGR5⁺ cells ($31.2 \pm 14.0 \%$, $n = 6$) and 5-FU-treated LGR5⁻ cells ($0.8 \pm 0.8 \%$, $n = 6$). **b,** The tumor initiation ability of untreated LGR5⁺ cells (0.50 ± 0.15 g, $n = 15$), untreated LGR5⁻ cells (0.21 ± 0.06 g, $n = 15$), 5-FU-treated LGR5⁺ cells (0.18 ± 0.05 g, $n = 8$) and 5-FU-treated LGR5⁻ cells (0.31 ± 0.19 g, $n = 8$). **c,** Representative picture showing the organoid initiation ability of above four groups. Black arrow: initiated organoids. Scale bar = 1000 μ m. **d,** Pictures showing 5-FU-treated LGR5⁺ cells and 5-FU-treated LGR5⁻ cells initiated tumors. Source data are provided as a Source Data file.



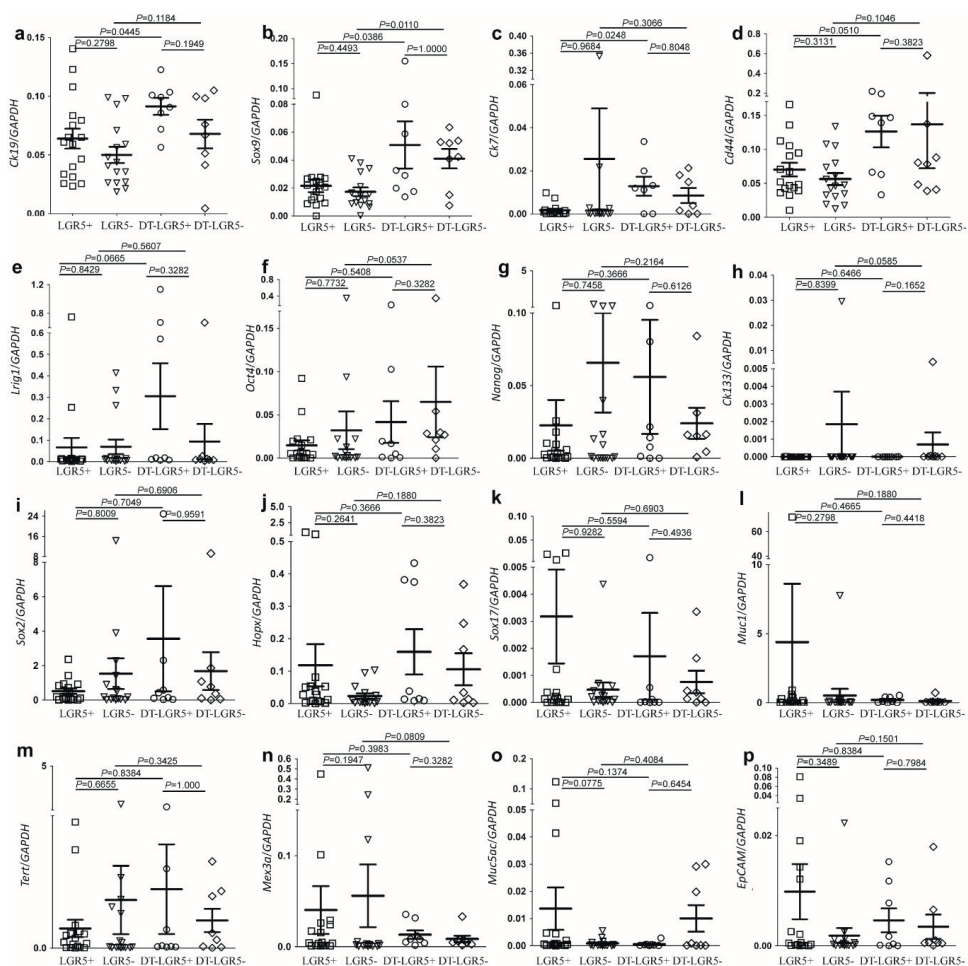
Supplementary Figure 9 | Genome-wide transcriptomic analysis of 5-FU treatment on LGR5^{+/-} cells.

a, A Volcano plot showing the most significantly differentially expressed genes between 5-FU treated LGR5⁺ cell/LGR5⁻ cells. **b**, Gene enrichment analysis (Wiki2019) of the differentially expressed genes between 5-FU treated LGR5⁺ cell/LGR5⁻ cells. **c**, A Volcano plot showing the most significantly differentially expressed genes between 5-FU treated/untreated LGR5⁻ cells. **d**, Gene enrichment analysis (Wiki2019) of the differentially expressed genes between 5-FU treated/untreated LGR5⁻ cells. Source data are provided as a Source Data file.



Supplementary Figure 10 | Targeting LGR5 impedes the tumor growth. **a-b**, Outline of the experimental strategies used to test the effect of DT administration during tumor growth (**a**) and at tumor initiation (**b**). **c-d**, Growth curves showing the effects of DT administration during the entire experimental period (Left, DT-I) and following DT intervention during tumor growth (Right, DT-M) for organoid strain 1 (**c**) and strain 2 (**d**). Mean \pm SEM. Red arrow: onset of DT administration ($n = 4$ for Page | 186

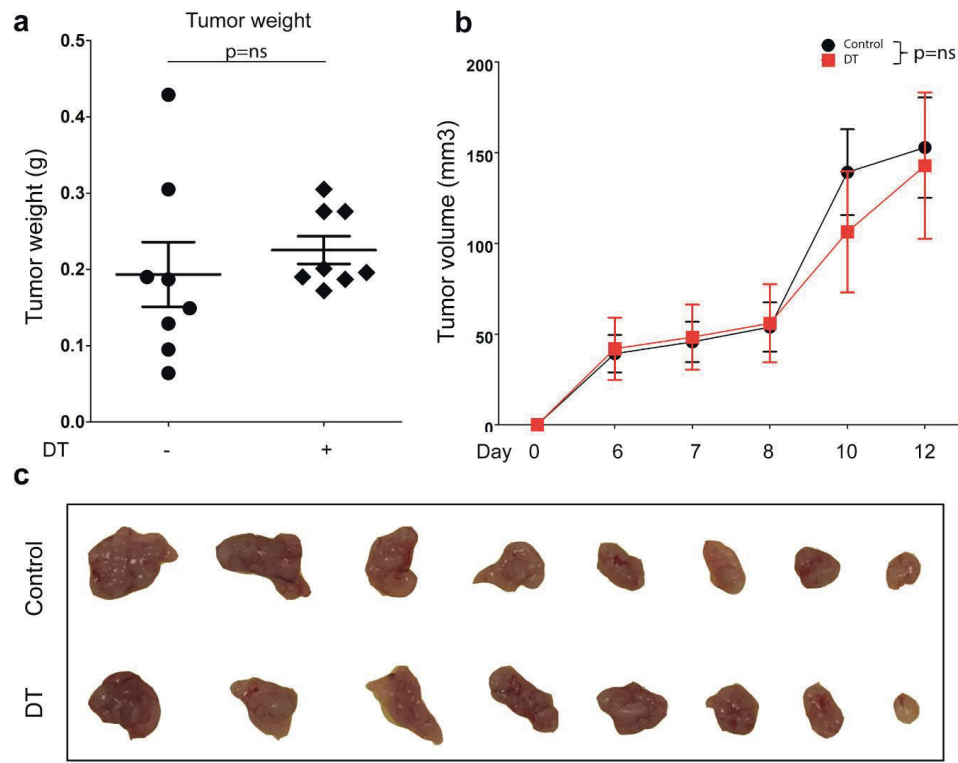
each time point). **e**, Representative FACS pictures (upper channel, with LGR5-GFP⁺ expression) and tumor pictures (lower channel, with tumor weights) showing that the same tumor strains, collected from a single mouse, shows variable LGR5 expression. **f**, tumors collected from six individual mice (transplanted with same strain and same amount of organoid; collected on the same day, non-treated tumors) showing that smaller tumors have relatively higher LGR5 expression. Source data are provided as a Source Data file.



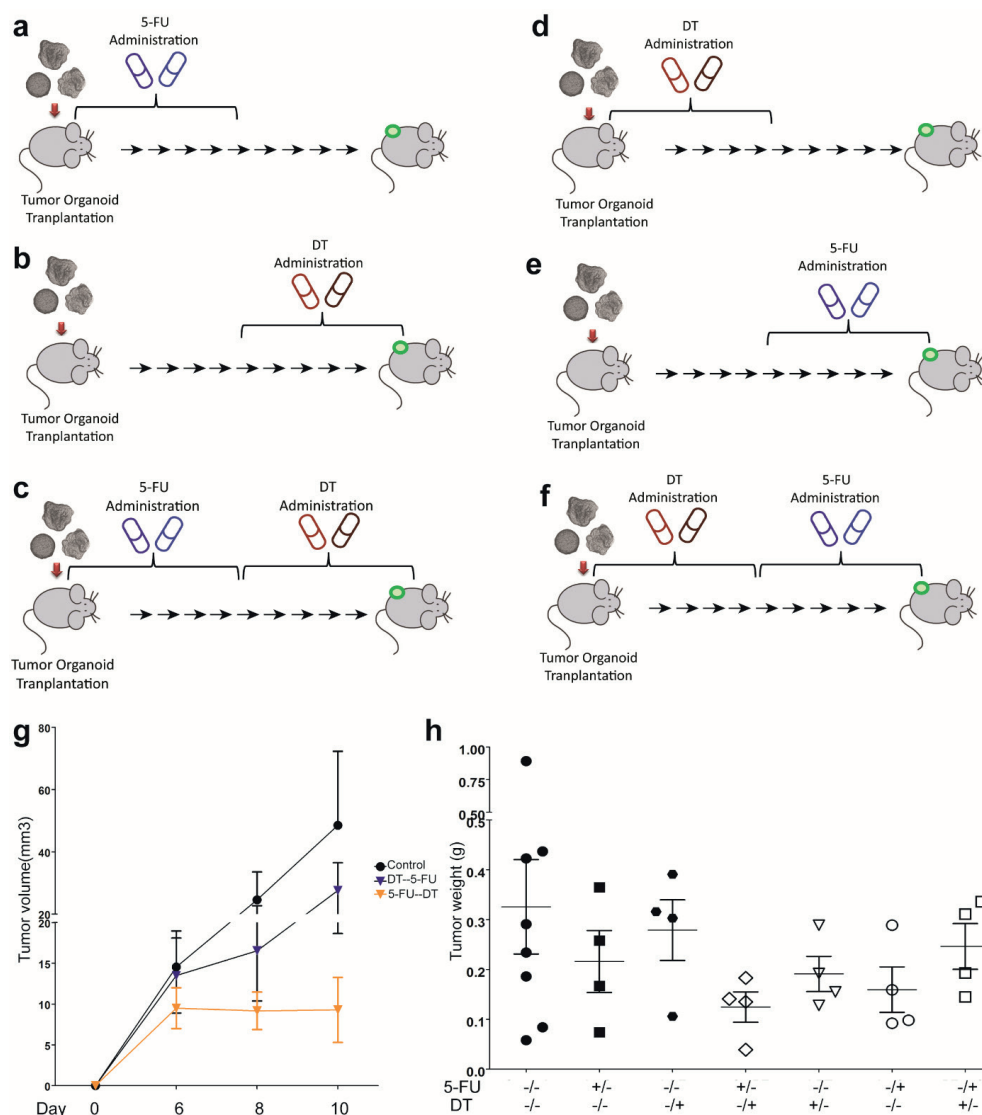
Supplementary Figure 11 | The expression profile of untreated/DT-treated LGR5⁺ and LGR5⁻ cells.

a-p, The expression of stem cell/tumor stem cell markers in LGR5⁺/LGR5⁻ and DT treated tumor isolated LGR5⁺/LGR5⁻ cells was analyzed using qRT-PCR and related to a reference gene. Mean ± SEM.

Source data are provided as a Source Data file.



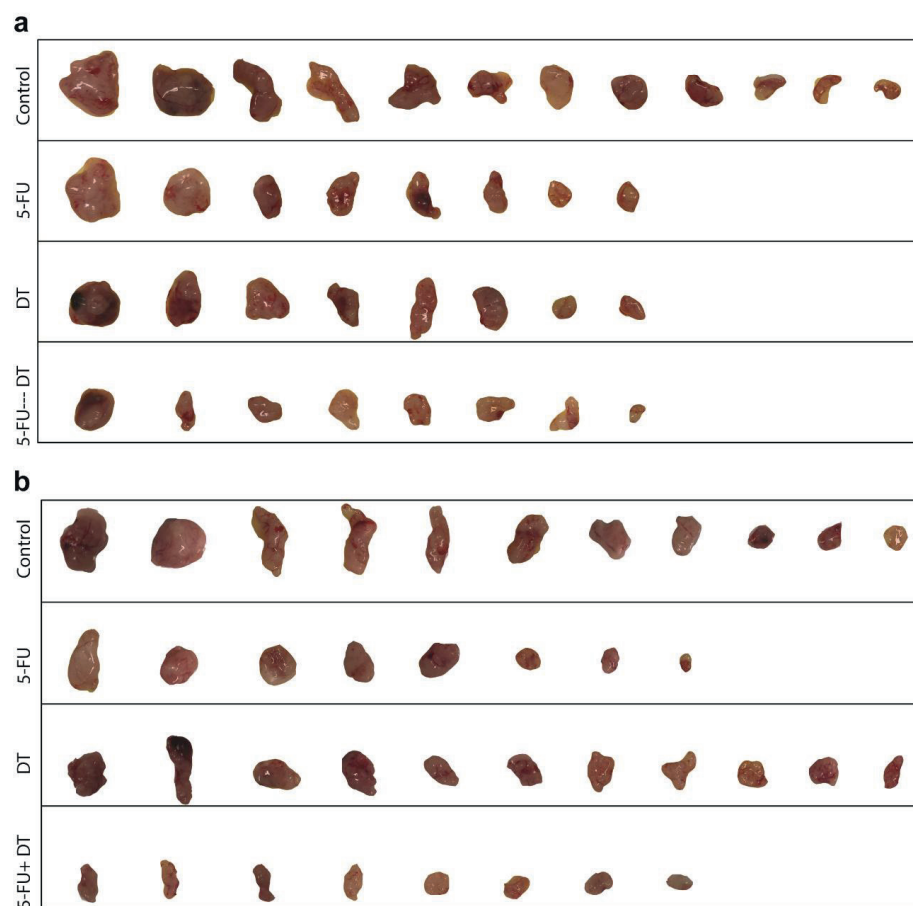
Supplementary Figure 12 | Wide type tumor organoids do not respond to DT administration. **a**, The weight of tumors initiated by wild type organoids from control, the DT-treated group following sacrifice of the animals involved (Control vs. DT: 0.19 ± 0.042 g vs. 0.23 ± 0.018 g, $n = 8$, $P = ns$, Mean \pm SEM). **b**, Representative growth curve showing tumor volume in the control group and the DT-treated group ($n = 4$). **c**, Representative pictures showing the tumors from the control group and DT administrated group. Source data are provided as a Source Data file.



Supplementary Figure 13 | Effects of combining DT treatment with conventional anti-cancer therapy.

a, 5-FU control: 5-FU was administrated during the first half of the experiment period and tumor volume was assessed continuously. **b**, DT control: animals were treated with DT during the second half of the experiment period and tumor volume was assessed continuously. **c**, Combination strategy 1: 5-FU was administrated during the first half and DT was treated during the second half of the experiment period. Tumor volume was assessed continuously. (**a** and **b** are the relevant control groups for **c**). **d**, DT control: DT was administrated during the first half of the experiment period and tumor volume was assessed continuously. **e**, 5-FU control: 5-FU was administrated during the second half of the

experiment period the and tumor volume was assessed continuously. **f**, Combination strategy 2: First DT was applied (first half of the experiment) followed by 5-FU treatment (second half of the experiment) (**d** and **e** are the relevant control groups for **f**). **g**, Representative growth curve showing tumor volumes of the control, Combination strategy 1 (5-FU--DT) and Combination strategy 2 (DT--5-FU) group ($n = 4$). **h**, Weight of tumors from the different groups described above at the end of the experiment. +/-: Treatment was administrated for the first half of the experiment; -/+ : Treatment was administrated for the second half of the experiment; -/-: No treatment. Mean \pm SEM. Source data are provided as a Source Data file.



Supplementary Figure 14 | Combination of LGR5 lineage ablation with conventional therapy. a-b, Pictures showing the tumors from the different groups.

Supplementary Table 1 | Allograft tumor

Allograft Tumor						
Initiated Tumor Code	Isolated Cell Popualtion	Original Strain	Injected Cell Number	Initiated Tumor Weight(g)	Tumor Formation Time	Immunodeficient mice type
1	LGR5+	SAL1	72	0.58	23	Nude mice
	LGR5-		72	0.27	23	Nude mice
2	LGR5+	SAL1	57	0.44	23	Nude mice
	LGR5-		57	0.01	23	Nude mice
3	LGR5+	SAL1	90	0.14	23	Nude mice
	LGR5-		90	0.11	23	Nude mice
4	LGR5+	SAL1	167	0.22	23	Nude mice
	LGR5-		167	0.08	23	Nude mice
5	LGR5+	AL43	66	2.28	38	Nude mice
	LGR5-		66	0.45	38	Nude mice
6	LGR5+	AL43	53	1.11	38	NSG
	LGR5-		53	0.43	38	NSG
7	LGR5+	AL43	57	0.51	38	NSG
	LGR5-		57	0.77	38	NSG
8	LGR5+	SAL2	237	0.8	26	Nude mice
	LGR5-		237	0.05	26	Nude mice
9	LGR5+	SAL2	699	0.23	26	Nude mice
	LGR5-		699	0.1	26	Nude mice
10	LGR5+	SAL1	182	0.53	26	Nude mice
	LGR5-		182	0.09	26	Nude mice
11	LGR5+	SAL1	127	0.18	26	Nude mice
	LGR5-		127	0.61	26	Nude mice

Supplementary Table 2 | Clinical-pathological data of Erasmus cohort

Table. Patient characteristics	
Characteristic	HCC patients (n=74)
Age at surgery (years)	
Mean \pm SD	60 \pm 15,9
Median (range)	63 (11-82)
Sex – no. (%)	
Male	45 (60,8)
Female	29 (39,2)
Race – no. (%)	
White	61 (82,4)
African	6 (8,1)
Asian	6 (8,1)
Not reported	1 (1,4)
Etiology – no. (%)	
No known liver disease	21 (28,4)
Alcohol	16 (21,6)
Hepatitis B	9 (12,2)
NASH	8 (10,8)
Hepatitis C + Alcohol	6 (8,1)
Hepatitis B + Alc/HepC/NASH	5 (6,8)
Hepatitis C	5 (6,8)
Fibrolamellar HCC	3 (4,1)
Hemochromatosis + NASH	1 (1,4)
Hepatitis status – no. (%)	
Hepatitis B or C positive	25 (33,8)
Chronic Hepatitis B	14 (18,9)

Chronic Hepatitis C	12 (16,2)
Cirrhosis – no. (%)	
Yes	21 (28,4)
No	53 (71,6)
Tumor differentiation – no. (%)	
Good	8 (10,8)
Moderate	40 (54,1)
Poor	14 (18,9)
Unknown	12 (16,2)
Vascular invasion – no. (%)	
Yes	29 (39,2)
No	38 (51,4)
Unknown	7 (9,5)
Number of lesions – no. (%)	
1	40 (54,1)
>1	34 (45,9)
Size of largest lesion (cm)	
Mean ± SD	7,7 ± 5,6
Median (range)	6,1 (1-24)
AFP level before resection (ug/l)	
Mean ± SD	6661,1 ± 407289,4
Median (range)	8 (1-3118700)

Supplementary Table 3 | Antibody

Antibody	Antibody clone/ reference	Raised	Origin
CD45	56-0451-82	Mouse	eBioscience
AFP	SAB3500533- 100UG	Goat	Sigma
HNF4a	ab41898	Mouse	Abcam
EpCAM	ab71916	Rabbit	Abcam
Cytokeratin 19	ab52625	Rabbit	Abcam
GFP	A-11122	Rabbit	Invitrogen/Life Technologies
Alexa Fluor® 488 AffiniPure Donkey Anti- Goat IgG (H+L)	705-545-147	Donkey	Bio-Connect
Donkey anti-Rabbit IgG (H+L) Secondary Antibody, Alexa Fluor® 594 conjugate	R37119	Donkey	Thermo fisher
Donkey anti-mouse IgG (H+L) Secondary Antibody, Alexa Fluor® 594 conjugate	R37115	Donkey	Thermo fisher

Supplementary Table 4 | Primer

Gene name	Gene Symbo	Sequence	
Leucine-rich repeat-containing G-protein coupled receptor 5	Mouse- <i>Lgr5</i>	Fw	CTG ACT TTG AAT GGT GCC TCG
		Re	ATG TCC ACT ACC GCG ATT AC
Cytokeratin-19	Mouse- <i>Krt19</i>	Fw	GTG AAG ATC CGC GAC TGG T
		Re	AGG CGA GCA TTG TC AAT CTG
Transcription factor SOX-9	Mouse- <i>Sox9</i>	Fw	CGA CTA CGC TGA CCA TCA GA
		Re	GAC TGG TTG TTC CCA GTG CT
CD133	Mouse- <i>Prom1</i>	Fw	TCT GTT CAG CAT TTC CTC AC
		Re	TCA GTA TCG AGA CGG GTC
CD44	Mouse- <i>CD44</i>	Fw	CGT CCA ACA CCT CCC ACT AT
		Re	AGC CGC TGC TGA CAT CGT
Keratin, type II cytoskeletal 7	Mouse- <i>Ck7</i>	Fw	ATC CGC GAG ATC ACC ATC
		Re	ATG TGT CTG AGA TCT GCG ACT
Leucine-rich repeats and immunoglobulin-like domains protein 1	Mouse- <i>Lrig1</i>	Fw	AAGGGAACCTCAACTGGCGAG
		Re	ACGTGAGGCCTTCAATCAGC
Octamer-binding transcription factor 4	Mouse- <i>Oct4</i>	Fw	CTGTAGGGAGGGCTTCGGGCACTT
		Re	CTGAGGGCCAGGCAGGAGCACGAG
Homeobox protein NANOG	Mouse- <i>Nanog</i>	Fw	AGGGTCTGCTACTGAGATGCTCTG
		Re	CAACCACTGGTTTTCTGCCACCG
SRY (sex determining region Y)-box 2	Mouse- <i>Sox2</i>	Fw	GGCAGCTACAGCATGATGCAGGAGC
		Re	CTGGTCATGGAGTTGTACTGCAGG
Homeodomain-only protein	Mouse- <i>Hopx</i>	Fw	CATCCTTAGTCAGACGCGCA
		Re	AGGCAAGCCTTCTGACCGC
Telomerase reverse transcriptase	Mouse- <i>Tert</i>	Fw	GCAGGTGAACAGCCTCCAGACAG
		Re	TCCTAACACGCTGGTCAAAGGGAAGC

RNA-binding protein MEX3A	Mouse- <i>Mex3a</i>	Fw	ACACCACGGAGTGCCTTC
		Re	GTTGGTTTTGGCCCTCAGA
Mucin 5AC	Mouse- <i>Muc5ac</i>	Fw	GGACCAAGTGGTTTGACACTGAC
		Re	CCTCATAGTTGAGGCACATCCCAG
Epithelial cell adhesion molecule	Mouse- <i>Epcam</i>	Fw	CGCAGCTCAGGAAGAATGTG
		Re	TGAAGTACACTGGCATTGACG
SRY-box 17	Mouse- <i>Sox17</i>	Fw	GGCGCAGCAGAATCCAGA
		Re	CCACGACTTGCCGAGCAT
Cell surface associated or polymorphic epithelial mucin	Mouse- <i>Muc1</i>	Fw	CCCCAGTTGTCTGTTGGGGTC
		Re	GGATTCTACCACCACGGAGCC
Glyceraldehyde 3-phosphate dehydrogenase	Mouse- <i>Gapdh</i>	Fw	TCACCACCATGGAGAAGGC
		Re	GCTAAGCAGTTGGTGGTGCA
Beta-glucuronidases	Human- <i>GUSB</i>	Fw	CAGGTGATGGAAGAAGTGG
		Re	GTTGCTCACAAGGTCACAG
Hypoxanthine phosphoribosyltransferase 1	Human- <i>HPRT1</i>	Fw	GCTATAAATCTTTGCTGACCTGCTG
		Re	AATTACTTTTATGTCCCTGTTGACTGG
Phosphomannomutase 1	Human- <i>PMM1</i>	Fw	CGAGTTCTCCGAAGTGGAC
		Re	CTGTTTTTCAGGGCTTCCAC
Leucine-rich repeat-containing G-protein coupled receptor 5	Human- <i>LGR5</i>	Fw	TCAGTCAGCTGCTCCGAAT
		Re	CGTTTCCCGCAAGACGTAAC

Supplementary Note:

Description for Supplementary Data

[1] Supplementary Data 1

Content:

The detailed information for *Lgr5-DTRGFP* mice which used to induce liver cancer, including:

1)The mice code

2)The mice background

3)Primary Code: The corresponding code of initiated primary organoid strain. Black mark: the tissue did not initiate an organoid strain or the strain was already lost due to infection in the following culture.

4)Post Den Time (Month): The sacrifice time after the induction of DEN.

5)DEN Administration (Week): Time passed between administration of DEN and sacrifice.

6)Tissue Type: S: tumor surrounding tissue; T: tumor tissue. S—T: initially marked with tumor surrounding tissue and then characterized as tumor.

7)Percentage of LGR5-expressing cells (%): The percentage of LGR5-expressing cells within each tissue.

8)Allograft Strains: The strain code which initiated allograft tumor in the immunodeficient mice.

Remarks: In total, 41 mice were monitored. 10 (mice code: 8,12,17,18,21,22,29,31,35,41) out of 41 mice liver did not show obvious tumor formation. After the following characterization, 2 (mice code: 8, 22) out of 10 were proven to be liver tumor.

Mouse Code	Mice Background	Primary Code	Post Den Time (Month)	DEN Administration (Week)	Tissue Type	Percentage of LGR5-expressing cells (%)	Allograft Strains
M1	B6	PT1	7	6	S	0,28	
		PT2			T	0,16	
M2	B6	PT3	7	6	S	0,79	
		PT4			T	1,1	

M3	B6	PT5	12	6	S	0,16	
		PT6			T	0,18	
M4	B6	PT7	9	6	S	0,57	
		PT8			T1	5,66	AL8
		PT9			T2	0,32	
		PT10			T3	5,61	AL10
M5	B6	PT11	9	6	S	0,22	
		PT12			T	2,5	
M6	B6&C3H	PT13	5	17	S	0	AL13
		PT14			T	2,75	
M7	B6	PT15	13	6	S	0,4	
		PT16			T	2,07	
M8	B6	PT17	13	6	S--T	0,31	AL17
M9	B6	PT18	12	6	S	1,1	
		PT19			T	3,05	
M10	B6	PT20	15	6	S	0,85	
		PT21			T1	2,85	
		PT22			T2	1,43	
M11	B6	PT23	15	6	S	0,89	
		PT24			T	0,17	
Mouse Code	Mice background	Primary code	Post Den time	DEN		Lgr5 expression	Allograft strains
M12	B6&C3H	PT25	3	11	S	0,18	

M13	B6	PT26	10	17	S	0,062	
		PT27			T	0,3	
M14	B6	PT28	13	6	S	0,33	
		PT29			T1	0,47	
		PT30			T2	2,15	
M15	B6	PT31	13	6	S	0	
		PT32			T1	0,45	
		PT33			T2	0,5	
M16	B6	PT34	13	6	S	0,12	
		PT35			T	1,71	
M17	B6	PT36	13	6	S	0,72	
M18	B6	PT37	13	6	S	0,24	
M19	B6	PT38	13	6	S	3,41	AL38
		PT39			T	1,11	
M20	B6	PT40	16	6	S	0,15	
		PT41			T	0,22	
M21	B6	PT42	14	6	S	0,33	
M22	B6&C3H	PT43	7	17	S--T	0,77	AL43
M23	B6&C3H	PT44	7	17	S	3,08	
		PT45			T1	3,29	
		PT46			T2	0,05	AL46
Mouse Code	Mice background	Primary code	Post Den time	DEN		Lgr5 expression	Allograft strains

M24	B6&C3H	PT47	7	17	S	25	
		PT48			T1	46,1	
		PT49			T2	55,6	
		PT50			T3	51,2	
M25	B6	PT51	14	6	T	4,63	
M26	B6	PT52	14	6	S	0,021	
		PT53			T	0	
M27	B6&C3H	PT54	7	17	T	7,73	
M28	B6	PT55	8	17	S	20,3	
		PT56			T1	10,7	
		PT57			T2	1,67	
		PT58			T3	0,48	
		PT59			T4	4,66	
M29	B6	PT60	15	6	S	0,4	
M30	B6&C3H	PT61	8	17	T1	2,62	AL61
		PT62			T2	7,01	AL62
		PT63			T3	10,5	
M31	B6&C3H	PT64	8	17	S	0,3	
M32	B6	PT65	15	6	S	20,3	
		PT66			T1	1,04	
		PT67			T2	8,03	
M33	B6	PT68	15	6	T1	47,9	
		PT69			T2	17,4	

		PT70			T3	4,69	
Mouse Code	Mice backgroud	Primary code	Post Den time	DEN		Lgr5 expression	Allograft strains
M34	B6	PT71	15	6	S	17,4	
		PT72			T1	3,86	
		PT73			T2	21,6	
M35	B6	PT74	15	6	S	0,22	
M36	B6	PT75	15	6	S	0,25	
		PT76			T	3,41	
M37	B6	PT77	15	6	T1	1,41	
		PT78			T2	0,23	
		PT79			T3	0,65	
M38	B6&C3H	PT80	8	17	S	0,26	
		PT81			T	0,14	
M39	B6	PT82	13	6	T1	0,29	
		PT83			T2	5,13	
		PT84			T3	0,18	AL84
		PT85			T4	8.90	AL85
M40	B6&C3H	PT86	7	17	T1	14,6	
		PT87			T2	6,82	
		PT88			T3	13,9	
M41	B6&C3H	PT89	8	17	S	0,21	

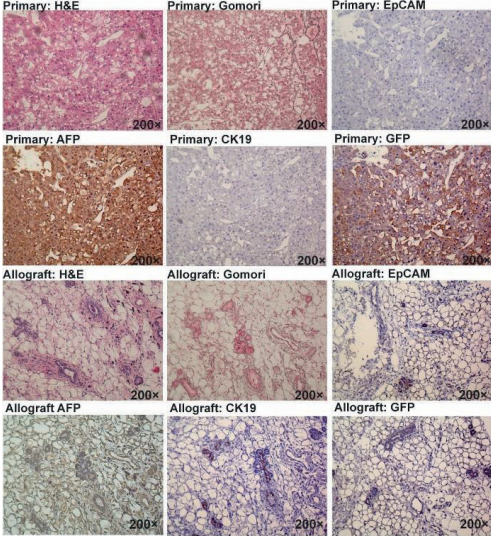
Group Code	Group	Tissue Number	Lgr5 Expression
A	The collected mice liver tissue	89	5.583%
B	The mice liver which did not initiate tumor	8	0.325%
C	Tumor surrounding tissue	34	2.930%
D	Tumor tissue	55	7.294%

[2] Supplementary Data 2

Content:

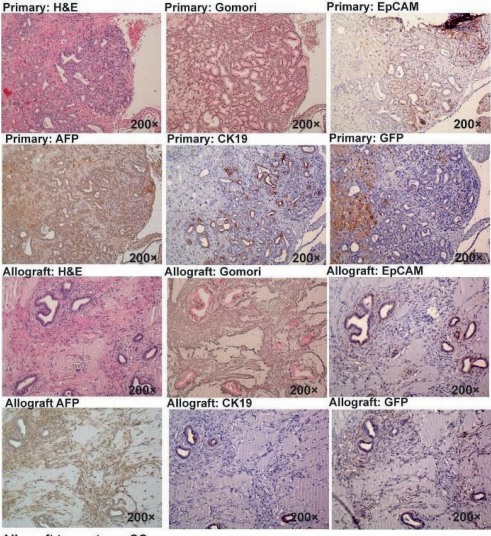
The H&E/Gomori/EpCAM/AFP/CK19/GFP staining of primary/allograft tissues for all the allograft strains.

AL62



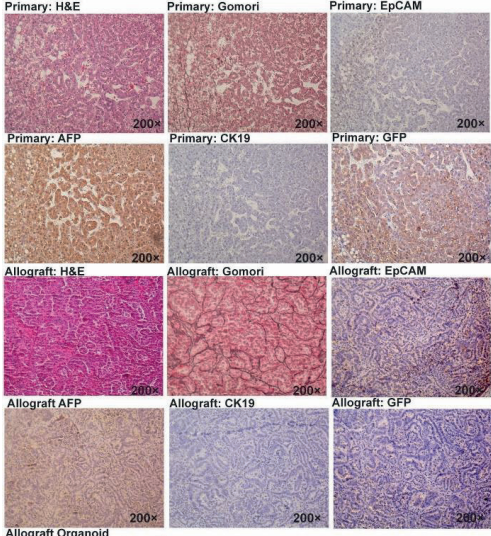
Allograft tumor type: unclear
Strain lost due to stop proliferation ex vivo

AL84

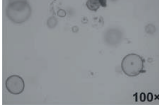


Allograft tumor type: CC
Strain lost due to stop proliferation ex vivo

AL61

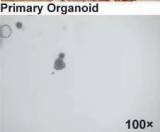
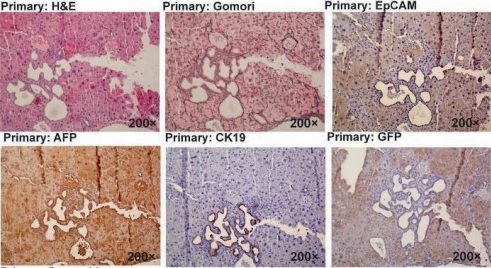


Allograft Organoid

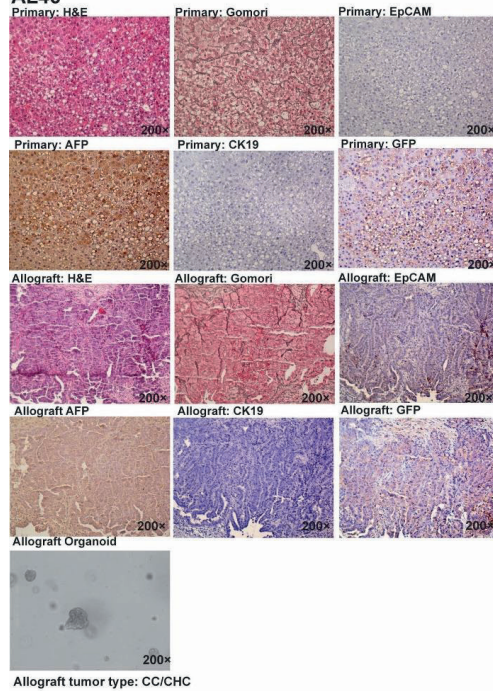
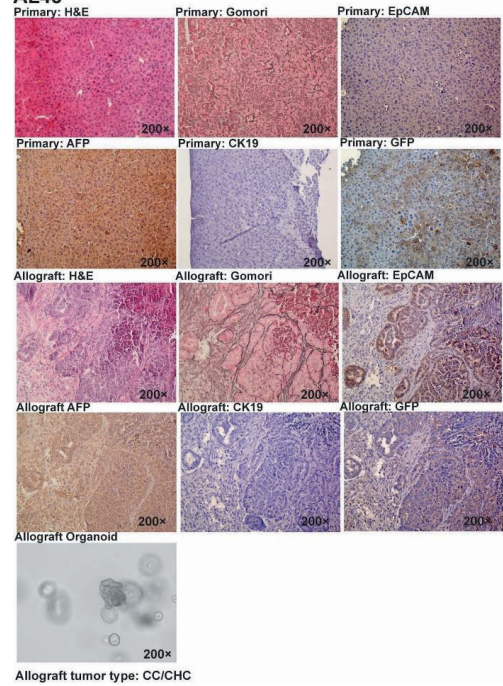
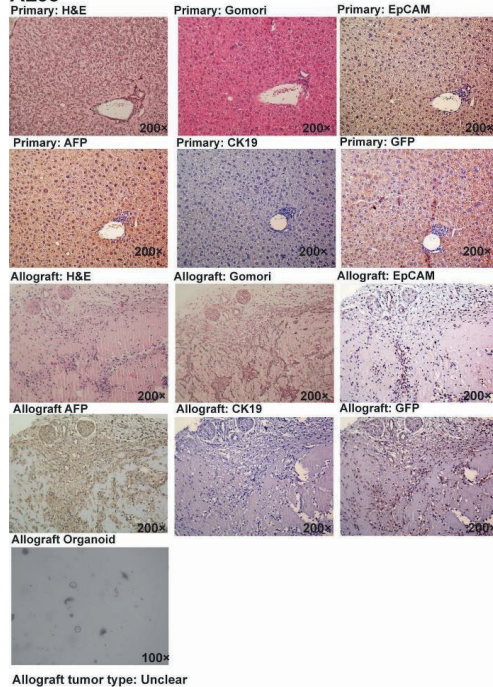
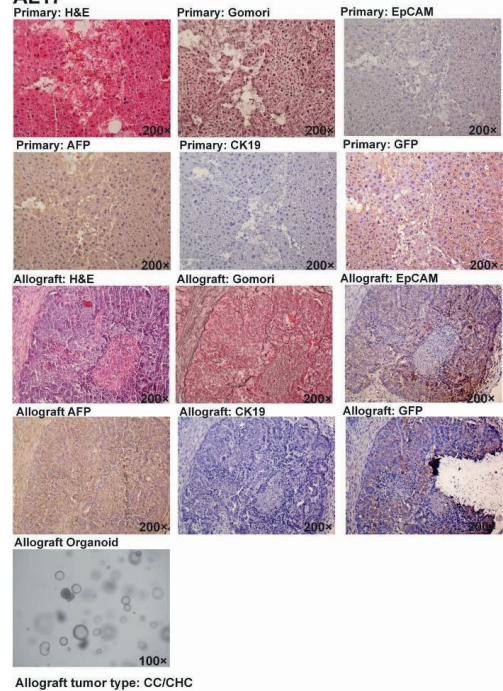


Allograft tumor type: CC/CHC

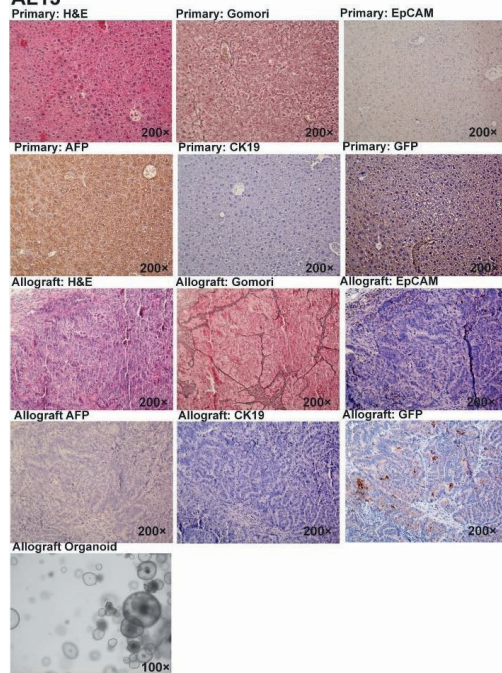
AL85



Allograft tumor type: Unclear
Strain lost due to stop proliferation ex vivo

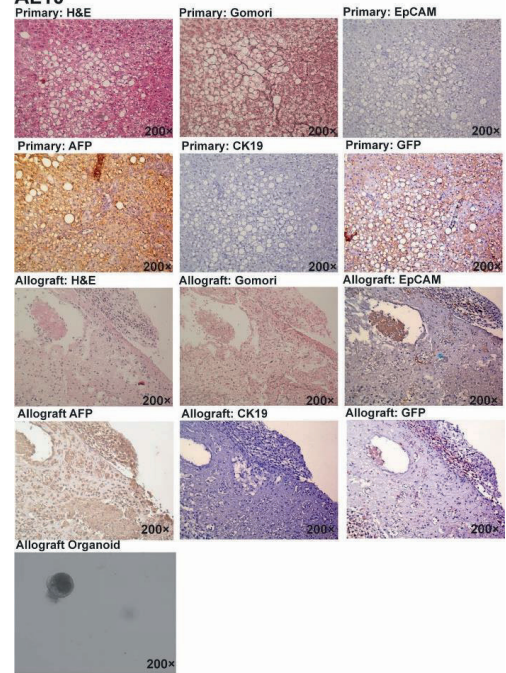
AL46**AL43****AL38****AL17**

AL13



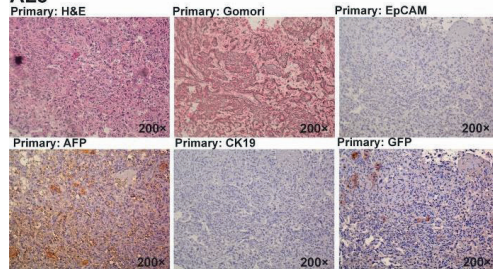
Allograft tumor type: CC/CHC

AL10



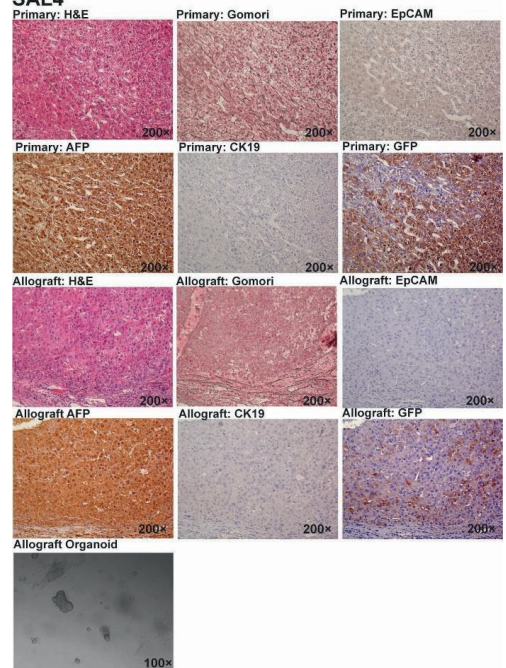
Allograft tumor type: Unclear

AL8



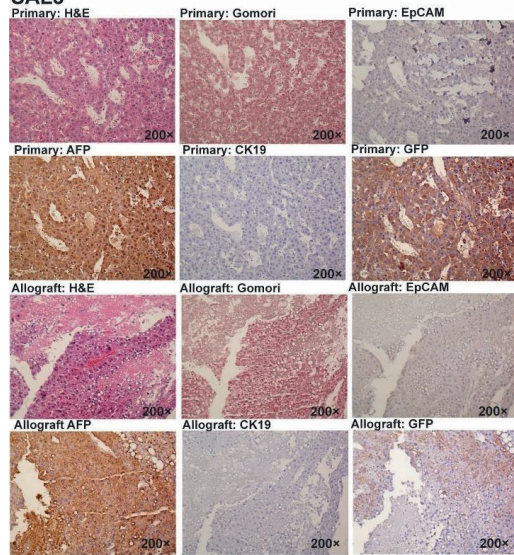
Allograft tumor type: Unclear
Strain lost due to stop proliferation ex vivo

SAL4



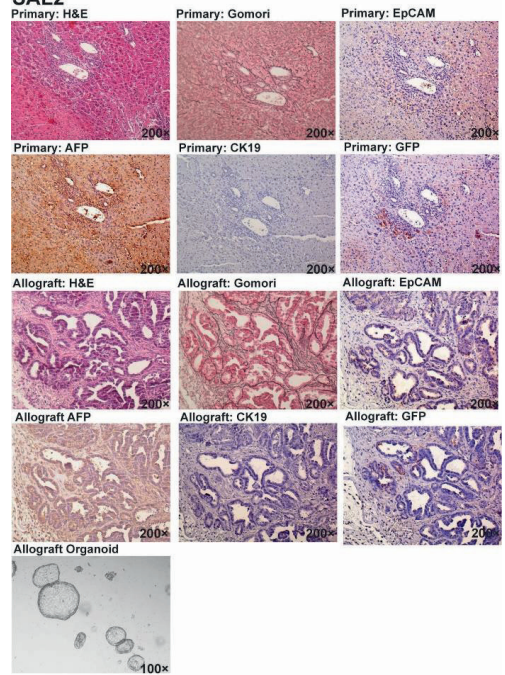
Allograft tumor type: HCC

SAL3



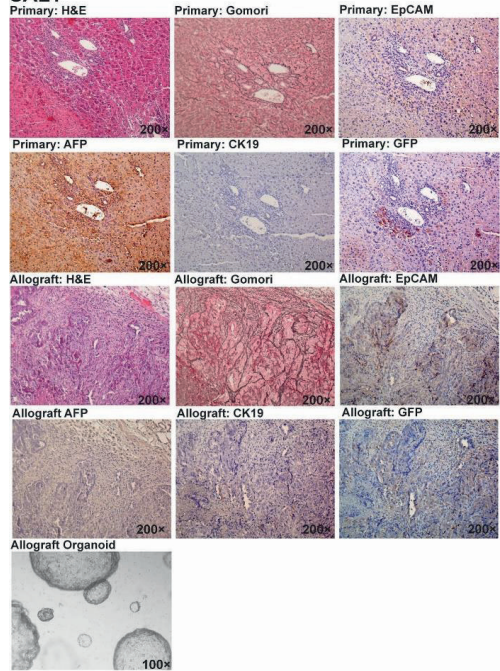
Allograft tumor type: HCC
Strain lost due to stop proliferation ex vivo

SAL2



Allograft tumor type: CC/CHC

SAL1



Allograft tumor type: CC/CHC

[3] Supplementary Data 3

Content:

Gene enrichment analysis of the differentially expressed genes between Untreated LGR5+ Vs. LGR5-, 5-FU-treated LGR5+ Vs. LGR5-, 5-FU-treated Vs. Untreated LGR5+ and 5-FU-treated Vs. Untreated LGR5- cells.

Treated LGR5+ Vs. LGR5-	
Pathway	Genes
Matrix Metalloproteinases WP441	MMP12;MMP9;MMP21
Glucocorticoid & Mineralcorticoid Metabolism WP495	HSD11B2;CYP21A1
Microglia Pathogen Phagocytosis Pathway WP3626	C1QA;FCER1G;NCF1
Striated Muscle Contraction WP216	TPM2;TCAP;TNNI3
Inflammatory Response Pathway WP458	COL1A1;CD28
Prostaglandin Synthesis and Regulation WP374	HSD11B2;ANXA8
Irinotecan Pathway WP475	UGT1A1
Osteoblast WP238	COL1A1
Estrogen metabolism WP1264	UGT1A1
Heart Development WP2067	HEY1;VEGFC
Calcium Regulation in the Cardiac Cell WP553	PRKCG;KCNB1;GJB6;ATP1B2;ADRB2
Glucuronidation WP1241	UGT1A1
Complement Activation, Classical Pathway WP200	C1QA
Eicosanoid Synthesis WP318	LTC4S
Hedgehog Signaling Pathway WP116	HHIP
GPCRs, Class B Secretin-like WP456	ADGRE1
Signal Transduction of S1P Receptor WP57	S1PR5
Spinal Cord Injury WP2432	MMP12;OMG;MMP9
Endochondral Ossification WP1270	COL10A1;MMP9
Dysregulated miRNA Targeting in Insulin/PI3K-AKT Signaling WP3855	COL1A1
Oxidative Stress WP412	UGT1A1
One Carbon Metabolism WP435	FOLH1
Peptide GPCRs WP234	CXCR3;CCR9
Eicosanoid metabolism via Lipo Oxygenases (LOX) WP4348	LTC4S
Monoamine GPCRs WP570	ADRB2
Retinol metabolism WP1259	NPC1L1
Parkinsons Disease Pathway WP3638	SNCAIP
Oxidation by Cytochrome P450 WP1274	CYP21A1
Oxidative Damage WP1496	C1QA
Non-odorant GPCRs WP1396	ADGRE1;CXCR3;CCR9;KISS1R;ADRB2;S1PR5
Metapathway biotransformation WP1251	UGT1A1;CYP21A1;HS3ST5
Wnt Signaling Pathway and Pluripotency WP723	PRKCG;HNF1A
Chemokine signaling pathway WP2292	NCF1;CXCR3;CCR9;PPBP
Wnt Signaling Pathway WP403	PRKCG
Lung fibrosis WP3632	MMP9
Complement and Coagulation Cascades WP449	C1QA
Alpha6-Beta4 Integrin Signaling Pathway WP488	COL17A1
GPCRs, Class A Rhodopsin-like WP189	GPR12;CXCR3;CCR9;ADRB2
Focal Adhesion WP85	COL1A1;VEGFC;THBS2
Adipogenesis genes WP447	PNPLA3;HNF1A
IL-2 Signaling Pathway WP450	CD53
Delta-Notch Signaling Pathway WP265	HEY1
GPCRs, Other WP41	ADRB2;S1PR5
Cytoplasmic Ribosomal Proteins WP163	RPL24
G Protein Signaling Pathways WP232	PRKCG
Amino Acid metabolism WP662	TAT
IL-6 signaling Pathway WP387	HNF1A
IL-3 Signaling Pathway WP373	MMP9
Neural Crest Differentiation WP2074	SNAI2
ESC Pluripotency Pathways WP339	HNF1A
Odorant GPCRs WP1397	GPR12;GPR61
Focal Adhesion-PI3K-Akt-mTOR-signaling pathway WP2841	COL1A1;ANGPT2;VEGFC;THBS2
Myometrial Relaxation and Contraction Pathways WP385	PRKCG
MAPK signaling pathway WP493	PRKCG
EGFR1 Signaling Pathway WP572	GM12260
PluriNetWork WP1763	PRKCG

Untreated LGR5+ Vs. LGR5-	
Pathway	Genes
Peptide GPCRs WP234	FPR1;SSTR1;TSHR
Myometrial Relaxation and Contraction Pathways WP385	MYL4;RGS5;ADCY4;RLN1
Macrophage markers WP2271	LYZ2
Matrix Metalloproteinases WP441	MMP8
Dopaminergic Neurogenesis WP1498	PITX3
Non-odorant GPCRs WP1396	FPR1;SSTR1;TSHR;CELSR3
Oxidation by Cytochrome P450 WP1274	CYP4X1
Striated Muscle Contraction WP216	MYL4
GPCRs, Class A Rhodopsin-like WP189	FPR1;SSTR1;TSHR
Metapathway biotransformation WP1251	CYP4X1;FMO2
Calcium Regulation in the Cardiac Cell WP553	RGS5;ADCY4
TYROBP Causal Network WP3625	HLX
Lung fibrosis WP3632	CMA1
Kit Receptor Signaling Pathway WP407	FGR
Purine metabolism WP2185	PNP2;ADCY4
PPAR signaling pathway WP2316	FABP2
Chemokine signaling pathway WP2292	FGR;ADCY4
G Protein Signaling Pathways WP232	ADCY4
Wnt Signaling Pathway and Pluripotency WP723	NKD2
IL-6 signaling Pathway WP387	FGR
GPCRs, Other WP41	CELSR3
Focal Adhesion WP85	FGR

[4] Supplementary Data 4

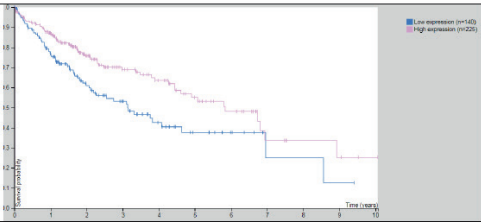
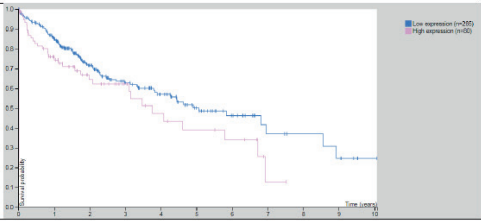
Content:

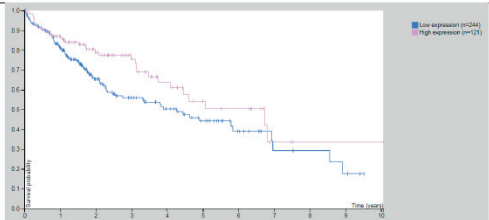
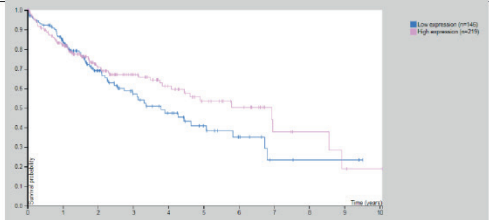
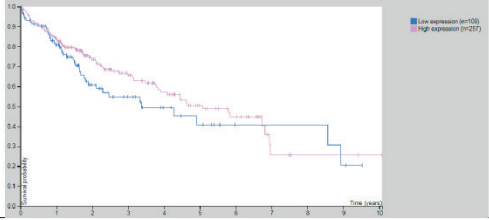
Gene: The differentially expressed genes between untreated LGR5+ cells and LGR5- cells.

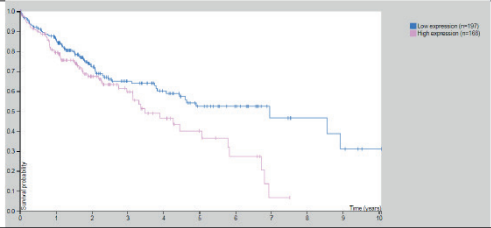
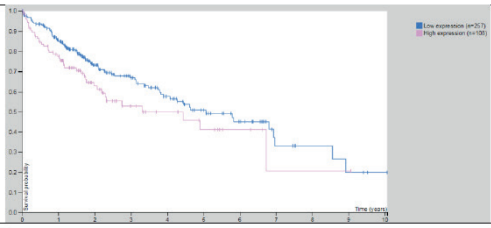
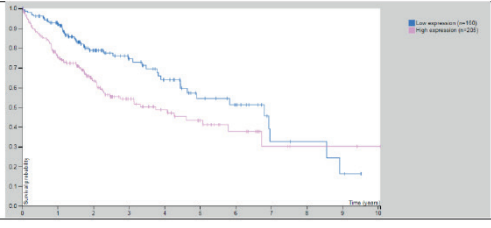
Gene description: The gene description.

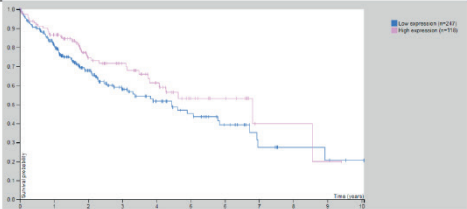
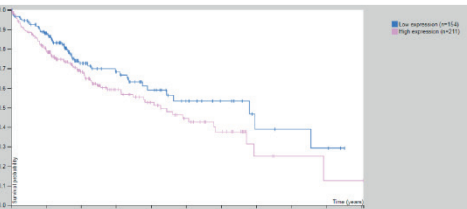
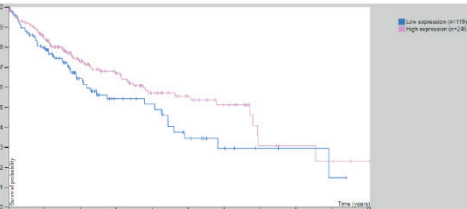
Survival Analyses: Online database (The Human Protein Atlas, <http://www.proteinatlas.org/>).

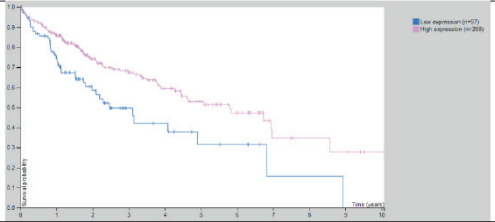
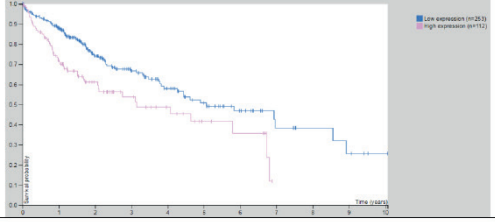
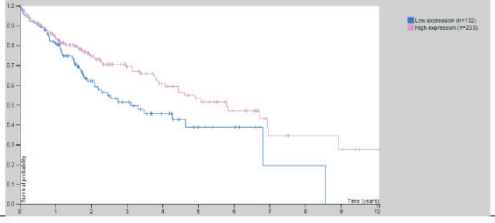
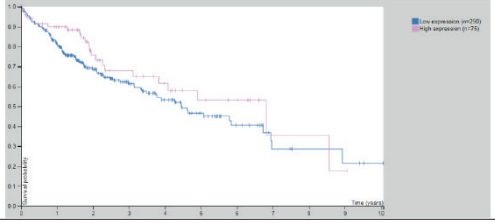
P value for Survival Analyses: Online database (The Human Protein Atlas, <http://www.proteinatlas.org/>).

Untreated LGR5+ vs. LGR5-			
Upregulated Gene	Gene description	Survival Analyses	P value for Survival Analyses
Gm11042			
AL589879.2			
1700003G13Rik			
Snord93			
Gm24325			
Gm8326			
Taf7l	TATA-box binding protein associated factor 7 like		0.0039
Gm11977			
Gm24328			
Gm15558			
B230112G18Rik			
Gm42586			
Rpl36-ps7			
2210017I01Rik			
Gm43058			
Gm38321			
4833428L15Rik			
Tm6sf1	Transmembrane 6 superfamily member 1		0.065
Gm18014			
Zfp572	Zfp572 zinc finger protein 572		
Kcnk4	Potassium two pore domain channel subfamily K member 4		

Spn	Sialophorin		0.040
Smtnl1	Smoothelin like 1		0.22
Gm12320			
Gm6976			
Gm24769			
Oas1h			
Tnfsfm13	tumor necrosis factor (ligand) superfamily, membrane-bound member 13		
Gm12227			
Gm12196			
Gm6568			
Gm15862			
Pitx3	Paired like homeodomain 3		
Rln1	Relaxin 1		
Fpr1	Formyl peptide receptor 1		0.20
4933429H19Rik			
RP24-530N5.5			
Gm26899			
Ube4bos3			
Gm25445			
4933402D24Rik			
Mmp8	Matrix		

	metallopeptidase 8		
2300005B03Rik			
Fabp2	Fatty acid binding protein 2		
4930562D21Rik			
Gm38058			
Sox2	SRY-box 2		0.018
Gm4795			
Gm12043			
Dsg4	membrane proteins		0.056
Gm15780			
Pnp2	Purine nucleoside phosphorylase		
Mcpt8	mast cell protease 8		
Nid1	Nidogen-1		0.0024
Tshr	Thyroid stimulating hormone receptor		
Dnajb8	DnaJ heat shock protein family (Hsp40) member B8		
Nlrp4c	NACHT, LRR and PYD domains-containing protein 4C		
Gm10392			
Sstr1	Somatostatin		

	receptor 1		
Gm13578			
Gm14822			
Erich5	Glutamate rich 5		0.087
Gm18301			
6430571L13Rik			
Gm11465			
Gm15982			
Nkd2	Naked cuticle homolog 2		
Myl4	Myosin light chain 4		
Gm15964			
Gm42807			
Gm9765			
Gm16177			
Khlh3	Kelch like family member 3		0.062
1700031P21Rik			
Gm24336			
Palm3	Paralemmin 3		0.047
Gm14019			
Gm13110			
Gm42682			
Slc16a9	Solute carrier family 16 member 9		

Ambp	Alpha-1-microglobulin/bikunin precursor		0.001
Gm37229			
Gm11764			
3110035E14Rik			
Gm6526			
Gm10030			
Mboat4	Membrane bound O-acyltransferase domain containing 4		0.0019
Gm14379			
Cma1	Chymase 1		0.015
1600002D24Rik			
Gm5093			
Cd300lg	CD300 molecule like family member g		
Rab37	RAB37, member RAS oncogene family		0.17
Gm28177			
Gm42500			
Hlx	H2.0 like homeobox		
Gm6226			
Gm37933			
Rai2	Retinoic acid induced 2		
Gm20056			
RP24-83C9.5			
Lyz2	Lysozyme C-2		
1700003M07Rik			
Gm5909			
Gm27033			
Gm13448			
Npm3-ps1			

[5] Supplementary Data 5

Content:

The detailed information for single cells isolated from DEN induced murine livers and allograft tumors, then used for organoid initiation, including:

- 1) Code: The corresponding tissues of DEN induced murine livers or allograft tumors. Green mark: the groups did initiate organoids after sorting.
- 2) Initiated organoid number for each group.
- 3) Organoid initiated efficiency (%) for each group.

Remarks: In total 89 tissues were collected. Among them, 71 tissues were sorted for following single cell initiation; 18 tissues were failed for the sort due to FACS machine issue or other technical reasons.

Primary Tissue						
Relative Organoid strain	Isolated LGR5 ⁺ cell number	Initiated organoid number	Organoid initiated efficiency (%)	Isolated LGR5 ⁻ cell number	Initiated organoid number	Organoid initiated efficiency (%)
PT1	0	0	0	1	0	0
PT2	1	0	0	7	0	0
PT3	10	1	10	17	0	0
PT11	307	0	0	8124	0	0
PT12	787	2	0.25	39066	20	0.05
PT13	24	0	0	332457	0	0
PT14	140	0	0	44901	0	0
PT15	58	0	0	186498	0	0
PT16	49	0	0	21632	0	0
PT17	59	0	0	221656	0	0
PT18	51	0	0	185640	0	0
PT19	81	0	0	8985	0	0
PT20	379	1	0.26	26090	75	0.29
PT21	611	1	0.16	13775	39	0.28
PT22	20	0	0	475	0	0
PT23	322	0	0	27748	0	0
PT24	3	0	0	8951	0	0
PT26	32	0	0	87	0	0
PT27	17	0	0	19104	30	0.16
PT28	17	0	0	8643	3	0.035
PT29	62	0	0	10809	22	0.20

PT30	124	0	0	6680	5	0.075
PT31	140	0	0	2692	0	0
PT32	41	0	0	6430	0	0
PT33	141	0	0	23853	10	0.042
PT34	36	0	0	2355	0	0
PT35	540	0	0	26689	0	0
PT36	265	0	0	86774	0	0
PT37	109	0	0	90979	0	0
PT38	1253	10	8.00	131695	0	0
PT39	1073	0	0	250982	0	0
PT40	115	0	0	1329	0	0
PT41	20	0	0	1464	0	0
PT42	181	0	0	1193	0	0
PT43	131	0	0	5998	0	0
PT44	71	0	0	76	0	0
PT45	740	3	0.41	1348	0	0
PT46	22	0	0	1485	0	0
PT47	2304	5	0.22	5356	0	0
PT48	845	1	0.12	859	0	0
PT49	482	1	0.21	418	1	0.24
PT50	385	2	0.52	444	0	0
PT51	140	5	3.57	189	1	0.53
PT52	12	0	0	594	0	0
PT53	1	0	0	180	0	0
PT54	6062	50	0.82	5767	0	0
PT55	407	0	0	2121	0	0
PT56	2282	364	16.0	3841	2	0.05
PT57	288	3	1.04	960	0	0
PT58	120	0	0	1613	0	0
PT59	821	23	2.8	758	0	0
PT60	30	0	0	1299	0	0
PT61	1879	0	0	2242	0	0
PT62	2881	10	3.5	4514	0	0
PT63	3510	27	7.7	1262	0	0
PT64	6	0	0	16	0	0
PT65	340	0	0	281	0	0
PT66	1425	0	0	1222	0	0
PT67	4404	3	0.00068	1026	0	0
PT68	9386	25	2.7	5129	0	0
PT69	93	0	0	128	0	0
PT70	1694	10	0.59	728	0	0
PT71	1526	14	0.92	1792	0	0
PT72	4482	6	0.13	4482	0	0

PT73	1101	4	0.36	1097	0	0
PT80	103	0	0	729	0	0
PT81	58	0	0	51	0	0
PT82	129	0	0	37	0	0
PT83	627	14	2.23	616	0	0
PT84	31	0	0	18	0	0
PT85	652	8	1.2	784	0	0

Allograft Tissue						
Relative Organoid strain	Isolated LGR5 ⁺ cell number	Initiated organoid number	Organoid initiated efficiency (%)	Isolated LGR5 ⁻ cell number	Initiated organoid number	Organoid initiated efficiency (%)
AL17	70	64	91.4	513	46	9,0
AL13	1026	233	22.7	663	5	0,8
SAL1	7	7	100	38	7	18,4
AL43	39	15	38.5	54	18	33,3
AL46	13	5	38.5	1	0	0,0
AL13.1	1646	180	10.9	1373	176	12,8
AL17.2	21	11	52.4	366	11	3,0
AL8.1	62	17	27.4	100	3	3,0
AL8.2	107	12	11.2	181	7	3,9
AL8.3	138	16	11.6	178	0	0,0

[6] Supplementary Data 6

Content:

The detailed information for single cells isolated from DEN induced murine livers, then injected directly into immunodeficient mice for tumor formation, including:

1)Code: The corresponding tissues of DEN induced murine livers and initiated allograft tumors.








Green mark: the groups did initiate tumors after sorting.

2) Injected cell number for each group.

3) Pictures of primary tumors and corresponding allograft tumors.

	Tissue Code	Injected Cell Type	Injected Cell Number	Tumor initiation
1	PT47	LGR5 ⁺ cells	3000	no
		LGR5 ⁻ cells	3000	no
2	PT50	LGR5 ⁺ cells	2000	SAL1
		LGR5 ⁻ cells	2000	SAL2
3	PT63	LGR5 ⁺ cells	2000	SAL3
		LGR5 ⁻ cells	2000	no
4	PT65	LGR5 ⁺ cells	6000	no
		LGR5 ⁻ cells	6000	no
5	PT67	LGR5 ⁺ cells	1000	no
		LGR5 ⁻ cells	1000	no
6	PT68	LGR5 ⁺ cells	16000	SAL4
		LGR5 ⁻ cells	16000	no
7	PT72	LGR5 ⁺ cells	5000	no
		LGR5 ⁻ cells	5000	no
8	PT73	LGR5 ⁺ cells	1000	no

		LGR5 ⁻ cells	1000	no
9	PT85	LGR5 ⁺ cells	3000	no
		LGR5 ⁻ cells	3000	no

Tissue code	Primary tumor	Allograft Tumor
SAL1		
SAL2		
SAL3	Picture lacking	
SAL4		

CHAPTER 7

Pregnane X Receptor Activation Constrains Mucosal NF- κ B Activity in Active Inflammatory Bowel Disease

J. Jasper Deuring¹, Meng Li¹, Wanlu Cao¹, Sunrui Chen¹, Wenshi Wang¹, Colin de Haar¹, C. Janneke van der Woude¹, Maikel Peppelenbosch¹

¹ Department of Gastroenterology and Hepatology, Erasmus MC-University Medical Center, Rotterdam, The Netherlands

PLoS One. 2019; 14(10): e0221924.

Introduction

Background: The Pregnane X Receptor (PXR) is a principal signal transducer in mucosal responses to xenobiotic stress. It is well-recognized that inflammatory bowel disease is accompanied by xenobiotic stress, but the importance of the PXR in limiting inflammatory responses in inflammatory bowel disease remains obscure at best.

Methods: We stimulate a total of 106 colonic biopsies from 19 Crohn's disease patients with active disease, 36 colonic biopsies from 8 control patients, colonic organoids and various cell culture models (either proficient or genetically deficient with respect to PXR) *in vitro* with the PXR ligand rifampicin or vehicle. Effects on NF- κ B activity are assessed by measuring interleukin-8 (IL-8) and interleukin-1 β (IL-1 β) mRNA levels by qPCR and in cell culture models by NF- κ B reporter-driven luciferase activity and Western blot for signal transduction elements.

Results: We observe a strict inverse correlation between colonic epithelial PXR levels and NF- κ B target gene expression in colonic biopsies from Crohn's disease patients. PXR, activated by rifampicin, is rate-limiting for mucosal NF- κ B activation in IBD. The correlation between colonic epithelial PXR levels and NF- κ B target gene expression was also observed in intestinal organoids system. Furthermore, in preclinical *in vitro* models of intestinal inflammation, including intestinal organoids, genetic inactivation of PXR unleashes NF- κ B-dependent signal transduction whereas conversely NF- κ B signaling reduces levels of PXR expression.

Conclusions: Our data indicate that the PXR is a major and clinically relevant antagonist of NF- κ B activity in the intestinal epithelial compartment during inflammatory bowel disease.

Introduction

Intestinal epithelial cells (IEC) form the physical barrier between the gut content and the *milieu interieur* and perform a multitude of functions in cellular physiology including absorption of nutrients and water but also constitute a first line of defense against pathogenic and xenobiotic challenge to the body [1, 2]. The interaction between IEC functionality in innate immunity and xenobiotic detoxification remains largely obscure but is likely relevant in pathophysiology as pathogenic and xenobiotic stress often occurs concomitantly in the intestine [3], and breakdown of barrier function by specific epithelial subtypes underpins inflammatory bowel disease (IBD) [4]. Xenobiotics are often the result of metabolism by specific bacteria, which fits well with the insight that altered microbial composition is linked to the clinical course of IBD [5] as well as reaction to therapy [6]. Various receptor systems are involved in the detection by IEC of xenobiotic components present in the in the intestinal lumen, in particular the plasma membrane-localized G-protein-coupled receptors GPR41, GPR43, and GPR109A and the nucleus-localized receptors aryl hydrocarbon receptor, farnesoid X receptor and pregnane X receptor (PXR) [7]. With respect to the nuclear receptors, the aryl hydrocarbon receptors protects stem cells against challenge to their genome by genotoxic compounds through stimulating the production of interleukin 22 by lymphocytes [8] from the diet, whereas generally speaking this receptor has a regulatory influence on immunity through Src-mediated stimulation of indoleamine 2,3-dioxygenase 1 [9], an enzyme that is a key element in relay pathway between arginine and tryptophan metabolism that mediates immunosuppression [10]. For other xenobiotic-sensing nuclear receptors in general and PXR in particular, their potential functionality in limiting intestinal inflammation is less clear-cut.

Intriguingly, however, the PXR locus is associated with susceptibility to IBD, suggesting that this receptor is clinically relevant in constraining in intestinal inflammation [11, 12]. In apparent agreement, stimulating PXR in rodents during experimental colitis ameliorates inflammation and reduces disease [13-17]. Mechanistically these effects may relate to intestinal NF- κ B activation. NF- κ B is a master regulator of inflammatory responses of the genome [18] and its importance for the pathogenesis for inflammatory bowel disease is undisputed [19]. Importantly PXR deficient mice display more severe NF- κ B-driven small intestinal inflammation than their non-mutant littermates [20] whereas effects of PXR activation in experimental colitis also correlate to NF- κ B activation [21]. It thus rational to propose that also in human disease, PXR activation constrains NF- κ B activation and IBD. The functionality, however of PXR activation in clinical inflammatory bowel disease and its relation to NF- κ B activation remains, however, largely unexplored.

Prompted by the above-mentioned considerations we decided to explore the role of PXR activation in human IECs and clinical IBD. Our study shows that PXR activity is the major rate-limiting pathway constraining mucosal NF- κ B activity in active IBD and provides insight into PXR signals, which are much more important in pathology than previously thought.

Furthermore, our results imply that modulation of PXR activity holds significant clinical promise in the management of IBD.

Materials and methods

Cell lines

All cell lines were originally obtained from the ATTC. Human colorectal adenocarcinoma cell lines CACO2 and LS174t and hepatocellular carcinoma cell lines Huh7 were cultured in Dulbecco's modified Eagle's medium from Invitrogen-Gibco, complemented with 10% fetal calf serum, 100 IU/ml penicillin and 100 ug/ml streptomycin according to routine procedures [22]. Cell lines were used to investigate the function of PXR expression. All cell lines needed to passage twice a week and were cultured according standard culture conditions.

Gene knockdown

To study the NF- κ B inhibiting potential of PXR activation, a PXR knockdown LS174t cell was created to test the specificity of PXR. The LS174t cell line was transduced with the lenti-virus, containing small interference RNA for PXR (siPXR), similarly as described before [23]. The transduced cells were cultured with 100 uM puromycin (Sigma-Aldrich) for three weeks to select for cells that harbor the siPXR.

Reagents

NF- κ B was in-vitro activated by 2 μ l *E. coli* lysate (ELI), a centrifuged 50 ml o/n *E. coli* (DH5 α , Invitrogen) culture taken up in 500 ul dH₂O. PXR was activated by 100 μ M Rifampicin (Sigma-Aldrich). Recombinant human TNF α (Perotech, USA) was dissolved in phosphate-buffered saline in stock solution of 100 μ g/ml.

Biopsies

This study was conducted with approval of the Ethic committee of the Erasmus MC University Medical Center in Rotterdam. All patients gave written informed consent. During endoscopy biopsies were taken from patients with a known history at least 6 months of CD and from patients referred for colonoscopy but without intestinal abnormalities, further described as control patients. Also patients were asked for additional blood samples. CD was diagnosed according to international guidelines and only the results of the control biopsies were used if there were no abnormalities on pathology, when there was no history of IBD, and no familiar history of IBD. For each patient the biopsies were taken from the ascending colon ($n=3$), the transversum ($n=3$) and the descending colon ($n=3$).

Culture of human intestinal organoids

Human intestinal organoids were cultured as described previously [24]. Briefly, intestinal tissues were re-suspended in advanced DMEM/F12 (supplemented with 1% GlutaMAX™ Supplement, 10 mM HEPES) with growth factors, and collected by centrifugation. Crypts were finally suspended in Matrigel (Corning, Bedford, USA), and placed 40 µL/well in a 24-well plate. Organoids were cultured in expansion medium after the Matrigel had solidified. Organoid expansion medium was refreshed every 2–3 days, and organoids were passaged every week.

Histology

One biopsy from each location was fixed in 4% formaldehyde solution, dehydrated and embedded in paraffin for histological scoring. Four microM slices from the formalin fixed paraffin embedded (FFPE) tissue specimens were stained with hematoxylin and eosin (Sigma-Aldrich) according to previously described procedures [25]. Three observers have independently examined each biopsy, in a blinded fashion. Discrepancies were reassessed to reach agreement.

Stimulation of the biopsies

The freshly taken biopsies were immediately placed in ice-cold regular culture medium (DMEM) for transport. Before stimulating the biopsies, they were washed three times with ice-cold PBS containing antibiotics to prevent infection. The biopsies were then stimulated for 18 h at 37 °C with 100 µM Rifampicin (Sigma-Aldrich) or solvent. Stimulated biopsies were directly lysed in Tripure (Roche, Switzerland) for RNA and protein extraction, according to the manufacturer's protocol. After the Tripure extraction, the RNA samples were purified using the RNA II extract kit from Macherey Nagel (Bioke) according to the manufacturer's protocol.

Peripheral blood mononuclear cells

Peripheral blood mononuclear cells (PBMC) were isolated from fresh blood using Ficoll (Gibco) according standard procedures. The isolated PBMC were stimulated with 100 µM Rifampicin for 18 h at 37 °C followed by lysing of the PBMC in Tripure (Roche) for RNA isolation.

Quantitative Real-Time Polymerase Chain Reaction (PCR)

Gene expression of GapdH, Ywaz, IL-8, IL-1 , CYP3A4, Sult1a, and PXR were measured via quantitative real-time PCR with the StepOne Real-Time PCR system and the StepOne v2.0 software (Applied biosystem, Darmstadt, Germany). The primer sequences are shown in **Supplementary Table 1**. All genes were analysed using the same qPCR program as described before [26]. Gene expression is plotted as fold change using the deltaCt method [27]. The data from patients with multiple colonic biopsies were averaged.

Luciferase activity measurement of CACO2-based NF-κB luciferase reporter cell lines

Luciferase reporter cells were created by transducing cells with lentiviral vectors expressing the firefly luciferase gene under the control of the NF-κB promoters. The luciferase activity

was measured with a LumiStar Optima luminescence counter (BMG Lab Tech, Offenburg, Germany). The cells were cultured and measured as described previously [28, 29].

Protein analysis

The p-p65 (catalogue no. 3037, Cell Signaling Technology) and p-Akt (catalogue no. 11055-2, Signalway Antibody) protein expression was measured using conventional Western blot as described before [30]. The IL-8 protein expression in the protein solution isolated from the TriPure fraction was measured using ELISA [31], Human IL-8 ELISA Ready-SET-Go! (eBioscience). Immunohistochemistry for NF- κ B target genes was performed as described earlier [32].

Statistics and software

All the graphs and the statistical analyses were performed using the Graphad Prism 5.0 software package for Windows. Data from the paired biopsies were non-parametric statistically analyzed using the Wilcoxon matched pairs test. Correlations were determined using the Spearman's rank correlation coefficient. A two-tailed *P* value <0.05 was accepted as statistically significant. Images were composed using Adobe Photoshop CS5.

Ethical statement

The work has been approved by the Medical Ethical Committee of the Erasmus Medical Center (Medisch Ethische Toetsings Commissie Erasmus MC), and that subjects gave informed consent to the work.

Results

PXR activation is rate-limiting for mucosal NF- κ B activation in IBD

To investigate the effects of PXR stimulation on mucosal NF- κ B activation, we decided to contrast the effect of the canonical PXR ligand rifampicin [33] to solvent control on NF- κ B target gene levels in colonic biopsies. For this experimentation we obtained 106 biopsies from 19 CD patients and 36 biopsies from 8 controls. Demographic patient characteristics are presented in **Supplementary Table 2**. Five additional patients with quiescent CD and 4 controls agreed to donate blood samples. We concluded that this set of patient materials should allow us to make meaningful statements on potential effects of PXR stimulation on mucosal NF- κ B activation.

The expression of the NF- κ B target genes *IL-8* and *IL-1 β* has been shown previously to represent a valid reflection of NF- κ B-mediated transcriptional activity [34]. Indeed, when non-stimulated biopsies were investigated for the mRNA levels of these cytokines we observed that expression of either *IL-8* and *IL-1 β* mRNA levels (**Figs 1A** and **1B**, respectively) or IL-8 protein levels (**Figs 1C** and **1D**, respectively) were markedly higher in biopsies of patients with active inflammation when compared to biopsies from controls or CD patients with quiescent disease. Thus we decided to use expression levels of these two cytokines as a surrogate measure for assessing the effect of PXR stimulation on mucosal inflammation. Importantly, challenge of biopsies with Rifampicin did not significantly reduce the *IL-8* or *IL-1 β* mRNA expression in the biopsies from control and quiescent CD patients (**Figs 1A** and **1B**), indicating that outside the context of active IBD, PXR activity is not a rate-limiting factor with respect to NF- κ B-directed gene expression. However, Rifampicin stimulation caused a 35 fold reduction of *IL-1 β* mRNA expression in the biopsies with active inflammation ($p < 0.01$, **Fig 1B**). Thus PXR stimulation can constrain inflammatory gene expression in active IBD but does not affect constitutive levels of inflammatory cytokines in quiescent IBD or in the colonic mucosa of non-IBD individuals.

PXR activation limits NF- κ B activation in the epithelial compartment

Intestinal PXR expression is especially prominent in the epithelium and is less evident in the stromal and immunological compartment, suggesting that the effects observed following rifampicin stimulation relate to the epithelial compartment [35]. Nevertheless, since the biopsies, especially those of patients with active CD, contain a large number of lymphocytes we wanted to determine if these cells contribute to the observed PXR-mediated reduction of NF- κ B signaling. Therefore, we investigated the effect of Rifampicin on PBMC isolated from blood. No PXR mRNA were detected in any of the PBMC fractions. Rifampicin stimulation does not influence the *IL-8* mRNA expression in PBMC from controls and CD patients (**Supplementary Fig 1A**). Furthermore the expression of PXR target gene *Sult1a* is not altered (**Supplementary Fig 1B**). Hence, mononuclear cells such as stromal cells do not seem to be important in the PXR-mediated inhibition of NF- κ B in human intestinal biopsies. This notion

was confirmed in experiments in which we tested the effects of rifampicin in TNF α -stimulated human colonic organoids, which are devoid of non-epithelial components. In apparent agreement with the intestinal epithelium being an important mediator of PXR effects, we observed marked reduction of *IL-8* and *IL-1 β* mRNA levels following Rifampicin treatment, whereas such effects were much less pronounced in intestinal organoids not stimulated by TNF α (**Figs 1E and 1F**). In the context of IBD, the organoid derived from the inflamed tissue show similar cytokines expression pattern with Rifampicin treatment (**Figs 1G and 1H**). Thus PXR-mediated inhibition of pro-inflammatory gene expression in the inflamed intestine prominently involves the IEC compartment.

Mutual repression of PXR and NF- κ B signaling in IBD

Having established that the PXR can negatively regulate NF- κ B-dependent gene transcription in IBD, we subsequently we decided to establish the potential relevance this observation. To this end, we determined *PXR* expression in our patient cohort and related this expression to NF- κ B pathway activity as judged by *IL-8* and *IL-1 β* mRNA levels. We observed that expression of *PXR* is largely similar in control biopsies and in biopsies from quiescent CD patients. However, although not significant ($p=0.15$) *PXR* expression levels seemed to be reduced in biopsies from active CD patients (**Fig 2A**). When *PXR* expression was related to the expression of NF- κ B target genes, we observed a statistically significant correlation between *PXR* expression and NF- κ B activity (**Fig 2B**; $r=-0.6$, $p<0.01$), suggesting that PXR status is important for controlling inflammation in IBD.

To further investigate this relationship between *PXR* expression and NF- κ B signaling, patients were stratified into three groups according to their *PXR* mRNA expression level after Rifampicin treatment (**Figs 2C and S3**): patients that had lower *PXR* expression following Rifampicin ($n=5$), patients that had higher *PXR* expression following Rifampicin stimulation ($n=10$) and four patients that did not show changes in *PXR* expression following Rifampicin application. Using this stratification, it emerges that Rifampicin-mediated down regulation of *IL-8* expression correlates well with induction of *PXR* expression (**Fig 2D**; $p<0.05$), further highlighting the PXR-dependent nature of the anti-inflammatory action of Rifampicin in colonic biopsies. The overall upregulation of *PXR* expression seen in the Rifampicin-stimulated biopsies confirms the efficacy of stimulating *PXR* expression through the Rifampicin challenge (**Fig 2E**). It thus appears that the level of *PXR* activity is the rate-limiting factor with respect to NF- κ B-directed gene expression in active IBD and conversely the amount of NF- κ B activity is an important negative regulator for *PXR* expression. The latter notion was supported by observation made in intestinal organoids. *PXR* expression was repressed when NF- κ B pathway TNF α stimulate in the intestinal organoids, although *PXR* still increased with Rifampicin treatment (**Fig 2F**). Rifampicin could also stimulate *PXR* expression in organoids deprived from IBD patient, but in the inflamed group the increase was held (**Fig 2G**). Thus it appears that *PXR* activation and NF- κ B pathway are mutually exclusive in the context of the colon IEC.

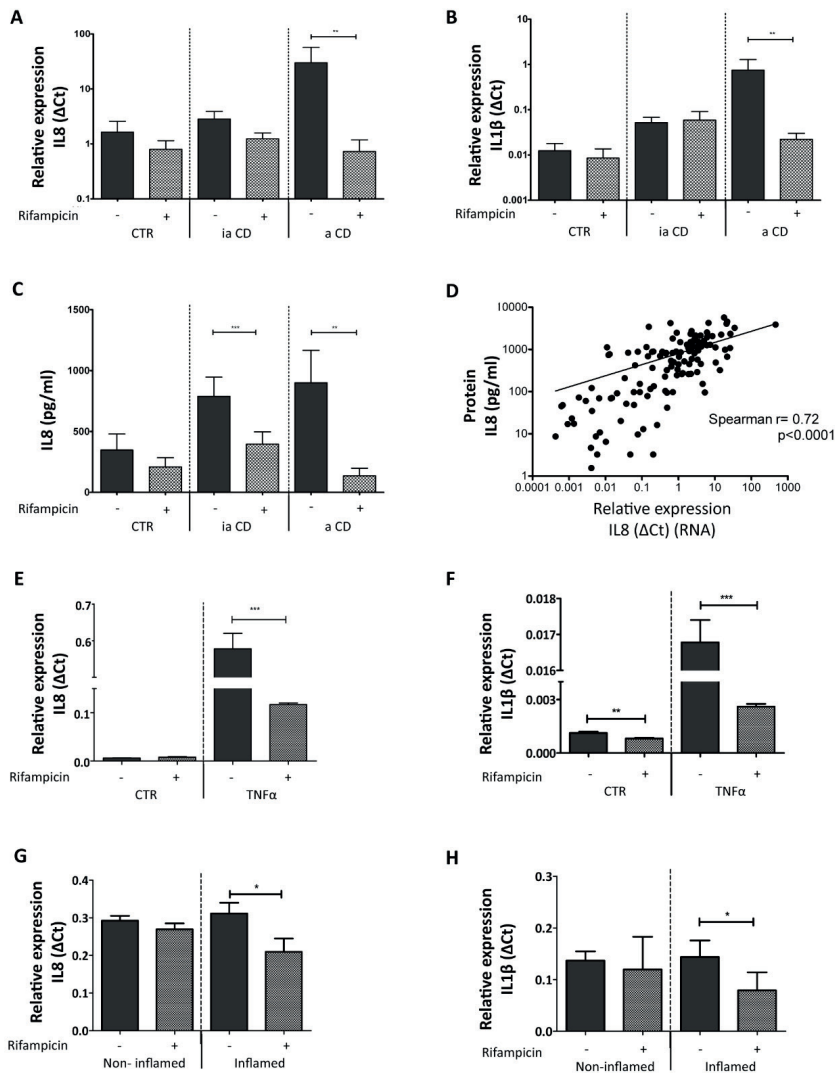


Fig 1. Effects of with rifampicin treatment on cytokine expression in human intestinal biopsies. **(A)** IL-8 mRNA expression in human intestinal biopsies. The graph represents the mean IL-8 mRNA expression on a log scale, from biopsies stimulated with solvent only (0.1 % (v/v) DMSO) or 100 μ M Rifampicin for 18 h at 37 $^{\circ}$ C. CTR are the biopsies from control patients ($n=36$), ia CD signifies biopsies from CD patients without active intestinal inflammation ($n=66$), and a CD indicates biopsies from CD patients with active intestinal inflammation ($n=40$). **(B)** IL-1 β mRNA expression in human intestinal biopsies. For this graph the same labeling applies as in A. The error bar denotes SEM, ** $p<0.01$. **(C)** IL-8 protein expression in human intestinal biopsies. ELISA was used to measure the IL-8 protein concentration from biopsy homogenates. The same biopsies were used as for the mRNA expression analysis in A and B. The error bar is SEM, ** $p<0.01$, *** $p<0.001$. **(D)** Correlation between IL-8 mRNA levels and protein levels. The IL-8 mRNA expression ($dCt=\delta Ct$) is plotted against the IL-8 protein (pg/mL) measured *per* biopsy. The Spearman correlation is depicted as well, $r=0.72$, $p<0.0001$. **(E)** & **(F)** IL-8 mRNA levels and IL-1 β levels, respectively, as measured in human intestinal organoids. The graph represents the mean IL-8 mRNA expression stimulated with solvent only (0.1 % (v/v) DMSO) or 100 μ M Rifampicin for 18 h at 37 $^{\circ}$ C. The TNF α group was treated with 10 ng/ml TNF α for 24 h while the CTR group was stimulated with solvent only. **(G)** & **(H)** IL-8 and IL-1 β expression in the intestinal organoid

from the patient of inflammation bowel disease. The non-inflamed group represents the organoid derived from non-inflamed tissue and the inflamed group represents the organoid derived from inflamed tissue of the same patient.

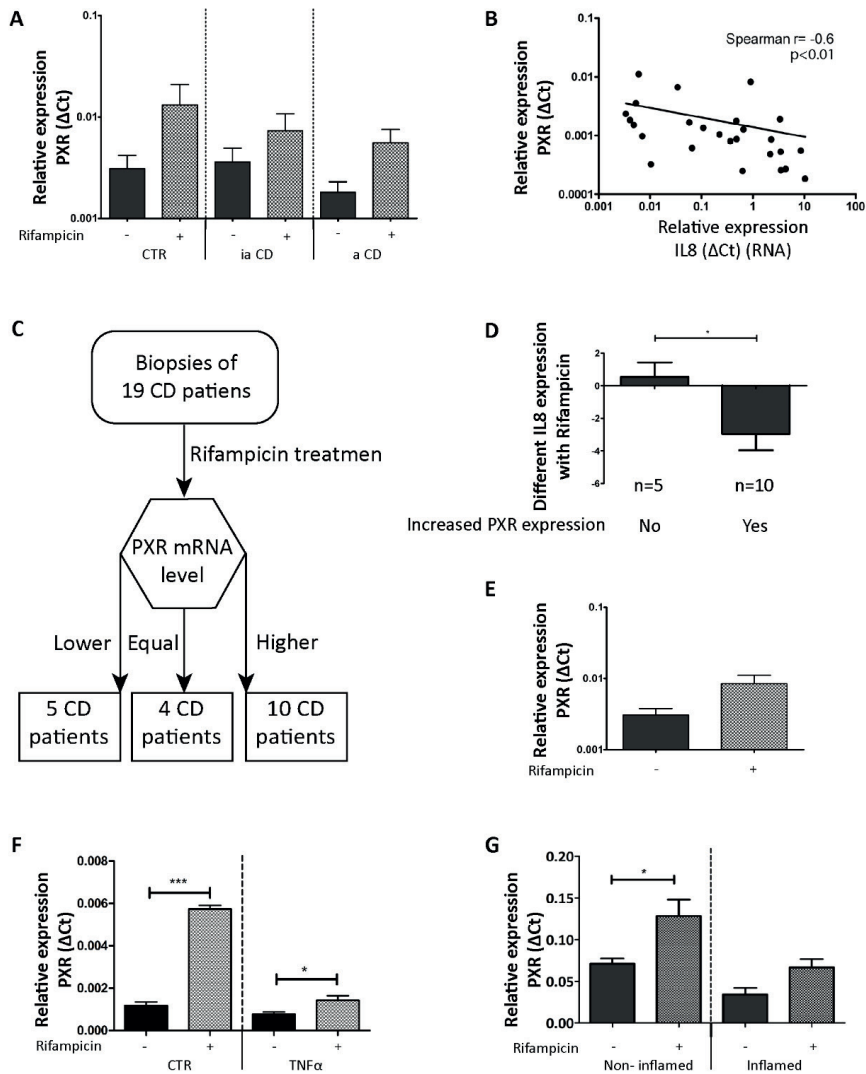


Fig 2. PXR expression levels and relation to NF-κB activity. **(A)** PXR mRNA levels in human intestinal biopsies. CTR are the biopsies from control patients ($n=36$), ia CD signifies biopsies from CD patients without active intestinal inflammation ($n=66$), and a CD indicates biopsies from CD patients with active intestinal inflammation ($n=40$). The error bar is SEM. **(B)** Correlation between IL-8 mRNA levels and PXR mRNA levels in non-rifampicin-challenged biopsies. **(C)** Flowchart used for dividing CD patients into groups based on induction of PXR expression by Rifampicin treatment. The CD patients were divided into three groups: Group 1 (5 CD patients) show lower PXR expression after the Rifampicin treatment; Group 2 (4 CD patients) have equal expression of PXR before and after Rifampicin treatment; Group 3 (10 CD patients) have increased PXR expression after the Rifampicin treatment. **(D)** Effects of rifampicin on IL-8 expression as stratified by the effects of Rifampicin on PXR expression. The error bar is SEM, $*p < 0.05$. **(E)** PXR expression in all biopsies with or without Rifampicin stimulation. The error bar is SEM, $p=0.056$. **(F)** PXR mRNA expression in human intestinal organoids. The graph represents the mean PXR mRNA expression measure when stimulated with solvent only (0.1 % (v/v) DMSO) or 100 μM Rifampicin for 18 h at 37 °C. The TNFα

group was treated with 10 ng/ml TNF α for 24 h while the CTR group was stimulated with solvent only. The error bar is SEM. * p <0.05. *** p <0.001. (G) PXR mRNA expression in non-inflamed and inflamed intestinal organoids from IBD patient. The same methodology as in Fig 1G was used. The error bar is SEM. * p <0.05.

PXR mediates NF- κ B inhibition

Direct support for the notion that PXR is important for restricting NF- κ B activation in the epithelial compartment came from experiments in which we investigated the effect of PXR expression *per se* on NF- κ B inhibition. We used the LS174t cells, a generally used model for colonic epithelial cells that recapitulates many aspects of normal enterocyte physiology [36] and generated two derivatives, the LS174t (siPXR) clone that lacked PXR expression and LS174t (nt) as a transfection control (**Fig 3A**). Consistently, induction of *CYP3A4* (the PXR target gene) was corrupted with PXR gene down-regulation (**Fig 3B**), but not in the control cells. Following stimulation of NF- κ B with *E. Coli* lysate, IL-8 expression was enhanced in the cells lacking PXR as compared to controls, which was significantly higher than its expression in cells with PXR expression (p <0.05; **Fig 3C**). We confirmed this difference by showing a decreased p-p65 and p-Akt protein expression in the LS174t (nt) cell line (**Figs 3D and 3E**). It demonstrated in this model cell line, PXR activity also constitutes the rate-limiting step in NF- κ B-dependent gene expression. Conversely, activating NF- κ B signaling reduces PXR levels in LS174t (nt) cells (**Fig 3F**). Thus these *in vitro* experiments showed that the negative relationship between NF- κ B and PXR signaling is cell-autonomous and provide strong support for the notion that the presence of PXR represents an important target constraining NF- κ B signalling in the mucosal epithelial compartment.

Mutual repression of PXR and NF- κ B signaling

In order to further understand the relationship between PXR and NF- κ B signaling, we also measured the NF- κ B target genes IL-8 and IL-1 β the in human epithelial colorectal adenocarcinoma cell line CACO2 [37]. As expected, NF- κ B signaling was inhibited by Rifampicin treatment in TNF α -challenged monolayers (**Figs 4A and 4B**). Conversely, induction of PXR by Rifampicin treatment was constrained in the presence of TNF α (**Fig 4C**). To establish that the rifampicin effects observed truly related to differences in NF- κ B transcriptional activity we constructed a CACO2 clone containing a NF- κ B reporter as described before [38]. The results show that also in this experimental system stimulation with rifampicin counteracts NF- κ B activity (**Fig 4D**). In conclusion, PXR activity is the major rate-limiting pathway constraining mucosal NF- κ B activity in active IBD and conversely active NF- κ B signaling represses PXR expression. Thus targeting PXR emerges as a rational strategy for the management of IBD.

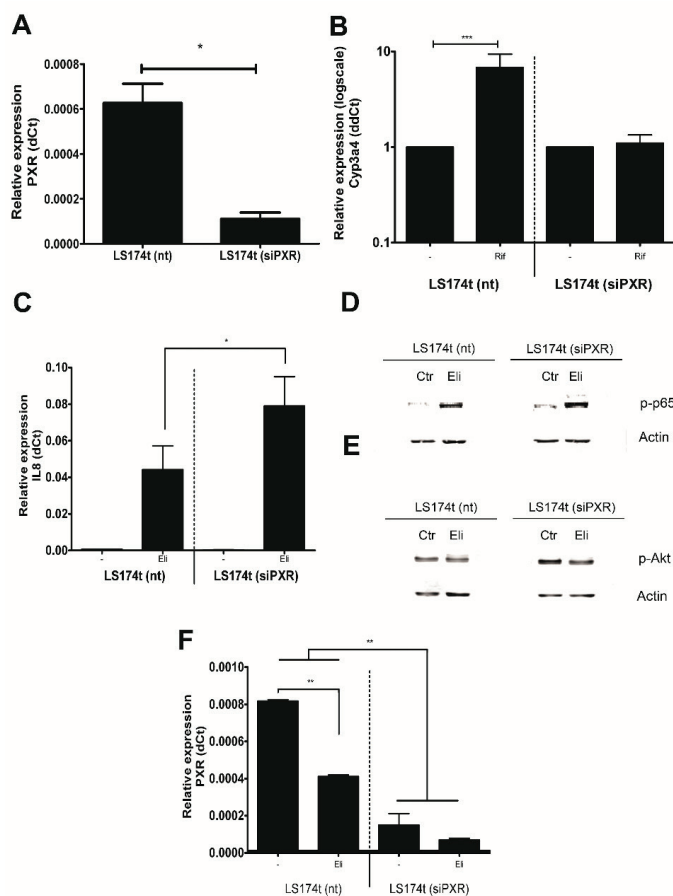


Fig 3. Effects of PXR knock down on NF- κ B signaling. **(A)** PXR mRNA expression in a LS174t cell line stably transduced with a non-targeting siRNA (nt) or an siPXR. The graph represents PXR mRNA expression in LS174t cells from three independent experiments. The error bar is SD, * $p < 0.05$. **(B)** LS174t (nt) and LS174t (siPXR) cells stimulated with 100 μ M Rifampicin for 16 h at 37 $^{\circ}$ C. The relative mRNA expression of the PXR target gene *CYP3A4* is presented in the graph. The error bar is SD, *** $p < 0.001$. **(C)** IL-8 mRNA expression in LS174t cells. Both cell lines were stimulated with 2 μ l *E. coli* lysate (ELI). The error bar is SD, * $p < 0.05$. **(D)** Activated NF- κ B subunit p65 protein (p-p65) expression in LS174t cells. The same stimulation methods were used as in C. β -actin protein expression is used as a loading control. **(E)** Activated Akt (p-Akt) protein expression in LS174t cells. **(F)** PXR mRNA expression in LS174t cells. The error bar is SD, ** $p < 0.01$.

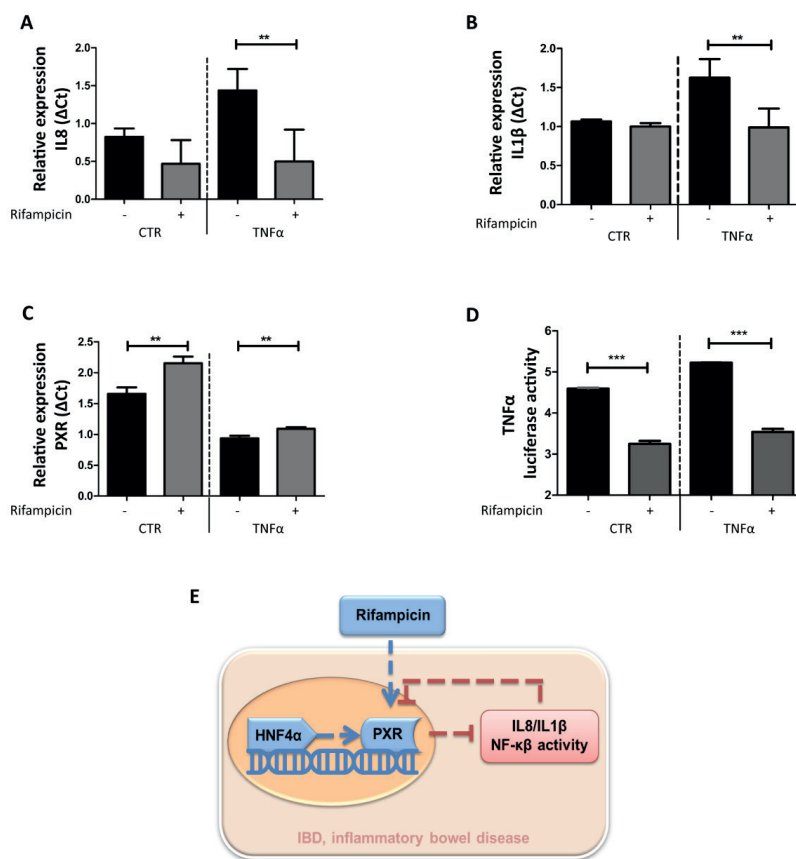


Fig 4. PXR and NF-κB axis activity in CACO2 cells. (A) & (B) IL-8 and IL-1β mRNA expression in CACO2 cells, respectively. CACO2 cells were stimulated with solvent only (0.1 % (v/v) DMSO) or 100 μM Rifampicin for 16 h at 37 °C. The TNFα group was treated with 10ng/ml TNFα for 24 h while the CTR group was stimulated with solvent only. The error bar is SEM, and ** $p < 0.01$. (C) PXR expression in CACO2 cells. (D) TNFα luciferase activity in CACO2 cells. The same stimulation methods were used as in A. (E) Schematic diagram illustrating the mutual repression of PXR and NF-κB.

Discussion

Active IBD is associated with the imbalanced immune response against intestinal microbial challenge. Xenobiotic and inflammatory signaling in response to microbiological constituents appear a certain extent mutually exclusive. Hence it is important to understand how xenobiotic receptor systems interact with epithelial immunity, especially in the context of IBD. Here we demonstrate that NF- κ B signaling on one hand and the PXR receptor on the other hand restrain each other's activity and that in the context of active IBD the PXR pathway is a major rate-limiting factor for NF- κ B-dependent epithelial gene expression (**Fig 4E**). Our observations have substantial consequences in our thinking of IBD and open the possibility that by targeting PXR signaling therapeutic benefit may be achieved, especially in those patients with epithelial hyper-activation of NF- κ B signaling.

Earlier studies already demonstrated a role for defective xenobiotic resistance mechanisms in effector T cells for preventing Crohn's-like ileitis in experimental animals [39], the present study extends this concept into the epithelial compartment as well and indicates the importance of such mechanisms for active inflammatory responses. It is tempting to speculate why such mechanisms might exist, but a possibility is limiting NF- κ B-dependent signaling and subsequently reduced inflammation facilitates regenerative responses. In apparent agreement with this notion is that Pregnane X receptor agonists enhance intestinal epithelial wound healing and repair of the intestinal barrier following the induction of experimental colitis [13]. Consistent with a critical role for PXR in constraining epithelial inflammatory responses are also the genetic studies that link genomic variation in PXR in susceptibility to IBD [11, 12], although a recent meta-analysis revealed that PXR gene polymorphisms may not be significantly associated with IBD susceptibility. It is, however, tempting to suggest that in certain patient populations aberrant PXR induction failed to control epithelial NF- κ B induction and thus predisposing to disease. It would thus also be interesting to study the relation between such polymorphisms and the success of therapy to keep patients in remission, also in view of the association we see in the present study between PXR signaling and active disease. Larger studies containing cohorts are thus essential to clarify the association between *PXR* polymorphisms and the natural history of IBD. Disregarding the exact importance of genetic variance in the *PXR* gene, it is evident from the present study that PXR signaling constitutes a powerful anti-inflammatory mechanism capable of counteracting epithelial inflammation in active IBD. Stimulation of PXR may have clinical possibility, not only because of its capacity to limit inflammation, but also because such an action may improve bone mineralization [40, 41] and bone mineralization is a problem in inflammatory bowel disease [42, 43], whereas the lipophilic ligands used for PXR stimulation may conceivably also have chemopreventive effects with respect to the development of IBD-associated colorectal cancer [44]. We thus feel that our observation call for controlled studies assessing the potential of PXR agonists as a rational therapeutic strategy in IBD.

Acknowledgements

We thank our patients for their consent and our coworkers for their support during this study.

Funding Statement

M.L. [201506100033] and S.C. [201606760056] are supported by a China Scholarship Council stipend, MPP is grateful to the Dutch Society for the Replacement of Animal Testing and ZONMW (2016/22827/ZONMW) for the financial support of this work. The sponsors were not involved study design, data collection and analysis, decision to publish, or preparation of the manuscript.

Competing interests: The authors have declared that no competing interesting exist.

References

1. Peterson LW, Artis D. Intestinal epithelial cells: regulators of barrier function and immune homeostasis. *Nat Rev Immunol*. 2014;14(3):141-53.
2. Deuring JJ, de Haar C, Kuipers EJ, Peppelenbosch MP, van der Woude CJ. The cell biology of the intestinal epithelium and its relation to inflammatory bowel disease. *Int J Biochem Cell Biol*. 2013;45(4):798-806.
3. Schiering C, Wincent E, Metidji A, Iseppon A, Li Y, Potocnik AJ, et al. Feedback control of AHR signalling regulates intestinal immunity. *Nature*. 2017;542(7640):242-5.
4. Parikh K, Antanaviciute A, Fawcner-Corbett D, Jagielowicz M, Alicino A, Lagerholm C, et al. Colonic epithelial cell diversity in health and inflammatory bowel disease. *Nature*. 2019;567(7746):49-55.
5. Ananthakrishnan AN, Bernstein CN, Iliopoulos D, Macpherson A, Neurath MF, Ali RAR, et al. Environmental triggers in IBD: a review of progress and evidence. *Nat Rev Gastroenterol Hepatol*. 2018;15(1):39-49.
6. Hyams JS, Davis Thomas S, Gotman N, Haberman Y, Karns R, Schirmer M, et al. Clinical and biological predictors of response to standardised paediatric colitis therapy (PROTECT): a multicentre inception cohort study. *Lancet*. 2019;393(10182):1708-20.
7. Sivaprakasam S, Bhutia YD, Ramachandran S, Ganapathy V. Cell-Surface and Nuclear Receptors in the Colon as Targets for Bacterial Metabolites and Its Relevance to Colon Health. *Nutrients*. 2017;9(8).
8. Gronke K, Hernandez PP, Zimmermann J, Klose CSN, Kofoed-Branzk M, Guendel F, et al. Interleukin-22 protects intestinal stem cells against genotoxic stress. *Nature*. 2019;566(7743):249-53.
9. Bessede A, Gargaro M, Pallotta MT, Martino D, Servillo G, Brunacci C, et al. Aryl hydrocarbon receptor control of a disease tolerance defence pathway. *Nature*. 2014;511(7508):184-90.
10. Mondanelli G, Bianchi R, Pallotta MT, Orabona C, Albini E, Iacono A, et al. A Relay Pathway between Arginine and Tryptophan Metabolism Confers Immunosuppressive Properties on Dendritic Cells. *Immunity*. 2017;46(2):233-44.
11. Glas J, Seiderer J, Fischer D, Tengler B, Pfennig S, Wetzke M, et al. Pregnane X receptor (PXR/NR1I2) gene haplotypes modulate susceptibility to inflammatory bowel disease. *Inflamm Bowel Dis*. 2011;17(9):1917-24.
12. Dring MM, Goulding CA, Trimble VI, Keegan D, Ryan AW, Brophy KM, et al. The pregnane X receptor locus is associated with susceptibility to inflammatory bowel disease. *Gastroenterology*. 2006;130(2):341-8; quiz 592.

13. Terc J, Hansen A, Alston L, Hirota SA. Pregnane X receptor agonists enhance intestinal epithelial wound healing and repair of the intestinal barrier following the induction of experimental colitis. *Eur J Pharm Sci.* 2014;55:12-9.
14. Dou W, Zhang J, Li H, Kortagere S, Sun K, Ding L, et al. Plant flavonol isorhamnetin attenuates chemically induced inflammatory bowel disease via a PXR-dependent pathway. *J Nutr Biochem.* 2014;25(9):923-33.
15. Zhang X, Wang Y, Ma Z, Liang Q, Tang X, Hu D, et al. Tanshinone IIA ameliorates dextran sulfate sodium-induced inflammatory bowel disease via the pregnane X receptor. *Drug Des Devel Ther.* 2015;9:6343-62.
16. Uehara D, Tojima H, Kakizaki S, Yamazaki Y, Horiguchi N, Takizawa D, et al. Constitutive androstane receptor and pregnane X receptor cooperatively ameliorate DSS-induced colitis. *Dig Liver Dis.* 2019;51(2):226-35.
17. Liu M, Zhang G, Zheng C, Song M, Liu F, Huang X, et al. Activating the pregnane X receptor by imperatorin attenuates dextran sulphate sodium-induced colitis in mice. *Br J Pharmacol.* 2018;175(17):3563-80.
18. Zhang Q, Lenardo MJ, Baltimore D. 30 Years of NF-kappaB: A Blossoming of Relevance to Human Pathobiology. *Cell.* 2017;168(1-2):37-57.
19. McDaniel DK, Eden K, Ringel VM, Allen IC. Emerging Roles for Noncanonical NF-kappaB Signaling in the Modulation of Inflammatory Bowel Disease Pathobiology. *Inflamm Bowel Dis.* 2016;22(9):2265-79.
20. Zhou C, Tabb MM, Nelson EL, Grun F, Verma S, Sadatrafiei A, et al. Mutual repression between steroid and xenobiotic receptor and NF-kappaB signaling pathways links xenobiotic metabolism and inflammation. *J Clin Invest.* 2006;116(8):2280-9.
21. Zhang J, Cao L, Wang H, Cheng X, Wang L, Zhu L, et al. Ginsenosides Regulate PXR/NF-kappaB Signaling and Attenuate Dextran Sulfate Sodium-Induced Colitis. *Drug Metab Dispos.* 2015;43(8):1181-9.
22. Voorneveld PW, Kodach LL, Jacobs RJ, Liv N, Zonneville AC, Hoogenboom JP, et al. Loss of SMAD4 alters BMP signaling to promote colorectal cancer cell metastasis via activation of Rho and ROCK. *Gastroenterology.* 2014;147(1):196-208 e13.
23. Wang W, Xu L, Liu P, Jairam K, Yin Y, Chen K, et al. Blocking Wnt Secretion Reduces Growth of Hepatocellular Carcinoma Cell Lines Mostly Independent of beta-Catenin Signaling. *Neoplasia.* 2016;18(12):711-23.
24. Yin Y, Bijvelds M, Dang W, Xu L, van der Eijk AA, Knipping K, et al. Modeling rotavirus infection and antiviral therapy using primary intestinal organoids. *Antiviral Res.* 2015;123:120-31.
25. Li Y, Deuring J, Peppelenbosch MP, Kuipers EJ, de Haar C, van der Woude CJ. IL-6-induced DNMT1 activity mediates SOCS3 promoter hypermethylation in ulcerative colitis-related colorectal cancer. *Carcinogenesis.* 2012;33(10):1889-96.

26. Deuring JJ, de Haar C, Koelewijn CL, Kuipers EJ, Peppelenbosch MP, van der Woude CJ. Absence of ABCG2-mediated mucosal detoxification in patients with active inflammatory bowel disease is due to impeded protein folding. *Biochem J.* 2012;441(1):87-93.
27. Livak KJ, Schmittgen TD. Analysis of relative gene expression data using real-time quantitative PCR and the 2(-Delta Delta C(T)) Method. *Methods.* 2001;25(4):402-8.
28. Hakim MS, Ding S, Chen S, Yin Y, Su J, van der Woude CJ, et al. TNF-alpha exerts potent anti-rotavirus effects via the activation of classical NF-kappaB pathway. *Virus Res.* 2018;253:28-37.
29. Wang W, Xu L, Brandsma JH, Wang Y, Hakim MS, Zhou X, et al. Convergent Transcription of Interferon-stimulated Genes by TNF-alpha and IFN-alpha Augments Antiviral Activity against HCV and HEV. *Sci Rep.* 2016;6:25482.
30. de Sousa RR, Queiroz KC, Souza AC, Gurgueira SA, Augusto AC, Miranda MA, et al. Phosphoprotein levels, MAPK activities and NFkappaB expression are affected by fisetin. *J Enzyme Inhib Med Chem.* 2007;22(4):439-44.
31. Camoglio L, Juffermans NP, Peppelenbosch M, te Velde AA, ten Kate FJ, van Deventer SJ, et al. Contrasting roles of IL-12p40 and IL-12p35 in the development of hapten-induced colitis. *Eur J Immunol.* 2002;32(1):261-9.
32. van Den Brink GR, ten Kate FJ, Ponsioen CY, Rive MM, Tytgat GN, van Deventer SJ, et al. Expression and activation of NF-kappa B in the antrum of the human stomach. *J Immunol.* 2000;164(6):3353-9.
33. Goodwin B, Hodgson E, Liddle C. The orphan human pregnane X receptor mediates the transcriptional activation of CYP3A4 by rifampicin through a distal enhancer module. *Mol Pharmacol.* 1999;56(6):1329-39.
34. Medzhitov R, Preston-Hurlburt P, Janeway CA, Jr. A human homologue of the Drosophila Toll protein signals activation of adaptive immunity. *Nature.* 1997;388(6640):394-7.
35. Blokzijl H, Vander Borgh S, Bok LI, Libbrecht L, Geuken M, van den Heuvel FA, et al. Decreased P-glycoprotein (P-gp/MDR1) expression in inflamed human intestinal epithelium is independent of PXR protein levels. *Inflamm Bowel Dis.* 2007;13(6):710-20.
36. Lee JH, Koh H, Kim M, Kim Y, Lee SY, Karess RE, et al. Energy-dependent regulation of cell structure by AMP-activated protein kinase. *Nature.* 2007;447(7147):1017-20.
37. Kalthoff S, Ehmer U, Freiberg N, Manns MP, Strassburg CP. Coffee induces expression of glucuronosyltransferases by the aryl hydrocarbon receptor and Nrf2 in liver and stomach. *Gastroenterology.* 2010;139(5):1699-710, 710 e1-2.
38. Xie W, Barwick JL, Downes M, Blumberg B, Simon CM, Nelson MC, et al. Humanized xenobiotic response in mice expressing nuclear receptor SXR. *Nature.* 2000;406(6794):435-9.
39. Cao W, Kayama H, Chen ML, Delmas A, Sun A, Kim SY, et al. The Xenobiotic Transporter Mdr1 Enforces T Cell Homeostasis in the Presence of Intestinal Bile Acids. *Immunity.* 2017;47(6):1182-96 e10.

40. Zambuzzi WF, Coelho PG, Alves GG, Granjeiro JM. Intracellular signal transduction as a factor in the development of "smart" biomaterials for bone tissue engineering. *Biotechnol Bioeng*. 2011;108(6):1246-50.
41. Ihunnah CA, Jiang M, Xie W. Nuclear receptor PXR, transcriptional circuits and metabolic relevance. *Biochim Biophys Acta*. 2011;1812(8):956-63.
42. Shi HY, Ng SC. The state of the art on treatment of Crohn's disease. *J Gastroenterol*. 2018;53(9):989-98.
43. Krajcovicova A, Hlavaty T, Killinger Z, Miznerova E, Toth J, Letkovsky J, et al. Combination therapy with an immunomodulator and anti-TNFalpha agent improves bone mineral density in IBD patients. *J Crohns Colitis*. 2014;8(12):1693-701.
44. Yang J, Yu J. The association of diet, gut microbiota and colorectal cancer: what we eat may imply what we get. *Protein Cell*. 2018;9(5):474-87.

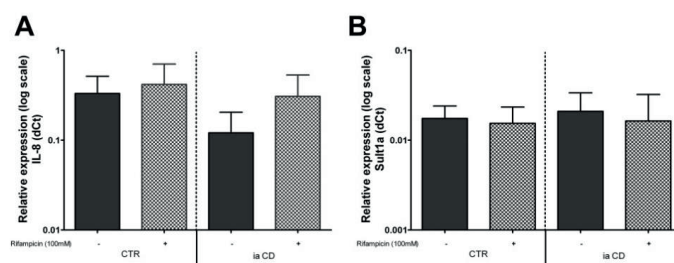
Supplementary data for

Pregnane X Receptor Activation Constrains Mucosal NF- κ B Activity in Active Inflammatory Bowel Disease

J. Jasper Deuring¹, [Meng Li](#)¹, Wanlu Cao¹, Sunrui Chen¹, Wenshi Wang¹, Colin de Haar¹, C. Janneke van der Woude¹, Maikel Peppelenbosch¹

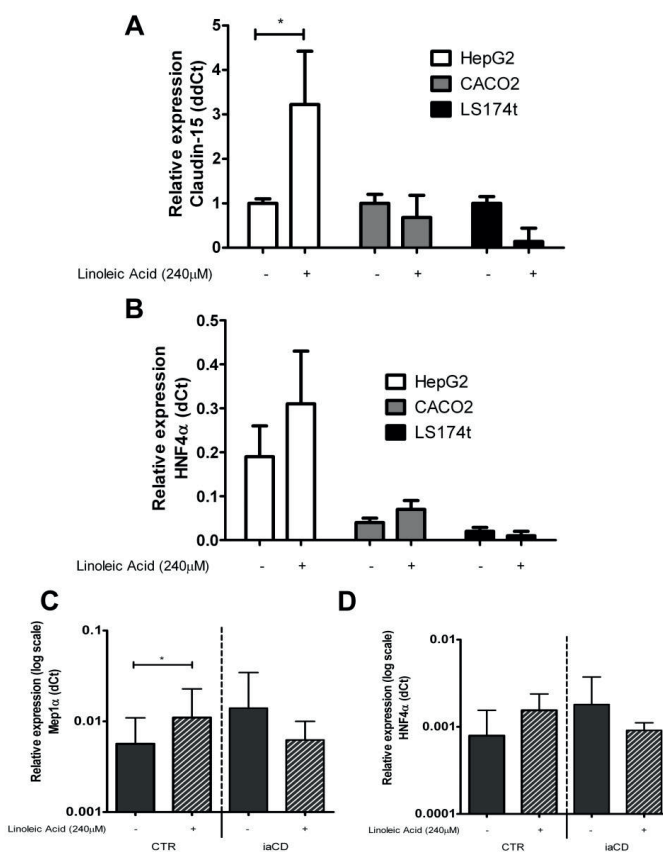
Table of contents

- S1 Fig The effect of rifampicin on PBMC
- S2 Fig Cancer cells with HNF4 α stimulation
- S3 Fig The increase of PXR mRNA expression by rifampicin treatment
- S4 Fig The expression levels of PXR target genes in organoids
- S5 Fig The expression levels of PXR target genes
- S1 Table. Primers used for qRT-PCR
- S2 Table. Patients information with rifampicin
- S3 Table. Patients information with linoleic acid



S1 Fig: The effect of rifampicin on PBMC

A) IL-8 mRNA expression in PBMC. PBMC isolated from peripheral blood samples of CD patients and healthy individuals were stimulated for 18h at 37°C with solvent (0.1% (v/v) DMSO) or 100 mM rifampicin. Ctr is the mean IL-8 expression of the healthy individuals (n=4) and ia CD is the mean IL-8 expression of the inactive CD patients (n=5). The error bar is SD. B) Sult1a mRNA expression in PBMC. Same methodology as used in A was used.



S2 Fig: Cancer cells with HNF4a stimulation

A) HNF4a target gene Claudin-15 expression in cancer cell lines. Hepatocyte cancer cell line HepG2 and colon cancer cell line CACO2 and LS174t were stimulated with 240 mM linoleic acid for 18h at 37°C. The graph represents the mean relative Claudin-15 expression per cell lines and with or without linoleic acid stimulation line. The error bar is SD, * $p < 0.05$. B) HNF4a expression in cancer cell lines. Same methodology as in A was used. The graph represents the mean expression of HNF4a per cell line. The error bar is SD. C) HNF4a target gene Mep1a expression in biopsies. Biopsies from two CD patients and three healthy individuals were stimulated with solvent (1% (v/v) PBS) or 240 mM Linoleic acid for 18 h at 37°C. The graph represents the mean Mep1a expression per group. CTR are the controls and iaCD are CD patients with quiescent disease. The error bar is SD. D) HNF4a expression in biopsies. Same methodology as in C) was used. The graph represents the mean HNF4a expression per group. The error bar is SD.

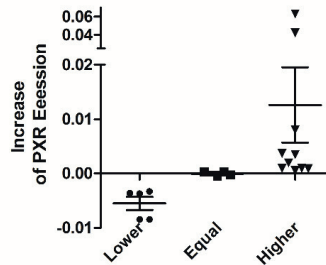
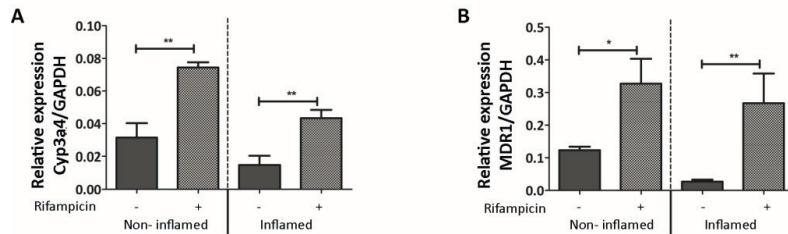


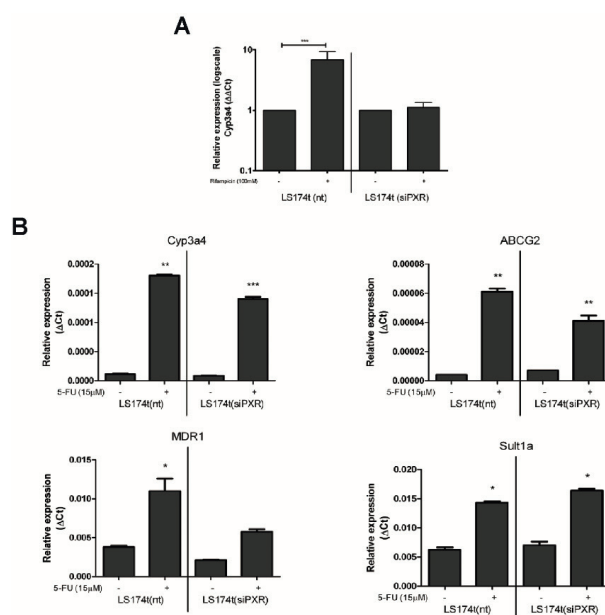
Figure S3: The increase of PXR mRNA expression by Rifampicin treatment

19 samples were treated with Rifampicin to induce the expression of PXR. The samples were divided into three groups: Group 1 (n=5) show lower PXR expression after the Rifampicin treatment; Group 2 (n=4) have equal expression of PXR before and after Rifampicin treatment; Group 3 (n=10) have increased PXR expression after the Rifampicin treatment. The graph represents the mean increase of PXR expression. The error bar is SEM.



S4 Fig: The expression levels of PXR target genes in organoids

A) & B) Cyp3a4 and MDR1 expression in the intestinal organoids from the patient with inflammation bowel disease. The non-inflamed group represents the organoid derived from non-inflamed tissue and the inflamed group represents the organoid derived from inflamed tissue of the same patient. Error bar is SEM. Organoids were cultured with (+) or without (-) Rifampicin. * $p < 0.05$, ** $p < 0.01$.



S5 Fig: The expression levels of PXR target genes

A) PXR specific stimulation by 100 mM rifampicin. This graph represents the average, of two independent experiments performed in duplo, mRNA expression of Cyp3a4. Error bar is SD, *** $p < 0.001$. B) The expression of multi drug resistant associated genes. The mRNA expression of the indicated genes was measured in the LS174t (nt) cells and the LS174t (siPXR) cells stimulated with 15 mM 5-FU for 72 h. These graphs represent the average of two independent experiments. Error bar is SD. The increase in expression was compared per cell line to the un-stimulated cells using a non-parametric t-test, * $p < 0.05$, ** $p < 0.01$ and *** $p < 0.001$.

Table S1: Primer sequences

Primer name	Sequence from 5' to 3'
GapdH_fw	GCATTGCCCTCAACGACCAC
GapdH_rev	CCACCACCCTGTTGCTGTAG
YWHAS_fw	ACTTTTGGTACATTGTGGCTTCAA
YWHAS_rev	CCGCCAGGACAAACCACTAT
IL8_fw	CACTGCGCCAACACAGAAATTA
IL8_rev	ACTTCTCCACAACCTCTGCAC
IL1b_fw	CCCTAAACAGATGAAGTGCTCCTT
IL1b_rev	GTAGCTGGATGCCGCCAT
Cyp3a4_fw	CAGGAGGAAATTGATGCAGTTTT
Cyp3a4_rev	GTCAAGATACTCCATCTGTAGCACAGT
HNF4a_fw	ACATGGACATGGCCGACTAC
HNF4a_rev	TGCCTCAATCTGGCGAGACG
Claudin-15_fw	TGAGGTGGGTGGATTACTTG
Claudin-15_rev	TGTTGAAGGCGTACCAGGAG
Mep1a_fw	TCAAGCCCTATGAAGGAGAG
Mep1a_rev	CCTTATAGGCACATCCTTGG
Sult1a_fw	GCACCCACCCTGTTCTCTAC
Sult1a_rev	ACCACGAAGTCCACGGTCTC
PXR_fw	ATGGCAGTGTCTGGAACACTAC
PXR_rev	CAGTTGACACAGCTCGAAAG

Table S2: Baseline characteristics of patients treated with rifampicin

	CD	Control
Total number of patients	19	8
Mean age, yr (SD)	44 (16.6)	62 (3.5)*
Gender (M/F)	5/14	3/4
Mean duration of disease, yr (SD)	13 (8.8)	-
# Smoking (%Yes)	4 (25)	2(33)
# Familial IBD (%Yes)	5 (36)	-
Concomitant medication:		
- none	1	-
- aminosalicylates	3	-
- corticosteroids	4	-
- immunosuppressives	9	-
- biological	5	-
# Biopsies colon	106	36

* The healthy controls are significantly older than the CD patients p=0.002.

Table S3: Baseline characteristics of patients treated with linoleic acid

	Linoleic acid		Linoleic acid +/- Rifampicin	
	CD	Control	CD	Control
Total number of patients	2	3	2	3
Mean age, yr (SD)	38(7.7)	49(12.9)	50(0.7)	45(6.4)
Gender (M/F)	1/1	2/1	1/1	2/1
Mean duration of disease, yr (SD)	17(7.1)	-	5.5(0.7)	-
# Smoking (%Yes)	0(0)	0(0)	0(0)	1(33)
# with familiar link to IBD (%Yes)	0(0)	-	1(50)	-
Concomitant medication:				
- none	0	-	1	-
- aminosalicylates	1	-	1	-
- corticosteroids	0	-	0	-
- immunosuppressives	0	-	0	-
- biological	1	-	0	-
# Biopsies colon	10	8	10	8

CHAPTER 8

Risk for complications in cancer patients treated with checkpoint inhibitors

Meng Li¹, Qiuwei Pan¹, Maikel P. Peppelenbosch¹

¹ Department of Gastroenterology and Hepatology, Erasmus MC-University Medical Center, Rotterdam,
The Netherlands

Based on *Clinical Gastroenterology and Hepatology* 2017 Oct;15(10):1637.

Abstract

Despite the tremendous progress of cancer treatment, many cancers remain highly refractory to conventional chemotherapy and only become manifest when curative surgery is no longer an option. Immunotherapy has emerged as an exciting adjuvant approach and involves stimulating responses of the immune system to combat cancer. Recently, especially immune check-point inhibitors have proven instrumental in the management of various cancers by counteracting the mechanisms that limit the host immune response and have been proven in various settings to constrain tumor growth. They are considered to have ushered a new era of cancer management. Unfortunately, the side effects of check point inhibitors substantially limit their use and adequate management of these side effects without compromising anti-cancer activity remains a challenge. Here we have performed a study of the published contemporary literature and conference proceedings and present a theoretical evaluation of the side effects involved and suggest better tailored treatments based on molecular characteristics.

Introduction

Cancer is one of the major causes of mortality throughout the world and is the second leading cause of death in the United States and thus is a major public health problem [1]. Cancer remains such a devastating disease mainly because therapies are often ineffective and recurrence remains unacceptably high. In recent years the use of immunomodulating therapy applied to treat various cancers has increased. Immunotherapies for cancer specifically activate the immune system to mount responses against malignant cells and is as thus an adjuvant therapy. As such therapies are often successful in patients resistant to other type treatment, they have offered new hope for cancer patients. Among immune therapies for cancer, checkpoint inhibitors are shown effective. The pathways targeted by these medications include cytotoxic T lymphocyte associated antigen 4 (CTLA-4) and programmed death-1 (PD-1) which mediate cell cycle arrest and apoptosis of immune cells attacking cancers [2]. Constituted from different monoclonal antibody therapeutics to stimulate immune responses for a variety of cancers, check point inhibitors have in a short time become one the most successful therapies for cancer.

However, with better understanding of immunoregulatory mechanisms and more inhibitors approved to be used in clinical settings, more side effect cases related with checkpoint inhibitors are being reported as well and reveal another side to this apparent success story [3-5]. Here, we review the application and side effects of check point inhibitors for cancer and discuss existing and emerging possibilities that translate the promise of immunotherapy into clinical reality with minimal associated toxicities.

Check point inhibitors

Check point inhibition is an immunomodulatory strategy used to boost immune responses against the cancer [6]. It is well known that cancer cells have numerous mechanisms to silence the local immune system and the result is cancer progression even in immunocompetent individuals [7]. The check point inhibitors physiologically activate immune responses, including T cell activation, proliferation and cytokine and target lymphocyte receptors to counteract the immune system tolerance evoked by the oncological process. With respect to the latter, immunology tolerance of tumors is mainly mediated by the co-stimulatory pathway, and mainly includes aberrant activity the programmed death-1 receptor (PD-1) and its ligand (PD-L) and the cytotoxic T lymphocyte associated antigen 4 (CTLA-4) [8,9]. Currently there are several immune check point inhibitors as commercially available drugs and more drugs are in clinical trial procedure (Figure 1). Ipilimumab an anti-cytotoxic T-lymphocyte-associate protein (CTLA)-4 humanized antibody, was the first to be indicated for the treatment of metastatic melanoma. PD-1 targeting drugs, nivolumab and pembrolizumab, were approved for multiple advanced malignancies, including non-small cell lung cancer [10].

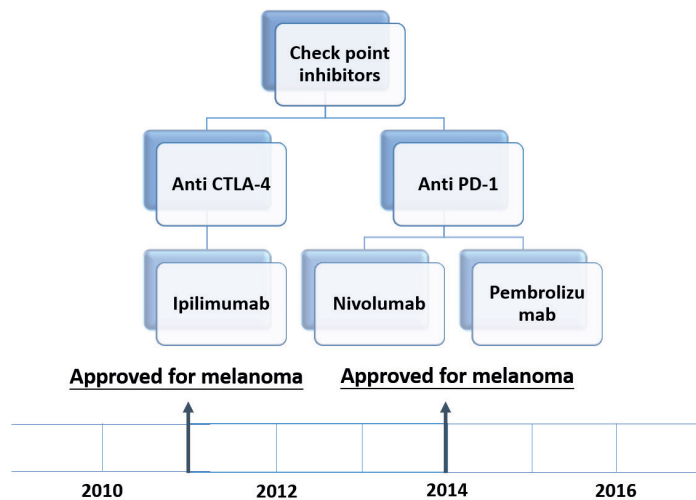


Figure 1 general introduction

Checkpoint inhibitors appear to offer an advantage compared with conventional chemotherapy and the survival curves indicate increased patient remission. But immune checkpoint inhibitors are hampered by side effects, prominently including IBD-like colitis.

Side effects

Check point inhibitors comes with a broad spectrum of side effects related to excessive immune activation, and this is reported in many studies. The most common side effects encountered are colitis and hepatitis and thus involve the gastrointestinal system [11]. Type 1 diabetes and acute kidney injury are also among the most frequently reported side effects of the immune checkpoint inhibitor therapy (Figure 2). Since in the majority situation five cycles of therapy would induce pancreatic dysfunction, it is necessary to closely monitor pancreatic function in addition to the evaluation of other systems [12]. Initiation of steroids and supportive therapy with medicine for symptom treatment could solve the problems in a majority of cases. However, there were a few cases that developed side effects without optimized follow up treatment and failed to consider the cell-based underlying mechanism of check point inhibitors.

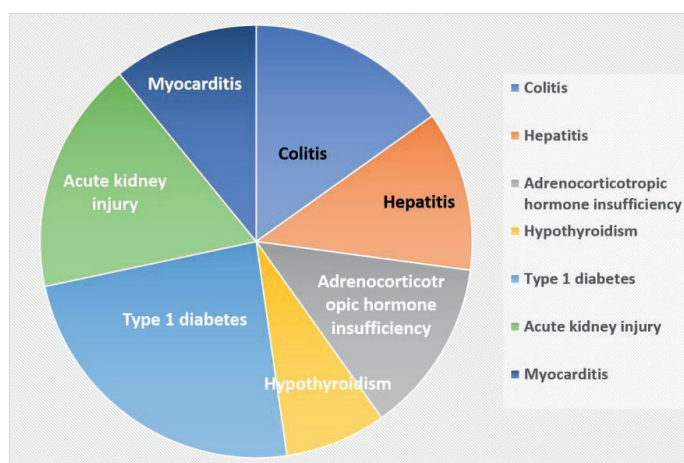


Figure 2 The common side effects of checkpoint inhibitors.

In this context, we read with interest the case described by Yanai *et al* in which these investigators described a patient who developed ulcerative colitis under uveal melanoma-indicated nivolumab therapy [13]. Nivolumab is an immunologic check-point inhibitor that combats oncologic disease by removing regulatory control on the T-cell compartment and thus up-regulating cytotoxic T-cell-mediated antitumor immunity. The resulting up-regulation of T-cell immunity, however, can be accompanied by autoimmunity, and colitis is especially a side effect of immune check-point inhibition [14]. In the described case the colitis was managed successfully by infliximab therapy.

Anti-tumor necrosis factor (TNF)- α medication in general and infliximab in particular has revolutionized the treatment of inflammatory bowel disease. Intriguingly, however, infliximab does not counteract colitis through neutralization of soluble TNF- α , as also evident from the failure of the anti-TNF- α medication etanercept to control colitis [15]. In contrast, infliximab binds directly to membrane-bound TNF- α on lymphocytes and causes T-cell apoptosis [16]. Indeed, the clinical efficacy of infliximab shows a strict correlation with T-lymphocyte apoptosis in patients in vivo [17]. Therefore, infliximab should be expected to counteract the clinical effect of nivolumab in oncologic disease by impairing T-cell-mediated immunity. Hence, infliximab thus is not a rational choice for counteracting nivolumab-induced colitis.

There are other options to manage nivolumab-associated colitis available that do not interfere with nivolumab-mediated anticancer immunity (eg, vedolizumab). However, we also would like to point to the study by Kubo *et al* that documented the efficacy of mesalazine in controlling nivolumab-associated colitis [18]. Mesalazine is safe, inexpensive, and is not expected to counteract nivolumab-induced anticancer immunity. If the observations of Kubo *et al* are confirmed, mesalazine would constitute a superior alternative to infliximab [18].

Discussion

The loss of the immunological balance has been confirmed as one of cancer hallmarks [19]. Check point inhibitors, as a promising anticancer treatment, represents one of the most successful approach for treating multiple cancers, such as metastatic melanoma, non-small cell lung cancer (NSCLC) and cervical cancer [20]. Currently, there are two classes of immunotherapy that have been approved for clinical use. Numerous other cancer types, including breast cancer, were treated by check point inhibitors in clinical trials [21]. Such therapy, however, is complicated by side effects, prominently including IBD-like colitis. The side effect profile of check point inhibitors is consistent with their mechanism of action, which is the reason that different side effect pattern emerged between CTLA-4 and PD-1 targeting antibodies. The most common side effects include gastro-intestinal, hepatic and endocrine events and they are also the most frequent and earliest side effects. Furthermore, side effects also depend on tumor-related factor, such as the primary site of the cancer.

To understand the immunity and microbiome driving colitis, we decided to evaluate whether current strategies are rational in terms of the contemporary biomedical literature. We evaluated studies recent years how the mitigate the effects involved and conclude that some of the strategies involved, especially anti-TNF, which has proven spectacularly successful in managing IBD-dependent colitis [22], may not be the best choice to manage the side effects of these anti-cancer drugs in this respect. Generally speaking, we feel that this issue needs much more attention to improve quality of life and minimize side effects on patients. Also we would like to mention that with respect to preventing inflammation-related cancer, in the IBD field substantial experience might also benefit physicians managing inflammatory liver diseases. Now days improved techniques for immune cell manipulation and engineering have create fresh path to new treatment and that may generate more promising immunotherapies, which will play a more important role in the treatment of cancer.

Reference

1. Siegel, R.L.; Miller, K.D.; Jemal, A. Cancer statistics, 2020. *CA Cancer J Clin* **2020**, *70*, 7-30, doi:10.3322/caac.21590.
2. Farkona, S.; Diamandis, E.P.; Blasutig, I.M. Cancer immunotherapy: the beginning of the end of cancer? *BMC Med* **2016**, *14*, 73, doi:10.1186/s12916-016-0623-5.
3. Okiyama, N.; Tanaka, R. Varied immuno-related adverse events induced by immune-check point inhibitors - Nivolumab-associated psoriasiform dermatitis related with increased serum level of interleukin-6. *Nihon Rinsho Meneki Gakkai Kaishi* **2017**, *40*, 95-101, doi:10.2177/jsci.40.95.
4. Izzedine, H.; Gueutin, V. [Immune check point inhibitor-associated renal toxicity]. *Nephrol Ther* **2019**, 10.1016/j.nephro.2019.05.006, doi:10.1016/j.nephro.2019.05.006.
5. Kumar, P.; Saini, S.; Prabhakar, B.S. Cancer immunotherapy with check point inhibitor can cause autoimmune adverse events due to loss of Treg homeostasis. *Semin Cancer Biol* **2019**, 10.1016/j.semcancer.2019.01.006, doi:10.1016/j.semcancer.2019.01.006.
6. Sharma, P.; Allison, J.P. Immune checkpoint targeting in cancer therapy: toward combination strategies with curative potential. *Cell* **2015**, *161*, 205-214, doi:10.1016/j.cell.2015.03.030.
7. La-Beck, N.M.; Jean, G.W.; Huynh, C.; Alzghari, S.K.; Lowe, D.B. Immune Checkpoint Inhibitors: New Insights and Current Place in Cancer Therapy. *Pharmacotherapy* **2015**, *35*, 963-976, doi:10.1002/phar.1643.
8. De Felice, F.; Musio, D.; Cassese, R.; Gravina, G.L.; Tombolini, V. New Approaches in Glioblastoma Multiforme: The Potential Role of Immune- check Point Inhibitors. *Curr Cancer Drug Targets* **2017**, *17*, 282-289, doi:10.2174/1568009616666160813183738.
9. De Felice, F.; Marchetti, C.; Palaia, I.; Ostuni, R.; Muzii, L.; Tombolini, V.; Benedetti Panici, P. Immune check-point in cervical cancer. *Crit Rev Oncol Hematol* **2018**, *129*, 40-43, doi:10.1016/j.critrevonc.2018.06.006.
10. Sharma, P.; Allison, J.P. The future of immune checkpoint therapy. *Science* **2015**, *348*, 56-61, doi:10.1126/science.aaa8172.
11. Bajwa, R.; Cheema, A.; Khan, T.; Amirpour, A.; Paul, A.; Chaughtai, S.; Patel, S.; Patel, T.; Bramson, J.; Gupta, V., et al. Adverse Effects of Immune Checkpoint Inhibitors (Programmed Death-1 Inhibitors and Cytotoxic T-Lymphocyte-Associated Protein-4 Inhibitors): Results of a Retrospective Study. *J Clin Med Res* **2019**, *11*, 225-236, doi:10.14740/jocmr3750.
12. Guleria, I.; Gubbels Bupp, M.; Dada, S.; Fife, B.; Tang, Q.; Ansari, M.J.; Trikudanathan, S.; Vadivel, N.; Fiorina, P.; Yagita, H., et al. Mechanisms of PDL1-mediated regulation of autoimmune diabetes. *Clin Immunol* **2007**, *125*, 16-25, doi:10.1016/j.clim.2007.05.013.
13. Yanai, S.; Nakamura, S.; Matsumoto, T. Nivolumab-Induced Colitis Treated by Infliximab. *Clin Gastroenterol Hepatol* **2017**, *15*, e80-e81, doi:10.1016/j.cgh.2016.09.017.

14. Postow, M.A. Managing immune checkpoint-blocking antibody side effects. *Am Soc Clin Oncol Educ Book* **2015**, 10.14694/EdBook_AM.2015.35.76, 76-83, doi:10.14694/EdBook_AM.2015.35.76.
15. Sandborn, W.J.; Hanauer, S.B.; Katz, S.; Safdi, M.; Wolf, D.G.; Baerg, R.D.; Tremaine, W.J.; Johnson, T.; Diehl, N.N.; Zinsmeister, A.R. Etanercept for active Crohn's disease: a randomized, double-blind, placebo-controlled trial. *Gastroenterology* **2001**, *121*, 1088-1094, doi:10.1053/gast.2001.28674.
16. Van den Brande, J.M.; Braat, H.; van den Brink, G.R.; Versteeg, H.H.; Bauer, C.A.; Hoedemaeker, I.; van Montfrans, C.; Hommes, D.W.; Peppelenbosch, M.P.; van Deventer, S.J. Infliximab but not etanercept induces apoptosis in lamina propria T-lymphocytes from patients with Crohn's disease. *Gastroenterology* **2003**, *124*, 1774-1785, doi:10.1016/s0016-5085(03)00382-2.
17. Van den Brande, J.M.; Koehler, T.C.; Zelinkova, Z.; Bennink, R.J.; te Velde, A.A.; ten Cate, F.J.; van Deventer, S.J.; Peppelenbosch, M.P.; Hommes, D.W. Prediction of antitumour necrosis factor clinical efficacy by real-time visualisation of apoptosis in patients with Crohn's disease. *Gut* **2007**, *56*, 509-517, doi:10.1136/gut.2006.105379.
18. Kubo, K.; Kato, M.; Mabe, K. Nivolumab-Associated Colitis Mimicking Ulcerative Colitis. *Clin Gastroenterol Hepatol* **2017**, *15*, A35-A36, doi:10.1016/j.cgh.2017.03.026.
19. Hanahan, D.; Weinberg, R.A. Hallmarks of cancer: the next generation. *Cell* **2011**, *144*, 646-674, doi:10.1016/j.cell.2011.02.013.
20. Couzin-Frankel, J. Breakthrough of the year 2013. Cancer immunotherapy. *Science* **2013**, *342*, 1432-1433, doi:10.1126/science.342.6165.1432.
21. Hu, X.; Huang, W.; Fan, M. Emerging therapies for breast cancer. *J Hematol Oncol* **2017**, *10*, 98, doi:10.1186/s13045-017-0466-3.
22. Deuring, J.J.; Li, M.; Cao, W.; Chen, S.; Wang, W.; de Haar, C.; van der Woude, C.J.; Peppelenbosch, M. Pregnane X receptor activation constrains mucosal NF-kappaB activity in active inflammatory bowel disease. *PLoS One* **2019**, *14*, e0221924, doi:10.1371/journal.pone.0221924.

CHAPTER 9

General discussion and summary

Liver cancer, a group of diseases that prominently includes hepatocellular carcinoma (HCC) and cholangiocarcinoma (CCA), shows as rapid increase in an already high incidence and thus has become one of the most prevalent types of cancers worldwide [1,2]. Also because of inadequacy of current treatment options, liver cancer represents one of the most common causes of cancer related death and consequently this group of diseases is considered a major global public health challenge [3]. Progress with respect to improving clinical management is frustratingly slow and inadequate [4,5]. The work in this thesis was initiated from the notion that improved prevention and treatment of liver cancer requires better understanding of the molecular and cellular factors governing its initiation and that determine treatment success, including side effects. In addition further understanding of the processes restraining inflammatory responses in endodermal derivatives *per se* may also prove useful in this respect. Thus I also undertook to obtain better understanding of inflammatory bowel disease. The preceding chapters describe the fruits of these efforts, while in this chapter, I aim to summarize these results and discuss the main discoveries in light of body of contemporary biomedical literature.

Understanding the strategy taken requires an overview of existing relevant literature and thus prior providing an outline of this thesis, in [Chapter 1](#), I provide a concise review on selected aspects of the intracellular and extracellular signalling pathways controlling physiology in the liver and the intestine. To this end I discuss 1) the role of mitochondrial dynamics and mitochondrial electron transport chain in liver cancer; 2) the role of cancer-associated fibroblasts (CAFs), the major component of tumor microenvironment, in proliferation and angiogenesis of liver tumor cells, 3) the role of LGR5-marked tumor initiating cells in liver cancer, 4) the role of PXR levels with respect to NF- κ B target gene expression and the side effects of check point inhibition in inflammatory bowel disease (IBD). Together the knowledge provided enable me to explain the strategy taken when pursuing this thesis.

Mitochondria and cancer metabolism

Mitochondrial, comprised of outer membrane and inner membrane, play central roles in cell functions [6]. These cellular biochemical powerhouses show a highly dynamic morphological aspects in response to the alterations of metabolic environment, driven by constantly fission (division of mitochondria) and fusion (elongation of mitochondria) [7,8]. Various elements driving these changes in morphological aspect have been identified and include the outer mitochondrial membrane proteins Mfn1 and Mfn2, and the inner mitochondrial membrane protein OPA1 [9,10]. Previously, work in my host laboratory had shown that Hepatitis E virus infection induces mitochondrial fusion to facilitate viral replication by interfering with cell-autonomous innate immunity (Yijin Wang, thesis, ISBN: 978-94-6169-903-9). The importance of these morphological alterations in the context of liver cancer had, however, not been addressed prompting my further investigations in this respect.

In [Chapter 2](#), I present the fruits of these efforts showing that inhibiting mitochondrial fusion in HCC cell lines and CCA tumor organoids, causes cell growth to be inhibited in vitro and

abrogates in vivo tumor formation in mice. I found that the inhibition of fusion triggered apoptosis, pointing to an anti-apoptotic role of mitochondrial fusion in HCC, an effect hitherto not reported in the biomedical literature. My results appear, however, to be in line with previously reported findings that mitochondrial fusion proteins are essential for maintenance of the mitochondrial membrane structure, maintaining mitochondrial matrix homogeneity and also for mitochondrial genome integrity, which are all vital for cell survival [11,12]. Mechanistically, my findings most likely relate to my observation that dysfunction of mitochondrial fusion provoked increased ROS production while concomitantly oxygen consumption and ATP production were compromised in the liver cancer cells examined. This fits well with previous studies that indicated that mitochondrial dynamics and ROS processes influence each other in various other types of cancer [13,14]. Clearly, mitochondrial fusion dysfunction has pleiotropic effects on multiple cell functions and my study has probably only uncovered a small part of these.

On the other hand, mitochondrial fission and its key regulator Drp1 had already been widely studied in various types of cancers. Drp1 has been reported to be overexpressed in so-called oncocytic thyroid tumors, but decreased in malignant colon and lung cancer tissues, whereas no change was observed in breast and prostate cancer [15,16]. Thus, Drp1 effects in oncological disease are context dependent. Overall, fission is thought to be pro-tumorigenic, although it remains a matter of debate whether it has pro- or anti-apoptotic function [17]. In MYC transformed cells, it has been demonstrated that fusion promotes mitochondrial metabolism to support cell proliferation [18-20]. The lack of clarity in this respect prompted me to performed genome-wide transcriptomic analysis in liver cancer. Consistent with the work cited above, the inhibition of fusion affected most predominantly expression of genes associated with metabolic pathways. Functionally, I demonstrated that the knockdown of mitochondrial fusion genes inhibited oxygen consumption and ATP production in HCC cell lines and CCA tumor organoids; as the latter two processes are the hallmarks of mitochondrial metabolism, it appears that fusion is directly necessary for appropriate mitochondrial functionality. Although fission has been widely recognized as pro-tumorigenic, it has also been reported to decrease mitochondrial oxygen consumption rate and ATP production in malignant cells [21]. The morphodynamics and functions of mitochondria are rather multifaceted, highly depending on the cancer types and specific context. Thus, the distinct observations from different studies appear but may not be necessarily in contradiction with each other. Further investigations are necessary to address this issue.

Besides critical functions for cellular bioenergetics, in cancer mitochondria also provide tumor cell anabolism, calcium homeostasis, and govern cell death by controlling apoptotic and pyroptotic processes [22,23]. Metabolic reprogramming universally occurs in cancer [24]. Mitochondrial electron transport chain (ETC) process two electron flows in mitochondrial ETC to produce ATP: Complex I/III/IV, with as a substrate NADH and complex II/III/IV, with as a substrate succinic acid [25]. Due to the large local electron flow, the ETC is the major source of mitochondrial ROS and is also vital for mitochondrial membrane potential maintenance [26].

Therefore, mitochondria electron transport chain may provide a valuable therapeutic option for the future treatment of liver cancer, reminiscent to the situation my colleague dr Changbo Qu encountered with respect to cell autonomous viral immunity [27,28]. The similarities of mitochondrial function in viral disease and cancer are intriguing and deserve further exploration.

To this end in [Chapter 3](#), I targeted mETC complex I and III by gene knock down or employing inhibitors such as metformin. It found that liver cancer cell growth was inhibited both in vitro and during in vivo tumor formation in mice such inhibition stimulated cell apoptosis. These results indicate mETC may represent intriguing therapeutic targets in liver cancer. Recently an intensive research effort has been focusing on drugs like metformin, a well-known inhibitor of complex I [29,30]. Previous studies demonstrated that metformin showed anti-cancer effects via inhibition of complex I and activation of AMP-activated protein kinase (AMPK) [31]. In search for more efficient drugs, I analyzed inhibitors of complex I, complex II, complex III and complex IV and found that mETC complex I (ROT and Met) and III (AMA and MYXO) inhibitors produced obvious inhibition of HCC cells survival and growth in a dose-dependent manner, while complex II (TTFA) and IV (KCN) inhibitors evoked slight inhibition of HCC cell vitality. However and maybe resembling the situation encountered with hepatitis virus research. the exact mechanisms by which mitochondrial ETC modulates this apoptotic process remain to be elucidated. The labyrinthine complexity of the HCC process is an obvious impediment of progress in this area.

Cancer associated fibroblasts

Following investigations of the liver cancer cell interior, I decided to explore the dependency of these cells on their environment. The cancer-associated fibroblasts (CAFs), as a major component of tumor microenvironment, play a role in cancer progression and drug resistance in general [32,33]. I attempted to study their role in liver cancer by creating a model that is essentially a co-culture system of CAFs and cancer cells. I reasoned that employing such cultures I might establish a 'more clinically relevant' tumor model to better mimic the real situation *in vivo*. Among the possible cellular interactions of cancer cells with the tumor microenvironment, the interaction between cancer cells and fibroblasts is thought to contribute to tumor initiation, progression and metastasis in many cancer types, even if its role in liver cancer remains large uncharacterized [34,35]. Enticingly, these models could also be used to test anticancer agents [36]. Thus I decided this angle of the liver cancer process.

In [Chapter 4](#), I present an organoid-based co-culture model that integrates tumor organoids with CAFs. I observe that proliferation of tumor cells is significantly promoted in co-cultures when compared with the control group. As situation in vivo is more reminiscent to co-cultures I feel that the reciprocal interaction between tumor organoids and fibroblasts I uncovered should be interpreted as that the co-culture system would be more suitable for drug screening as compared to conventional technology. In addition, this system should help dissecting the role of the tumor microenvironment in the liver cancer process. Underlying mechanisms that

explain the effects of co-culture include the induction of the epithelial-to-mesenchymal transition (EMT) in the cancer cells (a precursor of metastasis), induction of increased stemness (associated with therapy resistance) and metabolic reprogramming (a widely observed hallmark of cancer cells). In conjunction these CAF-mediated effects on tumor cells may explain tumor progression and therapy resistance [37-40]. Despite the progress in the field with respect to understanding CAF biology, I feel my model is significant importance to the field because most of the current studies are based on in vitro assays working with a limited number of immortalized cell lines, while my model involves working directly with cells derived from patients and captures the variety in cell types better. I hope these studies may give more insight to the activity of CAFs and interaction between CAFs and cancer cells in turn producing superior therapy.

However, despite the large amount of work that has been done, more efforts are needed in this area. If, however, they prove successful, it may well prove possible to translate CAF-directed anti-cancer strategies from the bench to the clinic.

Cancer stem cells

Understanding the biology of cancer stem cells remains challenging, but may ultimately also lead to improved therapy. In this thesis I tried to use organoids to obtain better understanding of cancer stem cells. Organoids are stem cell derived organ-like 3D structures. Organoids system not only offer a promising platform for stem cell research, but could also be used for modeling a wide range of diseases, including inflammatory bowel disease (IBD) as I showed in this thesis [41,42]. Stem cells in cancer are considered to be responsible for tumor initiation and growth, therapy resistance and tumor recurrence [43,44]. LGR5, the leucine-rich-repeat-containing G-protein-coupled receptor 5, marks a group of stem cells proliferating after liver injury induced by carbon tetrachloride (CCL4) [45]. LGR5 in cancer cells marks a cancer stem cell population in intestinal and colorectal carcinoma. The role of this group of stem cells in liver cancer remained, however, obscure at best.

My study demonstrated LGR5 cells were induced by DEN injection (a procedure that provokes pre-cancerous liver damage often progressing further). Furthermore, I observed tumor that LGR5 cells have a much stronger initiation ability (the capacity to seed new organoids) in established organoid culture systems from primary liver tumors and also with respect to in vivo tumor initiation capacity. I describe the findings involved in [Chapter 5](#) and [Chapter 6](#). I also observed that the percentage of LGR5 cells was significantly higher in tumor tissue compared with the tumor surrounding tissue. Studies in colon cancer indicate that depletion of LGR5 compartment can impede both the growth of the primary tumor as well as metastasis [46]. Upon tissue injury, reprogramed LGR5 cells are induced apparently by modulating the Wnt homeostatic program, as well as through activation of epidermal growth factor receptor signaling [47]. The canonical Wnt/ β -catenin signalling governs diverse developmental, homeostatic and pathological pathways. Without Wnt ligands and R-sponding ligands present,

the default fate of LGR5 cells is to differentiate and I think this especially relates to the effects seen in this chapter [48].

An important point highlighted by my studies is that targeting the cancer stem cell system is useful as it abrogates the potential of the cancer to recover from chemotherapeutic insult. The apparent advantage of specifically targeting cancer stem cells such as LGR5 cells is that it opens a window to more superior therapeutic effect of existing therapies, potentially leading to long-term clinical benefit. If the observations seen can be extrapolated to other cancers as well, my studies may thus help generating a framework for developing a novel therapeutic regimens for oncological disease in general.

Inflammatory bowel disease

IBD has two major distinct phenotypes: Crohn's disease (CD) and ulcerative colitis (UC). CD is characterized by trans-mural and patchy inflammation that can occur along the entire GI tract but mostly involves the terminal ileum and colon (although not the rectum), while UC is characterized by superficial inflammation typically involving the large intestine only [49,50]. IBD is a multifactorial disease of a chronic nature and relatively well accessible to study as for instance compared to hepatitis. It is thus tempting to study IBD also for understanding how chronic inflammation in endodermal derivatives can progress to cancer. Indeed, IBD can progress to IBD related colorectal cancer (CRC) and my host had significantly contributed to understanding the processes involved and how to manage patients in this respect, further justifying investigating this disease rather as hepatitis itself in my quest to better understand the liver cancer process [51-54]. Earlier studies demonstrated defective xenobiotic resistance mechanisms in effector T cells for preventing Crohn's-like ileitis in experimental animals [55]. Pregnane X receptor (PXR) agonists enhance intestinal epithelial wound healing and repair of the intestinal barrier following the induction of experimental colitis [56]. It is fair to say that the exact functionality of xenobiotic receptors remains poorly understood in IBD. As xenobiotic signaling is also important in the liver, I decided to investigate the mechanisms involved better.

In [Chapter 7](#), I investigated correlation of PXR levels with NF- κ B target gene expression in IBD and explored side effects of check point inhibition. Treatment with rifampicin reduces NF- κ B activity showing that PXR activity is a rate-limiting step with respect to CD-associated NF- κ B activity. These effects were also verified in-vitro. Our data suggest that the presence of PXR is the main mechanism counteracting and limiting the epithelial NF- κ B activity in patients with active IBD. Modulation of PXR activity thus holds therapeutic promise in the clinical management of CD and it would be interesting to see if also for liver inflammation a similar situation hold true.

Interestingly, immune check point inhibition is an immunomodulatory strategy used to boost immune responses and is also explored in the context of liver cancer [57]. Such therapy, however, is complicated by side effects, prominently including IBD-like colitis. Also building

substantial expertise in the host laboratory with respect to understanding the immunity and microbiome driving colitis, I decided to evaluate whether current strategies are rational in the context of the body of the contemporary biomedical literature [58]. We evaluated studies recent years how the mitigate the effects involved and conclude that some of the strategies involved, especially anti-TNF (which has proven spectacularly successful in managing IBD-dependent colitis, insight to which also my host department contributed [59]) may very well be not the optimal option to manage the side effects of these anti-cancer drugs in this respect. I discuss this issue in [Chapter 8](#). Generally speaking, I feel that this issue needs much more attention to improve quality of life and that oncologists would benefit to seek the opinion of IBD-specialized physicians before embarking on check point-directed therapy. Also I would like to mention that with respect to preventing inflammation-related cancer, in the IBD field substantial experience is now available to might also benefit physicians managing inflammatory liver diseases.

Overall I have tried in this thesis to address many aspects of cancer and also inflammation in the field of gastroenterology and hepatology and I hope the studies described in the above of this thesis will finally contribute to better management of such diseases.

Reference

1. Bray, F.; Ferlay, J.; Soerjomataram, I.; Siegel, R.L.; Torre, L.A.; Jemal, A. Global cancer statistics 2018: GLOBOCAN estimates of incidence and mortality worldwide for 36 cancers in 185 countries. *CA Cancer J Clin* **2018**, *68*, 394-424, doi:10.3322/caac.21492.
2. Yang, J.D.; Hainaut, P.; Gores, G.J.; Amadou, A.; Plymoth, A.; Roberts, L.R. A global view of hepatocellular carcinoma: trends, risk, prevention and management. *Nat Rev Gastroenterol Hepatol* **2019**, *16*, 589-604, doi:10.1038/s41575-019-0186-y.
3. Scudellari, M. Drug development: try and try again. *Nature* **2014**, *516*, S4-6, doi:10.1038/516S4a.
4. Forner, A.; Reig, M.; Bruix, J. Hepatocellular carcinoma. *Lancet* **2018**, *391*, 1301-1314, doi:10.1016/S0140-6736(18)30010-2.
5. Yang, J.D.; Roberts, L.R. Hepatocellular carcinoma: A global view. *Nat Rev Gastroenterol Hepatol* **2010**, *7*, 448-458, doi:10.1038/nrgastro.2010.100.
6. Ortmayr, K.; Dubuis, S.; Zampieri, M. Metabolic profiling of cancer cells reveals genome-wide crosstalk between transcriptional regulators and metabolism. *Nat Commun* **2019**, *10*, 1841, doi:10.1038/s41467-019-09695-9.
7. Chen, H.; Chomyn, A.; Chan, D.C. Disruption of fusion results in mitochondrial heterogeneity and dysfunction. *J Biol Chem* **2005**, *280*, 26185-26192, doi:10.1074/jbc.M503062200.
8. Chen, H.; Detmer, S.A.; Ewald, A.J.; Griffin, E.E.; Fraser, S.E.; Chan, D.C. Mitofusins Mfn1 and Mfn2 coordinately regulate mitochondrial fusion and are essential for embryonic development. *J Cell Biol* **2003**, *160*, 189-200, doi:10.1083/jcb.200211046.
9. Nunnari, J.; Suomalainen, A. Mitochondria: in sickness and in health. *Cell* **2012**, *148*, 1145-1159, doi:10.1016/j.cell.2012.02.035.
10. Chan, D.C. Mitochondria: dynamic organelles in disease, aging, and development. *Cell* **2006**, *125*, 1241-1252, doi:10.1016/j.cell.2006.06.010.
11. Cogliati, S.; Frezza, C.; Soriano, M.E.; Varanita, T.; Quintana-Cabrera, R.; Corrado, M.; Cipolat, S.; Costa, V.; Casarin, A.; Gomes, L.C., et al. Mitochondrial cristae shape determines respiratory chain supercomplexes assembly and respiratory efficiency. *Cell* **2013**, *155*, 160-171, doi:10.1016/j.cell.2013.08.032.
12. Frezza, C.; Cipolat, S.; Martins de Brito, O.; Micaroni, M.; Bezoussenko, G.V.; Rudka, T.; Bartoli, D.; Polishuck, R.S.; Danial, N.N.; De Strooper, B., et al. OPA1 controls apoptotic cristae remodeling independently from mitochondrial fusion. *Cell* **2006**, *126*, 177-189, doi:10.1016/j.cell.2006.06.025.
13. Huang, Q.; Zhan, L.; Cao, H.; Li, J.; Lyu, Y.; Guo, X.; Zhang, J.; Ji, L.; Ren, T.; An, J., et al. Increased mitochondrial fission promotes autophagy and hepatocellular carcinoma cell survival through

- the ROS-modulated coordinated regulation of the NFKB and TP53 pathways. *Autophagy* **2016**, 12, 999-1014, doi:10.1080/15548627.2016.1166318.
14. Hu, J.; Zhang, Y.; Jiang, X.; Zhang, H.; Gao, Z.; Li, Y.; Fu, R.; Li, L.; Li, J.; Cui, H., et al. ROS-mediated activation and mitochondrial translocation of CaMKII contributes to Drp1-dependent mitochondrial fission and apoptosis in triple-negative breast cancer cells by isorhamnetin and chloroquine. *J Exp Clin Cancer Res* **2019**, 38, 225, doi:10.1186/s13046-019-1201-4.
 15. Ferreira-da-Silva, A.; Valacca, C.; Rios, E.; Populo, H.; Soares, P.; Sobrinho-Simoes, M.; Scorrano, L.; Maximo, V.; Campello, S. Mitochondrial dynamics protein Drp1 is overexpressed in oncocytic thyroid tumors and regulates cancer cell migration. *PLoS One* **2015**, 10, e0122308, doi:10.1371/journal.pone.0122308.
 16. Downregulation of Drp1, a fission regulator, is associated with human lung and colon cancers. **2018**, 50, 209-215, doi:10.1093/abbs/gmx137.
 17. Maycotte, P.; Marin-Hernandez, A.; Goyri-Aguirre, M.; Anaya-Ruiz, M.; Reyes-Leyva, J.; Cortes-Hernandez, P. Mitochondrial dynamics and cancer. *Tumour Biol* **2017**, 39, 1010428317698391, doi:10.1177/1010428317698391.
 18. Graves, J.A.; Wang, Y.; Sims-Lucas, S.; Cherok, E.; Rothermund, K.; Branca, M.F.; Elster, J.; Beer-Stolz, D.; Van Houten, B.; Vockley, J., et al. Mitochondrial structure, function and dynamics are temporally controlled by c-Myc. *PLoS One* **2012**, 7, e37699, doi:10.1371/journal.pone.0037699.
 19. Dang, C.V. MYC, metabolism, cell growth, and tumorigenesis. *Cold Spring Harb Perspect Med* **2013**, 3, doi:10.1101/cshperspect.a014217.
 20. Stine, Z.E.; Walton, Z.E.; Altman, B.J.; Hsieh, A.L.; Dang, C.V. MYC, Metabolism, and Cancer. *Cancer Discov* **2015**, 5, 1024-1039, doi:10.1158/2159-8290.CD-15-0507.
 21. Serasinghe, M.N.; Wieder, S.Y.; Renault, T.T.; Elkholi, R.; Asciolla, J.J.; Yao, J.L.; Jabado, O.; Hoehn, K.; Kageyama, Y.; Sesaki, H., et al. Mitochondrial division is requisite to RAS-induced transformation and targeted by oncogenic MAPK pathway inhibitors. *Mol Cell* **2015**, 57, 521-536, doi:10.1016/j.molcel.2015.01.003.
 22. Kroemer, G.; Pouyssegur, J. Tumor cell metabolism: cancer's Achilles' heel. *Cancer Cell* **2008**, 13, 472-482, doi:10.1016/j.ccr.2008.05.005.
 23. Vyas, S.; Zaganjor, E.; Haigis, M.C. Mitochondria and Cancer. *Cell* **2016**, 166, 555-566, doi:10.1016/j.cell.2016.07.002.
 24. Schwartz, L.; Supuran, C.T.; Alfarouk, K.O. The Warburg Effect and the Hallmarks of Cancer. *Anticancer Agents Med Chem* **2017**, 17, 164-170, doi:10.2174/1871520616666161031143301.
 25. Mitchell, P. Coupling of phosphorylation to electron and hydrogen transfer by a chemi-osmotic type of mechanism. *Nature* **1961**, 191, 144-148, doi:10.1038/191144a0.
 26. Zhao, R.Z.; Jiang, S.; Zhang, L.; Yu, Z.B. Mitochondrial electron transport chain, ROS generation and uncoupling (Review). *Int J Mol Med* **2019**, 44, 3-15, doi:10.3892/ijmm.2019.4188.

27. Rohlena, J.; Dong, L.F.; Ralph, S.J.; Neuzil, J. Anticancer drugs targeting the mitochondrial electron transport chain. *Antioxid Redox Signal* **2011**, *15*, 2951-2974, doi:10.1089/ars.2011.3990.
28. Qu, C.; Zhang, S.; Li, Y.; Wang, Y.; Peppelenbosch, M.P.; Pan, Q. Mitochondria in the biology, pathogenesis, and treatment of hepatitis virus infections. *Rev Med Virol* **2019**, *29*, e2075, doi:10.1002/rmv.2075.
29. He, C.; Jiang, S.; Jin, H.; Chen, S.; Lin, G.; Yao, H.; Wang, X.; Mi, P.; Ji, Z.; Lin, Y., et al. Mitochondrial electron transport chain identified as a novel molecular target of SPIO nanoparticles mediated cancer-specific cytotoxicity. *Biomaterials* **2016**, *83*, 102-114, doi:10.1016/j.biomaterials.2016.01.010.
30. Urrea, F.A.; Weiss-Lopez, B.; Araya-Maturana, R. Determinants of Anti-Cancer Effect of Mitochondrial Electron Transport Chain Inhibitors: Bioenergetic Profile and Metabolic Flexibility of Cancer Cells. *Curr Pharm Des* **2016**, *22*, 5998-6008, doi:10.2174/1381612822666160719122626.
31. Foretz, M.; Guigas, B.; Bertrand, L.; Pollak, M.; Viollet, B. Metformin: from mechanisms of action to therapies. *Cell Metab* **2014**, *20*, 953-966, doi:10.1016/j.cmet.2014.09.018.
32. Kalluri, R.; Zeisberg, M. Fibroblasts in cancer. *Nat Rev Cancer* **2006**, *6*, 392-401, doi:10.1038/nrc1877.
33. Allaoui, R.; Bergenfelz, C.; Mohlin, S.; Hagerling, C.; Salari, K.; Werb, Z.; Anderson, R.L.; Ethier, S.P.; Jirstrom, K.; Pahlman, S., et al. Cancer-associated fibroblast-secreted CXCL16 attracts monocytes to promote stroma activation in triple-negative breast cancers. *Nat Commun* **2016**, *7*, 13050, doi:10.1038/ncomms13050.
34. Houthuijzen, J.M.; Jonkers, J. Cancer-associated fibroblasts as key regulators of the breast cancer tumor microenvironment. *Cancer Metastasis Rev* **2018**, *37*, 577-597, doi:10.1007/s10555-018-9768-3.
35. Friedrich, J.; Seidel, C.; Ebner, R.; Kunz-Schughart, L.A. Spheroid-based drug screen: considerations and practical approach. *Nat Protoc* **2009**, *4*, 309-324, doi:10.1038/nprot.2008.226.
36. Aref, A.R.; Huang, R.Y.; Yu, W.; Chua, K.N.; Sun, W.; Tu, T.Y.; Bai, J.; Sim, W.J.; Zervantonakis, I.K.; Thiery, J.P., et al. Screening therapeutic EMT blocking agents in a three-dimensional microenvironment. *Integr Biol (Camb)* **2013**, *5*, 381-389, doi:10.1039/c2ib20209c.
37. Kalluri, R. The biology and function of fibroblasts in cancer. *Nat Rev Cancer* **2016**, *16*, 582-598, doi:10.1038/nrc.2016.73.
38. Brabletz, T.; Kalluri, R.; Nieto, M.A.; Weinberg, R.A. EMT in cancer. *Nat Rev Cancer* **2018**, *18*, 128-134, doi:10.1038/nrc.2017.118.
39. Su, S.; Chen, J.; Yao, H.; Liu, J.; Yu, S.; Lao, L.; Wang, M.; Luo, M.; Xing, Y.; Chen, F., et al. CD10(+)GPR77(+) Cancer-Associated Fibroblasts Promote Cancer Formation and

- Chemoresistance by Sustaining Cancer Stemness. *Cell* **2018**, *172*, 841-856 e816, doi:10.1016/j.cell.2018.01.009.
40. Mishra, R.; Haldar, S.; Placencio, V.; Madhav, A.; Rohena-Rivera, K.; Agarwal, P.; Duong, F.; Angara, B.; Tripathi, M.; Liu, Z., et al. Stromal epigenetic alterations drive metabolic and neuroendocrine prostate cancer reprogramming. *J Clin Invest* **2018**, *128*, 4472-4484, doi:10.1172/JCI99397.
 41. Huch, M.; Dorrell, C.; Boj, S.F.; van Es, J.H.; Li, V.S.; van de Wetering, M.; Sato, T.; Hamer, K.; Sasaki, N.; Finegold, M.J., et al. In vitro expansion of single Lgr5+ liver stem cells induced by Wnt-driven regeneration. *Nature* **2013**, *494*, 247-250, doi:10.1038/nature11826.
 42. Deuring, J.J.; Li, M.; Cao, W.; Chen, S.; Wang, W.; de Haar, C.; van der Woude, C.J.; Peppelenbosch, M. Pregnane X receptor activation constrains mucosal NF-kappaB activity in active inflammatory bowel disease. *PLoS One* **2019**, *14*, e0221924, doi:10.1371/journal.pone.0221924.
 43. Sun, J.H.; Luo, Q.; Liu, L.L.; Song, G.B. Liver cancer stem cell markers: Progression and therapeutic implications. *World J Gastroenterol* **2016**, *22*, 3547-3557, doi:10.3748/wjg.v22.i13.3547.
 44. Chang, C.W.; Lo, J.F.; Wang, X.W. Roles of mitochondria in liver cancer stem cells. *Differentiation* **2019**, *107*, 35-41, doi:10.1016/j.diff.2019.04.001.
 45. Cao, W.; Chen, K.; Bolkestein, M.; Yin, Y.; Verstegen, M.M.A.; Bijvelds, M.J.C.; Wang, W.; Tuysuz, N.; Ten Berge, D.; Sprengers, D., et al. Dynamics of Proliferative and Quiescent Stem Cells in Liver Homeostasis and Injury. *Gastroenterology* **2017**, *153*, 1133-1147, doi:10.1053/j.gastro.2017.07.006.
 46. Shimokawa, M.; Ohta, Y.; Nishikori, S.; Matano, M.; Takano, A.; Fujii, M.; Date, S.; Sugimoto, S.; Kanai, T.; Sato, T. Visualization and targeting of LGR5(+) human colon cancer stem cells. *Nature* **2017**, *545*, 187-192, doi:10.1038/nature22081.
 47. Gregorieff, A.; Liu, Y.; Inanlou, M.R.; Khomchuk, Y.; Wrana, J.L. Yap-dependent reprogramming of Lgr5(+) stem cells drives intestinal regeneration and cancer. *Nature* **2015**, *526*, 715-718, doi:10.1038/nature15382.
 48. Yan, K.S.; Janda, C.Y.; Chang, J.; Zheng, G.X.Y.; Larkin, K.A.; Luca, V.C.; Chia, L.A.; Mah, A.T.; Han, A.; Terry, J.M., et al. Non-equivalence of Wnt and R-spondin ligands during Lgr5(+) intestinal stem-cell self-renewal. *Nature* **2017**, *545*, 238-242, doi:10.1038/nature22313.
 49. Vermeire, S.; Van Assche, G.; Rutgeerts, P. Laboratory markers in IBD: useful, magic, or unnecessary toys? *Gut* **2006**, *55*, 426-431, doi:10.1136/gut.2005.069476.
 50. Shivananda, S.; Lennard-Jones, J.; Logan, R.; Fear, N.; Price, A.; Carpenter, L.; van Blankenstein, M. Incidence of inflammatory bowel disease across Europe: is there a difference between north and south? Results of the European Collaborative Study on Inflammatory Bowel Disease (EC-IBD). *Gut* **1996**, *39*, 690-697, doi:10.1136/gut.39.5.690.

51. Ten Hove, J.R.; Shah, S.C.; Shaffer, S.R.; Bernstein, C.N.; Castaneda, D.; Palmela, C.; Mooiweer, E.; Elman, J.; Kumar, A.; Glass, J., et al. Consecutive negative findings on colonoscopy during surveillance predict a low risk of advanced neoplasia in patients with inflammatory bowel disease with long-standing colitis: results of a 15-year multicentre, multinational cohort study. *Gut* **2019**, *68*, 615-622, doi:10.1136/gutjnl-2017-315440.
52. Li, Y.; Deuring, J.; Peppelenbosch, M.P.; Kuipers, E.J.; de Haar, C.; van der Woude, C.J. IL-6-induced DNMT1 activity mediates SOCS3 promoter hypermethylation in ulcerative colitis-related colorectal cancer. *Carcinogenesis* **2012**, *33*, 1889-1896, doi:10.1093/carcin/bgs214.
53. Li, Y.; de Haar, C.; Peppelenbosch, M.P.; van der Woude, C.J. SOCS3 in immune regulation of inflammatory bowel disease and inflammatory bowel disease-related cancer. *Cytokine Growth Factor Rev* **2012**, *23*, 127-138, doi:10.1016/j.cytogfr.2012.04.005.
54. Li, Y.; de Haar, C.; Chen, M.; Deuring, J.; Gerrits, M.M.; Smits, R.; Xia, B.; Kuipers, E.J.; van der Woude, C.J. Disease-related expression of the IL6/STAT3/SOCS3 signalling pathway in ulcerative colitis and ulcerative colitis-related carcinogenesis. *Gut* **2010**, *59*, 227-235, doi:10.1136/gut.2009.184176.
55. Cao, W.; Kayama, H.; Chen, M.L.; Delmas, A.; Sun, A.; Kim, S.Y.; Rangarajan, E.S.; McKevitt, K.; Beck, A.P.; Jackson, C.B., et al. The Xenobiotic Transporter Mdr1 Enforces T Cell Homeostasis in the Presence of Intestinal Bile Acids. *Immunity* **2017**, *47*, 1182-1196 e1110, doi:10.1016/j.immuni.2017.11.012.
56. Terc, J.; Hansen, A.; Alston, L.; Hirota, S.A. Pregnane X receptor agonists enhance intestinal epithelial wound healing and repair of the intestinal barrier following the induction of experimental colitis. *Eur J Pharm Sci* **2014**, *55*, 12-19, doi:10.1016/j.ejps.2014.01.007.
57. Chen, B.; Garmire, L.; Calvisi, D.F.; Chua, M.S.; Kelley, R.K.; Chen, X. Harnessing big 'omics' data and AI for drug discovery in hepatocellular carcinoma. *Nat Rev Gastroenterol Hepatol* **2020**, 10.1038/s41575-019-0240-9, doi:10.1038/s41575-019-0240-9.
58. van der Giessen, J.; Binyamin, D.; Belogolovski, A.; Frishman, S.; Tenenbaum-Gavish, K.; Hadar, E.; Louzoun, Y.; Peppelenbosch, M.P.; van der Woude, C.J.; Koren, O., et al. Modulation of cytokine patterns and microbiome during pregnancy in IBD. *Gut* **2020**, *69*, 473-486, doi:10.1136/gutjnl-2019-318263.
59. Colombel, J.F.; Sandborn, W.J.; Reinisch, W.; Mantzaris, G.J.; Kornbluth, A.; Rachmilewitz, D.; Lichtiger, S.; D'Haens, G.; Diamond, R.H.; Broussard, D.L., et al. Infliximab, azathioprine, or combination therapy for Crohn's disease. *N Engl J Med* **2010**, *362*, 1383-1395, doi:10.1056/NEJMoa0904492.

CHAPTER 10

Nederlandse samenvatting Dutch summary

Nederlandse samenvatting.

Met een gewicht van anderhalve kilogram is de lever het zwaarste interne orgaan van het lichaam. Bij de mens en meeste andere dieren is de lever een belangrijk en veelzijdig orgaan dat een belangrijke rol speelt in het metabolisme. De lever ligt achter de onderste ribben van de borstkas, rechtsboven in de buikholte en dus goed beveiligd tegen mechanisch trauma. Helaas wordt de lever wel vaak het slachtoffer van (chronische) virale infecties (denk aan hepatitis B en C), chemische toxiciteit (denk aan bijvoorbeeld schimmeltoxines zoals die op pinda's kunnen voorkomen) en ook door chronische ontsteking door vervetting. Uiteindelijk kan dergelijke belasting van de lever uitmonden in leverkanker, een ziekte die ongemeen dodelijk is omdat ze nauwelijks reageert op therapie anders dan chirurgie. In dit proefschrift probeer ik zowel ontsteking en haar interactie met giftige stoffen te begrijpen, de intracellulaire details van de leverkankercel op te helderen, en de rol van de verschillende cellen zoals die in leverkanker voorkomen te identificeren. Ook ga ik in op over hoe het beste met de bijwerkingen van nieuwe therapie van leverkanker om te gaan. Samen hoop ik dat deze studies een nieuw beeld geven van leverkanker en zullen bijdragen aan het ontwerpen van verbeterde behandeling. Een algemene inleiding alsmede een rechtvaardiging van de gekozen strategie is te vinden in hoofdstuk 1.

In hoofdstuk 2 en 3 van dit proefschrift neem ik de leverkankercel nader onder de loep en concentreer ik mij met name op de zogenaamde mitochondria. Een mitochondrion is een knobbelvormig organel met een diameter van ongeveer 1 micrometer dat de energiesynthese van de cel verzorgt. Het ligt voor de hand dat in een metabool actieve cel als de levercel mitochondria belangrijk zijn. Bij de afbraak van energierijke stoffen in het mitochondrion gedurende de zogenaamde citroenzuurcyclus worden energierijke elektronen geproduceerd die dan tijdens de oxidatieve fosforylering in de electronentransportketen weer worden gebruikt om ATP te produceren. ATP is een belangrijke energiebron voor zeer veel reacties in de cel. Ik laat in mijn proefschrift zien dat mitochondria door met elkaar te fuseren of juist te delen voortdurend van vorm veranderen. De leverkankercel blijkt erg gevoelig is voor interventies die ingrijpen op deze intracellulaire vormveranderingen van de mitochondria. Het ligt dus voor de hand om te suggereren dat dergelijke interventies een belofte inhouden voor wat betreft behandeling van leverkanker. De studies in dit proefschrift beperken zich tot experimenten in cellijnen en ook wel proefdieren. Er moet dus meer werk verzet worden voordat hier hardere uitspraken over gedaan kunnen worden. Gelijkaardig zie ook dat de electronentransportketen zelf een doelwit voor nieuwe behandeling van leverkanker kan zijn. Hier geldt echter hetzelfde voorbehoud. Desalniettemin is het duidelijk dat het mitochondrion een zwakke plek van de leverkankercel is, die uitnodigt tot verder onderzoek en heel wel een geschikt aangrijpingspunt kan zijn voor radicaal nieuwe vormen van therapie.

Het is echter belangrijk om te realiseren dat levertumoren complexe structuren zijn die een veelvoud aan celtypes bevatten. Zo zijn er immuuncellen en hun activatie kan helpen de tumor te bestrijden maar zal ook bijwerkingen kennen (waarover later meer). Maar er zijn ook

fibroblasten en ook niet alle tumorcellen zelf zijn gelijk. Dit aspect van leverkanker diep ik uit in hoofdstuk 4, 5 en 6. Meestal wordt voor preklinisch onderzoek gebruik gemaakt van cellijnsystemen die louter een geïmmortaliseerde variant van een enkele kankercel omvatten. Ik laat zien dat de eigenschappen van de kankercel alleen kunnen worden begrepen en worden geabstraheerd in de kweekschaal als ook de fibroblasten worden betrokken. De eigenschappen van de kankercellen veranderen als deze cellen meegekweekt worden. Eigenlijk vervullen deze fibroblasten een functie als warm bad voor de kankercellen, die daardoor veel minder gevoelig worden voor therapie. Ik postuleer dan ook dat dit de reden is dat preklinisch onderzoek met betrekking tot leverkanker tot nu toe zo slecht vertaalbaar blijkt naar de zieke mens. Ook laat ik zien dat een specifieke populatie van kankercellen heel belangrijk is bij terugkeer van ziekte na bijvoorbeeld chemotherapie. In modellen waarbij deze kankerstamcellen (een kleine fractie van alle kankercellen) genetisch werden geïnactiveerd bleek chemotherapie veel succesvoller. Dus naast de fibroblast zou ook dit celtype betrokken moeten worden bij het ontwerpen van rationele therapie voor leverkanker.

In hoofdstuk 7 schakel ik over naar ontsteking. Chronische ontsteking leidt tot kanker. In het laboratorium waar ik mijn onderzoek heb uitgevoerd is indrukwekkende expertise met betrekking tot inflammatoire darmziekten, een groep ziektes die veel beter toegankelijk is voor onderzoek dan ontsteking van de lever. Ik besloot dan ook deze groep ziektes te bestuderen en wel wat betreft de activatie van zogenaamde xenobiotische receptoren. Xenobiotica spelen een belangrijke rol bij pathologie van de lever, dus dit was een logische keuze. Ik karakteriseer de interactie van deze receptoren met het immuunsysteem en suggereer dat dergelijke interacties gebruikt kunnen worden om ontsteking te beperken. Verder onderzoek moet uitwijzen of dat dit ook voor de lever zou gelden.

De specifieke kennis met betrekking tot de ontsteking van darm aanwezig op de afdeling waar ik dit promotieonderzoek heb uitgevoerd, heb ik ook benut bij een studie naar de bijwerkingen van de zogenaamde immunocheckpointinhibitoren. Het antwoord van het immuunsysteem op kanker wordt vaak beperkt door de zogenaamde immunocheckpoints, die dan ook vaak in ruime mate in kankers aanwezig zijn. Door inhibitoren te geven van deze checkpoints wordt de volle kracht van het immuunsysteem bij het bestrijden van de ziekte opgeroepen. Een probleem zijn de bijwerkingen van deze medicatie en met name ontsteking van de dikke darm is problematisch. Ik analyseer de strategieën die wereldwijd worden gebruikt om deze bijwerkingen te verminderen en concludeer dat ze wellicht interfereren met het behandelings-effect van de immunocheckpointinhibitoren zelf. Ik draag mogelijke alternatieve strategieën aan in hoofdstuk 8.

In hoofdstuk 9 vat ik al deze bevindingen nog eens samen en bediscussieer ze in het licht van de huidige wetenschappelijke literatuur. Al overschauwend hoop ik met deze dissertatie een bijdrage te hebben geleverd aan het overwinnen in het gevecht tegen leverkanker.

Appendix

Acknowledgements

Publications

PhD portfolio

Curriculum Vitae

Acknowledgements

To obtain a PhD degree is a long journey full of unknowns and indeterminants. I would like to thank all people who walked this road with me.

First and foremost, I would like to give my wholehearted appreciation to my promotor, Prof. Dr. Maikel P Peppelenbosch, for offering me the precious opportunity to pursue my PhD and your four-year of supervising with great patience and sharing your immense knowledge with me. The first time you introduces the subproject of IBD to me, my feeling were very special because one of my close family members is suffering from this disease. It was the first time I felt my work is directly connected to my personal life even if my research work is far away from providing patient benefit.

I am also deeply indebted to my co-promoter Dr. Qiuwei Pan for his fundamental role in pursuing my doctoral work. His encouragement, support, and guidance throughout my PhD study made me survive from my PhD and finally resulted in me being able to present my work in this thesis.

I also want to express my deepest gratitude to my almost co-promoter Wanlu Cao for your sage advice and endless support. Learning from you has not only improved my research capabilities but also showed me an example as how to be a young scientist in the future.

To Luc, it is my honor to have you as my inner committee member. Thank you for your brilliant comments and pertinent suggestions for my projects and papers. It was an enjoyable time full with interesting discussions and meetings.

To Gwenny, it is a great experience to work with and study from you. It was generous of you to give so much kind advice and offer so much great help. Your hardworking, wisdom and passionate attitude continue to inspire me to learn new things and overcome the fear of the unknown.

To Jaap and Dave, thanks for the insightful comments and encouragement, but also for the questions which made me to widen my research view and provide novel perspectives like you did during our weekly meeting. Wish all the best to you.

My sincere thanks also go to Ron. Your encyclopaedic knowledge of experiments and their principles have impressed me so many times. I learned not only from the answers you gave to my questions but also a strict attitude to seek the truth.

To Henk, thanks for all enjoyable time as a desk neighbour and the countless of help and patience you provided. I will miss the time and best wishes to you and your family.

To Auke and Leonie, there are too many times you helped me out with my problems. I could not have imagined how the lab would be without you. Thanks so much and wish the best to you and your family.

My greatest gratitude also goes to Anthonie and Petra. You are always supportive when I sought your help. I am grateful for every experience and lesson I learned.

To Estella, thanks for your continuous support for work, time after time. I will miss the delicious dinners and the happy time we shared together.

To Jiaye, I am extremely grateful for your contribution during all stages of thesis preparation. Thanks for all the patience, encouragement and support.

To Ruby, thanks for your valuable suggestions and your help during our weekly meetings and project discussions.

To Sam, Dr. Nicolaas J. H. Raat and other members from the Laboratory of Experimental Anesthesiology of the Erasmus MC, it has been a great opportunity to collaborate with such excellent researchers and has broadened my horizon.

To Suk Yee, thanks for providing professional help with translation, all extraordinary patience and a constant sunshine smile.

To Pengyu and Shan, I feel so lucky to work with you during the past years. Thanks for the constant encouragement and valuable suggestions.

To my paranimfen Ling and Ruyi, I would like to express my heartfelt gratitude for all the support. You helped me out of my difficulties and supported me without a word of complaint.

To Changbo and Buyun, I would like to extend my sincere thanks to you, who have helped me make this thesis possible and to improve it with your valuable suggestions and support.

To all the co-authors, thanks for your contributions to my thesis and the journal publications.

Financial support from China Scholarship Council made a dream come true, thanks for the generous support from home.

To all honorable MDL members who have left and who are present, thanks for all the happy time and unconditional help. Best wishes to all!

真诚地感谢实验室的师弟师妹们，近朱者赤，见贤思齐，从你们的身上我学到了很多也得到了很多帮助，特别感谢你们一直以来的鼓励和包容，希望你们未来一切顺利。

感谢远在德国的平安师姐，一起旅行的时光和美好的分享是平淡生活中的甜点。希望你的所有美好愿望都能达成。

感谢我的硕士导师李锦军教授，您是我科研路上的领路人，为我打下了坚实基础。希望您和家人平安喜乐。

最后感谢我的家人，是你们的陪伴和支持给了我坚持下去的勇气和信心。把这篇毕业论文献给你们！

List of publications

Li, M.; Wang, L.; Wang, Y.; Zhang, S.; Zhou, G.; Lieshout, R.; Ma, B.; Liu, J.; Qu, C.; Verstegen, M.M.A., et al. Mitochondrial Fusion Via OPA1 and MFN1 Supports Liver Tumor Cell Metabolism and Growth. *Cells* 2020, 9, doi:10.3390/cells9010121.

Cao, W.; Li, M.; Liu, J.; Zhang, S.; Noordam, L.; Verstegen, M.M.A.; Wang, L.; Ma, B.; Li, S.; Wang, W., et al. LGR5 marks targetable tumor-initiating cells in mouse liver cancer. *Nat Commun* 2020, 11, 1961, doi:10.1038/s41467-020-15846-0.

Cao, W.; Liu, J.; Wang, L.; Li, M.; Verstegen, M.M.A.; Yin, Y.; Ma, B.; Chen, K.; Bolkestein, M.; Sprengers, D., et al. Modeling liver cancer and therapy responsiveness using organoids derived from primary mouse liver tumors. *Carcinogenesis* 2019, 40, 145-154, doi:10.1093/carcin/bgy129.

Liu, P.; Cao, W.; Ma, B.; Li, M.; Chen, K.; Sideras, K.; Duitman, J.W.; Sprengers, D.; Khe Tran, T.C.; Ijzermans, J.N.M., et al. Action and clinical significance of CCAAT/enhancer-binding protein delta in hepatocellular carcinoma. *Carcinogenesis* 2019, 40, 155-163, doi:10.1093/carcin/bgy130.

Ma, B.; Chen, K.; Liu, P.; Li, M.; Liu, J.; Sideras, K.; Sprengers, D.; Biermann, K.; Wang, W.; JNM, I.J., et al. Dichotomous functions of phosphorylated and unphosphorylated STAT1 in hepatocellular carcinoma. *J Mol Med (Berl)* 2019, 97, 77-88, doi:10.1007/s00109-018-1717-7.

Liu, J.; Ma, B.; Cao, W.; Li, M.; Bramer, W.M.; Peppelenbosch, M.P.; Pan, Q. Direct-acting antiviral agents for liver transplant recipients with recurrent genotype 1 hepatitis C virus infection: Systematic review and meta-analysis. *Transpl Infect Dis* 2019, 21, e13047, doi:10.1111/tid.13047.

Liu, J.; Cao, W.; Ma, B.; Li, M.; Peppelenbosch, M.P.; Pan, Q. Sofosbuvir directly promotes the clonogenic capability of human hepatocellular carcinoma cells. *Clin Res Hepatol Gastroenterol* 2019, 43, e79-e81, doi:10.1016/j.clinre.2018.11.016.

Qu, C.; Zhang, S.; Wang, W.; Li, M.; Wang, Y.; van der Heijde-Mulder, M.; Shokrollahi, E.; Hakim, M.S.; Raat, N.J.H.; Peppelenbosch, M.P., et al. Mitochondrial electron transport chain complex III sustains hepatitis E virus replication and represents an antiviral target. *FASEB J* 2019, 33, 1008-1019, doi:10.1096/fj.201800620R.

Li, M.; Pan, Q.; Peppelenbosch, M.P. Should Nivolumab-Induced Colitis Be Treated by Infliximab? *Clin Gastroenterol Hepatol* 2017, 15, 1637, doi:10.1016/j.cgh.2017.05.012.

Deuring JJ, Li M, Cao W, Chen S, Wang W, de Haar C, van der Woude CJ, Peppelenbosch M. Pregnane X receptor activation constrains mucosal NF- κ B activity in active inflammatory bowel disease. *PLoS One*. 2019 Oct 3;14(10):e0221924.

Chen L, Tian H, Li M, Ge C, Zhao F, Zhang L, Li H, Liu J, Wang T, Yao M, Li J. Derivate isocorydine inhibits cell proliferation in hepatocellular carcinoma cell lines by inducing G2/M cell cycle arrest and apoptosis. *Tumour Biol*. 2016 May;37(5):5951-61.

Li M, Zhang L, Ge C, Chen L, Fang T, Li H, Tian H, Liu J, Chen T, Jiang G, Xie H, Cui Y, Yao M, Li J. An isocorydine derivative (d-ICD) inhibits drug resistance by downregulating IGF2BP3 expression in hepatocellular carcinoma. ***Oncotarget***. 2015 Sep 22;6(28):25149-60.

PhD portfolio

Name of PhD student:	Meng Li
EMC:	Department of Gastroenterology and Hepatology
PhD period:	October 2015 – July 2020
Promotor:	Prof. dr. Maikel P Peppelenbosch
Co-promotor:	Dr. Qiuwei Pan

PhD training

Seminars

2015-2019, Weekly MDL seminar program in experimental gastroenterology and hepatology (attending) (42 weeks/year) (ETCS, 9.0);

2015-2019, Weekly MDL seminar program in experimental gastroenterology and hepatology (presenting) (2 times/year) (ETCS, 4.6);

2015-2019, Biweekly research group education (attending) (21 times/year) (ETCS, 4.3);

2015-2019, Biweekly research group education (presenting) (21 times/year) (ETCS, 4.6)

General academic and research skills: courses

2015 Course on biomedical research (XIV) (ETCS, 1.5);

2015 The survival analysis course (ETCS, 0.6);

2016 Workshop on NCBI & other open source software (ETCS, 1.0);

2016 Microscope image analysis: from theory to practice (ETCS, 0.8);

2016 Introduction to laboratory animal science (ETCS, 3.0);

2017 Targeting mitochondria (ETCS, 2.0);

2018 Erasmus MC Molecular Medicine Day (ETCS, 0.7);

2019 Course on scientific integrity (ETCS, 0.3);

2019 The gene expression data analysis using R: How to make sense out of your RNA-seq/microarray data (ETCS, 2.0);

Special lectures and conferences

2016 The Erasmus Medical Center Molecular Medicine Day, Rotterdam, the Netherlands

2017 World Congress on Targeting Mitochondria, Berlin, Germany (Poster presentation)

Mitochondrial fusion fuels liver tumor cell metabolism and growth

2017 The Erasmus Medical Center Molecular Medicine Day, Rotterdam, the Netherlands

2018 The Erasmus Medical Center Molecular Medicine Day, Rotterdam, the Netherlands (Poster presentation)

Mitochondrial fusion fuels liver tumor cell metabolism and growth

2019 The Erasmus Medical Center Cancer Institute Research Day, Rotterdam, the Netherlands

2019 The Erasmus Medical Center Organ On Chip (OOC), Rotterdam, the Netherlands

Academic awards

China Scholarship Council (CSC) Scholarship (201506100033)

Other activities

Reviewer of articles for scientific report

Curriculum vitae

Meng Li was born in Oct. 30, 1988, in Harbin, Heilongjiang province, China. She grew up with her beloved parents.

In 2007, she graduated from high school of her hometown and went to the medical college of Fudan University at Shanghai. After obtaining the medical degree in 2012, she started a master study on cancer research under the supervision of Prof. Jinjun Li and graduated three years later.

In 2015, she had an opportunity to start her PhD research under the supervision of Prof. Maikel P Peppelenbosch and Dr. Qiuwei Pan at the department of Gastroenterology and hepatology, Erasmus Medical Center, the Netherlands. With the financial support of China Scholarship Council, she focused her study on controlling gastroenterology and hepatology growth: the role of intracellular and extracellular signalling.